CONCRETE FLUIDITY EFFECTS ON BOND OF PRESTRESSED TENDONS FOR LIGHTWEIGHT BRIDGE GIRDERS

By

JAKE PERKINS

B.S., Kansas State University, 2006

A THESIS

Submitted in partial fulfillment of the requirements for the degree

MASTER OF SCIENCE

Department of Civil Engineering
College of Engineering

KANSAS STATE UNIVERSITY
Manhattan, Kansas

2008

Approved by:

Major Professor
Dr. Robert J. Peterman

Abstract

With limited research being conducted solely on lightweight concrete prestressed bond and current development-length equations based on tests performed on normal-weight members, more investigation on lightweight concrete prestress bond is necessary. Additionally, the effects of water-reducing agents on normal-weight and lightweight concrete need further exploration. The aim of this study was to examine these areas using two locally available lightweight aggregates from Kansas and one from North Carolina to determine if lightweight prestressed concrete bridge girders are a useful alternative for the Kansas Department of Transportation. The lightweight concrete mixes developed were capable of attaining 5000 psi compressive strength in 16 hours and 7000 psi in 28 days. During the large block pull-out test, the average maximum force at pull-out and first observable slip was higher for the block cast with a three-inch slump then the companion specimen poured at a nine-inch slump. During flexural testing, the two beams not reaching nominal moment capacity, KC-9 and STA-9, failed in compression without strand end slip. The moment capacity was considerably greater for three-inch slump members than the companion specimen placed with nine-inch slump concrete.

Table of Contents

List of Figures

List of Tables

Acknowledgements

I would like to thank the Federal Highway Administration and the Kansas Department of Transportation for funding this project. I am truly grateful to live, be educated, and work in a state and country that is supportive of my profession and education . Additionally, I would like to thank the industry support of Buildex Incorporated, Stalite Corporation, Don Logan and the Stresscon Corporation, and the Monarch Cement Company.

I would like to thank Dr. Peterman for his continuous support and guidance throughout the project. I would also like to thank Dave Meggers, Bureau of Research and Materials Kansas Department of Transportation, for guiding the project in the direction that would be most beneficial for the state of Kansas and the Federal Highway Administration.

Additionally, this project would not have been possible without the support of my fellow graduate students; Sarah Larson, Patrick Sheedy, and Joey Holste. The under-graduate students Lisa Beck, Ryan and Logan Benteman, Brady Hedstrom, and Jordan Dettmer played a significant role in completing this project and all of their efforts are greatly appreciated.

1 Background

The concept of prestress concrete has been around since 1872 when a California engineer, P.H. Jackson, attempted to prestress individual pieces of concrete arches with metal rods. Again in 1888, a German engineer patented a system of prestress slabs. However, all these attempts failed due to loss of prestress force in the member caused by concrete creep plus relaxation of the steel (Nawy, 2006). Through the work of R. E. Dill and W. H. Hewett, America, prestress concrete became widely used due to the concept of incremental tightening of un-bonded rods that could be adjusted as time-dependent losses occurred. Their prestress developments were used in circular water tanks and pipes. At the same time, advancements in linear prestressing were being made in France by Eugene Freyssinet with the use of high-strength ductile steel. After World War II, many structures had to be replaced quickly, which further advanced use of linear prestressed members. In the 1930s and the 1960s more process improvement and design methods were refined due to the work of engineers like T. Y. Lin. Today, prestress members are used in commercial buildings, offshore structures, power-generation plants, single- and multiple-span bridges, cable-stay bridges, and segmental bridges (Nawy, 2006).

Many research projects have been conducted since the 1950s to study the topics of transfer length, development-length, time-dependent losses, shear capacity, detensioning methods, and other aspects of prestress members. In 1988, the Federal Highway Administration (FHWA) put temporary restrictions on use of pretensioned members for bridges. The restrictions were based upon the findings of Cousins et al. at North Carolina State University. Their study reported that the American Association of State Highway Transportation Officials' (AASHTO) development-lengths equations for flexural members were up to 29% shorter than required. The FHWA terminated use of 0.6-inch diameter strands, increased strand spacing to four times the strand diameter, and increased the AASHTO development-length by a factor of 1.6 for members deeper then 24 inches (Canfield (2005). The restrictions spurred research across the country to more accurately model transfer and development-length design equations. The *American Concrete Institute 318-05 Building Code Requirements for Structural Concrete* (ACI 318-05) Section 12.9 defines transfer length as shown in Equation 1-1.

$$l_d = \left(\frac{f_{se}}{3000}\right) d_b + \left(\frac{f_{ps} - f_{se}}{1000}\right) d_b$$

l_d = Development-Length

f_{se} = Effective Stress in Prestressing Steel (1-1)

f_{ps} = Stress in Prestressing Steel at Nominal-Moment Capacity

d_b = Nominal Diameter of Prestress Strand

The commentary to Section 12.9 explicitly states that the code equation is based upon tests performed on normal-weight concrete. The commentary also states that the first term in Equation 1-1 represents the transfer length. Section 11.4 of ACI 318-05 states that for shear design the transfer length should be taken as 50-bar diameters (ACI Committee 318, 2005).

AASHTO has the same required development-length as ACI, Equation 1-1, except for deeper members, where a 1.6 multiplier is required. The AASHTO transfer length is 60-bar diameters and not taken as the first term in the development-length equation like ACI. Neither transfer nor development-length are a function of concrete material properties, but of strand stress and diameter.

1.1 *Importance of Bonding in Prestressed Concrete Members*

Transfer length, $L_{tr,}$ the distance required to transfer tensile forces in the prestressing tendon to a compressive stress in the concrete, plays an important role in designing members for shear and flexure. Often the most critical area for shear resistance in a beam is within the transfer length. Additionally, the strand stress at nominal-moment capacity not only depends on the transfer length, but on accurate knowledge of the development-length, L_d. Development-length is the distance the strand must be bonded to reach the maximum stress at nominal-moment capacity, f_{ps}. There are three mechanisms by which the prestressing force is transferred to the concrete member; adhesion, friction resistance, and mechanical interlock (Barnes et al., 2003).

1.1.1 Adhesion

Cohesive bonding takes place between the paste in the concrete mix and the prestressing strand. However, when the force in the tendons is transferred from the prestress forms to the members, the strand breaks the cohesive bonds with the concrete. Therefore, adhesion does not play a significant role in bond (Barnes et al., 2003).

1.1.2 Frictional Resistance

When the prestressing tendon is tensioned, the strand contracts in the radial direction. When the concrete is poured, it cures around the contacted diameter. When the strand is cut and released to the member, it expands in the radial direction causing normal forces to develop, often referred to as the Hoyer effect. The normal force between the strand and the concrete creates frictional force (Barnes et al., 2003).

1.1.3 Mechanical Interlock

Most seven-wire prestressing steel is formed by twisting the seven individual wires into a single strand in a helix shape. When the strand is tensioned and the concrete is poured and cures around the tendon, a bearing interface between the strand and the concrete is formed. In order for the strand to slip, it most break through the bearing surface, or twist as it slips through the helix-shape mold of the concrete. Adding to the mechanical interlock are small pieces of concrete that break off when the prestress force is transferred to the member, causing wedging action between the steel and concrete (Barnes et al., 2003).

1.2 *Uses of Lightweight Concrete in Kansas*

In July 1953, the Kansas Department of Transportation (KDOT), at the time known as the State Highway Commission of Kansas, released its findings of a one-year study titled *Availability and Suggested Usages of Lightweight Concrete for Kansas Highway Construction*. The research department, authors of the study, identified two Kansas lightweight aggregate suppliers that would be suitable, Buildex Corporation near Ottawa, and Carter-Waters Corporation near Kansas City. Both companies produced an expanded-shale aggregate by heating the rock in a rotary kiln. The study discussed structures already in use with lightweight

concrete, suggested concrete mix designs for each aggregate, described the general quality of lightweight concrete, and estimated the in-place cost of the two lightweight concrete mixes. After the 1953 study, KDOT wrote a set of specifications for use of lightweight concrete (Research Department, State Highway Commission of Kansas, 1953).

The first documented use of lightweight concrete by KDOT was on two bridges in 1955. The lightweight mixes were used only for the bridge deck. The two structures, termed the "Turner bridge" and the "Willard bridge," were viewed to initially perform as well as normal-weight concrete mixes of the time. According to a report released by KDOT's research department in December 1955, aggregates used for the two bridges came from the local producers discussed above. In the same report, the Research Department announced a revised set of lightweight concrete specifications for construction to take place in 1956. Changes in the revised specifications were due to observations during batching and placing the lightweight concrete the previous year (Research Department, State Highway Commission of Kansas, 1955).

However, several years after construction was completed on the Turner and Willard bridges, it was noticed the lightweight bridge decks began to expand. Over several years, the lightweight decks began to show large cracks associated with the expansion. Several other bridges, constructed before the problems with the Turner and Willard bridges were evident, later experienced the same expansion problems. Due to the severe damage, KDOT decided to end use of lightweight concrete. Unfortunately, no documented investigation took place as to why the bride decks expanded.

1.3 *Water-Reducing Admixtures in Prestress Members*

Recently research has been conducted, Larson et al (2007) and Peterman (2007), on the effects of high-fluidity concrete and its implications on bond of prestress tendons. Fluid mixes are often produced with water-reducing admixtures that allow prestress plants to use low water-to-cementicious material ratios, maintain workability, achieve smooth finish on members, use less cement per cubic yard, and attain concrete compressive strength in time to detension strands and strip forms. Today, many prestress plants use a polycarboxylate-based superplasticizer, a high-range water reducer meeting ASTM C-1017 which allows plants to obtain slumps of 3 inches up to self-consolidating concrete (SCC) with a spread of 28 inches with a low water-to-cement ratio. Before the advent of superplasticizer, batch plants used low-, mid- and high- range

water reducers in many different combinations that achieved the desired slump or spread. The effects of polycarboxylate-based superplasticizer on the bond of prestress tendons have only recently been investigated and require more research.

1.4 *Current Use of Lightweight Aggregates*

Currently KDOT does not use lightweight concrete on any bridges. However, several Kansas counties have used lightweight bridge decks with aggregate from the same two rock quarries used in 1955 by KDOT, with varying degrees of success. Today both quarries used in the 1950s are owned by Buildex Corporation. Other states and local governments across the country have used lightweight aggregates from those same quarries with good long-term results.

With many Kansas bridges being located in rural areas, lightweight prestressed bridge girders could be a desirable, cost-effective alternative to normal-weight concrete girders. Many of the bridges require long travel distances for precast girder deliveries; lightweight members allow for the possibility of shipping multiple beams on one truck. Additionally, lightweight precast girders would reduce the required crane size, decrease foundation size, and increase span-to-depth ratio.

With minimal research being conducted solely on lightweight concrete prestress bond and current development-length equations based on test performed on normal-weight members, more investigation on lightweight concrete prestress bond is necessary. Effects of water-reducing agents on normal-weight and lightweight concrete need further exploration. The aim of this study was to examine these areas using two locally available lightweight aggregates from Kansas and one from North Carolina to determine if lightweight prestress bridge girders are a useful alternative for KDOT.

1.5 *Scope of Study*

Section 2.0 reviews the important literature and research that pertain to lightweight concrete and prestress bond.

Section 3.0 reports on coarse- and fine-aggregate gradation, absorption, moisture content, cement, and admixtures used to develop the mixes used in the study.

Section 4.0 reports on material specifications, concrete mix design, trial batch procedures, fresh concrete test procedures, finalized mix designs, hardened concrete test procedures, core sampling of existing lightweight bridge decks, and large-scale batching procedures.

Section 5.0 discusses the large-block pull-out test and strand preparation, cage construction, form fabrication, concrete casting, and test procedures that were required.

Section 6.0 discusses flexural member lengths, cross sections, forms, strand tensioning, concrete casting, surface-strain measurements, end-slip measurements, strand detensioning, and testing setup and procedures.

Section 7.0 reports on results of the hardened concrete test, modulus of elasticity, creep, shrinkage, petrographic examination of bridge deck core samples, large-block pull-out test, transfer lengths, and flexural testing.

Section 8.0 discusses results from section 7.0, and makes relevant conclusions and recommendation based upon test results.

2 Literature Review

This section is a review of the pertinent literature available that guided the research project. Articles related to lightweight concrete uses and behavior are discussed, as well as prestress bond testing and flexural prestress member behavior.

2.1 *Lightweight Aggregate Properties and Behavior*

Bremner (1986) studied the interaction between aggregates and the mortar matrix surrounding the aggregates. Researchers compared aggregate and mortar interaction for both normal-weight and lightweight coarse-aggregates. The study found that the ratio of normal-weight aggregate stiffness to matrix stiffness can vary from three to five, leading to high-stress concentrations at the aggregate interface. It was reported that the mismatch for normal aggregate can be minimized by decreasing water-to-cement ratio and air voids. The study also reported that the ratio of lightweight aggregate stiffness to matrix stiffness can be less then normal-weight mixes and approach one. This can be achieved by matrix-entrained air levels from 5 to 7% and use of "usual" water-to-cement ratios, in the short range of elastic behavior of lightweight aggregate. The similar modulus for lightweight mixes reduces stress concentrations, reduces micro cracking, and subsequently increases durability and strength.

Holm and Bremner (1991) reviewed the long-term performance of lightweight aggregate used in a variety of structures. Researchers reported increased use of lightweight aggregate is a result of better long-term durability, increased strength-to-density ratio, and use of equal weight but increased cover for reinforcing. The authors credit the high durability to the manufacturing process. When the rock is heated, a non-interconnected cell structure is formed that retains water and is able to provide additional moisture to the surrounding paste during curing. When the rock is heated, strength decreases, which allows for compatible stresses at the aggregate and paste interface when a load is applied. The additional moisture and similar modulus to the paste allow for a fully developed contact zone at the aggregate edge. The authors reviewed a study where lightweight concrete prisms were exposed to severe weather for 10 years and performed as well as normal-weight specimens. This was confirmed by showing equal maintenance costs of 2000

short-span, lightweight precast bridges in Alberta, Canada, to similar bridges cast with normal-weight concrete.

Harmon (2007) reviewed the structural properties of lightweight expanded-shale aggregate. The paper defined lightweight structural concrete as a mix made with aggregate conforming to ASTM 330 that can obtain compressive strength of at least 2500 pounds per square inch (psi), and has a unit weight of 115 pounds per cubic foot (pcf) with allowances up to 120 pcf. The author listed some of the benefits of lightweight aggregate as lower dead load, longer spans, decreased story height, less reinforcing steel, and reduced foundation size. The aggregate reviewed achieved the low density through the rotary kiln process that heats and expands the aggregate at 2200°F. The mined rock is fed into a kiln 11 feet in diameter and 160 feet long. The rock is gradually heated as it moves toward the "burn zone" where the specified temperature is reached. This allows internal gases in the rock to mobilize and form unconnected cells. The rock is then forced-air cooled, crushed to size, and mixed to meet the required gradation. The lightweight aggregate can be used to produce concrete mixes of equal strength of a normal-weight mix. Additionally, for high-strength concrete, the lightweight aggregate can produce mixes with a lower elastic modulus.

Brown et al. (1995) evaluated the long-term performance of a lightweight bridge constructed in 1964 in Fanning Springs, Florida. The prestressed girders and deck were cast with a lightweight mix consisting of an expanded clay and siliceous sand. Each span was 121 feet long and consisted of six girders tied to the deck to achieve composite-member resistance. The structure was the first lightweight bridge constructed in the state so the DOT performed extensive deflection and strain response after construction was completed. In 1992, researchers performed the same load test to compare the results found 34 years earlier. They found the deflection and strain measurements in 1992 matched closely with those found in 1968. Additionally, results showed the dynamic deflection response matched closely with results found in the laboratory. They also revealed the lightweight mixes performed as well as and in some cases better than normal-weight concrete in the laboratory tests. Researchers contributed the positive performance of the lightweight mixes to the similar modulus of the aggregate and the surrounding matrix.

The Federal Highway Administration (1985) released *Criteria for Designing Lightweight Concrete Bridges* in 1985. The report was compiled to give design engineers useful information from previous lightweight projects and to study situations where lightweight bridges are advantageous. The paper stated that expanded shale, clay, and slate are the most common types of structural lightweight aggregates. The report also stated that the commercial sector had already adopted use of lightweight concrete and found it beneficial for the transportation of precast members. Use of lightweight aggregate in bridges had been primarily limited to decks on steel girders at that time. Performance of the lightweight decks had been largely satisfactory and issues related to poor performance of the lightweight decks were related to concrete specifications, understanding the behavior of the aggregate, and field placement. The report also reviewed the properties of lightweight aggregates, performance of in-place bridges, and the economics of lightweight concrete.

The ACI Committee 213 (2003) released *Guide for Structural Lightweight-Aggregate Concrete* in 2003, a comprehensive report that covers mechanical and physical properties, mixing, and hardened concrete structural performance of lightweight concrete. The guide reported little difference in bond strength between lightweight and normal-weight structural mixes for deformed reinforcing bars. The guide reported that the literature available for development-length of prestress tendons showed conflicting results. Some of the literature showed ACI and AASHTO requirements to be conservative, while others have recommended a multiplier to increase the design requirements. In either case, the guide stated that use of high-quality aggregates is critical for lightweight prestress members. The report advised using greater prestress losses due to additional creep and shrinkage associated with lightweight mixes.

2.2 *Prestress Bond and Flexural Testing*

Buckner (1995) conducted a review summarizing five different studies of proposed models for calculating transfer length of prestress members. The models discussed were a result of the prestress research community developing more accurate design equations after the FHWA released a notice restricting use of seven-wire prestress strands. The ACI and AASHTO expression for development-length were based on grade 250, seven-wire strands. However, the current industry trend was use of low-relaxation, grade 270, seven-wire strand. The grade 270

strand is 6% larger and due to the low relaxation, imparts a greater force on the member at the time of release. Buckner analyzed the research conducted at the University of Tennessee at Knoxville (UTK), the Florida Department of Transportation (FDOT), Purdue University, McGill University, and the University of Texas at Austin (UTA). Based upon on his review, he proposed the transfer-length equation be a function of the force in the prestress tendon at the time of release, not the force after all time-dependent losses. Additionally, Buckner proposed that the development-length be a function of the strain in the strand at nominal-moment capacity after finding multiple bond failures in members with high steel strain at ultimate capacity. Buckner also proposed a 1.3 multiplier for strands cast with 12 inches of concrete below them.

Logan (1997) developed a test to evaluate bond performance of the prestressing strand. Half-inch diameter strand was obtained from several prestress plants across the country in order to collect a representative sample of tendons being used by the industry. The researcher designed a standard test specimen, large block pull-out test (LBPT), in which non-tensioned strands were tied to a reinforcing cage inside a rectangular concrete form. The strands were placed so that 18 inches of concrete was placed along the height of the tendon to bond to the standardized mix, with an additional 14 inches of strand extending above the top of the concrete. Once the concrete cured, the strands were than pulled out of the block with a hydraulic actuator. Flexural members were cast with the same strand used in concrete block test. Four different configurations of development-length with the same cross section were tested and compared with code equations for required embedment length. Logan looked at the surface condition of each strand. The color, rusting, and residue from the production process were analyzed and recorded. The study concluded strands pulled out of the concrete block at 36 kips or greater performed well in the flexural testing and had shorter transfer lengths than predicted by code equations. Strand with pull-out strengths of 12 kips or less performed poorly in flexural testing and failed due to strand slip. Logan found no consistent correlations between the surface condition of the strand and the quality of bond.

Barnes et al. (2003) conducted a research program to evaluate transfer length in ASSHTO type I girders. Researchers tested 186 transfer lengths in 36 plants across the country. One third of the girders had fully bonded strands; one third of the beams had 50% of the strands partially bonded; and the last third had 60 to 70% of the strands partially bonded. The research team looked at the effects of concrete strength, detensioning methods, rusted or bright strand, and

time. The research revealed that little correlation could be found for the transfer lengths without considering the varying concrete strengths at release. More specifically, little correlation could be found with varying concrete strengths without the square root of the compressive strength. When the method of prestress transfer was examined, it was found that the transfer length was not consistently greater or less when comparing the dead and live ends of a member for beams cast with bright strand and concrete release strengths 9500 to 15000 psi. Unfortunately, beams in the study with concrete release strengths 5000 to 7000 psi were simultaneously released, therefore live- and dead-end effects could not be examined for lower concrete strengths. Beams with rusted strand had live-end transfer lengths 30 to 50% greater than the dead end. The rusted strand had a lower average transfer length then the bright strand. However, the amount of scatter in the rusted-strand transfer-length data was so large, the upper- and lower-bound limits were similar to the bright strand which had a higher average transfer length. The author contributed the scatter to the inconsistency of rusting and surface rust detaching from the strand at release. The bright-strand transfer length increased on average by 1.13 and took place within the first 20 days. The end detensioned second showed a 10% increase in transfer length, and the end detensioned first exhibited no increase with time. The rusted-strand transfer length increased by 1.17 in the first 20 days, but no correlation was found with the method of release and concrete strength over time. The authors concluded there was no difference in transfer methods for beams with concrete strength at release greater then 7000 psi; use of rusted strand does not give predictable results; and on average, transfer lengths increased by 10 to 20% with time.

Peterman (2000) evaluated development-length equations for semi-lightweight concrete by using direct code equations for $f_{ps,}$ the maximum steel stress at nominal-moment capacity, and underestimating f_{se}, effective prestress force after all losses, giving the shortest realistic development-length a designer could calculate. The study also looked at effects of a flexural shear crack forming near the area of maximum strand stress in semi-lightweight members. Single-strand, development-length specimens were cast 8 inches wide and 12 inches deep, with a single strand 10 inches below the top surface. Initially, three multiple-strand T-beams were cast with a flange width of 36 inches, flange depth of 6.5 inches, stem width of 16 inches, step depth of 14.5 inches, and five strands located 19 inches below the top surface. Both the single-strand and multiple-strand beams were tested with a development-length of 6 feet and 1.5 inches. The designation strand A and B were used to decipher between the two different strand

manufacturers tested. Six, single-strand development-lengths were tested with strand designation A and six with strand designation B. From the first set of T-beams, two had strand A and one had strand B. All 12 single-strand members reached the design stress in the tendon. The two T-beams with strand A were able to reach nominal-moment capacity and failed in strand rupture. However, the T-beam with strand B failed just above nominal from a flexural shear crack caused by strand slip. The research team believed that the crack shifted the location of maximum strand stress from below the point load to a location d_p closer to the free end of the member. The embedment length was not sufficient to allow the strand to develop the required stress and slipped. The research team then developed a model that showed stirrups could carry part of the increased demand in the prestress tendon, if the critical section shifted toward the free end, when a flexural shear crack formed. Three more T-beams were cast, one with No.4 stirrups spaced at six-inches along the entire length, one with No.4 stirrups spaced at 3 inches on center in the middle portion of the beam, and the final T-beam with No.4 stirrups at 15 inches on center in the middle portion of the member. All three T-beams in the second set were cast with strand B, which was believed to have inferior bond as compared to strand A. The beam containing stirrups at 6inches on center failed in bond/web shear. The beam with stirrups at three-inch centers failed in flexure with strand rupture, and the third beam with stirrups at 15-inch centers failed in bond/web shear. The researchers believed that if a flexural shear crack forms near the area of maximum strand stress, then stirrups can prevent a bond failure when the maximum demanded tension force shifts toward the end of the member.

Girgis and Tuan (2005) looked at the effects of SCC on the development-length of prestressing tendons. Three concrete mixes were studied, two of which were SCC mixes with a viscosity modifying admixture (VMA), and a third that was a conventional mix with a lower dosage of superplasticizer and no VMA. For each mix, a full-scale bridge girder was cast and instrumented with Demec points to measure the transfer length. All girders were stressed with 0.6-inch diameter strands and was pre-qualified using the LBPT. Both SCC mixes and the conventional mix had pull-out strengths above the bench mark load of Logan's LBPT. The two SCC mixes had pull-out loads of 43.4 kips and 54.2 kips, while the conventional mix had a pull-out load of 48 kips. The SCC mixes had transfer lengths of 36 inches and 43 inches, which were both above ACI and AASHTO code equations. The conventional mix had a transfer length of 20 inches, which was below ACI and AASHTO code equations. Researchers concluded that SCC

mixes with a VMA admixture will lead to longer transfer lengths and low early compressive strengths, which affect early bond capacity.

Mitchell (2007) studied the effects of high-strength lightweight (HSLW) concrete on bond of deformed bars. Researchers tested 72 pull-out and push-in specimens with No.8 and No.11 bars. All tests were conducted with a hydraulic actuator, load cell, and LVDT at the gripped end of the bar and a linear potential differential transducer (LPDT) at the free end to capture first slip. Two monotonic loading rates and three cyclical loading rates with varying amplitude were used to evaluate the impact on bond stress. When tension specimens were pulled, the load-versus-actuator displacement plot remained linear until 40% of the maximum stress was obtained, the plot then decreased slope as friction and mechanical interlock engaged. The area under the curve for the deformed bars in the HSLW concrete was less than that of high-strength normal-weight (HSNW) concrete and therefore had less bond energy. Bond stress for the No. 11 bars was less than that of the No.8 bars. When the compression, push-in tests were run, it was also found that maximum slip was half of the maximum slip in tension and therefore gave lower bond energy compared to the tension test. When results of the varying monotonic loading rates were plotted, little effect was found on the No.8 bar. However, the No. 11 bar experienced lower maximum bond stress with the slower monotonic loading rates. For the three frequencies tested, the first five cycles had amplitudes that would not significantly damage the bond interface, while the last five cycles had amplitudes that would engage the mechanical interlock and friction of the aggregate. The bond stresses slowly decreased as the cycles continued, until the aggregate was sheared and lost bond. Researchers concluded that the bond stress on HSLW concrete was greater than that of HSNW concrete because of the brittle nature of the aggregate, and therefore it was unable to absorb the same amount of energy. Additionally, it was stated that good bond can be maintained under cyclical loading as long as the peak load does not induce the maximum slip achieved in the monotonic testing.

Petrou et al. (2000) investigated prestress piles experiencing excessive strand slip in several precast plants. The study examined concrete piles of varying shape and number of strands. The research team considered the effects of varying concrete strength, transverse steel, and as-cast depth of strand. They found no correlation between transverse steel and excessive strand slip. Additionally, the investigators made no clear distinction between concrete strength and bond capacity, except for its contribution to the top-strand effect. The study found that

strands close to the top of the form when the concrete was cast experienced 2.12 times more strand slip than stands at the bottom of the form. The research team suggested that the concrete at the bottom of the form had a higher compressive strength then the concrete at the top of the form at the time of release, thus causing larger transfer lengths for the top strands. However, investigators could not contribute the excessive strand slip to one factor, believing it likely to be a combined effect from changes in concrete materials, prestressing steel, strength of the concrete, and as-cast depth of an individual strand. Thus in order to maintain sufficient bond in prestress members, the authors suggested a quality assurance plan that monitors all materials used to produce the products.

Larson et al. (2007) performed a study to evaluate bond characteristics of SCC mixes. The study conducted preliminary bond assessments using the LBPT. The study also looked at transfer length, partial- and full-development-lengths, and the top-strand effect. LBPT results for the SCC block had an observed first slip below 16 kips and a pull-out strength of 36 kips, which are the minimum recommended loads. Evaluation of the top-strand effect was done by testing one cross section with an eight-inch width, 12-inch depth, and 10 inches of concrete cast above the strand. The companion section was 8 inches wide, 24 inches deep, and a block out at mid span that provided 10-inches of concrete cast above it as compared to 22 inches throughout the rest of the beam. Additionally, the research team cast T-beams that had five strands at a depth of 19 inches. Two lengths of T-beam were tested, one with 100% and one with 80% of the calculated development-length on each side of the constant-moment region. Crack formers were placed at the end of the development-length for both lengths to ensure the first crack would open at the ends of the constant-moment region. Researchers found a 10 to 20% increase in transfer length for all bottom strand beams 21 days after detensioning. However, top-strand beams experienced a 40 to 45% increase in transfer length in 21 days after detensioning. The research team used three different loading rates during flexural testing of the beams, all of which were relatively slow in order to capture end slip of the strand with a linear voltage displacement transducer (LVDT). One of the loading rates selected was modeled after the ACI 318-05 Section 20.3 load test procedure. All beams failed in flexure by strand rupture. The 100% development-length specimens broke above nominal-moment capacity, and the 80% development-length specimens broke above the calculated reduced-moment capacity.

Peterman (2007) published an article that encompassed more than two years of research focused on the effect of strand depth at casting with varying concrete fluidity and the effects on prestress tendon bond. The study was conducted at five plants across the nation viewed by the four major admixture producers to produce SCC mixtures representative of the industry. All strands in the study were pre-qualified using the test method developed by Logan (1997), except one strand intentionally introduced in the study known to have poor bonding characteristics. The inferior bonding strand was used to verify that the cross section selected would be sensitive enough to expose poor bonding strand. Early in the study, it was found that SCC mixes performed below the recommended pull-out load of Logan's 1997 study, even at compressive strengths considerably higher than required by the LBPT. A 15-inch deep and 10-inch wide cross section was cast with the strand two-inches from the bottom surface and again with the strand two-inches from the top surface for each of the SCC mixes. Every mix exhibited greater transfer lengths for the cross section with the strand two-inches from the top of the section. In several of the test mixes, the top-strand transfer length was double in comparison to the same mix with the strand two-inches from the bottom. Further research was conducted by the author to determine if the top strand effect was a function of the depth of fresh concrete cast above or below the strand. The two cross sections used for continuation of the study were both four-inches wide; however, one was 28 inches deep while the other was 16 inches deep. The four-inch width was selected to address confinement concerns with the original cross section. The strands were spaced six-inches apart along the height with two-inches of clear cover on the top and bottom for both sections. The author then compared the shallower cross section's end-slip readings with the bottom or top three strands of the deeper section. The author found a close correlation with end-slip reading and the strand distance from the top surface as opposed to distance from the bottom surface. Peterman stated bond could be a function of the amount of concrete below the strand at casting for high fluid mixes. The author also found for a given water-to-cement ratio, increasing fluidity decreased bond capacity. Testing the four-inch wide cross sections, transfer length of the members made with SCC were 30% longer than those cast with conventional concrete. Flexural testing of the sections showed SCC mixes had lower moment capacity with two failing below nominal. In addition, the author noted none of the rheological properties taken at the time of casting gave an indication of bond performance.

3 Material Properties

This section covers properties for the aggregates used to cast all large-block pull-out test and flexural specimens. Coarse- and fine-aggregate specific gravity, gradation, and absorption are discussed. Also, moisture content for the coarse-aggregates when in the saturated surface dry (SSD) conditions for varying times of soak are presented.

3.1 *Coarse-Aggregate Properties*

The three lightweight coarse-aggregates evaluated in this study were a manufactured lightweight rock. The two locally available coarse-aggregates used were expanded shale, and the third from North Carolina was an expanded slate. All three had a similar manufacturing process. After the rock were mined and crushed, they were placed in a kiln and heated. Internal gasses were freed from the extreme heat and form a cellular structure that was maintained after cooling. This process made the aggregate highly porous and decreased density. Due to its porous structure, lightweight aggregate is highly absorptive and moisture content can vary significantly based upon duration of the soak. A majority of the absorbed water is locked internally within the aggregate and changes the unit weight. Therefore, an average SSD specific gravity recommended by aggregate manufacturers was used for mix design. The volatile nature of the rock made quantifying the gradation, absorption, and moisture content crucial for accurately designing concrete mixes.

3.1.1 Kansas City Coarse-Aggregate

The first aggregate obtained from Buildex was mined in New Market, Missouri, termed Kansas City or KC in this paper, and was an expanded shale. The manufacturer's report for an ASTM blend of ½"x No.4, used in this study, had a specific gravity of 1.09, density of 37 pcf, saturated density of 52 pcf when stockpiled and saturated for seven to 14 days, and 22% absorption in 24 hours. The rock is rounded with a brown-gray color and noticeable fracture planes on the surface. The Kansas City aggregate is available in vacuum-saturated condition to help stabilize the moisture content. The vacuum-saturated aggregate was not used in this study so a direct comparison could be made with the other two aggregates. Figure 3-1 shows a sample of the KC aggregate.

Figure 3-1 Kansas City Aggregate

3.1.2 Marquette Coarse-Aggregate

The aggregate obtained from the Buildex Marquette quarry was an expanded shale. The manufacturer's report for an ASTM blend size ½" x No.4, used in this study, a specific gravity of 1.09, density of 37 pcf, saturated density of 52 pcf when stockpiled and saturated for seven to 14 days, and 24-hour absorption of 22%. The Marquette aggregate is angular with an orange-light brown color and noticeable fracture plans, and uneven surfaces. A sample of the aggregate is shown in Figure 3-2.

Figure 3-2 Marquette Aggregate

3.1.3 Stalite Coarse-Aggregate

Stalite aggregate was shipped from Salisbury North Carolina. Stalite is viewed by many precasters as one of the highest quality lightweight aggregates, therefore it was added to the project for comparison with the two locally available rocks. The North Carolina aggregate is an expanded slate. Stalite aggregate has a specific gravity of 1.46, SSD specific gravity of 1.52, dry loose density of 48 pcf, and a SSD loose density of 50 pcf. Stalite is an angular rock that is dark gray in color and contains smooth surfaces with noticeable voids. A sample of the aggregate is shown in Figure 3-3.

Figure 3-3 Stalite Aggregate

3.1.4 Coarse-Aggregate Gradation

The two coarse-aggregates received from Buildex, Kansas City and Marquette, and the third from Stalite were sieved to verify the manufacturer's gradation. The KDOT coarse-aggregate specification SCA-2 was chosen because it is required for structural concrete with crushed stone and also required for a well-graded aggregate compared to the other specifications. KDOT is currently changing specifications towards performance based. Therefore, selecting the well-graded SCA-2 gradation was the most logical way to meet future goals. Table 3-1shows the high and low ranges for the KDOT SCA-2 gradation.

Table 3-1 KDOT SCA-2 High- and Low-Gradation Limits

Sieve	Percent Retained Low	Percent Retained High	Percent Passing Low	Percent Passing High
3/4"	0	0	100	100
1/2"	0	35	65	100
3/8"	30	70	30	70
4	75	100	0	25
8	95	100	0	5

A portion of the Kansas City gradation fell above the SCA-2 high range. The workability of mixes with the Kansas City aggregate was better than those batched with the Stalite rock but less than the Marquette concrete mixes. Gradation for the Kansas City aggregate can be seen in Figure 3-4.

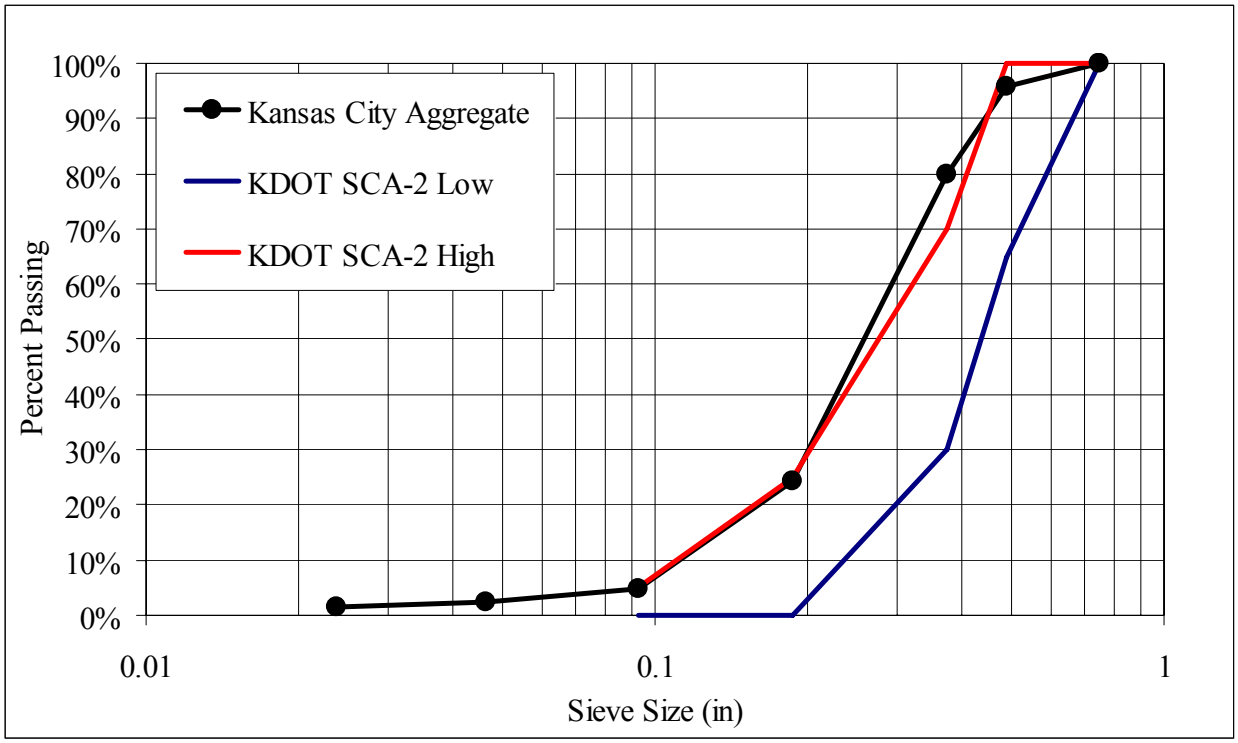

Figure 3-4 Kansas City Gradation with KDOT SCA-2 High- and Low-Gradation Limits

The Marquette aggregate met the SCA-2 requirements throughout the full-gradation range. The uniform gradation gave the greatest workability of all three coarse-aggregates. The sieve analysis is shown in Figure 3-5.

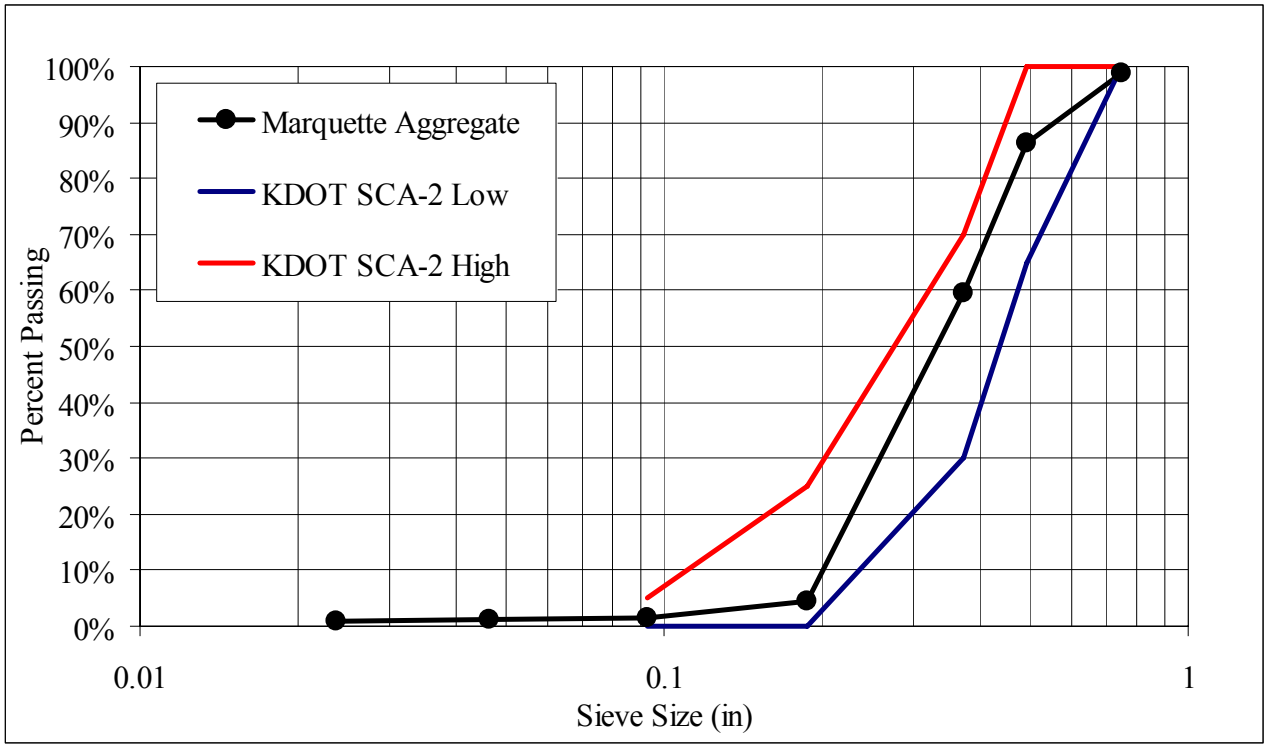

Figure 3-5 Marquette Gradation with KDOT SCA-2 High- and Low-Gradation Limits

The Stalite aggregate gradation fell outside the limits of the SCA-2 requirements. A larger percentage of the aggregate was retained on the $^{3}/_{4}$, $^{1}/_{2}$, and $^{3}/_{8}$-inch sieves. This made the rock coarsely graded and decreased workability. The Stalite sieve analysis with the SCA-2 high and low limits is shown in Figure 3-6.

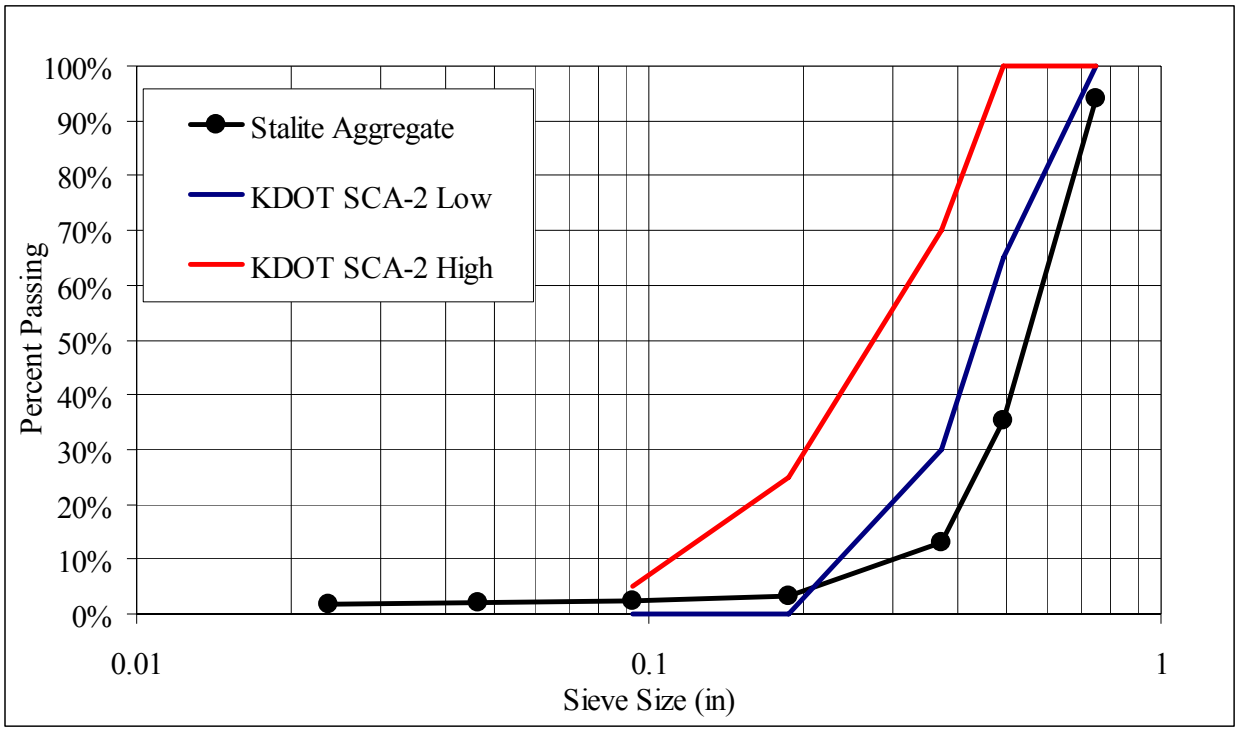

Figure 3-6 Stalite Gradation with KDOT SCA-2 High- and Low-Gradation Limits

3.1.5 Coarse-Aggregate Absorption and Moisture Content

Absorption of each aggregate in the study was found by following AASHTO T85. The specification requires the absorption rate to be recorded for a 24-hour period. However, due to the high porosity of lightweight aggregate, the study was carried out for 90 days. Within the first 24 hours Marquette had the highest rate of absorption. Stalite's absorption was significantly lower than the two local aggregates in the first 24 hours. Additionally, the Stalite rate of absorption quickly decreased compared to the other rocks. Figure 3-7 shows the 24-hour absorption rates for all three coarse-aggregates.

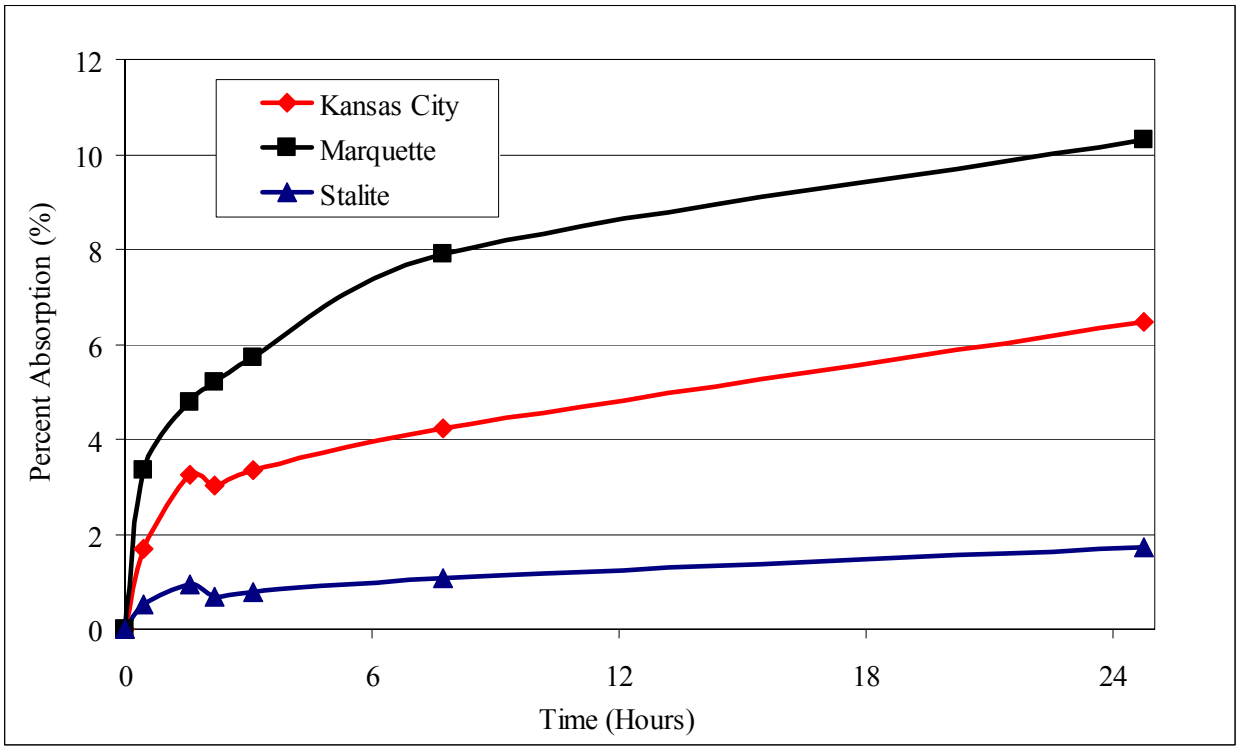

Figure 3-7 24-Hour Coarse-Aggregate Rate of Absorption

The 90-day test showed Marquette and Stalite's rate of absorption decreasing and approaching the maximum saturation. Kansas City absorption was lower in the 24-hour test; however, its rate of absorption did not decrease significantly and surpassed Marquette at day 46 and still continued to increase at day 90. All three aggregates matched the manufacturer's reported absorption within 4%. Figure 3-8 shows the 90-day absorption for all three aggregates.

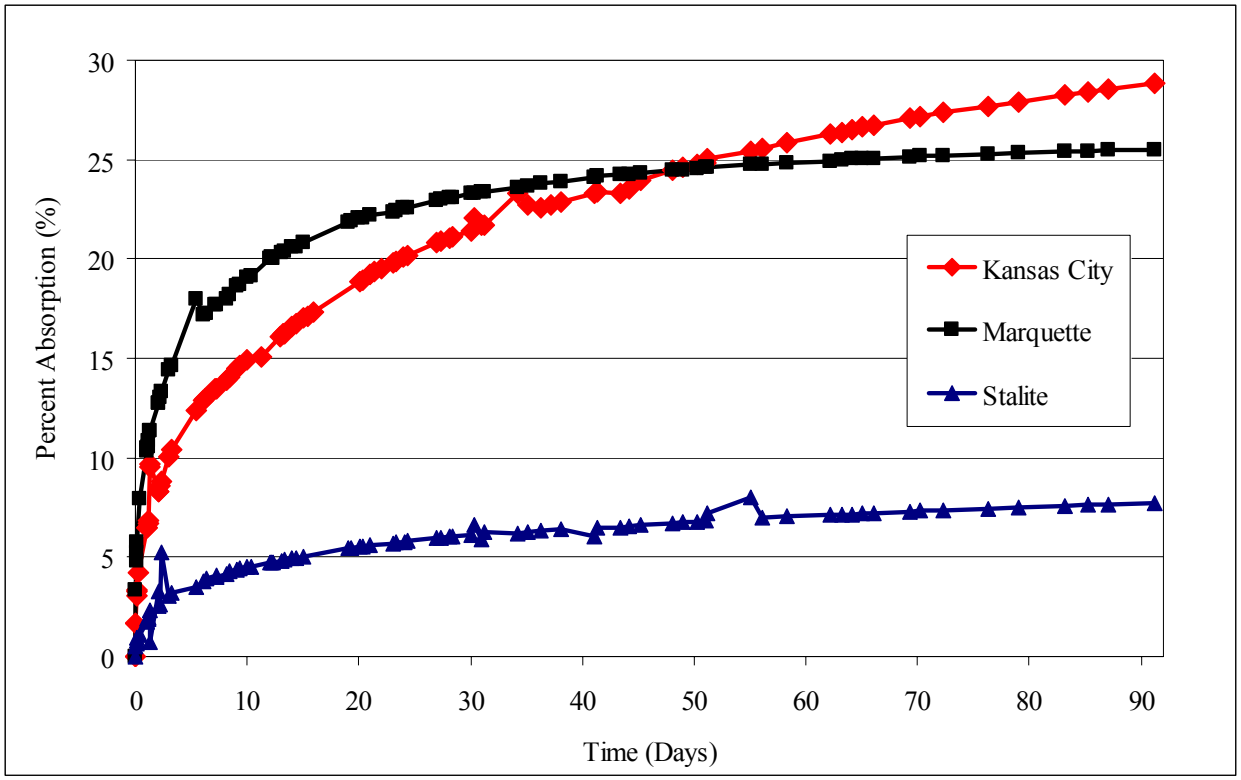

Figure 3-8 90-Day Coarse-Aggregate Rate of Absorption

3.1.6 Coarse-Aggregate Moisture Content and Free Surface Moisture

In order to perform mix designs using the absolute-volume method, moisture contents and free surface moisture were quantified to make adjustments to aggregate quantities and mixing water. Due to the high absorption level of lightweight aggregates, accurately knowing the moisture contents for varying durations of soak was important. To begin the test, each coarse-aggregate was placed in several buckets and filled with water. At days 1, 3, 7, 10, 14, 21, 28, and 60 a sample was removed from the bucket, strained for water, weighed wet, saturated surface dried, reweighed, placed in the oven and dried to a constant mass, and weighed again. The difference between the wet- and dry-moisture content was used to adjust the rock quantity, and the difference between the wet- and SSD-moisture content was used to adjust the mixing water.

Table 3-2 shows the wet- and SSD-moisture contents used when designing concrete mixes for each aggregate. Figure 3-9 shows the percent moisture content for the wet and SSD conditions for each aggregate. The difference between the wet- and SSD-moisture content is the percentage by weight of free water on the rock deducted from the mixing water. The percent

difference between the wet and SSD condition is shown in Table 3-3. The difference between the wet-moisture content and the x-axis is the percentage of the aggregate weight that was increased to account for the extra weight of water on and in the rock. It should be noted that there appeared to be an error in the day-14 data.

Table 3-2 Coarse-Aggregate Wet- and SSD-Moisture Contents

Percent Moisture Content						
Day	Marquette Wet	Marquette SSD	Kansas City Wet	Kansas City SSD	Stalite Wet	Stalite SSD
1	23.5	17.5	16.2	10.3	7.3	4.0
3	27.1	20.5	18.5	12.4	7.8	3.9
7	30.0	22.9	20.4	14.4	8.7	5.7
10	32.9	25.8	22.7	16.6	10.0	5.9
14	30.5	25.5	21.5	16.3	8.3	4.8
21	34.0	27.8	26.7	20.7	9.5	5.2
28	35.1	28.4	25.5	19.8	9.5	5.9
60	37.6	30.9	28.9	23.7	11.6	6.8

Table 3-3 Percent Difference Between Wet and SSD Condition

Percent Difference			
Day	Marquette	Kansas City	Stalite
1	6.0	5.9	3.2
3	6.6	6.1	3.8
7	7.2	6.0	3.0
10	7.1	6.2	4.1
14	5.1	5.1	3.5
21	6.2	6.0	4.2
28	6.8	5.7	3.5
60	6.6	5.2	4.7
Average Difference	6.4	5.8	3.8

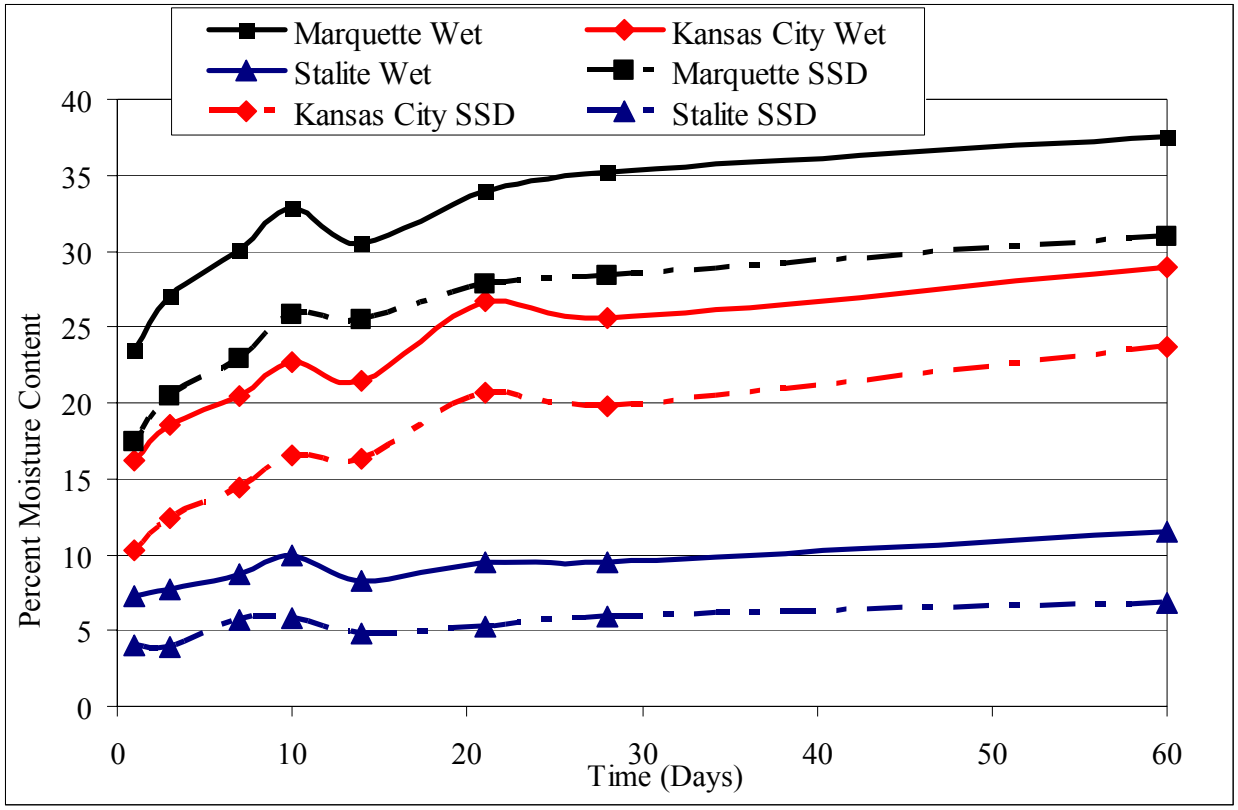

Figure 3-9 Coarse-Aggregate Percent Moisture Content Wet and SSD

3.2 *Fine-Aggregate Gradation*

The fine-aggregate used in the study was normal-weight sand. Lightweight sand was not selected because the target concrete unit weight was 115 pcf to 125 pcf. The sand was obtained from a local quarry, Midwest Concrete Materials. The fine-aggregate met the KDOT FA-A gradation specification. The FA-A gradation was selected because it required a uniform-aggregate distribution. Like the coarse-aggregate, the fine-aggregate specification had high and low limits for each sieve. The sand gradation fell between those limits for all sieves.

Table 3-4 shows the KDOT FA-A limits, and Figure 3-10 graphs the results from the sand-sieve analysis with KDOT high and low limits. Additionally, the sand had a fineness modulus of 4.26%. For all batches the sand was oven dried and the manufacturer's absorption of 2% was used. Therefore, no moisture content and absorption test was performed.

Table 3-4 KDOT FA-A High- and Low-Gradation Limits

Sieve	Percent Retained Low	Percent Retained High	Percent Passing Low	Percent Passing High
No. 4	0	0	100	100
No. 8	0	27	73	100
No.16	15	55	45	85
No. 30	40	77	23	60
No. 50	70	93	7	30
No. 100	90	100	0	10

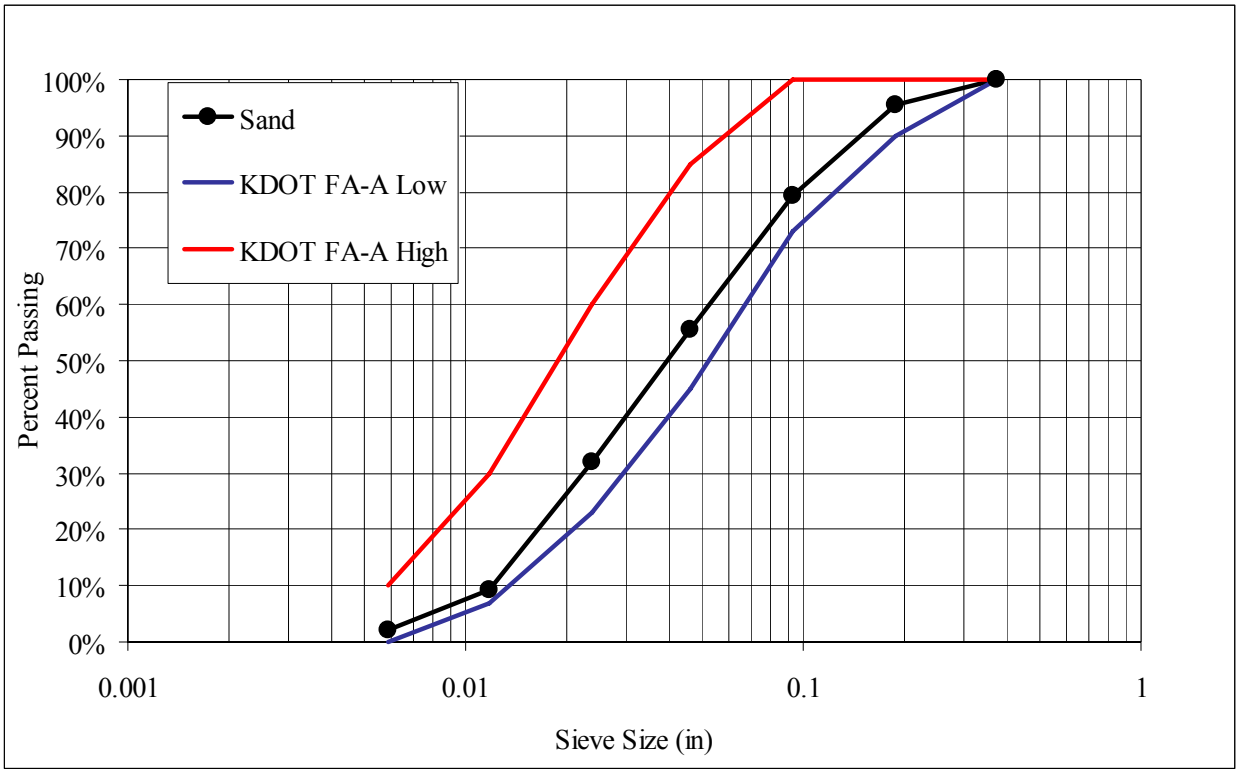

Figure 3-10 Sand Gradation with KDOT FA-A High- and Low-Limits

3.3 *Mixed-Aggregate Gradations*

The mixed-aggregate gradation for each rock was selected by choosing the lightest combination of fine and coarse aggregate while maintaining workability. The coarse-aggregate had a lower specific gravity than the sand, therefore a lighter mix was obtained by decreasing the amount of fine-aggregate. The aggregate ratios were adjusted until a gravimetric 118 pcf mix was reached for each mix. Actual unit weights varied between 122 pcf to 115 pcf depending upon the amount of entrained air. All coarse-to-fine aggregate ratios were calculated by volume instead of weight because of the lightweight-coarse aggregate. The three ratios are shown in Table 3-5. The targeted mixed-aggregate gradation was KDOT's MA-2. Like the other gradation specifications, the MA-2 was selected because of the required uniform-aggregate distribution. The high and low ranges can be seen in Table 3-6. The Kansas City mixed-aggregate gradation fell between the MA-2 high and low range for the smaller particles but was slightly above the high range for the larger aggregates as shown in Figure 3-11. The Marquette mixed-aggregate distribution was between the high and low limits for all sieves. The Marquette mixed-aggregate gradation is shown in Figure 3-12. The Stalite mixed gradation was between the high and low limits for the

smaller sieves but fell below the required aggregate distribution for the larger aggregates. The Stalite mixed-aggregate gradation is shown in Figure 3-13.

Table 3-5 Mixed-Aggregate Ratios by Volume

Coarse Aggregate	Percent Coarse Aggregate by Volume	Percent Fine Aggregate by Volume
Kansas City	56.0	44.0
Marquette	52.3	47.7
Stalite	56.4	46.3

Table 3-6 KDOT MA-2 High- and Low-Gradation Limits

Sieve	Cummlative Percent Retained Low	Cummlative Percent Retained High	Percent Passing Low	Percent Passing High
3/4"	0	0	100	100
1/2"	3	15	85	97
3/8"	15	30	70	85
4	33	50	50	67
8	45	67	33	55
16	64	80	20	36
30	78	90	10	22
50	87	96	4	13
100	95	100	0	5

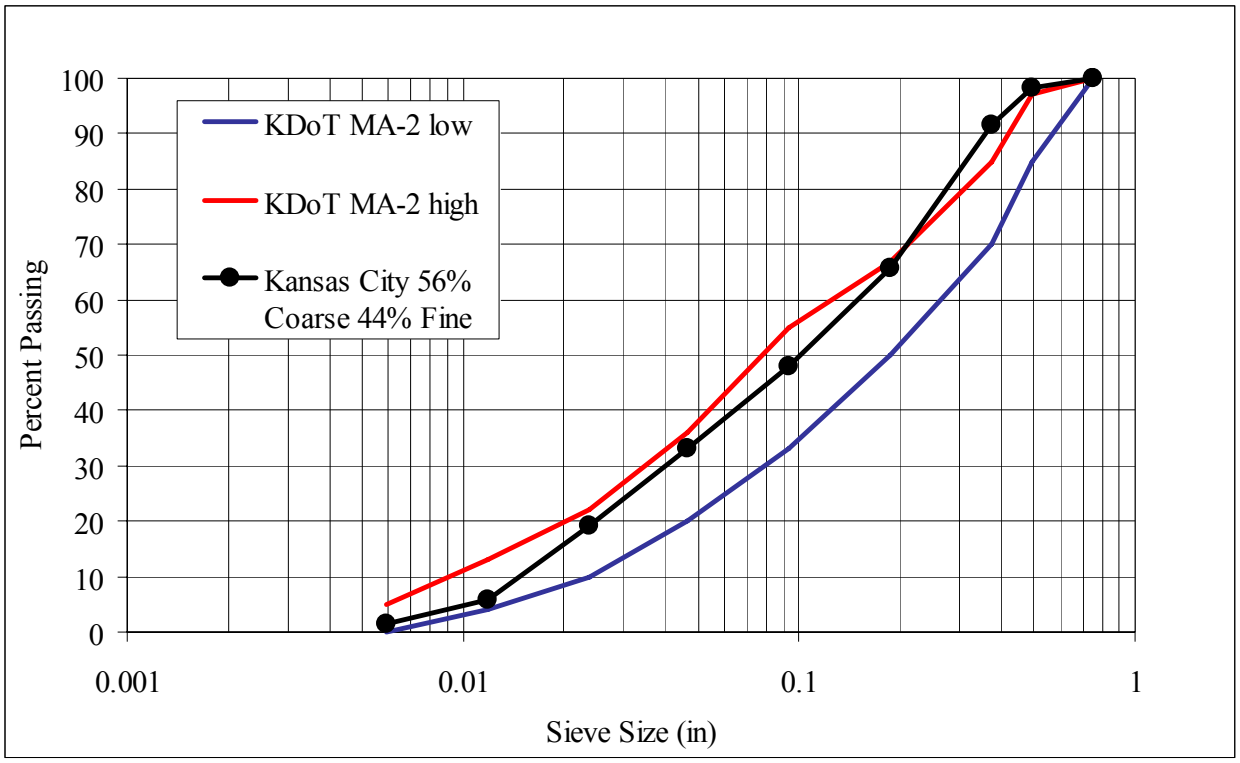

Figure 3-11 Kansas City Mixed-Aggregate Gradation

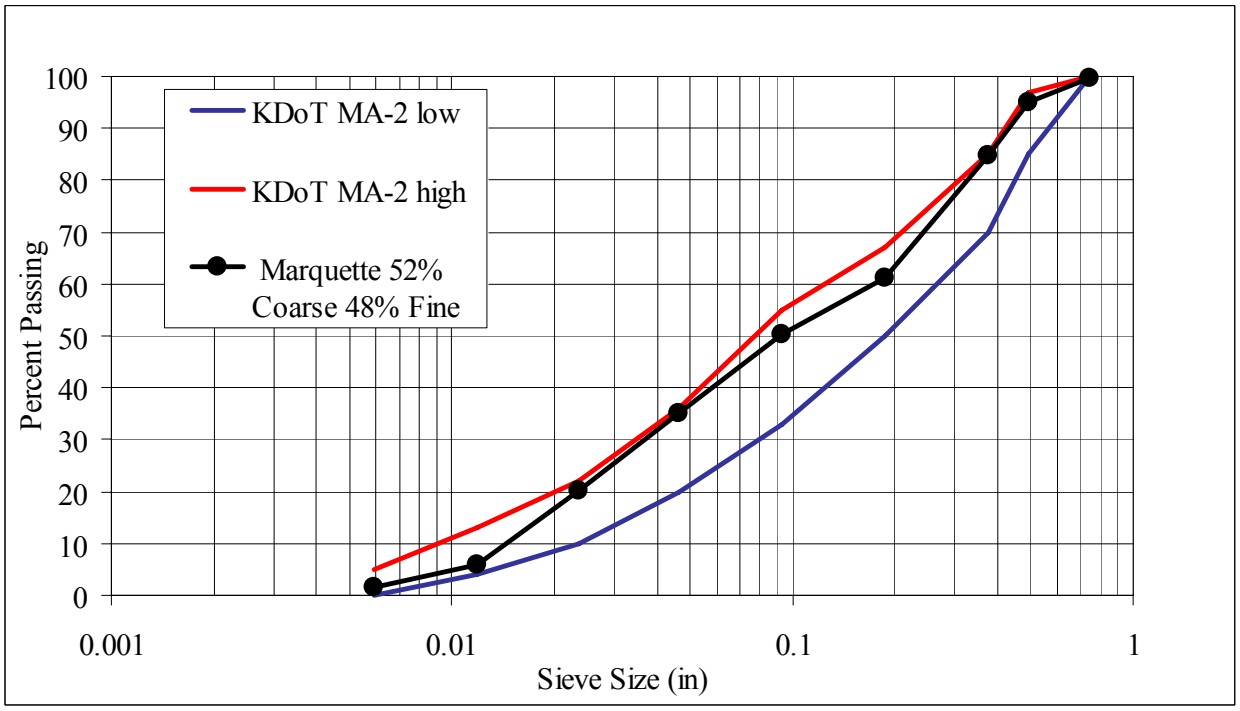

Figure 3-12 Marquette Mixed-Aggregate Gradation

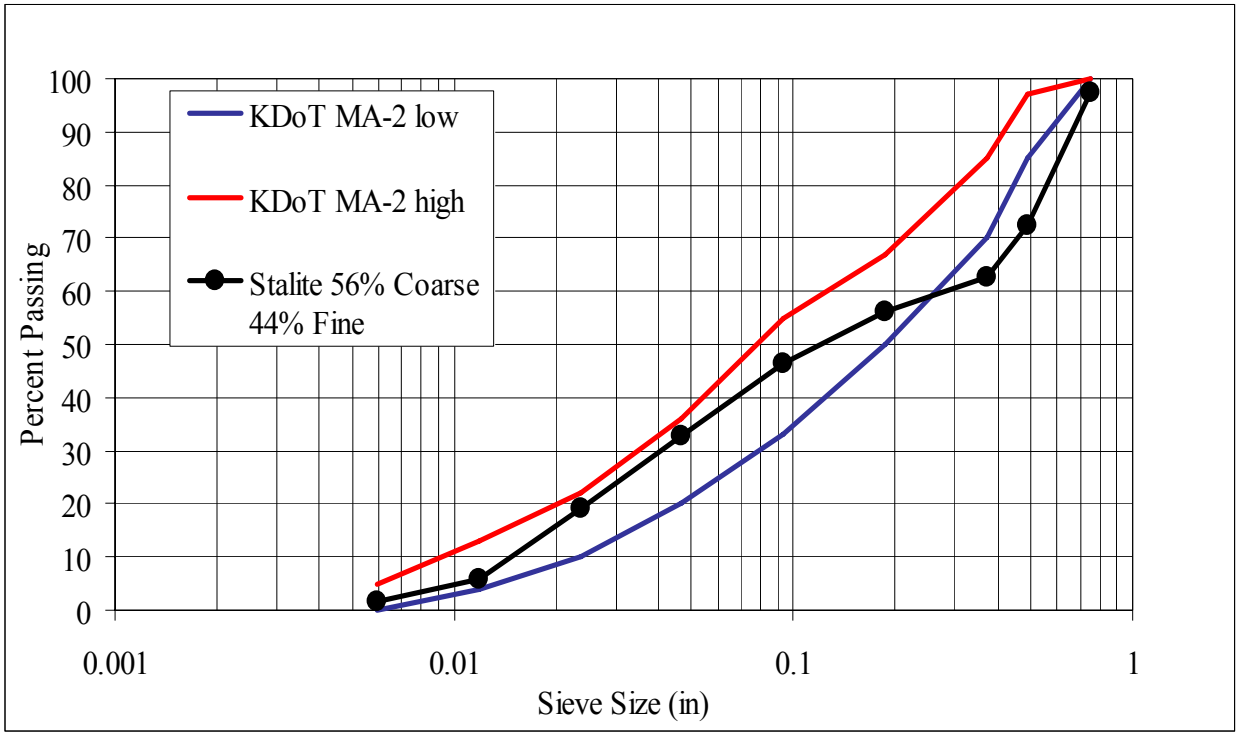

Figure 3-13 Stalite Mixed-Aggregate Gradation

3.4 *Cement*

Type III cement was used for all trial mixes and test specimens to achieve the high early strengths required in prestress plants. Two separate cement shipments were used. The first shipment was produced by Ash Grove Cement Company and the second by Lonestar Cement Company. Mortar cubes or blaine tests were not performed for either brand, but a sealed bucket was saved from each shipment if testing was required later.

3.5 *Admixtures*

The two admixtures used were an air-entrainer and superplasticizer. The air-entrainer used throughout the project was the Daravair 1000 produced by W. R. Grace. Adva Cast 530 was a type F polycarboxylate-based superplasticizer produced by W. R. Grace. Adva Cast 530 was selected because of its wide use in the prestress industry. The superplasticizer could be used to achieve a wide range of concrete fluidity.

4 Concrete Material Proportioning and Batching Procedure

This section discusses the trial mix process, fresh and hardened concrete test methods, and the finalized mix designs. Additionally, core sampling of existing lightweight bridges in Kansas and the large-scale matching procedure is explained.

4.1 *Material Specifications*

Concrete mixes were designed to meet KDOT specifications for rock, sand, and cement content. As mentioned in chapter 3, the specification for the coarse-aggregate was SCA-2, the fine-aggregate specification was FA-A, and the combined-gradation specification was the MA-2. The concrete mixes were designed to meet the KDOT Grade 5.0 Air Entrained (AE) Prestress Beam (PB) specification. The concrete mix specification Grade 50 AE PB with 30% or more on the No. 4 sieve for a mixed-aggregate gradation required 6.5% ± 1.5% air entrainment and a minimum cement content and water-to-cement ratio of 639 pound per cubic yard and 0.35, respectively.

4.2 *Absolute-Volume Method*

The absolute-volume, mix-design method was utilized to find design weights for each mix. The method uses the specific gravity and relative density of all materials in the concrete to calculate the weight of each ingredient required for a cubic yard of concrete. A target volume of 6.5% air was used in the mix designs, and the volume of admixtures was not included in the concrete design because of the small dosages required. As discussed in section 3.1, an SSD specific gravity was used for all coarse-aggregates. The specific gravities and relative densities are shown on a sample mix-design sheet in Figure 4-1.

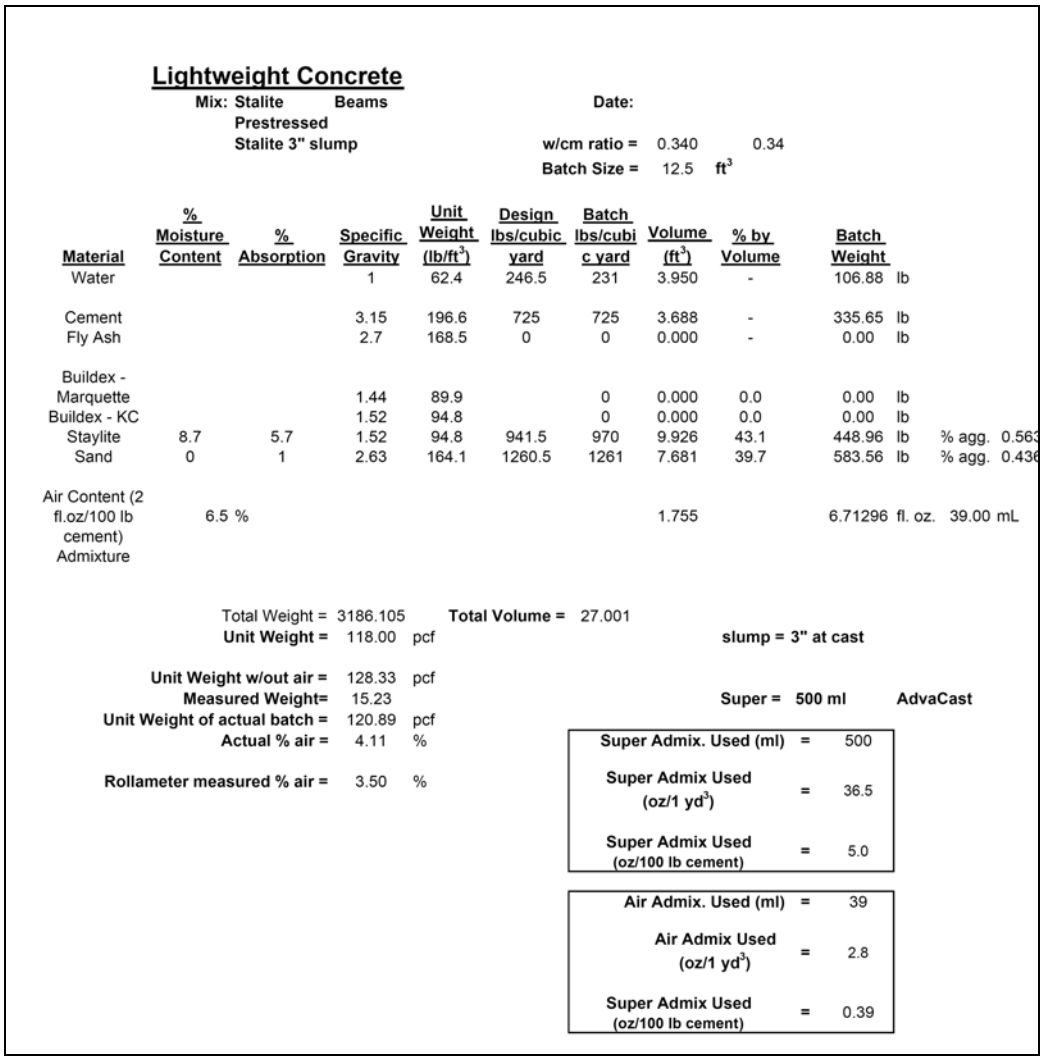

Lightweight Concrete

Mix: Stalite Beams Prestressed Stalite 3" slump **Date:**

w/cm ratio = 0.340 0.34

Batch Size = 12.5 ft^3

Material	% Moisture Content	% Absorption	Specific Gravity	Unit Weight (lb/ft^3)	Design lbs/cubic yard	Batch lbs/cubic yard	Volume (ft^3)	% by Volume	Batch Weight		
Water			1	62.4	246.5	231	3.950	-	106.88	lb	
Cement			3.15	196.6	725	725	3.688	-	335.65	lb	
Fly Ash			2.7	168.5	0	0	0.000	-	0.00	lb	
Buildex - Marquette			1.44	89.9		0	0.000	0.0	0.00	lb	
Buildex - KC			1.52	94.8		0	0.000	0.0	0.00	lb	
Staylite	8.7	5.7	1.52	94.8	941.5	970	9.926	43.1	448.96	lb	% agg. 0.563
Sand	0	1	2.63	164.1	1260.5	1261	7.681	39.7	583.56	lb	% agg. 0.436
Air Content (2 fl.oz/100 lb cement) Admixture	6.5 %						1.755		6.71296	fl. oz.	39.00 mL

Total Weight = 3186.105 **Total Volume =** 27.001

Unit Weight = 118.00 pcf **slump = 3" at cast**

Unit Weight w/out air = 128.33 pcf

Measured Weight= 15.23 **Super =** 500 ml AdvaCast

Unit Weight of actual batch = 120.89 pcf

Actual % air = 4.11 %

Rollameter measured % air = 3.50 %

Super Admix. Used (ml)	=	500
Super Admix Used ($oz/1\ yd^3$)	=	36.5
Super Admix Used (oz/100 lb cement)	=	5.0

Air Admix. Used (ml)	=	39
Air Admix Used ($oz/1\ yd^3$)	=	2.8
Super Admix Used (oz/100 lb cement)	=	0.39

Figure 4-1 Sample Mix-Design Sheet

4.3 *Trial Mixes*

The purpose of the trial mixes was to find the minimum cement content, water-to-cement ratio to make strength, the correct aggregate ratio to reduce unit weight but maintain workability, and the correct air-entrainer and superplasticizer dosage. Trial batches were made for mixes that could achieve a three-inch and nine-inch slump by varying only the add-mixture dosages. Slump, air-content, unit-weight, and compressive-strength cylinders were made and tested for the trial batches. Figures A-1 through A-3 in Appendix A show the fresh concrete properties for mixes made with Kansas City, Marquette, and Stalite, respectively. When performing the trial batches, all of the coarse-aggregate was saturated surface dried to alleviate errors in calculating free-mixing water on the surface of the aggregate. When trial batches were made, the material

was weighed in five-gallon buckets and then charged into the mixer in the order of rock, sand, cement, water, and add mixtures. The SSD condition of the rock is shown in Figure 4-2. The trial mixes were made in a Lancaster Counter-Current Batch Mixer. The machine is a 2.5-cubic-foot pan mixer and pictured in Figure 4-3.

Figure 4-2 Sample Saturated-Surface Dried Rock

Figure 4-3 Lancaster Mixer Used in Trial Batches

4.3.1 Slump Test

A slump test was conducted on the trial batches according to AASHTO T119. According to specifications, the test was designed to "monitor the consistency of unhardened concrete." The slump cone was filled in one-third layers, rodded 25 times per layer, and struck off at the top. The cone was gradually lifted from the concrete, then inverted and set back on the base. The distance between the top of the cone and the center of the concrete was recorded as the slump.

4.3.2 Volumetric Air-Content Test

Air content was measured for the trial batches using the volumetric method. The test was performed in accordance with AASHTO T196. The volumetric method of measuring air content was selected because the pressure method is not approved for use on mixes with high porous aggregates. The airmeter base was filled with fresh concrete in two layers, rodded 25 times per layer, and tapped 10 to 15 times per layer. The top of the base was struck off and cleaned. The top was then attached and the funnel inserted through the neck. A liter of isopropyl alcohol was added followed by water. The fluid level was adjusted until the bottom of the fluid meniscus was at the zero mark on the calibrated neck. The lid was then attached, and the airmeter was shook while being inverted to break the mix apart. Next the meter was rolled on the ground at a 45° angle to let the air rise to the top of the measuring device. The airmeter was set on the table; the cap was removed and the water concrete mixture was allowed to settle for several minute so any additional air could rise to the top. The liquid level on the calibrated neck indicated the air percentage in the concrete. A picture of the airmeter is shown in Figure 4-4.

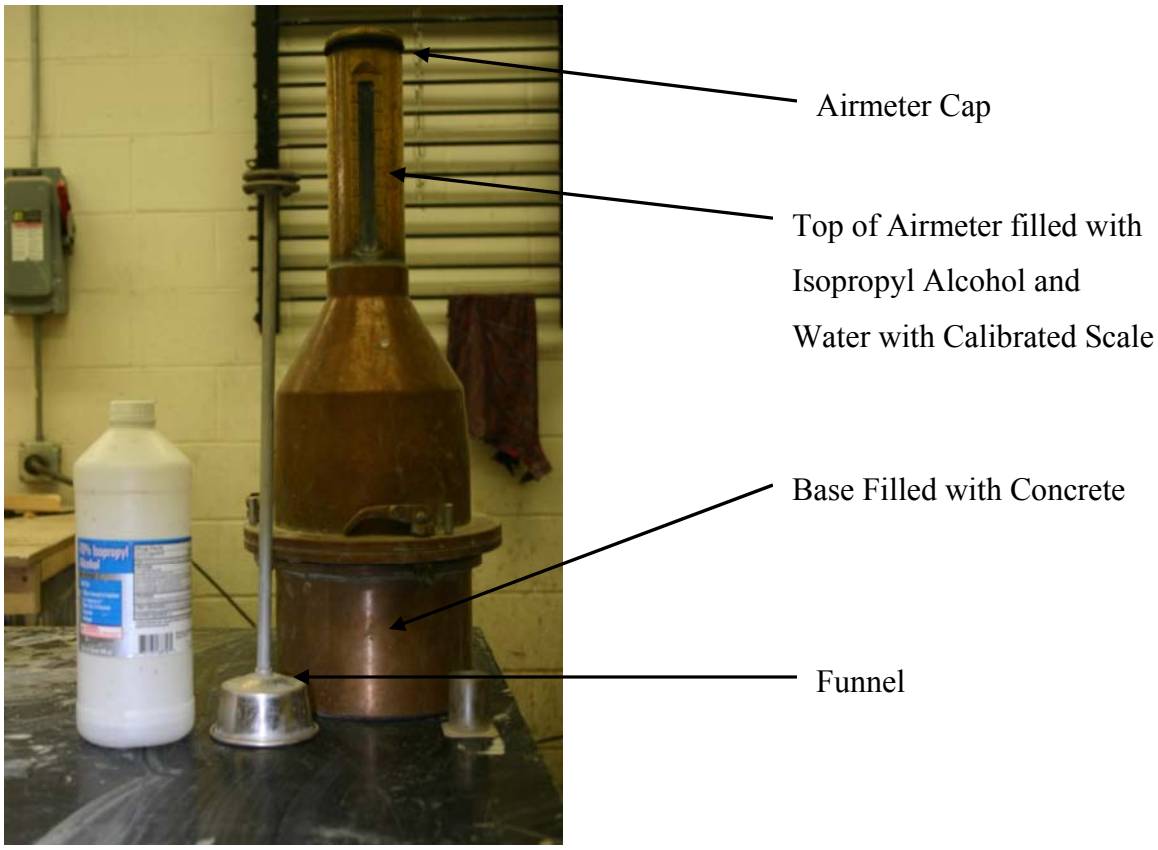

Figure 4-4 Airmeter Used to Measure Air Content of Fresh Concrete

4.3.3 Unit-Weight Test

The unit weight of the trial batches was found using AASHTO T121. The base of the airmeter pot was used as the known volume. When the base of the airmeter was filled to run the volumetric air test, it was placed on a scale before the top was put on. The known weight of the base was subtracted from the combined weight of the base filled with concrete and divided by the volume of the bottom of the airmeter to find the unit weight. The volume of the airmeter base was calibrated to verify the manufacturer's reported volume. A photo of the airmeter base on the scale is shown in Figure 4-5.

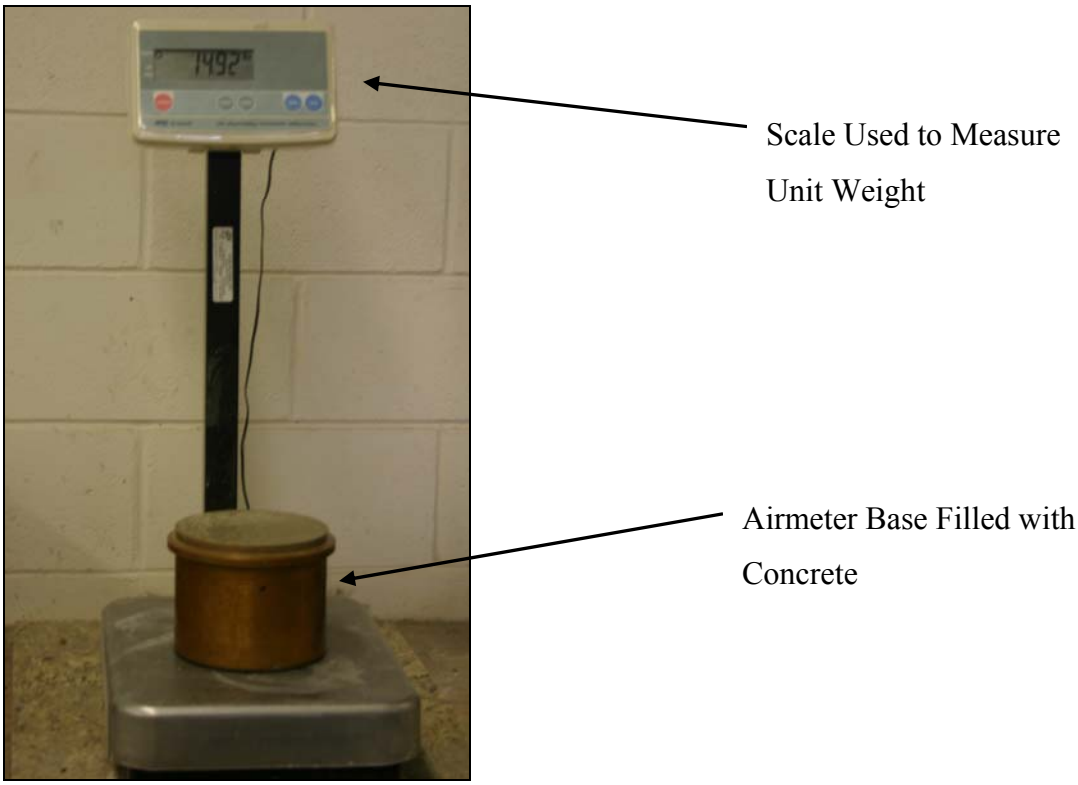

Figure 4-5 Weighing Fresh Concrete in Airmeter Base for Unit-Weight Calculation

4.3.4 Concrete Test Cylinders

Cylinders were made in accordance with AASHTO T126. During the concrete mix-design phase, four-inch by eight-inch cylinders were used to check the 16-hour compressive strength of trial mixes. The cylinders were filled in two layers and rodded 25 times per layer. Once the cylinders were filled, they were finished with a wood trowel to achieve a smooth even surface to facilitate compressive strength testing. The cylinders were then covered with an impermeable plastic to cure over night. Additionally, some cylinders were placed in a heat bath to simulate the heat generated by the concrete hydration process in a large member. Figure 4-6 shows four-inch by eight-inch and six-inch by 12-inch cylinders before the top surface was finished.

Figure 4-6 Compressive-Strength Specimens

4.4 *Finalized Mix Designs*

Based upon results from slump, air-content, unit-weight and compressive-strength tests, final mixes were found for each of the three coarse-aggregates. For each mix, a water-to-cement ratio of 0.34 with a cement content of 725 pounds per cubic yard was selected. The coarse-to-fine aggregate ratio for each mix is given in Table 3-5 and was kept constant for the different slump mixes. The finalized mix proportions, by weight, are shown in Table 4-1. The admixture dosages for each mix at a three-inch and nine-inch slump are given in Table 4-2. It should be noted if the initial slump was higher than desired, the batch was allowed to continue to mix so slump loss would occur.

Table 4-1 Finalized Mix Designs

Material	Kansas City	Marquette	Stalite
Water (lb)	247	247	247
Cement (Type III) (lb)	725	725	725
Coarse Aggregate (lb)	935	827	941.5
Sand (lb)	1267	1374	1260

Table 4-2 Admixture Dosages for Finalized-Concrete Mixes

Coarse Aggregate	Slump (inches)	Air-Entrianer Admixture oz./100 lb. of cement	Superplastisizer Admixture oz./100 lb. of cement
Kansas City	3	0.37	5.4
	9	0.35	6.1
Marquette	3	0.35	5.5
	9	0.30	6.1
Stalite	3	0.39	5.0
	9	0.32	6.2

4.4.1 Hardened Concrete Testing

Several hardened concrete material tests were performed to check if the mix was acceptable for structural applications. Once the concrete mixes were finalized, for each aggregate, compressive strength, split-tensile strength, and modulus of elasticity was checked at 16 hours, and 3, 7, 14, 21, and 28 days.

4.4.2 Concrete Compressive Strength

The cylinders described in 4.3.4 were tested according to AASHTO T22. Before the cylinders were tested, the diameter was measured twice at mid-height 90° apart. The cylinders were then placed between neoprene pads that were inside metal-extrusion controllers. The cylinders were loosely wrapped with a canvas cover to contain the debris when they broke. The cylinders were tested in a hydraulic testing machine. The compressive strength was taken as the average maximum stress of three cylinders from the same batch. The maximum stress for each individual cylinder was the peak load divided by the area found from the measured diameter. Figure 4-7 shows a cylinder in the hydraulic testing machine.

Figure 4-7 Compressive-Strength Cylinder in Hydraulic Testing Machine

4.4.3 Split-Tensile Strength

The split-tensile test was conducted in accordance with AASHTO T198. The test was only performed after the finalized mixes were designed. To perform the test six-inch by 12-inch cylinders were cast in the same procedure as the four-inch by eight-inch cylinders, except they were filled and rodded in three layers. At time of testing, the cylinder's length was measured and then placed in the load fixture and broken with the same hydraulic testing machine as the compressive cylinders. The formula given in AASHTO T198 to calculate the split-tensile strength is shown below in Equation 4-1. A picture of a cylinder in the load fixture is shown in Figure 4-8.

$$T = \frac{2P}{\pi l d}$$

$T =$ Tensile Strength (psi)

$P =$ Maximum Load (lb) 4-1

$l =$ Length of Specimen (in)

$d =$ Diameter of Cylinder (in)

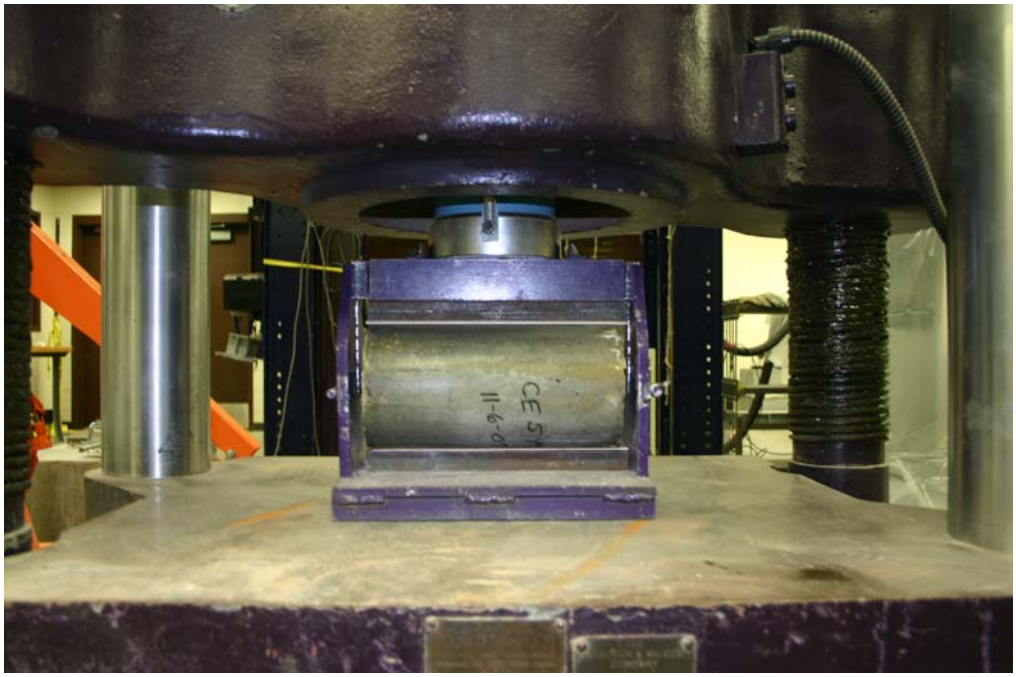

Figure 4-8 Split-Tensile Load Fixture in Testing Configuration

4.4.4 Modulus of Elasticity

The modulus of elasticity was found for the developed mixes. The test was run in accordance with ASTM C469. The four-inch by eight-inch cylinders were sulfur capped and mounted with a digital compresometer. They were then placed in an MTS digitally controlled hydraulic testing machine. The MTS system captured load and displacement within the compresometer gage length that was later used to calculate the strain. Each cylinder was loaded three times up to 40% of the compressive strength. The first cycle on a given cylinder was to seat the specimen and the compresometer. The next two cycles were used to calculate the modulus. For a given concrete age, three cylinders were tested and the modulus was taken as the average of the last two cycles of the three cylinders. The equation used to calculate the chord

modulus of elasticity is show in Equation 4-2. A picture of a cylinder mounted with the digital compresometer is shown in Figure 4-9.

$$E = \frac{(S_2 - S_1)}{\varepsilon_2 - 0.000050} \qquad 4\text{-}2$$

E = Chord Modulus of Elasticity (psi)

S_2 = Stress Corresponding to Ultimate Load (psi)

S_1 = Stress Corresponding to Strain of 0.000050

ε_2 = Longitudinal Strain Produced by Stress S_2

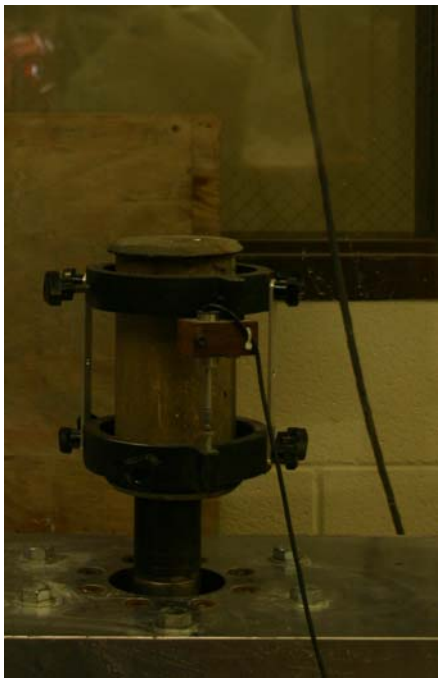

Figure 4-9 Cylinder Mounted with Compresometer for Modulus of Elasticity Testing

4.4.5 Creep and Shrinkage

Creep and shrinkage of concrete are important factors for calculating long-term prestress losses. Axial shortening caused by creep and shrinkage reduces the effective prestress force in the member. The ACI 209 Committee defines creep as time-dependent increase in strain in hardened concrete subject to sustained stress. Likewise, the committee defines shrinkage as the decrease with time of concrete volume. The committee noted the shrinkage definition includes drying, autogenous and carbonation shrinkage. To quantify these effects, creep and shrinkage prisms were made for the developed mixes. The test was conducted in conformance with

ASTM C512. Two creep specimens and two shrinkage specimens were made for each aggregate at a six-inch slump. The prisms were cast in four-inch by four-inch by 24-inch horizontal forms. The prisms were stripped within 24 hours and placed in a moist room for 28 days, after which the prisms were cut to 22-inch lengths providing 14 inches of length for mounting Whittemore surface-strain points, and four inches on each end of the prisms to avoid stress concentrations from the load fixtures for the creep specimens. The specimens were then capped with a high-strength sulfur-capping compound. After the prisms were sulfur capped, they were mounted with eight surface-strain points two inches apart on three sides of the members. Initial surface-strain readings were taken on the creep specimens before loading. The load frames consisted of three, one-inch threaded diameter rods; three, two-inch thick metal base and top plates, and three railroad car springs. The creep specimens were placed in the load frames and loaded to 40% or less of the 28-day compressive strength. Figure 4-10 shows a loaded creep specimen and companion shrinkage specimen. To monitor the loads placed on the specimens, a calibration curve was made from the gage pressure on the hydraulic pump used to load the creep members. Figure 4-11 shows the calibration curve used during loading.

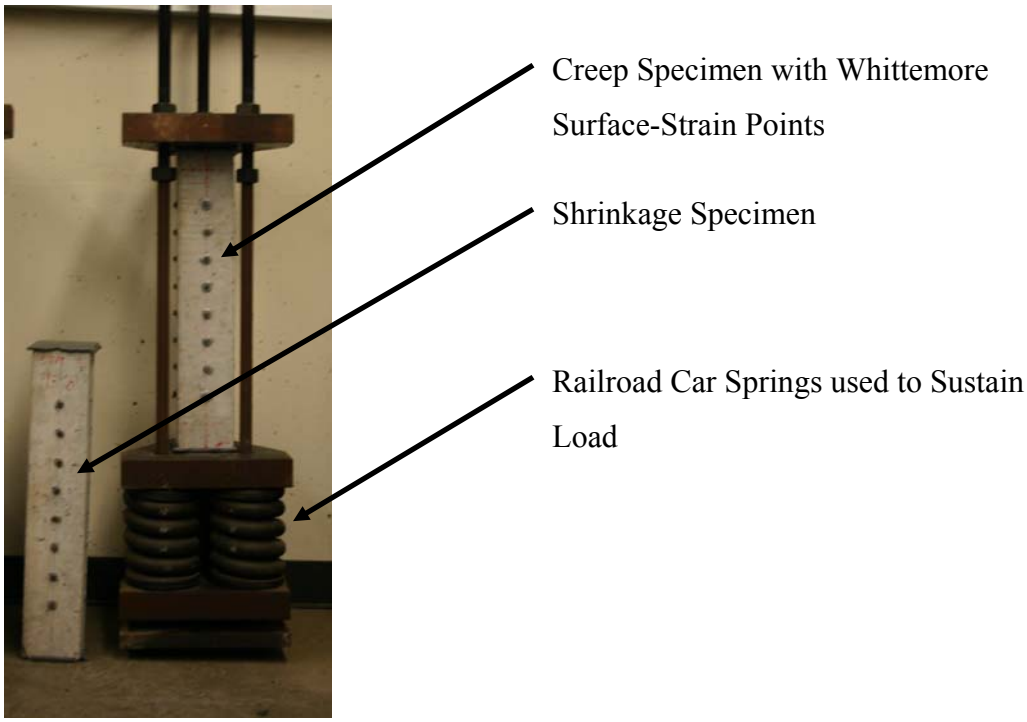

Figure 4-10 Loaded Creep Specimen and Companion Shrinkage Specimen

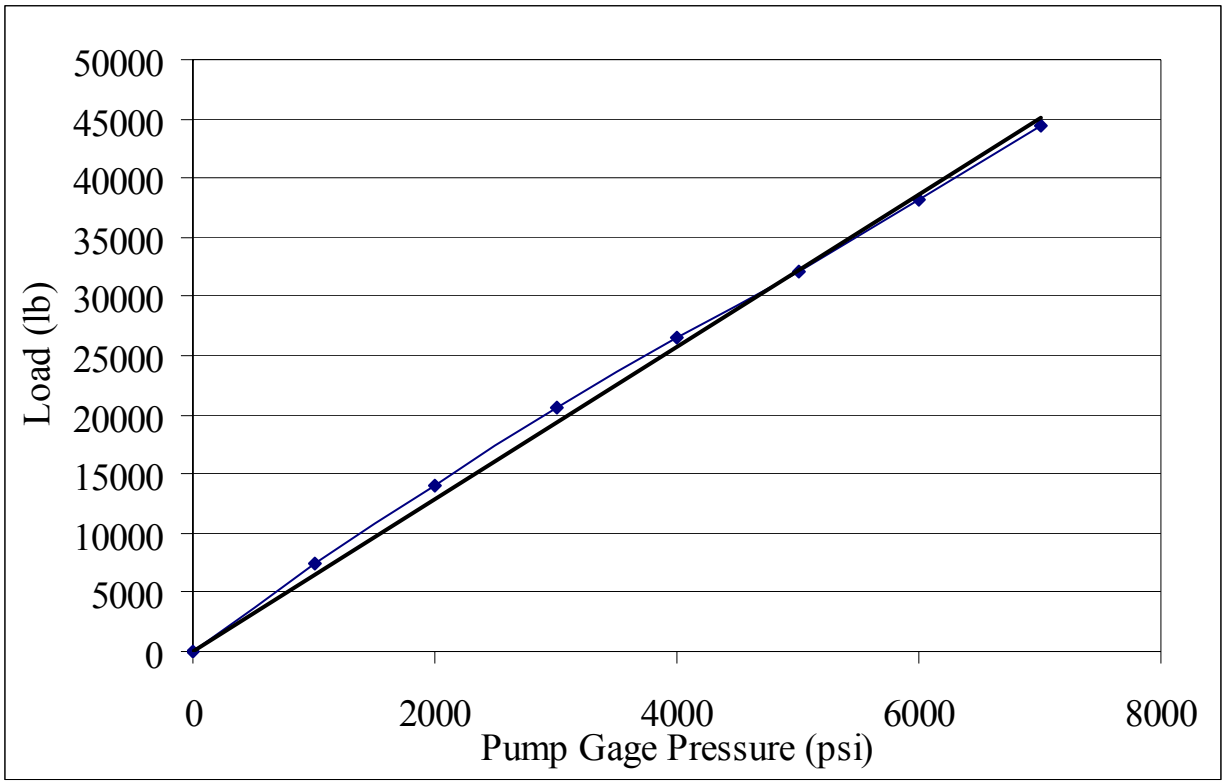

Figure 4-11 Calibration Curve Used to Load Creep Specimens

Surface-strain readings were taken immediately after loading the creep specimens to capture the elastic strain. Surface-strain readings were taken at the same time on the shrinkage members. Readings were taken on the creep and shrinkage specimens once a day for one week, once a week for one month, and monthly thereafter. ACI 209 gives an equation for the creep coefficient at any time t, as the measured ratio of creep strain per elastic strain. The creep strain is found by subtracting the initial strain at loading and the shrinkage strain from the strain reading at a given time interval. The ACI creep coefficient is shown in Equation 4-3 below.

$$\nu_t = \delta_t E_{ci} \qquad 4\text{-}3$$

ν_t = Creep Coefficent at Time t

δ_t = Creep Strain Per Unit Stress at Time t

E_{ci} = Initial Modulus of Elasticity at Time of Loading

The committee recommends an equation to predict the creep at any time based upon adjustments of constants in the equation to curve fit the experimental creep coefficient at the specified time intervals. ACI 209 Committee gives Equation 4-4 to predict the creep coefficient at any time period.

$$v_t = \frac{t^{\psi}}{d + t^{\psi}} v_u$$

$v_t =$ Creep Coefficient at Any Time t

$t =$ Time After Loading (days) 4-4

$\psi =$ Constant (0.40 to 0.80)

$d =$ Constant (6 to 30 days)

$v_u =$ Ultimate Creep Coefficent (1.30 to 4.15)

Likewise the ACI Committee gives Equation 4-5 to predict the shrinkage strain at any time. The constants of Equations 4-4 and 4-5 represent the shape and size factors for a given member and reflect the time dependency of shrinkage and creep. The constants for each mix were adjusted to curve fit the experimental shrinkage and creep strains at the specified time intervals (ACI Committee 209, 2005).

$$\left(\varepsilon_{sh}\right)_t = \frac{t^{\alpha}}{f + t^{\alpha}} \left(\varepsilon_{sh}\right)_u$$

$\left(\varepsilon_{sh}\right)_t =$ Shrinkage Strain at Any Time t

$t =$ Time After Loading (days) 4-5

$\alpha =$ Constant (0.90 to 1.10)

$f =$ Constant (20 to 130 days)

$\left(\varepsilon_{sh}\right)_u =$ Ultimate Shrikage Strain ($415x10^{-6}$ to $1070x10^{-6}$ in/in)

.

4.4.6 Core Sampling Existing Lightweight Bridges

To evaluate the long-term durability of lightweight mixes containing aggregate from the Buildex company, core samples were taken from two bridge decks in Kansas. One bridge is owned by Pottawatomie County south of Belvue, Kansas, near U.S. Highway 24 and spans the Kansas River; and the second is owned by Shawnee County north of Maple Hill, Kansas, near U.S. Highway 24 and spans the Kansas River. Both bridges have been reported to expand; however, the bridge in Shawnee County has shown excellent long-term durability while the bridge in Pottawatomie County has experienced significant cracking and surface spalling. Additionally, the Pottawatomie County bridge has been overlaid with asphalt. Three samples were taken from each bridge deck. The coring rig is shown in Figure 4-12 and the Maple Hill bridge deck after core sampling and patching was completed is shown in Figure 4-13. Not

clearly evident in Figure 4-13 is the excellent condition of the bridge deck and the minimal cracking that has taken place since its construction in 1975. At the bridge near Belvue, Kansas, one of the core samples was taken where the top half inch of the bridge deck had spalled off. This was done after noticing the top half inch of the first two cores taken from the deck were discolored at the top. A photo of the poor condition of the Belvue bridge deck is shown in Figure 4-14, and the discoloration of the top of the core samples is shown in Figure 4-15. Later in the study, a third bridge deck was cored for three concrete samples. The third bridge is owned by the state of Kansas and is located east of Randolph, Kansas, on State Highway 16 over Tuttle Creek Lake. The bridge was recently rehabilitated in 2005. The girder connections were replaced and the original lightweight concrete deck was replaced above the repaired girder connections with a normal-weight mix. Additionally, a polymer modified asphalt overlay was placed over the entire bridge beck more than 10-years ago. The deck replacement over the girder joints and the polymer overlay were done to address concerns with the bridge deck which was still expanding do to the lightweight aggregate. Cores from each bridge deck were sent to Construction Technology Laboratories (CTL) Group for a petrographic examination.

Figure 4-12 Drilling Rig Used to Core Bridge Deck Samples

Figure 4-13 Bridge near Maple Hill, Kansas, after Core Sampling

Figure 4-14 Bridge near Belvue, Kansas, Showing Poor Durability of Bridge Deck

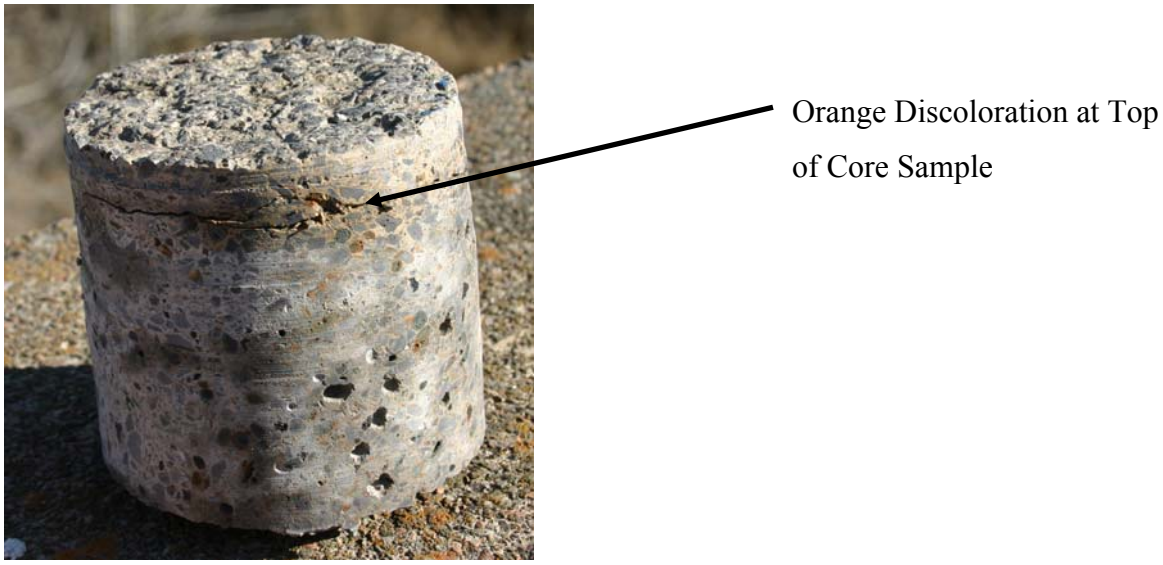

Figure 4-15 Core Sample from Bridge near Belvue, Kansas, Showing Discoloration at Top of Cylinder

4.5 *Large-Scale Batching Procedure*

To cast the six specimens for the LBPT and the 12 flexural specimens, batches of 12 cubic feet or greater were needed. To accommodate the large mixes, a 1.25-cubic-yard trailer drum mixer was used. The mixer was positioned under a hopper in which all of the rock, sand, and cement were dumped. The hopper was elevated on a wooden platform so the discharge elevation was at the same height as the mixer. The rock, sand, and cement were placed in 55-gallon barrels and raised to the top of the hopper with a fork lift. Figure 4-16 shows the mixer aligned with the hopper ready to be charged for batching. Figure 4-17 shows the hopper being charged during the batching procedure for one of the flexural members.

The material was pre-weighed with a crane scale except for the coarse-aggregate. The coarse-aggregate was put in a 55-gallon barrel and then filled with water and allowed to soak for seven days before batching. Immediately before batching, the water was drained from the barrel with a fine-mesh screen and perforated lid fabricated for the project. The material was then weighed with the crane scale. The batch weight of the coarse-aggregate was calculated to account for the moisture content of a seven-day soak. A picture of water draining from the aggregate is shown in Figure 4-18.

The mixing water was pre-weighed in an air tank before mixing. Once the water was added to the tank, an air compressor was hooked to the pressure vessel and pressurized to 30 psi. During batching, the water valve was opened and the pressure in the tank forced the mixing water out through a hose into the mixer already charged with rock, sand, and cement. A picture of the water tank is shown in Figure 4-19.

The admixtures were measured and poured into buckets with a portion of the mixing water. After 90% of the water had been added to the mix, the superplasticizer and then the air-entrainer were added. The remaining mixing water was used to clean out the admixture containers and dumped into the mixer.

Figure 4-16 Mixer and Hopper Used for Large-Scale Batching

Figure 4-17 Loading Sand into the Hopper with Fork Lift

Figure 4-18 Draining Water from Soaked Aggregate before Batching

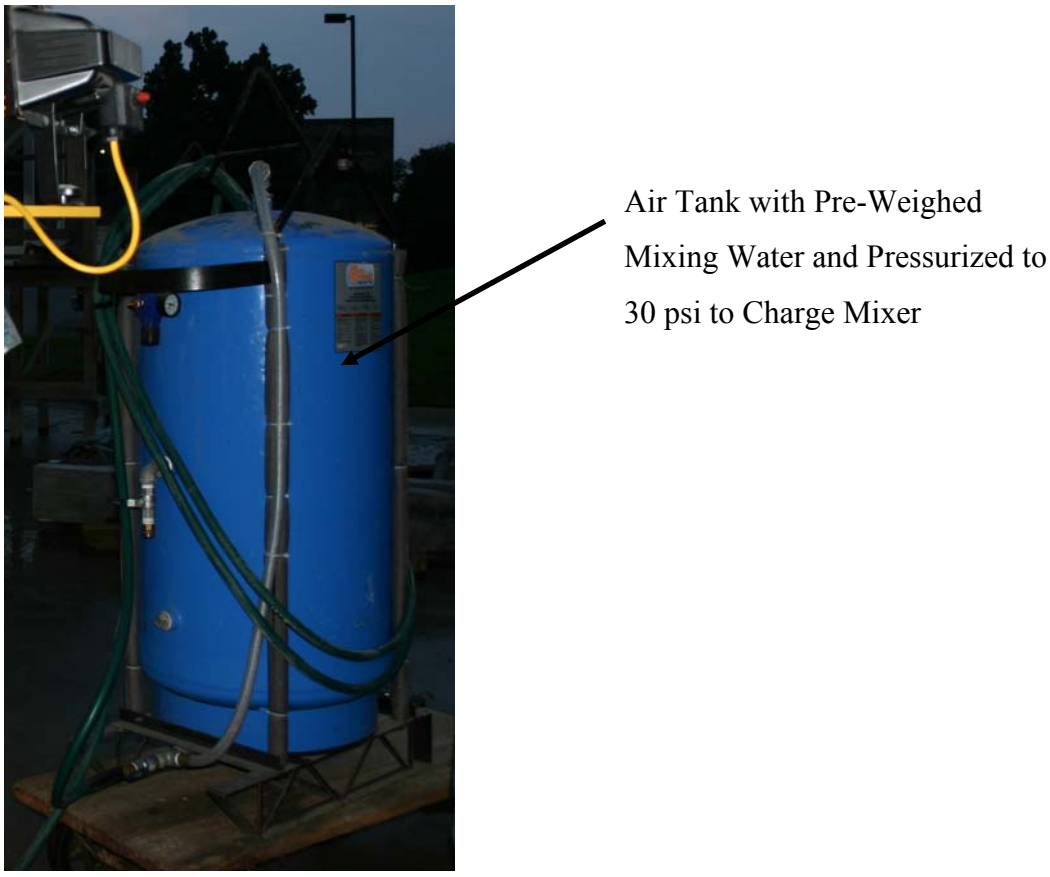

Figure 4-19 Water Tank Used to Charge Mixer for Large-Scale Batching

5 Large-Block Pull-Out Test

This section discusses the strand preparation, cage construction, form work, casting, and testing procedures used to perform the LBPT. The LBPT was performed with pre-qualified strand received from Don Logan, who developed the test. The test was not completed with the mix recommended by Logan. Instead, a control strand was used to test the bond performance of the lightweight mixes. A total of six blocks were tested, each containing one of the three aggregates at both a three-inch and nine-inch slump. The nomenclature used to label the six LBPTs is shown below in Table 5-1.

The same cross section was used as in Logan's test, except the length was adjusted for six strands instead of 18. The length of each specimen in the LBPT was 32-inches, and provided the same cover for each strand as Logan's 18 strand block. Additionally, Logan's testing procedure was followed for pulling the strands out of the block.

Table 5-1 LBPT Nomenclature

Coarse Aggregate	Slump (inches)	Specimen Name
Kansas City	3	KC-3
	9	KC-9
Marquette	3	MQ-3
	9	MQ-9
Stalite	3	STA-3
	9	STA-9

5.1 *Strand Preparation*

Five rolls of ½-inch-diameter prestressing strand were received from Don Logan with each roll containing four 30-foot strands. The strands were sealed and had minimal surface rust when removed from the packing. All strands were kept inside a climate-controlled lab and kept free from moisture. No qualitative surface testing was done because all of the strand came from the same manufacturer's large roll. A picture of the strand as received from Logan is shown in Figure 5-1.

Figure 5-1 Control Strand as Received from Don Logan

The strands were cut to 39-inch lengths for the test. On the bottom four inches of the strand, all individual wires were removed except for the center wire. The remaining center wire was fitted with a piece of clear plastic to inhibit bond but allowing the strand to rest on the bottom of the form. A picture of the sleeved portion is shown in Figure 5-2.

Figure 5-2 Bottom Sleeved Portion of Strand for LBPT

The next 18 inches of strand were the bonded length. The following two inches were duct taped and fitted with a piece of pvc pipe to prevent the top surface of the block from spalling during testing. The remaining 15 inches stuck out above the block and were used to grip the strand during testing. A picture of the strand prepared for casting is shown in Figure 5-3.

Figure 5-3 Strand Prepared for LBPT

5.2 *Cage Construction for LBPT*

The reinforcing cage used to hold the strands in place for the LBPT was made according to Logan's dimensions. No.3 stirrups, 16 inches tall and 18 inches wide with No.4 bars in each corner, were fabricated. A wood jig was constructed to ensure all cages were made to the same dimensions. A photo of the cage with the jig is shown in Figure 5-4. The longitudinal No. 4 bars were cut to the same length as the form so the steel cage would not move while placing the concrete. Legs were welded to the bottom of the cage to locate it at the correct height in the form. Additionally, the stirrups and longitudinal bars were tack welded together. However, the strands were tied to the cage with wire ties. Front and side elevations and top-plan view of the reinforcing cage and strand placement can be seen in Appendix A in Figure A-1 through Figure A-3.

Figure 5-4 Wood Jig Used to Construct Cage for LBPT

5.3 *Form Construction and Specimen Casting*

The form was constructed with two-inch by six-inch framing members and ¾-inch plywood sheeting. Each side of the form was placed on the wood base, screwed down, and then locked together at the top by two-inch by six-inch wood plates. The form was 24 inches in height, 24 inches wide, and 32 inches long. The base was built so a pallet jack could be placed underneath it to move the block after casting. The form was reused for each LBPT and was

sprayed with form release before each use. Care was taken so no form release contacted the strand. A photo of the form is shown in Figure 5-5.

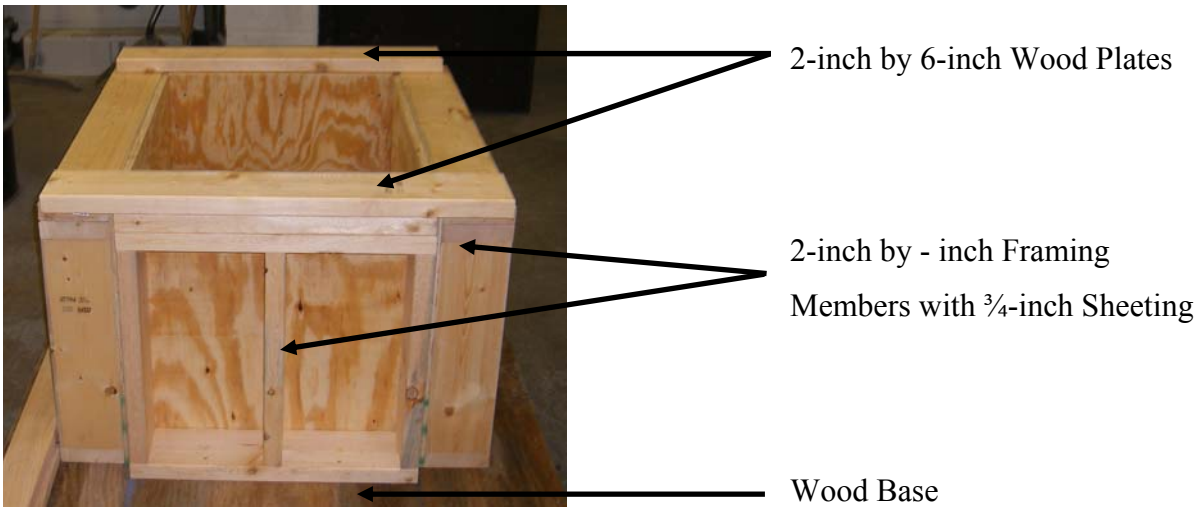

Figure 5-5 Form Used to Cast LBPT

Once the strands were prepared, attached to the cage, and placed in the form, the block was cast. The block was placed behind the mixer with a pallet jack, and the concrete was poured directly into the form. If the initial slump of the mix was higher than the required three-inch or nine-inch slump, the concrete was allowed to mix until the correct slump was reached. As concrete was poured, the block was vibrated. Once the form was filled, the block was put back into the climate-controlled lab and the vibrator was dipped into the concrete next to each strand once to ensure consolidation. Along with the slump, compressive-strength cylinders were made and the air content of the mix was tested. An electronic temperature recording gage, i-Button produced by Dallas Semi-Conductor, was placed in the center of the block and in one of the compressive-strength cylinders. The i-Button had wires soldered onto the top and bottom that came out of the top of the block and cylinder. The i-Buttons were read by connecting the wires to the com-port on a computer and the i-Button reader software. In their molds, the compressive-strength cylinders were placed in a heated water bath to match the maximum temperature developed in the block. A picture of the block just before placing the concrete is shown in Figure 5-6.

Figure 5-6 Casting an LBPT

5.4 *LBPT Testing Procedure*

Ten hours after the block was cast compressive-strength cylinders were broken periodically to determine when 5000 psi compressive strength was reached. Once the average of three cylinders reached 5000 psi, typically 12 to 16 hours, the block was positioned to begin testing. A bridging device was placed around one of the strands and the load frame was rested on top of the bridge plate with a chain hoist. The actuator inside of the load frame was then lowered down into place. At the end of the actuator was a 50-kip load cell to which the load fixture was attached. The load fixture was slipped around the strand and provided a bearing surface for the prestress chuck. The load frame was then repositioned until it was sitting level on the bridge plate. The chuck was then slipped over the strand and pressed against the load fixture. Figure 5-7 shows the test setup.

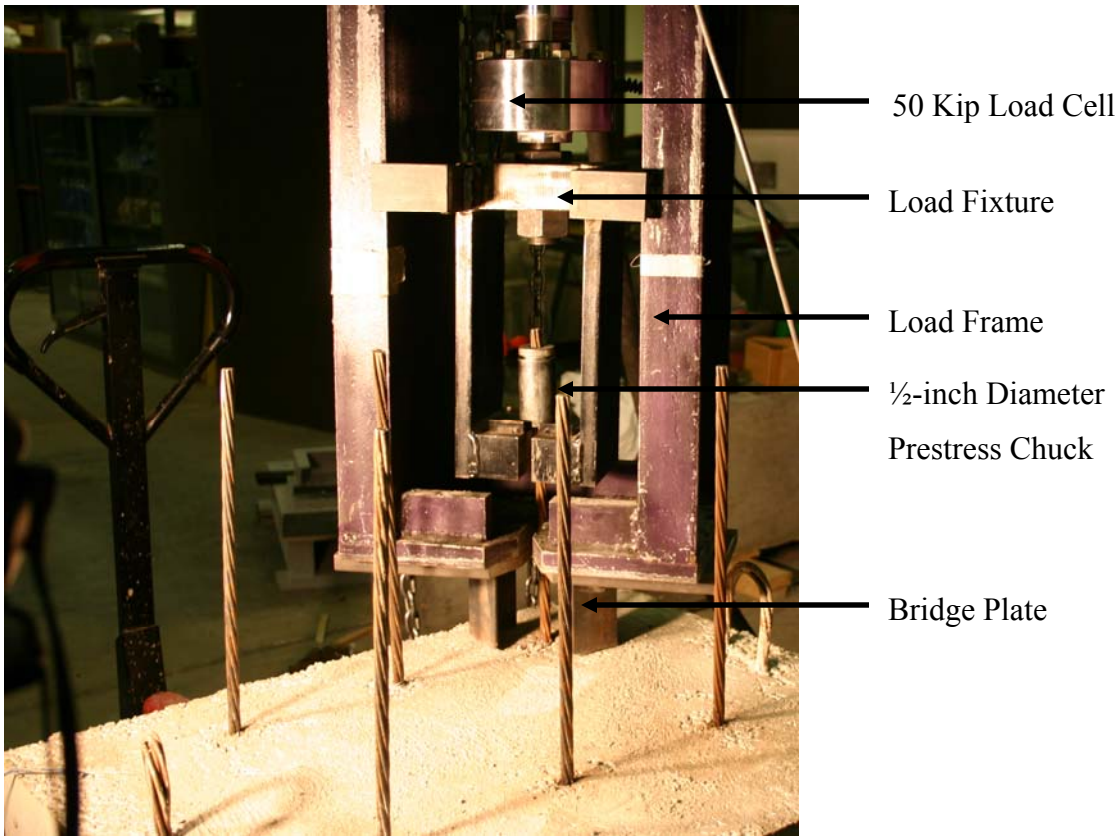

Figure 5-7 Load Fixture Setup for LBPT

The hydraulic actuator was controlled by the digital MTS testing software Basic Test Ware, and used to set the prescribed loading rate of 20 kips per minute. The data acquisition was set to capture force, actuator displacement, and first-slip signal once every 10 pounds. In order to capture the first slip of the strand, a digital camera was zoomed in at the interface of the strand and the top of the block, and the video was viewed on a large monitor. Once rigid body movement of the strand was detected, a button was pushed and a voltage signal was captured with the load and displacement in the data acquisition file. Figure 5-8 shows a test in progress with the monitor being viewed to capture first slip. The same setup and loading conditions were repeated for each strand in the block.

Figure 5-8 Capturing First Slip during Testing of an LBPT

6 Flexural Member Fabrication and Testing

This section covers flexural member cross section, forms and prestress bed, tensioning, casting, placement of Whittmore surface-strain points, end-slip readings, detensioning, and testing procedures. The LBPT gave a relative indication of the bond performance of the developed mixes for each lightweight aggregate at a three-inch and nine-inch slump. To evaluate the actual behavior of varying slumps on flexural-bond performance, beams were cast with both a three-inch and nine-inch slump with the same control strand received from Don Logan used in the LBPT. For each of the three lightweight mixes at both slumps, two beams were cast for a total of 12 beams. For each pour, the two beams differed by overall length. One beam was 190 inches in length, with the code-required development-length of 77 inches after all losses, a 36-inch constant-moment region, and a 77-inch development-length. The other beam had the same 36-inch constant-moment region, but had only 80% of the required development-length, 62 inches. An elevation of both beam lengths is shown in Figure 6-1. The two lengths allowed for the evaluation of the ACI 318-05 and *Precast Institute Design Handbook* (PCI) development-length equations, and the reduced-moment-capacity equation for underdeveloped strands. Table 6-1 gives the nomenclature used to label the flexural members (PCI Industry Handbook Committee, 2004).

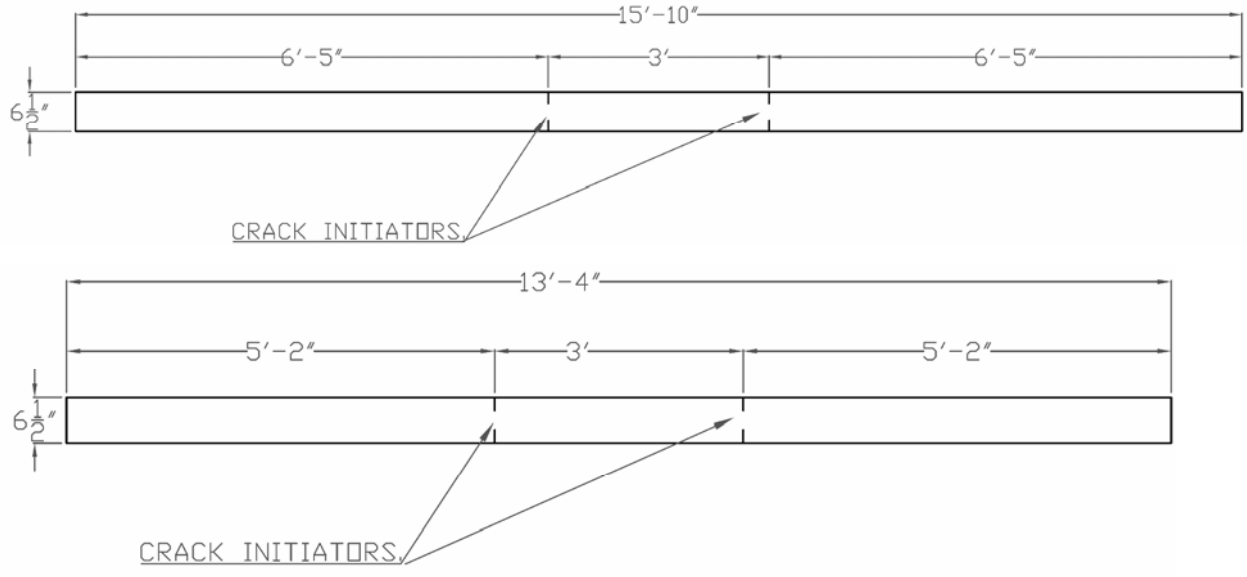

Figure 6-1 Elevation of Flexural Members

Table 6-1 Flexural Member Nomenclature

Coarse Aggregate	Slump (inches)	100% of Development Length	80% of Development Length
Kansas City	3	KC-3 100% L_d	KC-3 80% L_d
	9	KC-9 100% L_d	KC-9 80% L_d
Marquette	3	MQ-3 100% L_d	MQ-3 80% L_d
	9	MQ-9 100% L_d	MQ-9 80% L_d
Stalite	3	STA-3 100% L_d	STA-3 80% L_d
	9	STA-9 100% L_d	STA-9 80% L_d

6.1 *Cross Section for Flexural Members*

The author of *The Effects of As-Cast Depth and Concrete Fluidity on Strand Bond* (2007), Peterman, is currently investigating a cross section that would allow PCI member plants to use in their facilities to perform an "in house" bond test. Peterman's proposed cross section was used for this study. The width is eight inches at the top and three-inches at the bottom. The total height is six and one-half inches with a strand depth of four and one-half inches. The top one inch of the section is the full eight-inch width and then tapers to the three-inch width at the bottom for the remaining five and one-half inches. The narrower bottom is to address concerns that wide sections with a single strand do not accurately model larger members with closely spaced multiple strands because of the added confinement. A cross section of the flexural member is shown in Figure 6-2. The cross section contained no mild steel for flexural or shear reinforcing. However, one stirrup was placed two-inches from each end to stop cracks that may form during detensioning. Figure 6-3 shows a stirrup placed at the ends of the members.

The flexural capacities of the full-development-length and underdeveloped-length beams are shown in Appendix B. The nominal-moment capacity was calculated with KDOT and the PCI prestress losses. The shear capacity of the section was calculated as well. Even though shear stirrups are required by ACI 318-05 Section 11.5, they were not provided based on the Peterman et al. (2000) PCI Journal article showing shear stirrups can reduce the effects of poor flexural bond.

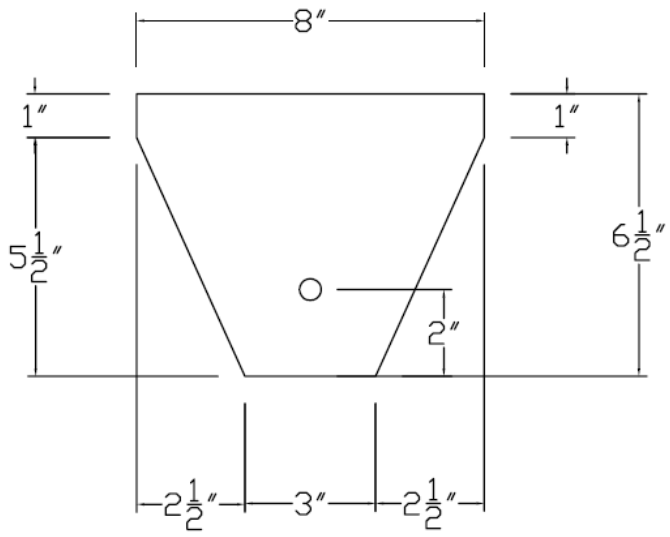

Figure 6-2 Cross Section of Flexural Members

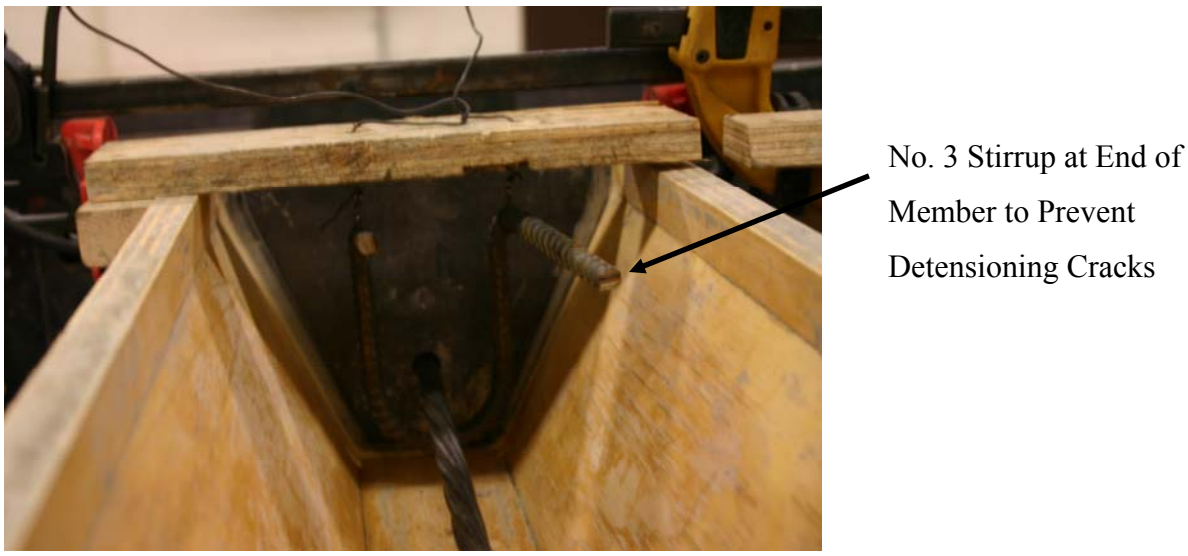

Figure 6-3 Stirrup Used to Stop Crack Propagation during Detensioning

6.2 *Prestress Bed and Forms for Flexural Members*

The prestress bed used to make all of the flexural members is located on the campus of Kansas State University. The bed has a casting length of 20 feet and is 4 feet wide with 23 feet between bulk heads. The forms were set adjacent to each other with enough distance to allow 12 inches between the strands for the two beams. A steel blockout was fabricated that served as the form cap on one end and butted against the bulk head.. The blockout allowed for a sudden release of both sides of the member, even after the opposite end had already been cut. One side

of each form was constructed to be removed before the member was detentioned to allow Whittmore strain-surface points to be attached. Also, both beams had crack formers placed at both ends of the constant moment. The crack formers ensured the first cracks would form at the end of the development-lengths during testing. One side of the crack formers was duct taped so no added resistance to cracking would be created by the concrete bonding to the plate. Figure 6-4 shows the prestress bed and forms ready for casting.

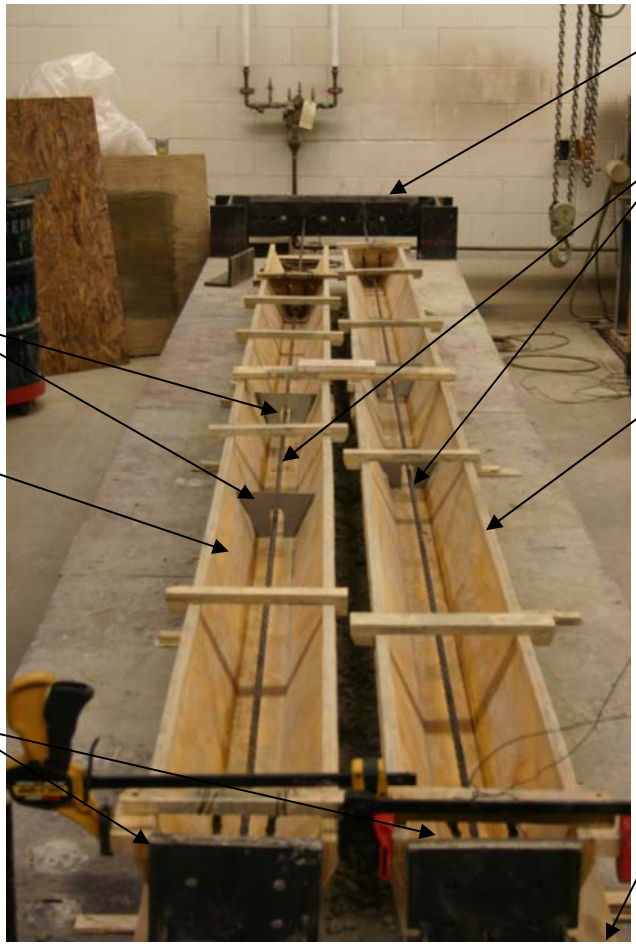

Figure 6-4 Prestress Bed and Forms Ready for Casting

6.3 *Strand-Tensioning Procedure*

To tension the strands for the flexural members, a post-tensioning jack was used. The post-tensioning jack had a power-seating chuck ram that pushed the chuck teeth into the strand to minimize seating losses. If a standard prestress chuck had been used, the shortening that would have taken place before the teeth locked to the strand would have caused a significant loss in

strand stress. The force in the strand was monitored two ways during tensioning. The first was a 50-kip load cell on the non-jacking end of the prestress bed and the second was a calibration curve for the pressure in the pump supplying the hydraulic fluid to the post-tensioning jack. The strand for the full development-length beam was tensioned first and the 80% development-length beam second. The first strand was over-jacked to account for losses that occur while tensioning the other strand. This jacking sequence was used for each pour. Figure 6-5 shows the post-tensioning jack used in the study. Figure 6-6 is a photo of the load cells used to monitor the force in the strand, and Figure 6-7 is the developed calibration curve for the hydraulic pump used to monitor the post-tensioning jack during tensioning.

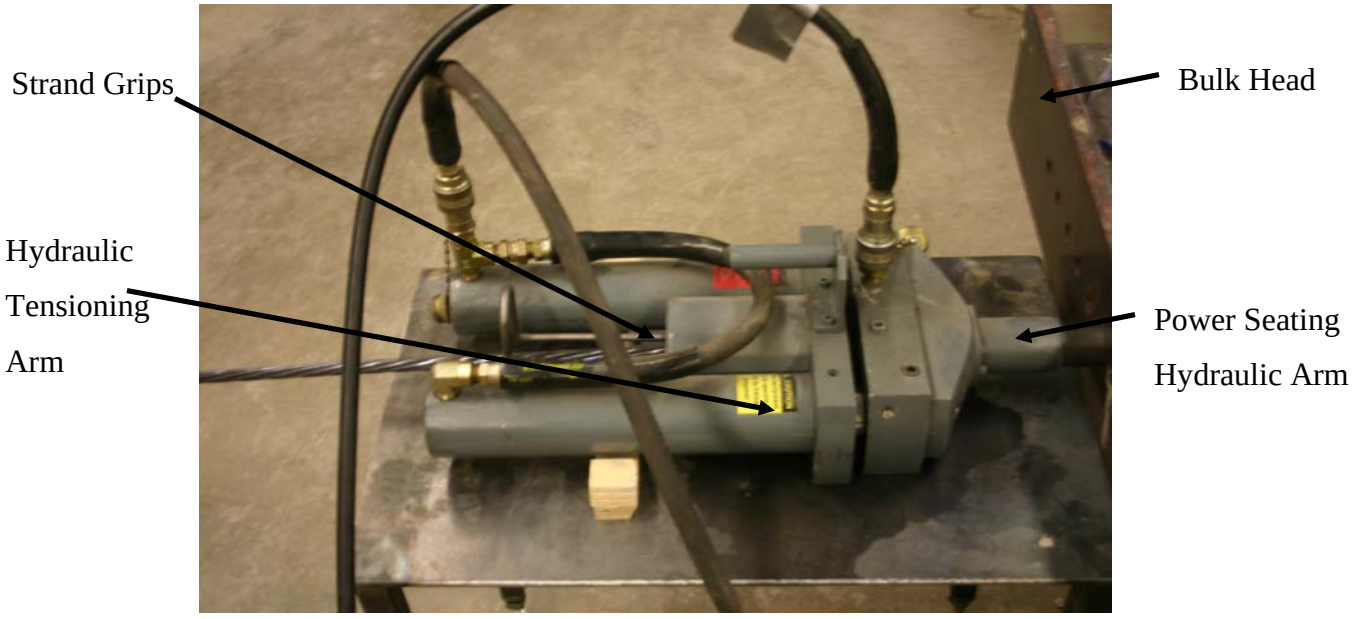

Figure 6-5 Post-Tensioning Jack Used to Tension Prestress Tendons

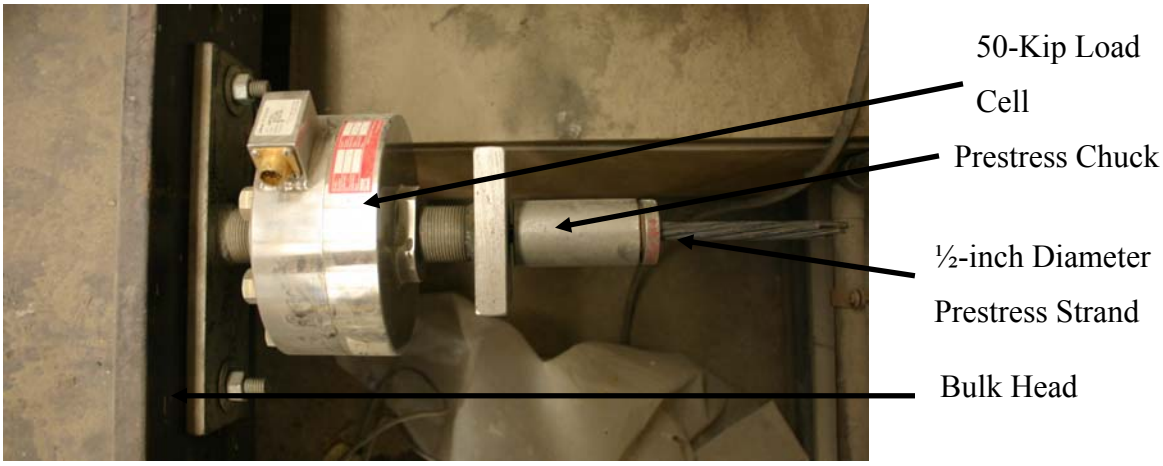

Figure 6-6 Load Cell Used to Measure Strand Force during Tensioning

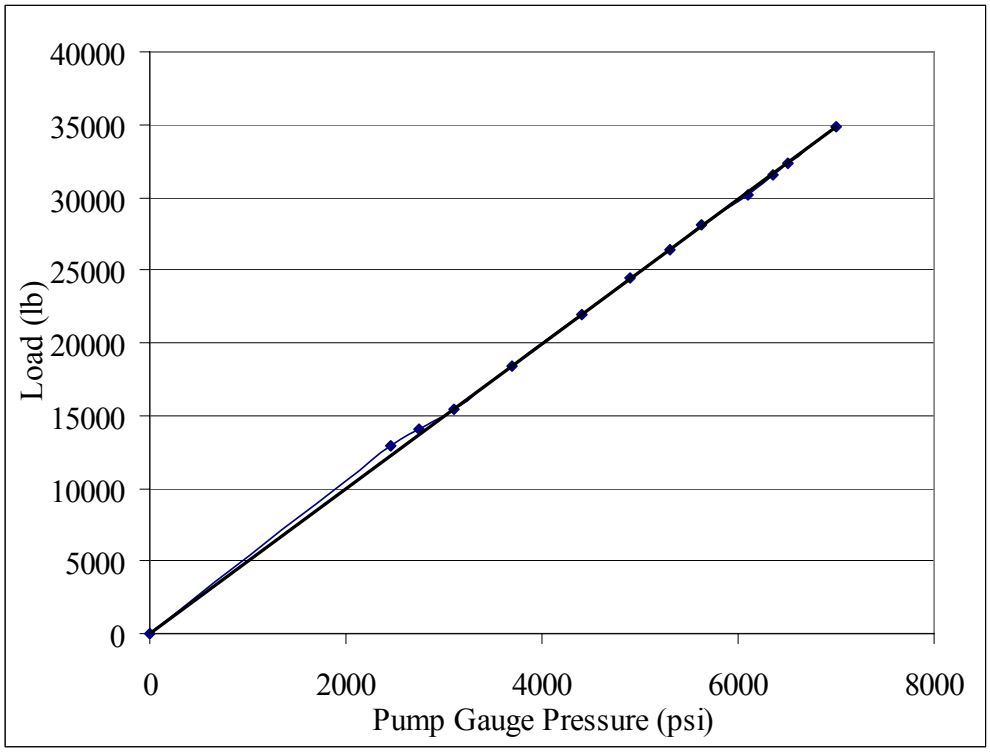

Figure 6-7 Post-Tensioning Pump Calibration Curve

6.4 *Casting Flexural Members*

All flexural members were batched as described in Section 4.6. If the initial slump was greater than the required three inches or nine inches, the concrete was allowed to mix until the desired slump was reached. The concrete was poured into wheel barrels and carried to the forms. The concrete was then scooped out of the wheel barrels and placed into the forms. The mix was vibrated as the concrete was placed along the length of the member to ensure good consolidation around the strand. The tops of the beams were finished with a wood trowel and lifting loops were inserted. Additionally, compressive-strength cylinders were made, unit weight was measured, and the air content of the mix was checked. Once the beams were finished, they were covered with a plastic tarp to cure. Figure 6-7 shows flexural member casting.

Figure 6-8 Flexural Member Casting

6.5 *Surface-Strain Measurements*

To measure the transfer length, concrete surface-strain measurements were taken. Stainless steel disks with a hole machined in the center were adhered to one side of each beam at the strand height along the development-lengths before detensioning. To align the stainless steel

disks, Whittemore points, a chalk line was snapped at strand height on the side of the beam. An aluminum bar, five-feet long with metal points machined two-inches apart with a tolerance of 0.001 inches, was used to glue and align the points to the beam. The center holes of the Whittemore points were placed over the points along the length of the bar; structural epoxy was placed on the back of the Whittemore points; and the bar was lifted and rotated onto the chalk line on the beam. Clamps were then used to hold the bar and points in place while the epoxy cured. Figure 6-9 shows a beam with Whittemore points attached.

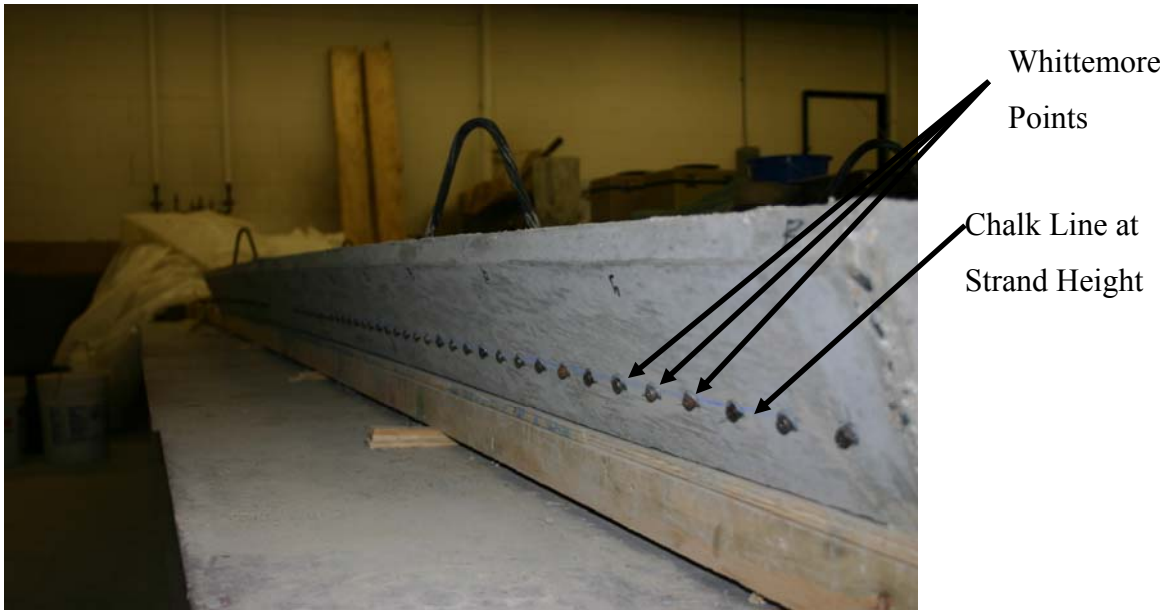

Figure 6-9 Whittemore Points Used to Measure Surface Strain

After all the points were adhered to the beam, a Whittemore gage was used to measure the distance between the centers of the Whittemore points. The gage length of the reader was eight inches plus or minus 0.0100 inches, with an accuracy of 0.0001 inches. Therefore, the distance between four Whittemore points was measured. The readings were taken before detensioning on days, 1, 2, 3, 4, 7, 14, 21; and before flexural testing. The Whittemore gage was sensitive to the position in which it was held; therefore, a block was made that rested against the beam and held the Whittemore gage perpendicular to the surface while readings were taken. Figure 6-10 shows the block and gage used to take all surface-strain readings. After the readings were recorded, the strains were calculated as shown in Equation 6-1.

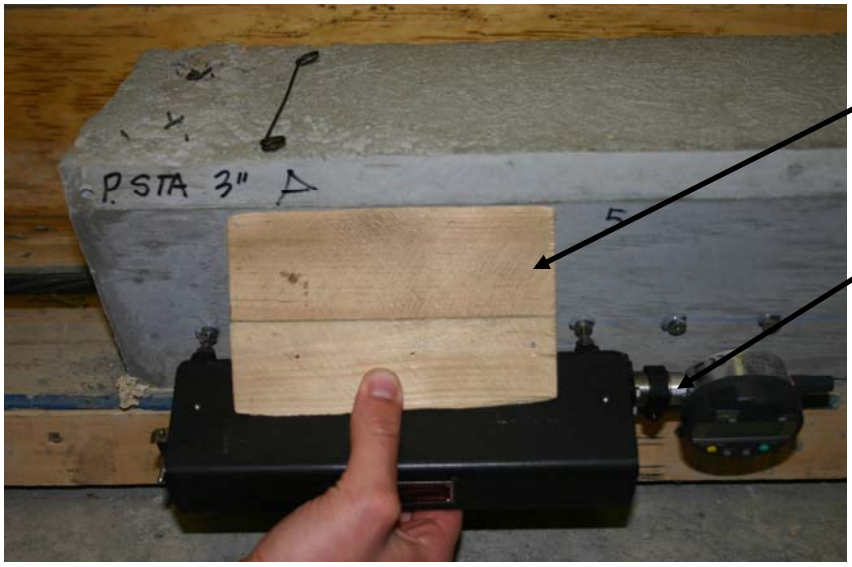

Figure 6-10 Gage and Block Used to Measure Surface Strain

$$\varepsilon_n = \frac{L_0 - L_n}{L_0} \qquad 6\text{-}1$$

ε_n = Strain on the nth day

L_0 = Measured Length Before Detensioning

L_n = Measured Length on nth day

A strain versus distance from end of beam plot was made for each day's readings. The plot showed a strain gradient that started at zero strain from both ends of the beam and increased to a maximum strain at the end of the transfer length. The transfer length was found using the strain values with a procedure prescribed by (Russell, B. W., and Burns, N. H., 1993). The strain at each point was smoothed by taking a moving three-point average to reduce any irregularities as shown in Equation 6-2. Next the average maximum strain was found by taking the average of the strain values in the plateau region of the curve that occur in between the transfer lengths. Finally, the transfer length was determined as the intersection of the smoothed curve and 95% of the average maximum strain.

$$(strain)_i = \frac{(strain)_{i-1} + (strain)_i + (strain)_{i+1}}{3} \qquad 6\text{-}2$$

i = The Current Strain Reading

6.6 *End-Slip Measurements*

End-slip measurements were also used to indirectly measure the transfer lengths. Mast's strand-slip theory as used by Logan (1997), Peterman (2007), and other publications was utilized to find the transfer length. A small notch was made on one of the seven wires on the prestress strand at both ends of the beams before detensioning. A digital caliper, with a precision of 0.001 inches and an alignment collar, was slipped into the notch and the distance between the notch and the end of the beam was recorded. Measurements were taken again at both ends of the beams after detensioning and days 1, 2, 3, 4, 7, 14, 21; and before flexural testing. The strand slip was taken as the difference between the length before detensioning and the measured length for a given day, minus elastic shortening. Assuming a straight-line variation in strand stress, zero stress at the free end of the beam to the full effective prestress force at the end of the transfer length, and the measured strand slip, the experimental transfer length was calculated. Equation 6-3 shows the derivation by which the experimental transfer length was calculated.

$$\Delta = \int_0^{L_{tr}} \frac{P(x)}{AE_{ps}} dx = \int_0^{L_{tr}} \frac{f(x)}{E_{ps}} dx = \int_0^{L_{tr}} \frac{f_{si}(x)}{E_{ps}} dx = \frac{f_{si} L_{tr}}{2E_{ps}}$$

$$L_{tr} = \frac{2\Delta E_{ps}}{f_{si}}$$

$\Delta =$ Measured Strand Slip

$P(x) =$ Prestress Force as a Function of Length

$f(x) =$ Strand Stress as a Function of Length 6-3

$A =$ Area of Prestressing Strand

$E_{ps} =$ Modulus of Elasticity of Prestress Strand

$f_{si} =$ Prestsress Tendon Stress After Detensioing

$L_{tr} =$ Transfer Length

Accuracy of the strand-slip measurements was sensitive to the position and force held by the digital caliper. It was also important to measure to the same point on the end of the beam each time readings were taken. Accuracy of the strand-slip measurements increased as more measurements were taken. Figure 6-11 shows a strand-slip measurements being taken.

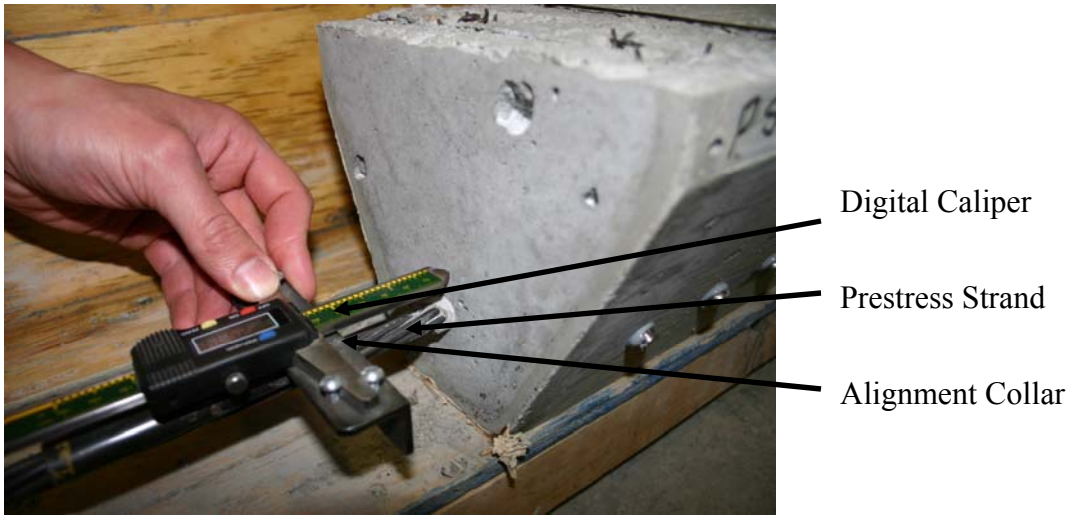

Figure 6-11 End-Slip Measurement

6.7 *Strand Detensioning*

After the initial surface-strain readings, strand-slip measurements and prestress force from the load cells were recorded as the flexural members were detensioned. A flame torch was used to cut the strands approximately 10 inches from the ends of the member. Torching at this distance allowed the individual wires to be twisted back into the original strand configuration if unraveling occurred during release. The torch was held several inches from the strands to preheat the tendon; the flame was then directed at individual wires burning through one at a time. The unrestrained end was detensioned first, giving a sudden release. The prestress force was then transferred to the blockouts at the opposite end of the beam. The blockouts pressing against the bulk heads allowed for a sudden release on the opposite end as well. Figure 6-12 show a free-end release and Figure 6-13 shows a restrained-end release.

Figure 6-12 Beam Free-End Detensioning

Figure 6-13 Beam Restrained-End Detensioning

6.8 *Flexural Member Setup and Testing Procedures*

All flexural members were tested between 28 and 33 days in the Kansas State University Structural Mechanics Laboratory. The beams were placed on concrete-bearing blocks and centered under the 22-kip MTS digitally controlled hydraulic actuator. Each end of the beam was then lifted and a roller and metal bearing plate was set underneath and leveled with a high-strength leveling compound, hydrocal. The rollers were placed three-inches from the end of the members. The rollers were used on both ends of the members so there was no restraint against rotation during loading. The three-foot spreader beam was then lowered to align the rollers underneath that were set and leveled with hydrocal on the flexural member. Figure 6-14 shows the end conditions of the beams, and Figure 6-15 shows the rollers underneath the spreader beam.

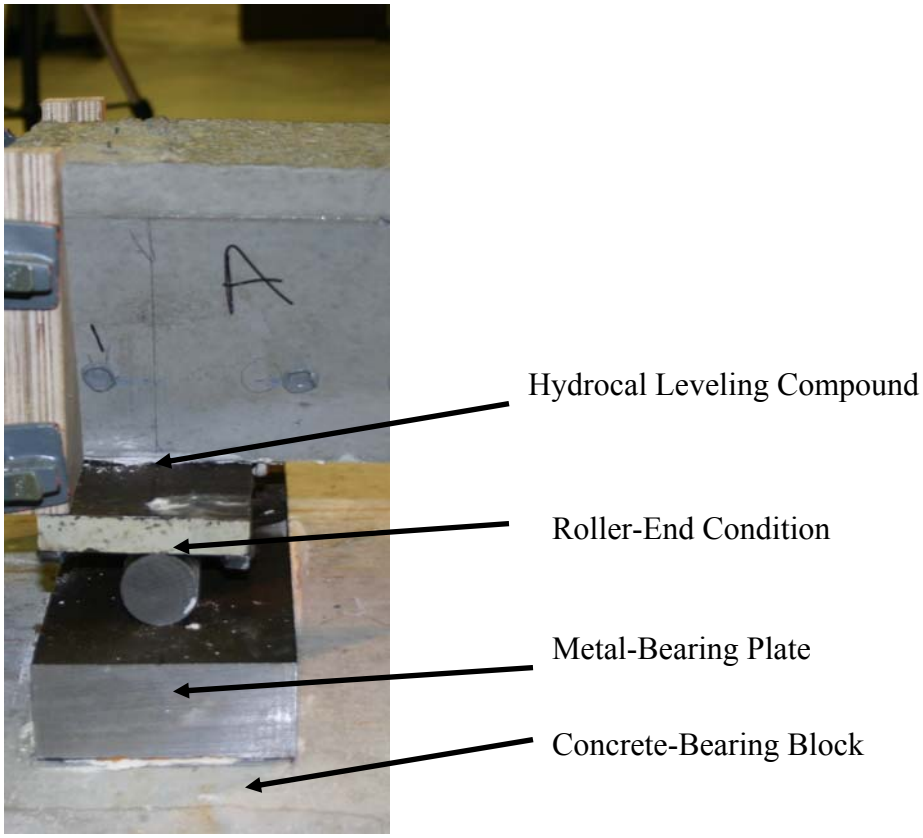

Figure 6-14 End Condition of Flexural Members

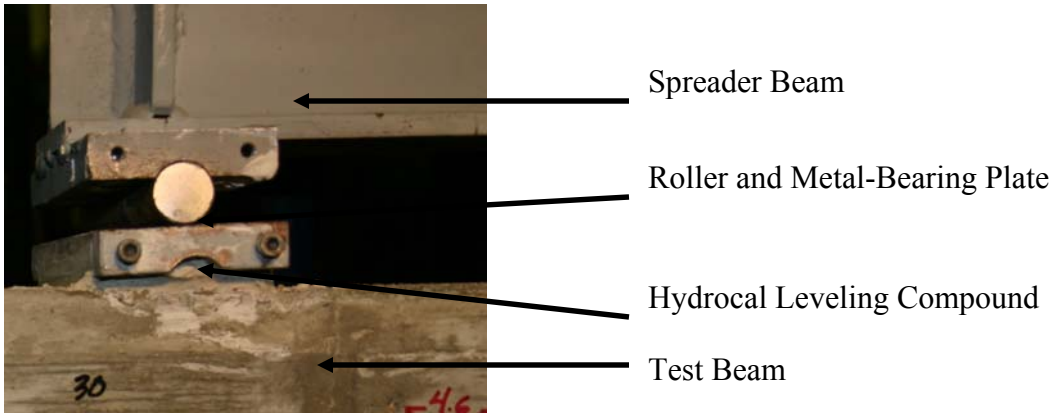

Figure 6-15 Roller Condition under Spreader Beam

Both ends of the flexural members were fitted with four-inch LVDT on the prestress strands. The strands were ground down so ¼-inch of the tendon stuck out from the ends of the member. Wood inserts that contoured the sides of the members were slid into place and a clamping fixture with an LVDT mount was secured around them. An LVDT was placed in the mount and centered on the center wire of the strand. A rubber band was then placed on two bolts at the front of the clamping fixture and looped around the LVDT to keep constant contact between the LVDT and the strand. A photo of the end-slip LVDTs is shown in Figure 6-16.

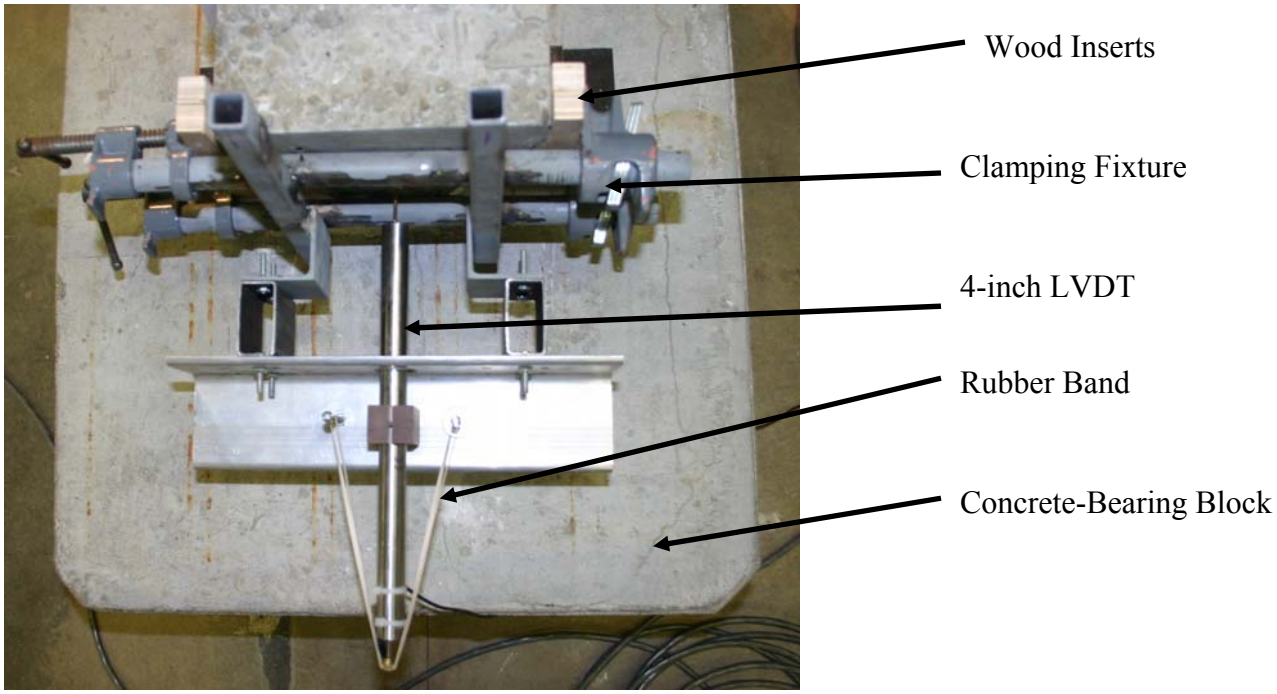

Figure 6-16 LVDT End-Slip Clamps

In addition to the end-slip LVDTs, two 10-inch mid-span LVDTs were used. They were placed at an equal distance on both sides of the beam from the longitudinal center line. The placement allowed the true vertical deflection to be captured if any out-of-plane deflection occurred. A steel alignment plate was adhered to the top of the beam with holes drilled at equal distances from the center. The LVDTs were placed in a stand and aligned over the drilled holes of the alignment plate.

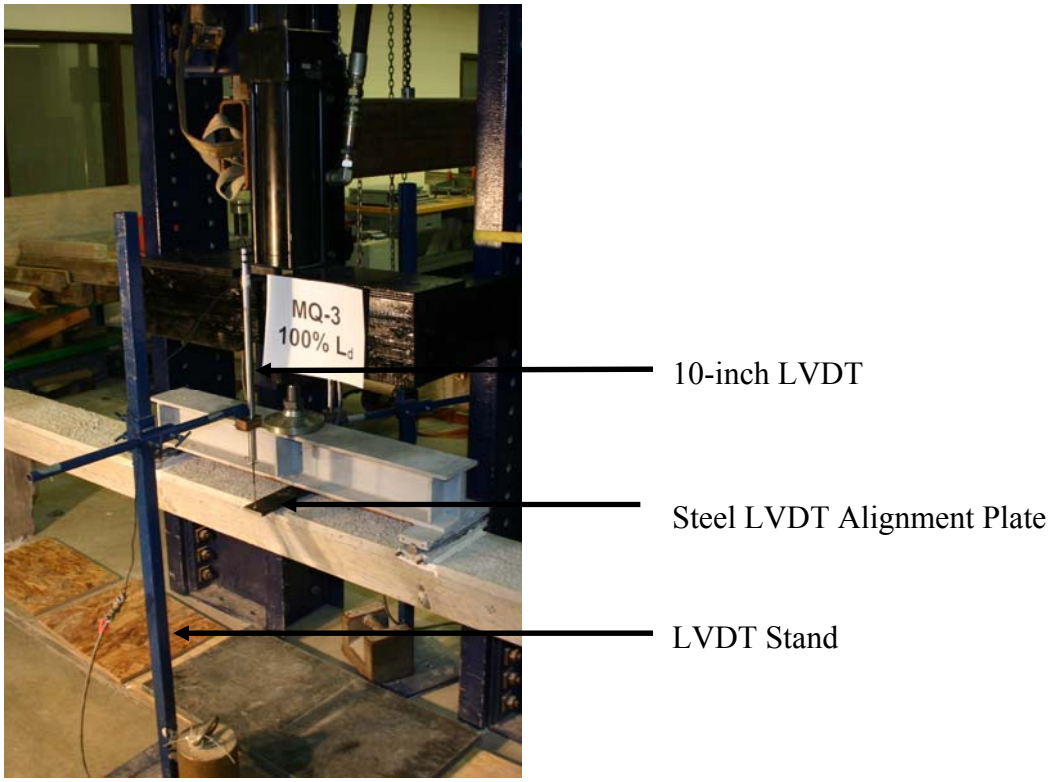

Figure 6-17 Mid-Span LVDTs for Flexural Members

After the beams were aligned, fitted with end- and mid-span LVDTs, and the spreader beam was lowered over the constant-moment region, loading began. Both the full-development-length and 80%-development-length beams had the same loading procedure, only the magnitude of the loads varied to account for the reduced-moment capacity of the underdeveloped beams. The loading procedure is described below.

- Ramp to 85% of nominal-moment capacity at 100 pounds per minute
- Hold 85% of nominal-moment capacity for 24 hours
- Ramp to nominal-moment capacity at 10 pounds per minute
- Hold nominal-moment capacity for 10 minutes
- Ramp to failure at 0.10 inches per minute

Ramping and holding to 85% of nominal-moment capacity was used based on recommendations from ACI 318-05 Chapter 20 *Strength Evaluation of Existing Structures,* Section 20.3.2. The loads were held for 24 hours to monitor creep in the member, loaded at the slower load rate of 10 pounds per minute to capture strand slip, and failed in displacement control at 0.10 inches per minute for safety concerns. Four separately activated data acquisitions were ran and recorded load, actuator displacement, both mid-span LVDTs, and the two end-slip LVDTs. The four separately queued data acquisition files were load, every 20 pounds; time, every five minutes during the 24-hour hold; and end-slip LVDTs, every 0.001 inches. Pictures were taken along the length of the beams after loading to 85% and full-moment capacity to record the flexural crack patterns. Later the crack patterns were drafted for comparison. All beams were loaded to failure. Figure 6-18 shows the full flexural member test setup.

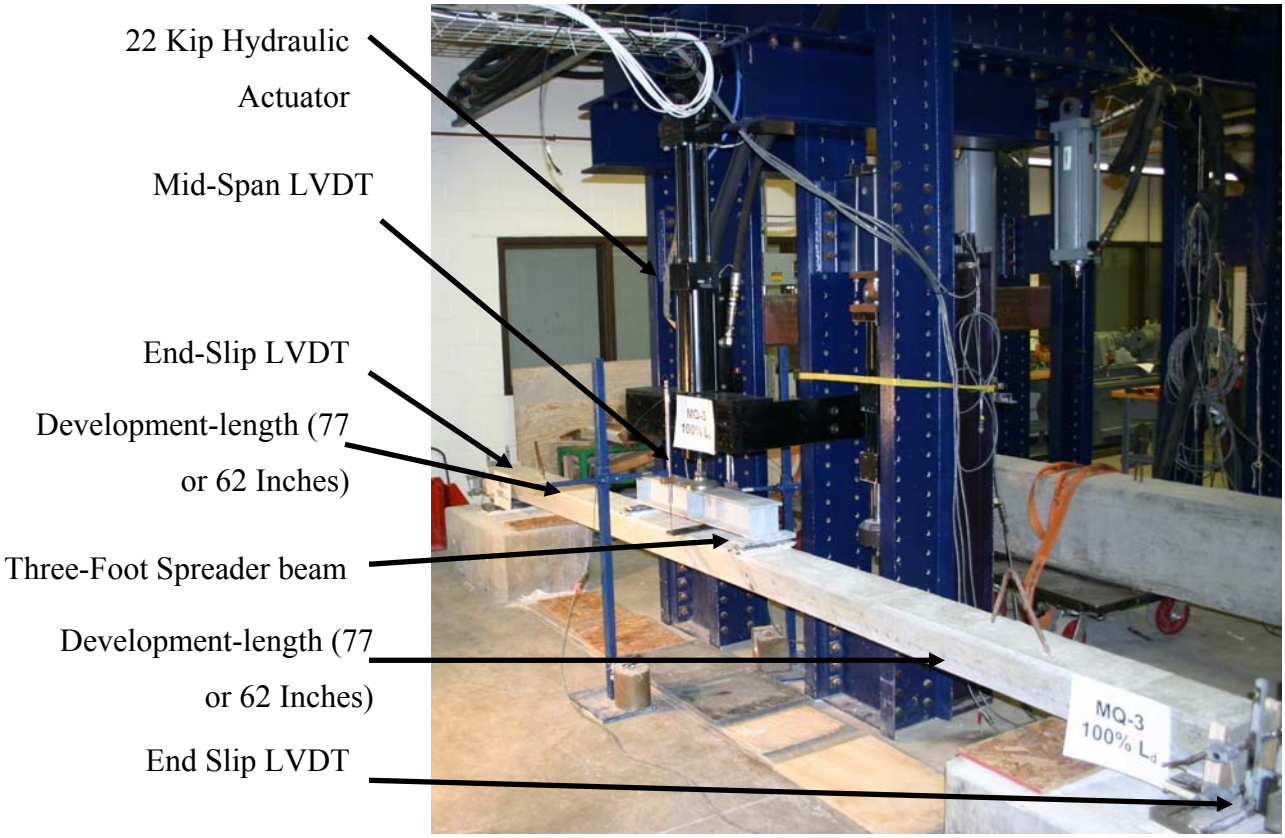

Figure 6-18 Test Setup for Flexural Members

7 Results

This section reports results from hardened concrete tests, petrographic examinations, LBPTs, surface-strain readings, end-slip readings, and flexural members. Compressive strength, split-tensile stress, modulus of elasticity, and creep and shrinkage results are given for each mix. Graphs of force versus actuator displacement and initial slip for each of the eight LBPTs are presented. Surface-strains data, end-slip measurements, crack diagrams, and moment versus mid-span deflection are reported for the 12 flexural members.

7.1 *Hardened- Concrete Properties Results*

Concrete cylinders were cast with the nine-inch slump flexural members to test at 16 hours, 3 days, 7 days, 14 days, 21 days, and 28 days to test the hardened concrete properties. The only variation in the three- and nine-inch slump mixes was the superplasticizer; therefore, the hardened concrete properties were determined with the nine-inch slump mixes for ease of concrete placement. All cylinders were stored in a lime bath until testing.

7.1.1 Concrete Compressive-Strength Results

Compressive cylinders were tested as specified in Section 4.5.1. All three of the mixes made the targeted compressive strength of 5000 psi in 16 hours. The Stalite mix had the greatest rate of strength gain followed by Marquette, then the Kansas City mix. Table 7-1 shows the averaged compressive strength of three cylinders for the stated test days. Figure 7-1 shows the rate of strength gain over time for the three mixes.

Table 7-1 Concrete Compressive-Strength Results

	Compressive Strength (psi)		
Day	**Marquette**	**Kansas Cty**	**Stalite**
16-hour	5360	5370	5160
3	6540	6660	6780
7	7330	6820	7290
14	7360	7200	7570
21	7740	6920	8060
28	7550	7200	8230

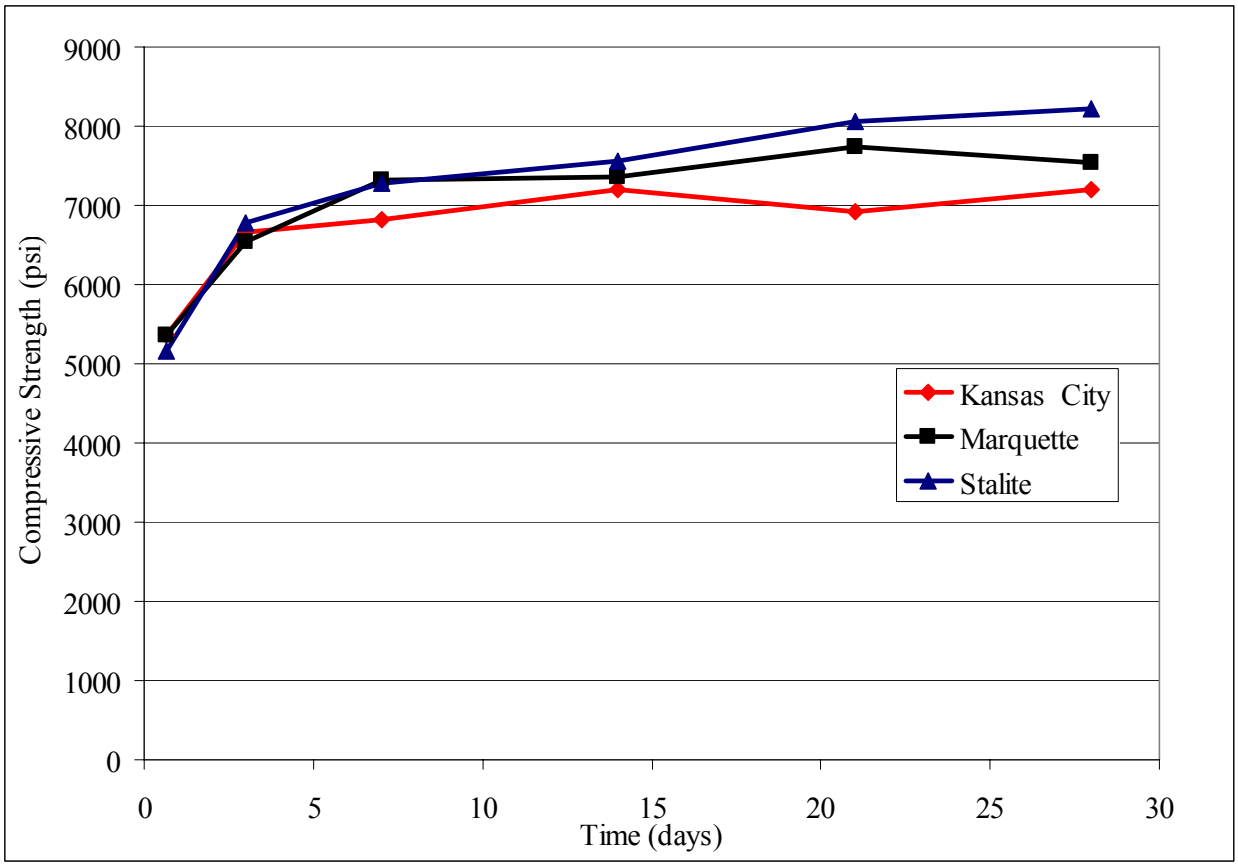

Figure 7-1 Developed-Concrete Mix Compressive-Strength Gains over Time

7.1.2 Split-Tensile-Strength Results

The split-tensile test was performed as described in Section 4.5.2. Reported values are an average of three cylinders. There is a general trend of increasing tensile stress with time; however, several cylinders broke at lower strengths than on the previous test day. This can be attributed to the brittle nature of the lightweight aggregate. The Marquette and Kansas City aggregate, an expanded shale, had visible fracture planes that can be broken by hand. Stalite, an expanded slate, had no visible fracture plans and exhibited increasing tensile strengths at each test period. Table 3-1 shows the results for the given time periods.

Table 7-3 shows the ACI 318-05 Section 9.5.2.3 predicted modulus of rupture for sand-lightweight concrete that is a function of the compressive strength as shown in Equation 7-1. The experimental compressive strength values of Table 7-1 were used to calculate the ACI 318-05 modulus of rupture, not the specified 5000 psi strength.

$$f_r = 0.85\left(7.5\sqrt{f_c'}\right)$$

f_r = Modulus of Rupture 7-1

f_c' = Concrete Compressive Strength (psi)

Table 7-2 Split-Tensile-Strength Results (psi)

Day	Marquette	Kansas City	Stalite
16-hour	400	360	310
3	340	390	440
7	450	430	480
14	410	390	470
21	500	470	480
28	430	460	420

Table 7-3 Predicted Modulus of Rupture from ACI 318-05 (psi)

Day	Marquette	Kansas City	Stalite
16-hour	454	408	352
3	386	442	499
7	510	488	544
14	465	442	533
21	567	533	544
28	488	522	476

7.1.3 Modulus of Elasticity Results

The test procedure described in Section 4.5.3 was used to determine the modulus of elasticity at specified test periods. The experimental values found following the ASTM C469 procedure, shown in Table 7-4, were lower than the values found using the ACI 318-05 Section 8.5 equation. The ACI expression for the modulus of elasticity is shown in Equation 7-2. The ACI predicted values were found using a unit weight of 122 pcf and the compressive strengths shown in Table 7-1. The ACI 318-05 predicted values are shown in Table 7-5. The lower modulus, of the lightweight mixes is a result of the lower modulus of the coarse-aggregate. The paste and the aggregate have similar modulus thus allowing the concrete matrix to deform uniformly with less cracking but with a greater magnitude as compared to a normal-weight concrete mix. Figure 7-2 shows the Kansas City-28 day stress-strain curve plotted from the

experimental data using the ASTM C469 procedure. All data collected to find the modulus of elasticity was plotted in the same manner. As shown in the graph, the first 30 to 40 data points were not plotted because of scatter caused by seating of the specimen. The experimental value for Stalite day three is not given because of an error during testing.

$$E_c = w_c^{1.5} 33\sqrt{f_c'} \qquad 7\text{-}2$$

E_c = Modulus of Elasticity of Concrete

w_c = Unit Weight of Concrete

f_c' = Specified Compressive Strength of Concrete

Table 7-4 Chord Modulus of Elasticity Results ASTM C469 (ksi)

Day	Marquette E_{chord}	City E_{chord}	Stalite E_{chord}
16-hour	2730	2610	3150
3	3130	3140	-
7	3380	3720	3370
14	3480	3420	3040
21	3110	3490	3160
28	3630	3690	3410

Table 7-5 Predicted Modulus of Elasticity from ACI 318-05 (ksi)

	Kansas		
Day	**Marquette**	**City**	**Stalite**
16-hour	3097	3100	3039
3	3421	3452	3483
7	3622	3493	3612
14	3629	3589	3680
21	3721	3519	3798
28	3675	3589	3837

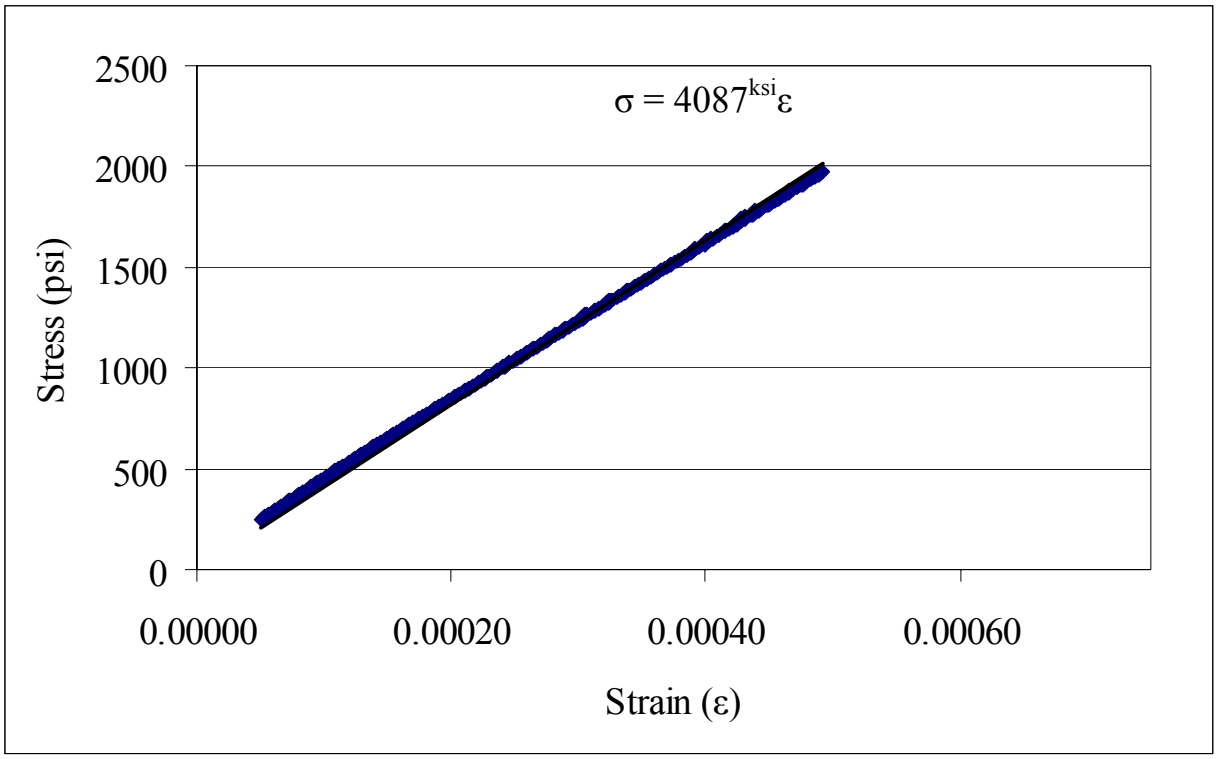

Figure 7-2 Kansas City Mix 28-Day Stress-Strain Plot Used to Determine Modulus of Elasticity

7.1.4 Creep and Shrinkage Results

The creep and shrinkage specimens had been in testing for seven months at the time this report was composed. ASTM C512 requires test duration of one year; however, data was plotted for the most current readings. The experimental data was used to find creep coefficients at specified time intervals with Equation 4-3. The ACI Committee 209 creep-prediction expression, given in Equation 4-4, was plotted against the values found with Equation 4-3. The constants ψ, d, and v_u of Equation 4-4 were varied until an acceptable curve fit was found. The constants found through the curve-fit process are shown on the corresponding graphs. Additionally, all of the constants were within the given ranges recommended by the ACI Committee. Figure 7-3 through Figure 7-5 give the curve-fit plots for the ACI creep-prediction equation with the experimental data. The ultimate creep coefficient, v_u, found using the curve-fit method, yielded similar results for all three mixes. The ACI Committee 209 states that the curve-fit method is a process to aid designers in predicting the long-term creep effects of structural members and provide a simplified approach for estimating the actual performance.

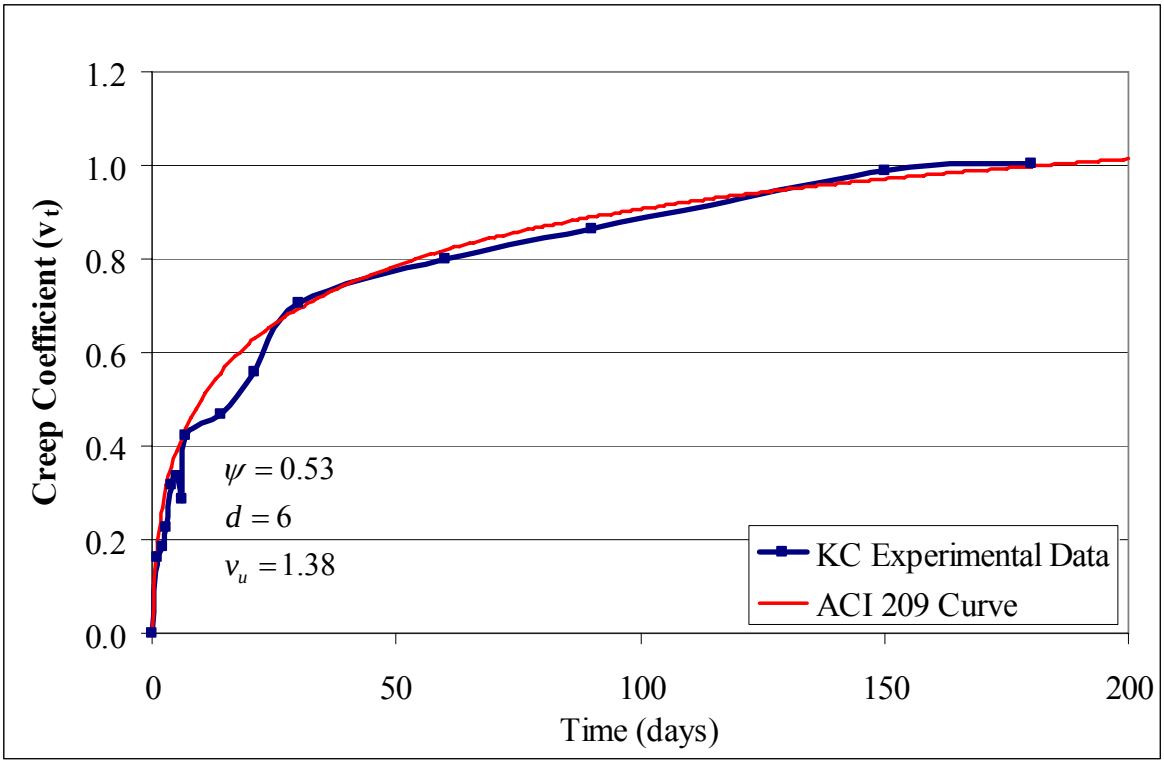

Figure 7-3 Creep Coefficient for Kansas City Mix

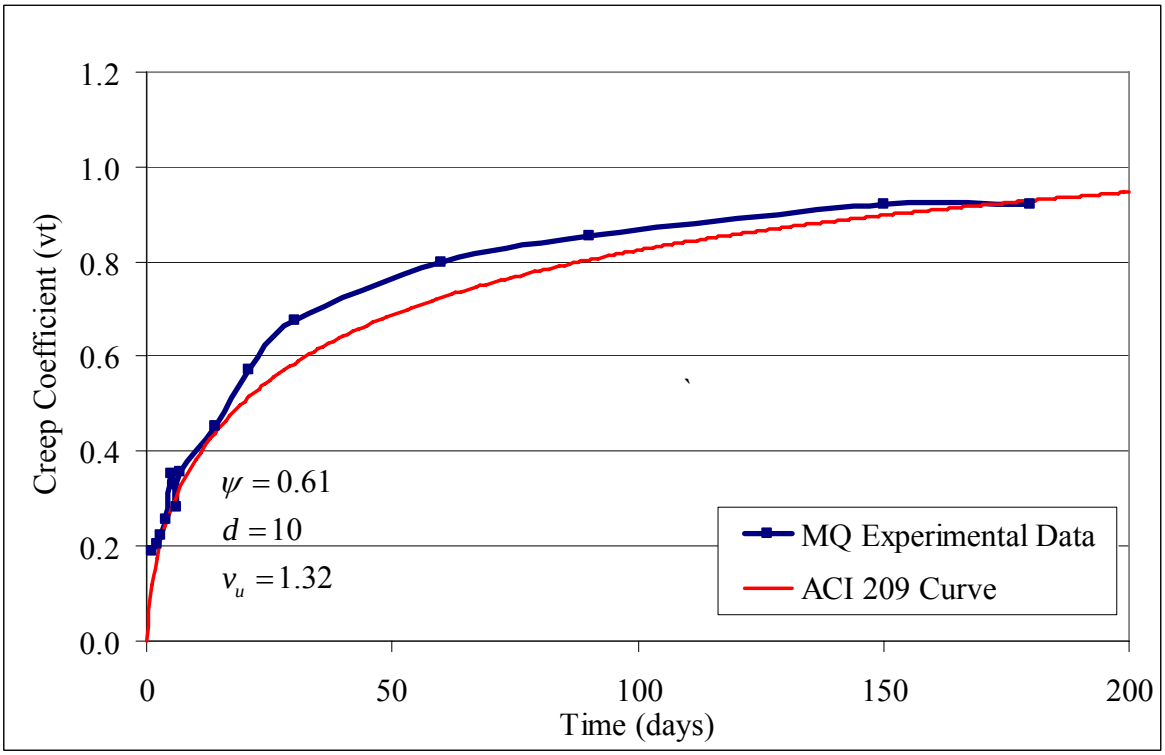

Figure 7-4 Creep Coefficient for Marquette Mix

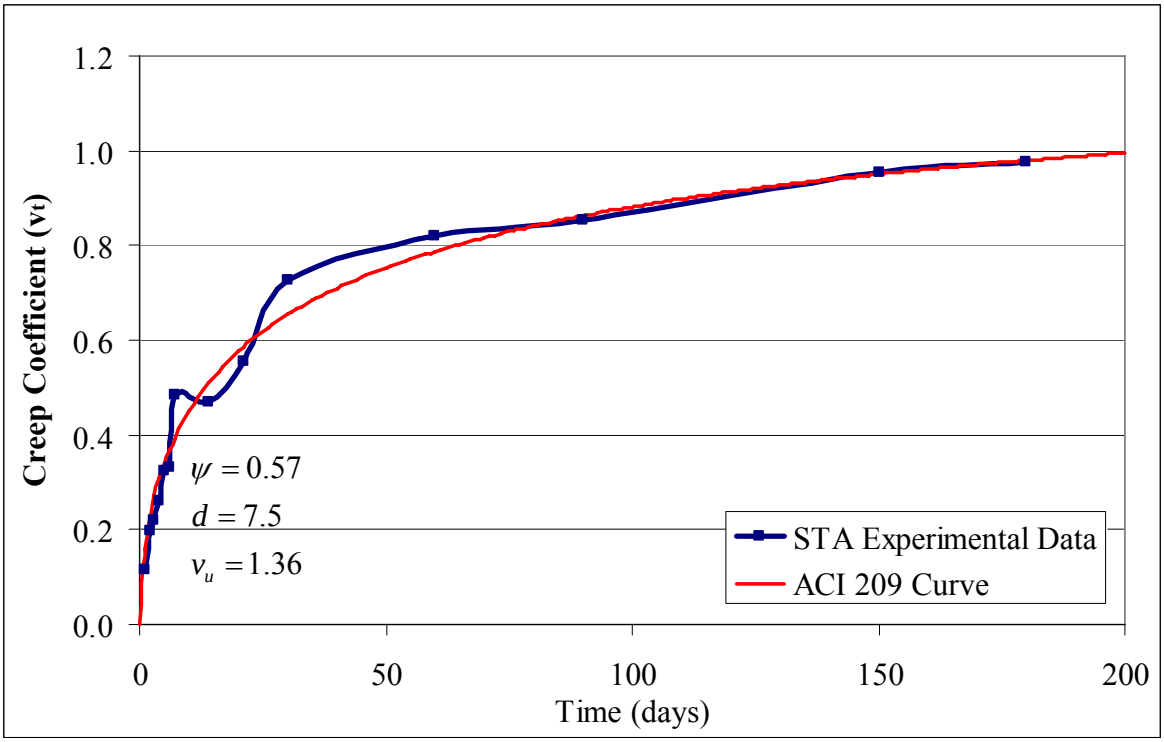

Figure 7-5 Creep Coefficient for Stalite Mix

The experimental data was used to find shrinkage strain at specified time intervals. The ACI Committee 209 ultimate shrinkage-strain expression, given in Equation 4-5, was plotted against experimental shrinkage strains at various time intervals. The constants t, ά, and $(\varepsilon_{sh})_u$, of Equation 4-5 were varied until an acceptable curve fit was found. The constants found through the curve-fit process are shown on the corresponding graphs. Additionally, all of the constants were within the given ranges recommended by the ACI Committee. Graphs of the ACI Committee's shrinkage-prediction expression with the experimental data are shown in Figure 7-6 through Figure 7-8. Data points for months four and five are missing due to repair and recalibrating the broken Whittemore gage. Additionally, there is an error on the day 21 readings for all of the mixes that may have been caused by a temperature fluctuation. The ultimate shrinkage-strain values found with the curve-fit method increased in magnitude with decrease in absorption of the coarse-aggregate. This may be due to the internal curing effect associated with high absorption of lightweight aggregates. The Kansas City aggregate had the highest level of absorption followed by Marquette and then Stalite. As the specimens cure, after final set, the

water in the pores of the aggregate are available for further hydration, therefore; reducing the drying shrinkage.

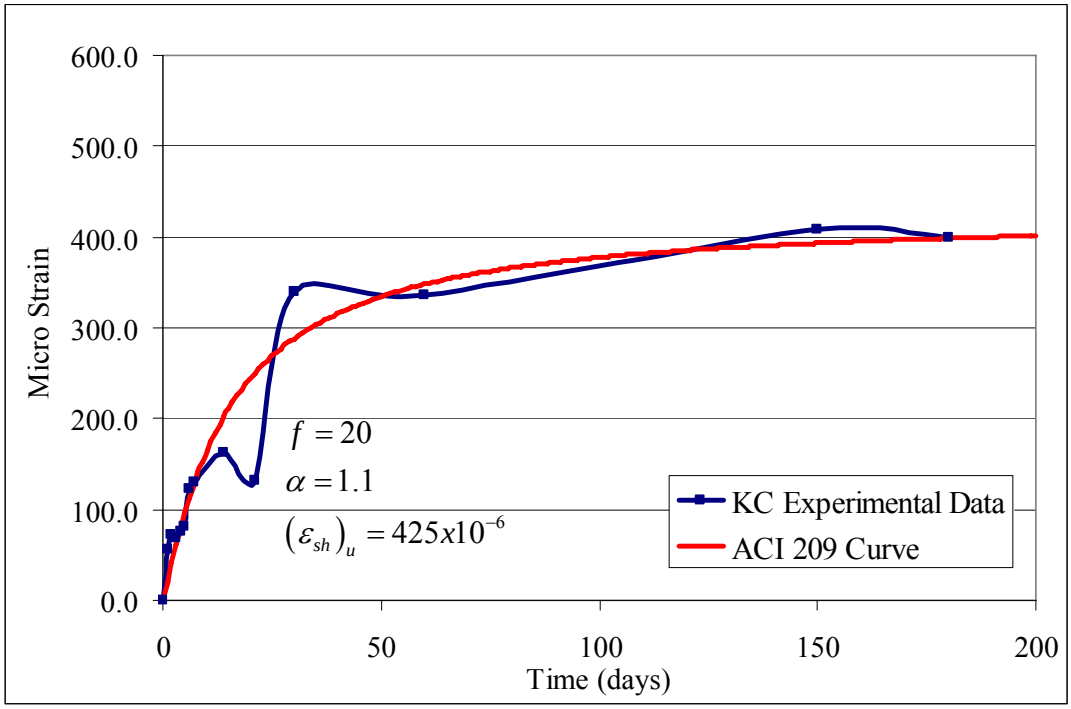

Figure 7-6 Shrinkage Strains for Kansas City Mix

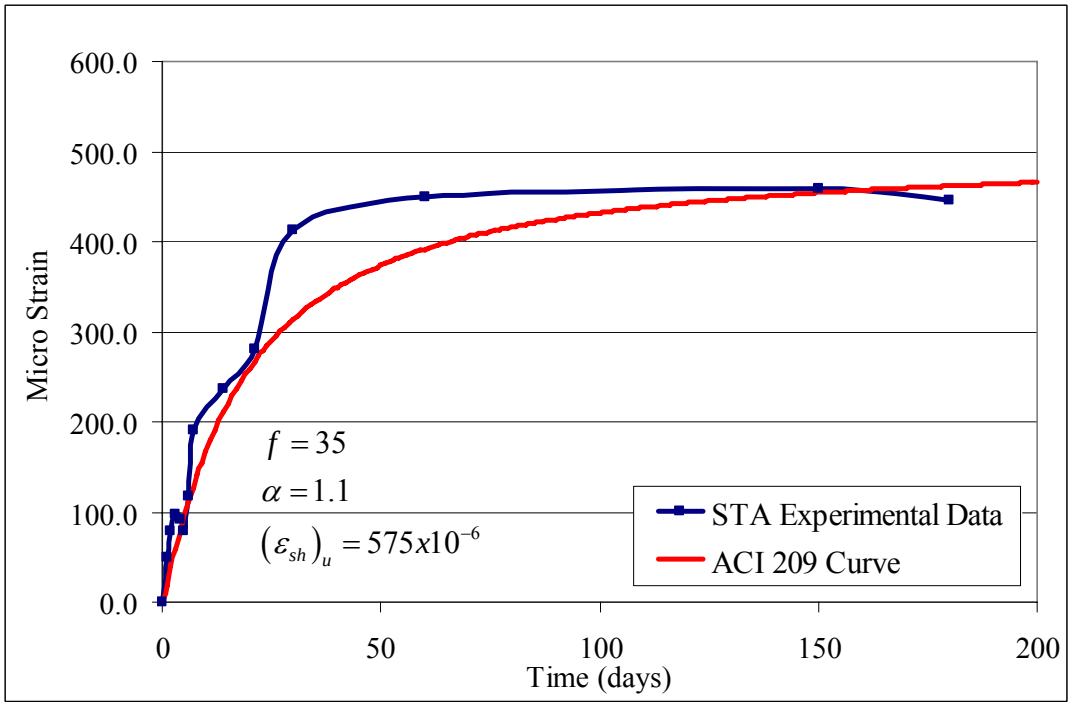

Figure 7-7 Shrinkage Strains for Marquette Mix

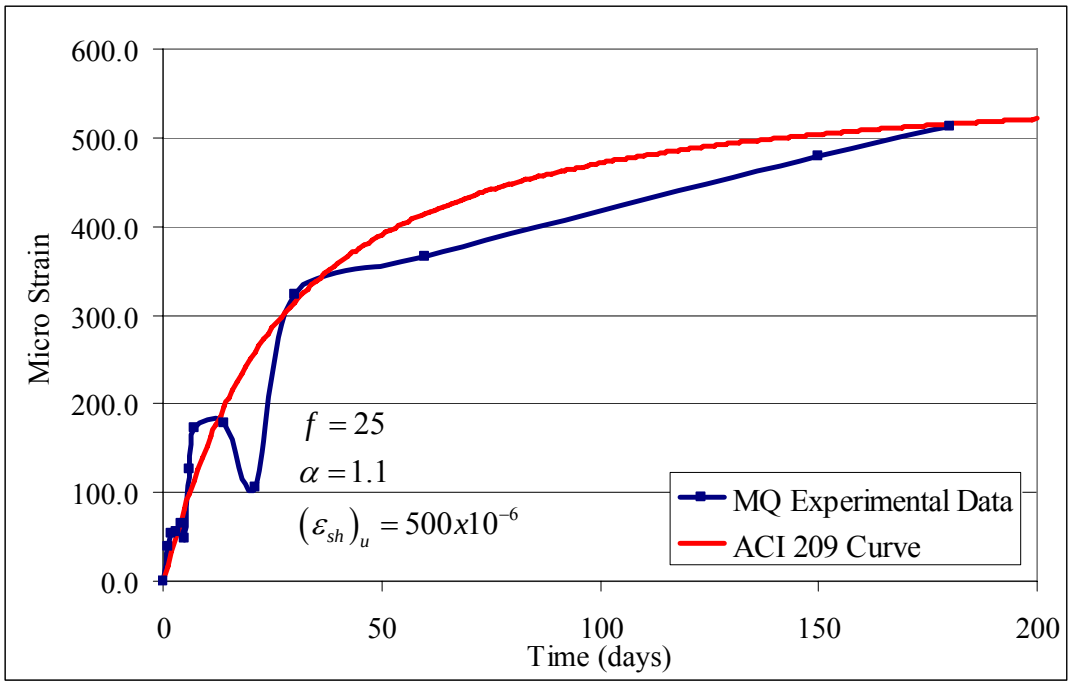

Figure 7-8 Shrinkage Strains for Stalite Mix

7.1.5 Petrographic Examination Results from Bridge Deck Core Samples

Results from the petrographic examination came in two separate reports. The first contained results from the bridge deck core samples taken from the bridges near Maple Hill and Belvue, Kansas. The second report contained results from the bridge near Randolph, Kansas. In the CTL report, the core sent for examination from the Maple Hill Bridge is referenced as MH1 and the two core samples from the Belvue Bridge are referenced as BNT1, Belvue No Top 1 as discussed in section 4.5.4, and B1, Belvue 1. The report states there was no top surface distress with B1, but found closely spaced parallel cracking two inches below the top-surface. The core fractured along these planes when struck. With further microscopic examination, it was reported that these cracks were formed by cyclical freezing and thawing while saturated in non-air-entrained concrete. Estimated total air content of the core was less than 1%. The core BNT1 had similar hairline cracking below the top surface and was attributed to cyclical freezing and thawing of non-air-entrained concrete. Total air content was estimated to be less then 1% as well. However, BNT1 was reported to have a rough and distressed top surface caused by freezing and thawing cycles. The core MH1 was reported to be in good condition with no signs

of top distress and minimal cracking in the core of the body. The estimated air entrainment of the cylinder is 3 to 5%. Both B1 and BNT1 were found to be composed of lightweight, manufactured, expanded-shale coarse and fine-aggregates. MH1 was found to be composed of lightweight, manufactured, expanded shale with a siliceous sand fine-aggregate. The estimated water-to-cement ratio for the Belvue Bridge cylinders was 0.50 to 0.65, while the Maple Hill Bridge cylinder had an estimated water-to-cement ratio of 0.45 to 0.55. None of the cylinders showed signs of alkali-silica reactivity.

The three cores taken from the bridge near Randolph, C1S2, C2S3, and C3S4, were found to have rough top surfaces below the polymerized overlay, with many fractured aggregates. The cause could be surface preparation for the asphalt overlay or cyclical freeze-thaw cycles. The cores contained micro-cracking throughout the core that could be attributed to shrinkage. The estimated air content for cores C1S2 was 1 to 3% and 2 to 4% for the other cores. The air content of all the cores was reported to be entrapped not entrained. All samples from the bridge were composed of lightweight, manufactured, expanded-shale coarse and fine-aggregate. Additionally, the estimated water-to-cement ratio for all of the cores was 0.45 to 0.55.

7.2 *Large-Block Pull-Out Test Results*

Logan's 1997 article stated that during testing the following should be recorded:

- Maximum load the strand attains before dropping off
- Approximate load at first noticeable strand movement
- Approximate distance the strand pulls out at maximum load
- General description of failure

The data was recorded; the average failure loads, displacements, and standard deviations were computed, then compared with the minimum recommended values. Logan stated that 0.5-inch diameter strand with an average pull-out capacity exceeding 36 kips had transfer lengths meeting ACI and AASHTO requirements, while strand with a pull-out load less than 12 kips had transfer lengths greater than the code requirements. Logan has since recommended a minimum load of 16 kips at first observable slip and a maximum coefficient of variation (COV) of 10% (Peterman, 2007).

Figure 7-9 shows the average maximum load and the standard deviation for the six blocks tested. The only mix meeting the recommended minimum load to ensure acceptable transfer lengths was MQ-3. MQ-9 and KC-3 were only a few kips short of meeting the minimum load requirement. For each aggregate, the mix with a nine-inch slump had a lower average maximum pull-out force than the companion three-inch slump mix. Only the two Marquette mixes fell below the maximum coefficient of variation of 10% specified by Logan. KC-9 coefficient of variation was well outside of the maximum range at 25.0%.

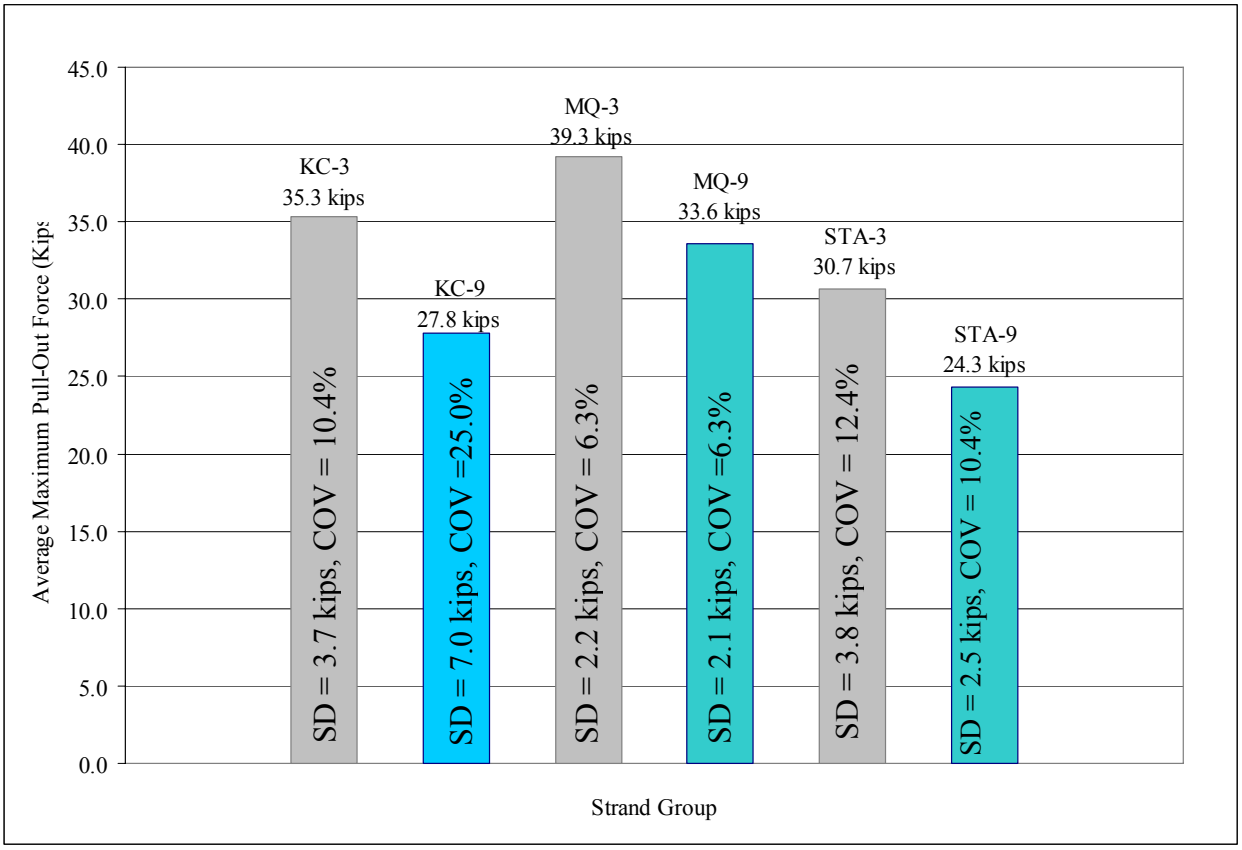

Figure 7-9 Average Maximum Force at Pull-Out

Figure 7-10 shows the average load at first observable slip of the strands. MQ-3 had the highest load at first slip, followed by STA-3 then KC-3. For all three aggregates, the mix with a three-inch slump had a higher load at first observable slip than the companion mix at nine-inch slump. Additionally, the difference in load at first slip between the three-inch slump and the nine-inch slump mix was the least for Marquette, followed by Kansas City, then Stalite.

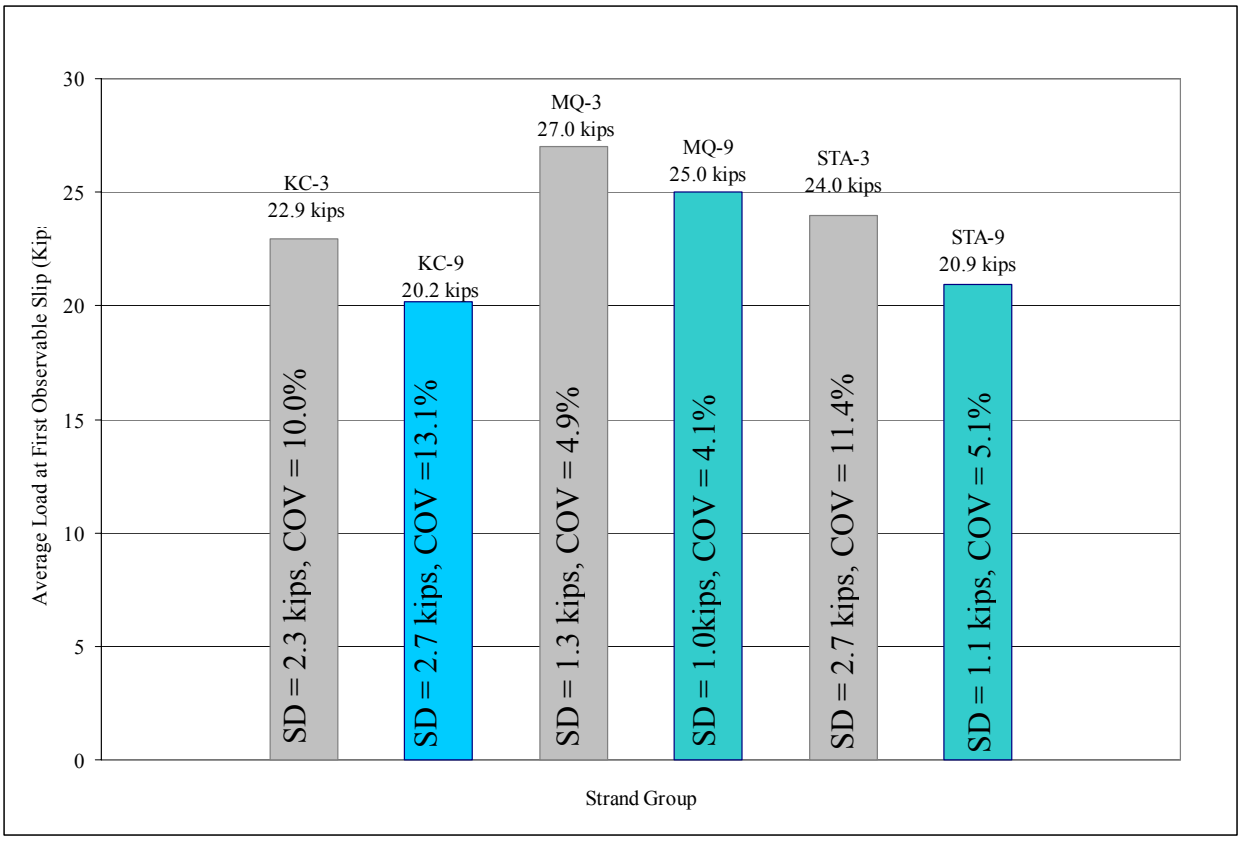

Figure 7-10 Average Load at First Slip

Figure 7-11 shows the average actuator displacement at first noticeable slip and pull-out force. It is important to note that the first slip was captured by visual inspection. Also, the displacements for all strands tested were zeroed at five kips to account for any "slop" in the load frame and to allow the bridge plate to seat on the concrete surface. All strands tested in this study experienced elastic stretch, gradual slip, followed by a sudden pull-out with load noise caused by the friction between the strand and the concrete block.

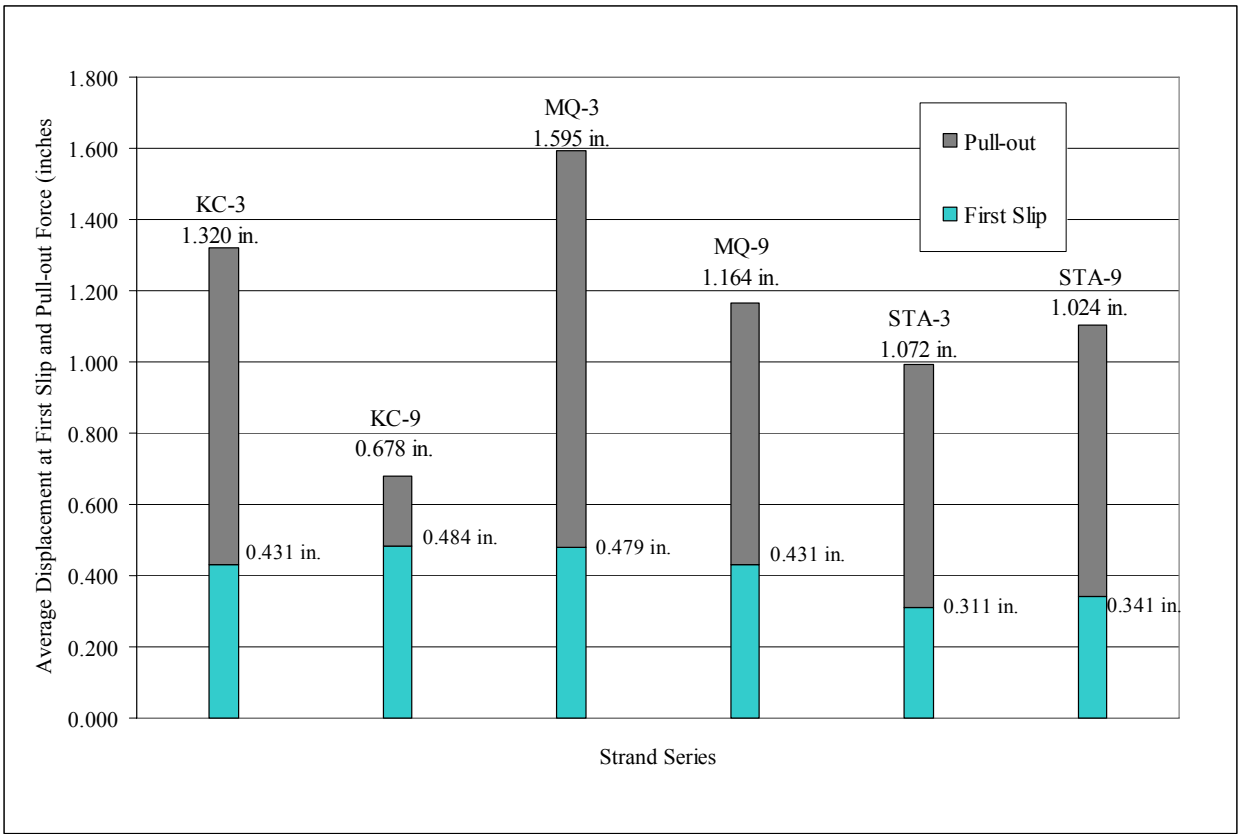

Figure 7-11 Average Actuator Displacement at First Slip and Pull-Out Force

Figure 7-12 shows the actuator displacement versus load for all blocks tested. In the figure, the displacements were averaged for all six strands at a given load. The displacements were zeroed at five kips for the reasons stated above. Since not of all of the strands reached the same maximum load for a given block, average displacements were taken for the strands that remained at a given load. Additionally, a five-point moving average was then taken to smooth the data. Despite the moving average, points of discontinuity still remained in the graph due to strands that pulled out at loads significantly higher or lower then the other strands in that block.

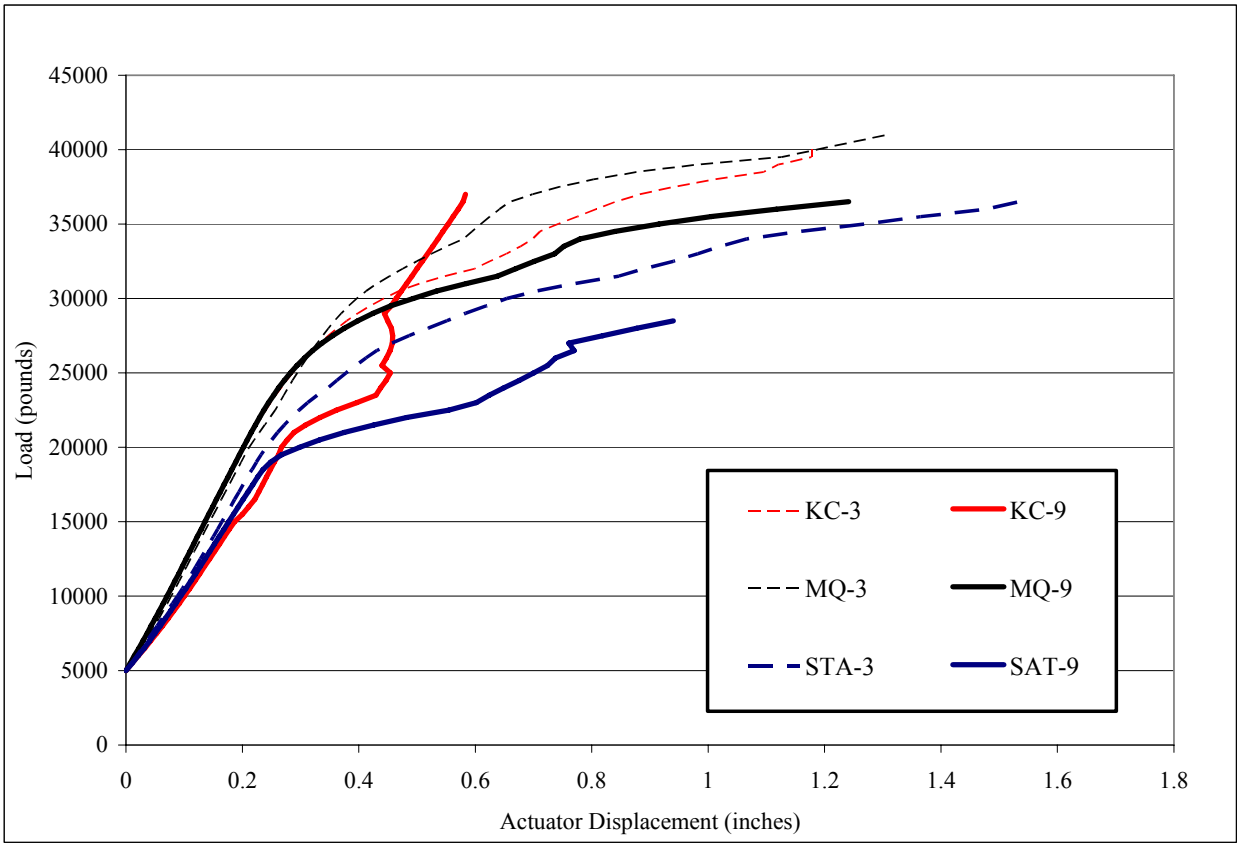

Figure 7-12 Average Displacement versus Average Load

After observing the high coefficient of variation found in average maximum load at pull-out, average load at first observable slip, and the points of discontinuity in the load versus displacement graph, the required data as stipulated by Logan and Figure 7-9 through Figure 7-12 were recalculated with only four strands per block, disregarding the strands with the highest and lowest maximum force at pull-out. Figure 7-13 shows the average maximum force at pull-out considering only four strands. Comparing Figure 7-9 and Figure 7-13, the average maximum force differs by one or zero kips for all blocks except for KC-9, which is five kips less in the four-strand average. KC-9 also has the highest coefficient of variation for both the four-strand and six-strand averages. The four-strand coefficient of variation for the blocks, except for the KC-9, fell below the minimum 10% specified by Logan. As in the six-strand average, only MQ-3 makes the recommended 36-kip minimum, with MQ-9 and KC-3 falling a few kips short of the specified minimum load.

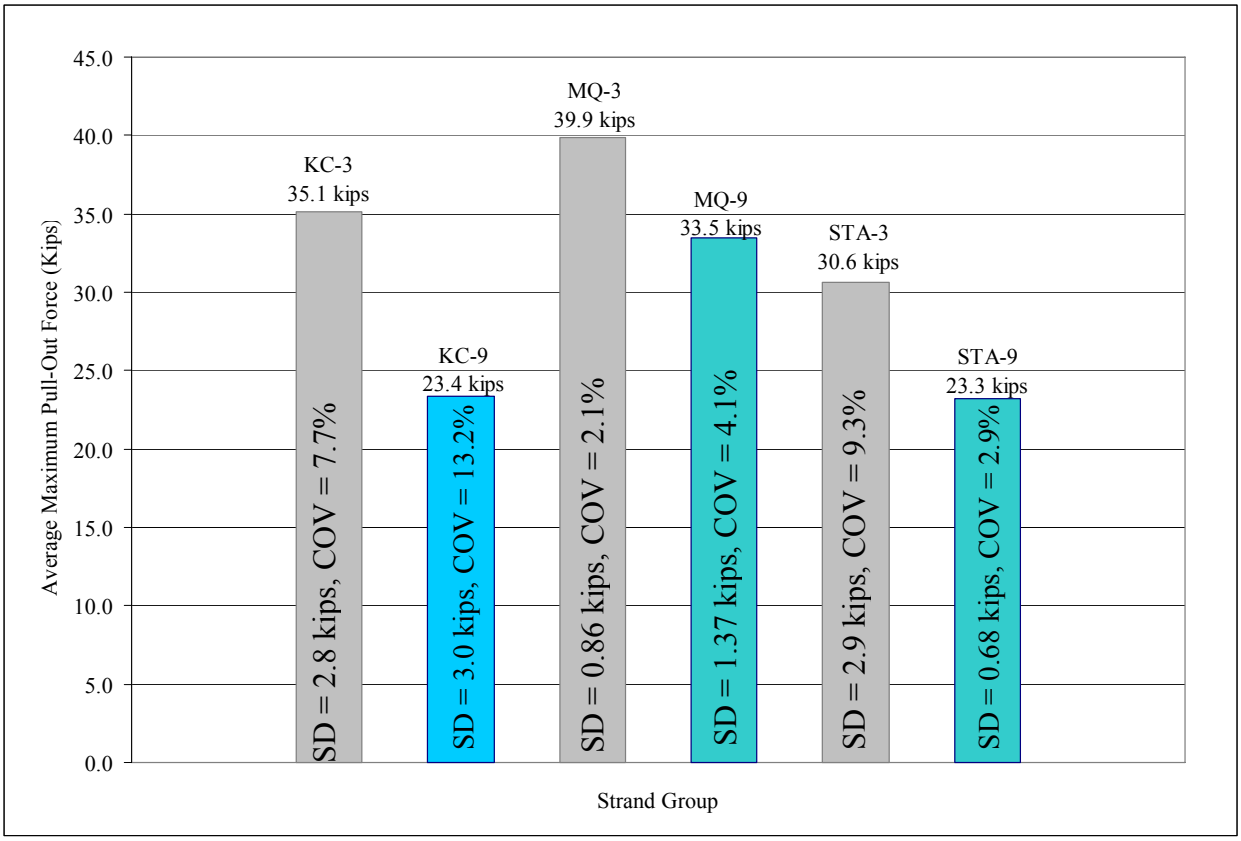

Figure 7-13 Average Maximum Force at Pull-Out (Four Strands)

Figure 7-14 shows the average force at first observable slip. All of the averaged loads were the same for the six-strand and four-strand averages except the KC-9, which increased 0.3 kips. The coefficient of variation decreased to 10% or less for the four strand averages except for KC-9. Figure 7-15 shows the average actuator displacement at first slip and at average maximum pull-out force. Figure 7-16 shows the actuator displacement versus load using only four strands. The same data treatment was used as in the six-strand plot. However, the curves were smooth and had fewer points of discontinuity. This provides a more predictable behavior for the bond capacity of each specimen.

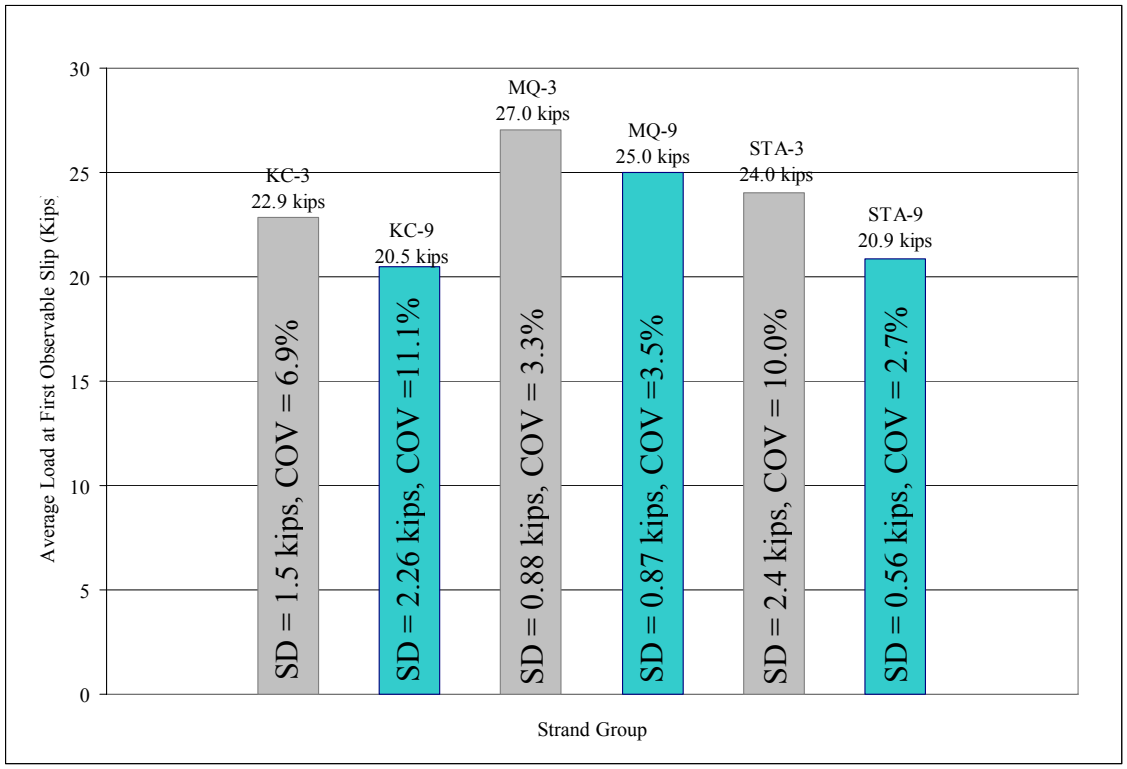

Figure 7-14 Average Load at First Slip (Four Strands)

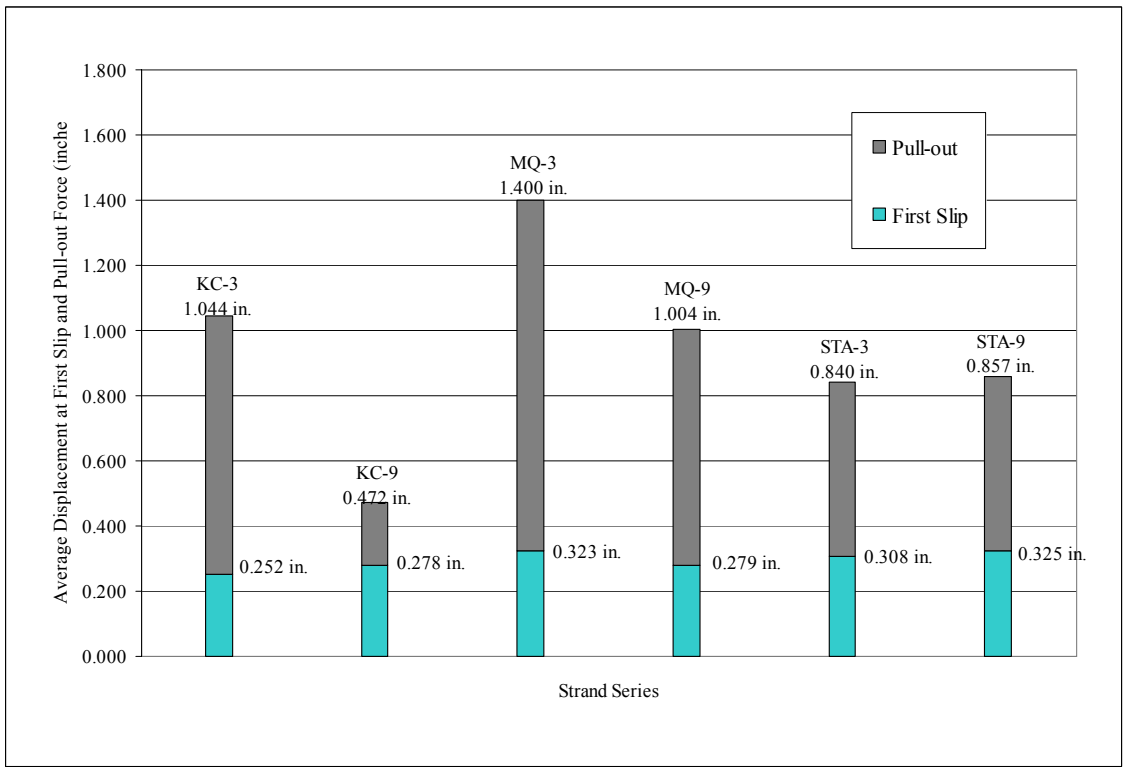

Figure 7-15 Average Actuator Displacement at First Slip and Pull-Out Force (Four Strands)

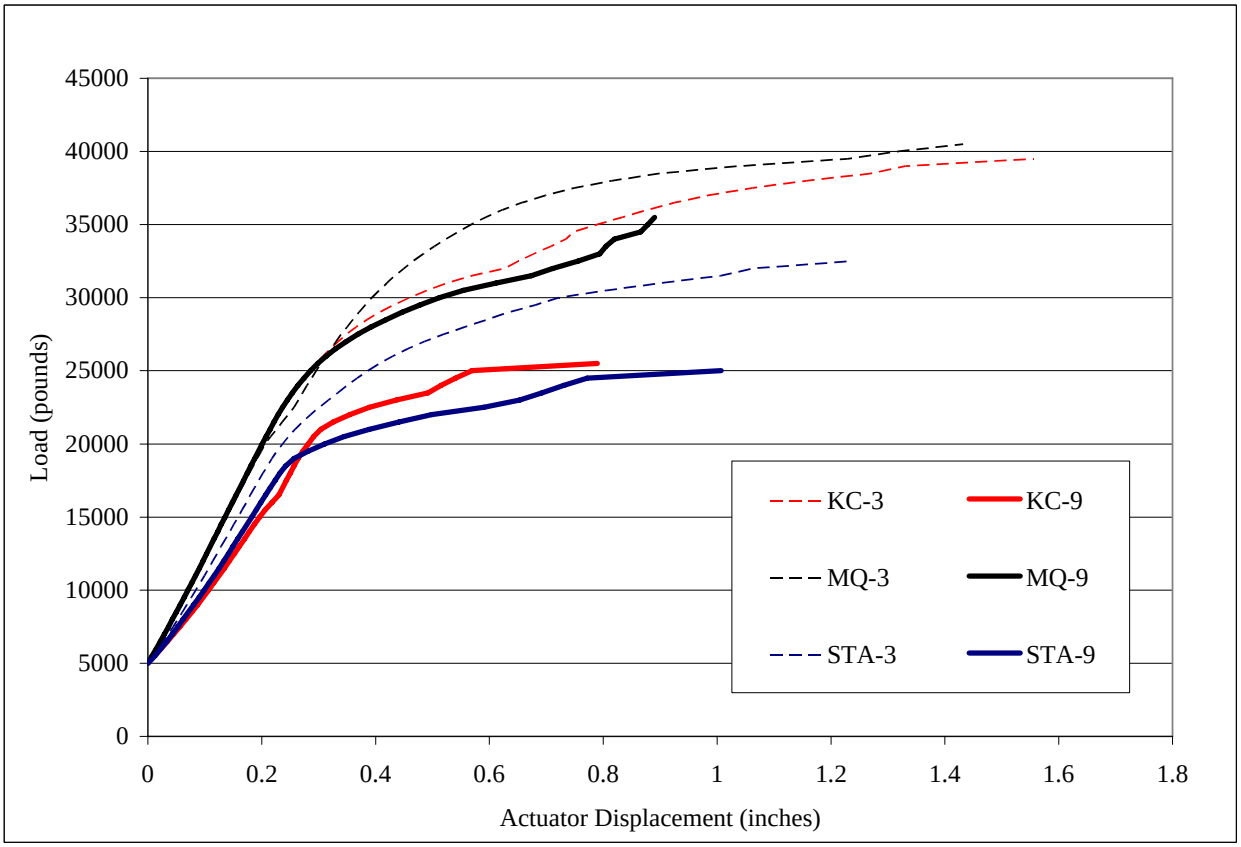

Figure 7-16 Average Displacement versus Average Load (Four Strands)

7.3 *Flexural Member Results*

As stated in chapter six, the flexural members were tested for transfer length with Whittemore points and end-slip readings. Additionally, the beams were mounted with LVDTs during loading at mid-span and on the ends of the members to capture deflection and strand slip during loading. Once loaded, the beams were marked and recorded for crack propagation at 85% and 100% of moment capacity. The following sections report results of those readings.

7.3.1 Flexural Member Strand-Force Results

When the strands were tensioned before casting, the strand for the full-development-length beam was pulled to 33 kips and the strand for the 80% development-length member was tensioned to 32.5 kips. After both strands were pulled and the chucks were power seated with the post-tensioning pump, both strands had a tension force of 29.5 kips. Due to relaxation of the strand and elastic shortening of the prestress bed, the two strands lost 0.10 to 5.0 kips. Table 7-6 shows the prestressing force just before detensioning for all flexural members.

Table 7-6 Flexural Member Strand Force before Detensioning

Coarse Aggregate	Slump (inches)	100% L_d Stand Force (pounds)	80% L_d Strand Force (pounds)
Kansas City	3	27,820	29,130
	9	28,180	29,940
Marquette	3	28,810	29,110
	9	28,500	29,110
Stalite	3	29,640	29,930
	9	30,480	29,600

7.3.2 Transfer-Length Results

As discussed in Section 6.5, transfer lengths were measured with the use of surface-strain plots. The 95% average maximum strain method prescribed by Russell and Barnes (1993) was utilized. Microsoft Excel was used to plot the strain profiles and the 95% average maximum strain along the length of the beams for each day's readings. A vertical line was projected down to the X-axis where the strain profile intersected the 95% average maximum strain value. The location on the X-axis where the vertical projection crossed was taken as the transfer length. Figure 7-17 shows KC-9 100% L_d as an example of how all the strain plots were treated to determine the transfer length. For each beam, development-lengths were found separately for both ends. Figure 7-18 shows the KC-9 100% L_d beam with the strain profiles for after detensioning; days 7, 14, 21; and before testing. In Appendix A, Figure A-4 through Figure A-14 show the strain profile for all other beams in the study. "End A" denotes the end detensioned second for the 100% development-length beams and "End A" denotes the end detensioned first for the 80% development-length members. KC-3 80% L_d was detensioned incorrectly providing a gradual release for end A and a harsh sudden release for end B. This can be seen in the strain profile at release for the member in Figure A-6. All of the plots show an increase in strain magnitude with time. However, the strains begin to converge at day 21 and just before testing, signifying the transfer lengths were stabilizing by the time of flexural testing. Additionally, the plots show a horizontal shift in the strain gradient with time indicating an increase in transfer length.

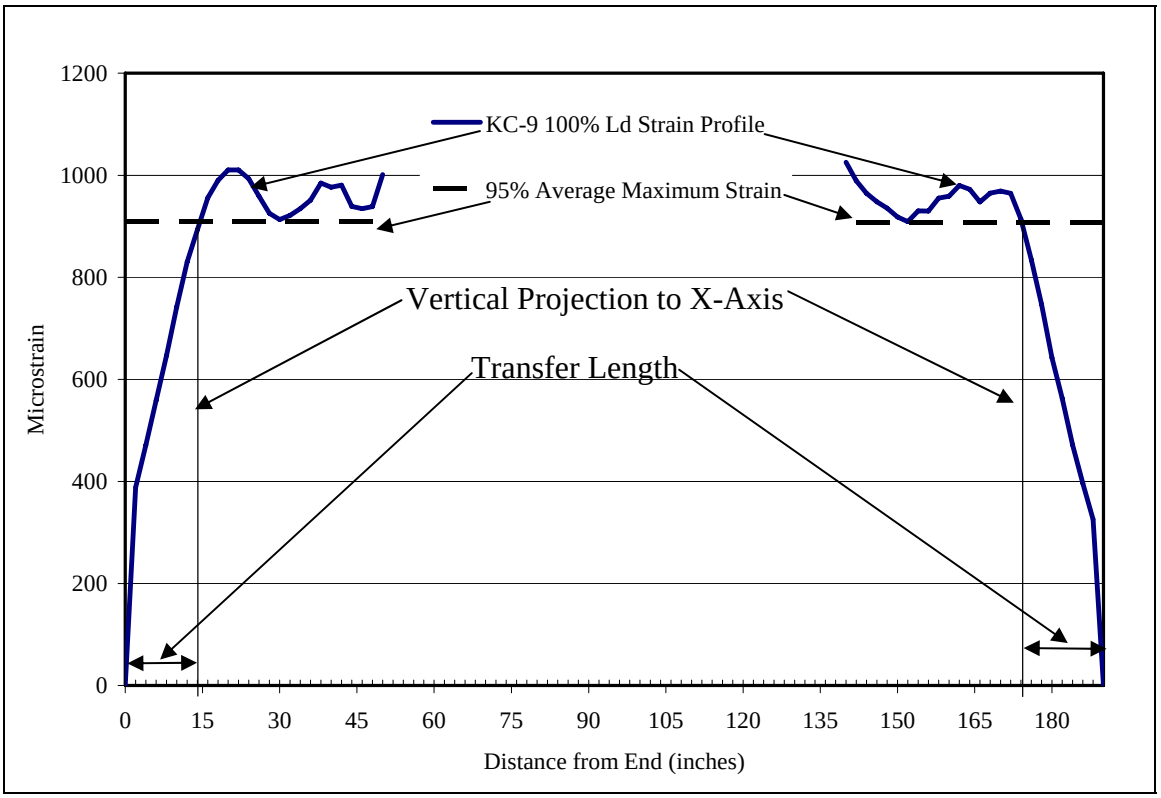

Figure 7-17 95% Average Maximum Strain Method Used to Determine Transfer Lengths

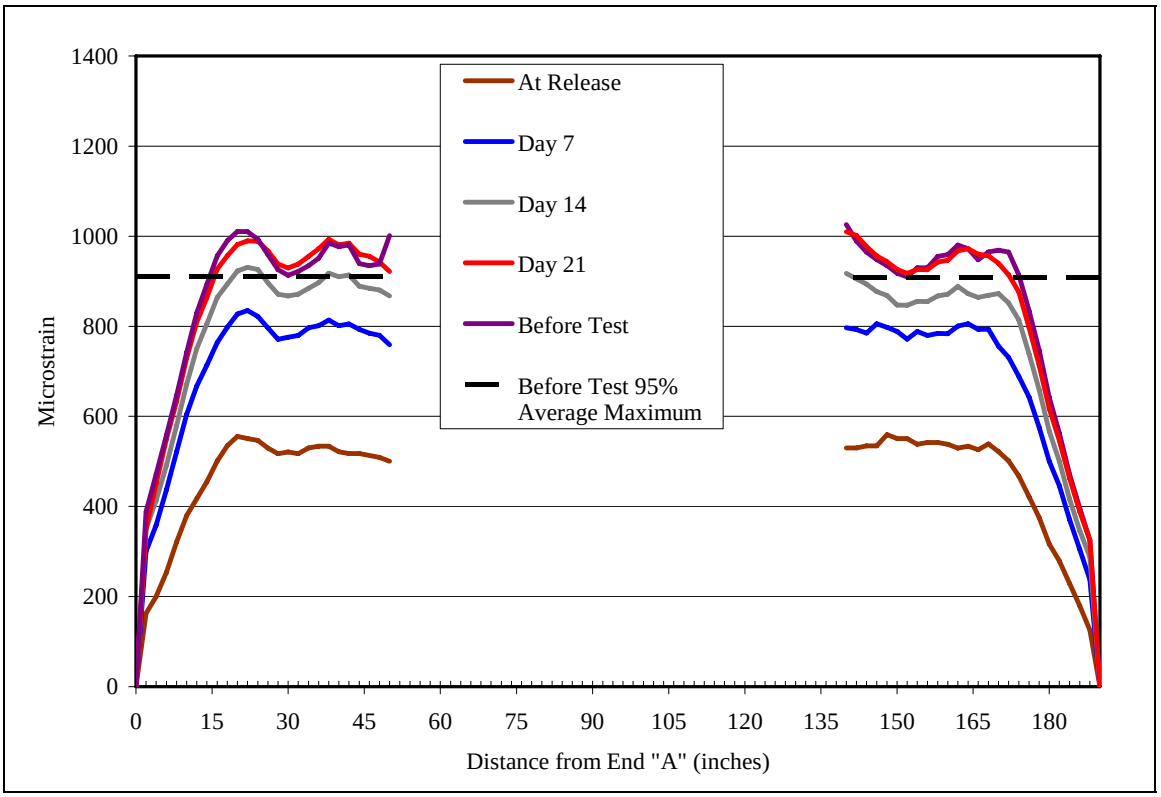

Figure 7-18 KC-9 100% L_d (Typical Strain Profiles)

Table 7-7 and Table 7-8 show the transfer lengths found with the 95% average maximum method. Table 7-7 gives the transfer lengths for the end detensioned first for 100% development-length beams, 80% development-length beams, and the two averaged together for each coarse aggregate at three-inch and nine-inch slumps. Table 7-8 presents the same data for the end detensioned second. The table shows that the transfer lengths are longer for the nine-inch slump mixes for each aggregate, except for STA-9 and STA-3 end detensioned first. Additionally, the end detensioned first had longer transfer lengths except for STA-9 and STA-3. The values reported were found with a three-point moving average that smoothed the strain profile as required by the 95% average maximum method; however, anomalies still existed in the data. In several cases, the 95% average maximum strain line intersected the strain profile at one of the outliers in the strain gradient, giving an inconsistent transfer length with respect to the reported values found on the days before and after it.

Table 7-7 Transfer Lengths 95% Average Maximum Method (End Detensioned First)

		100% L_d	80% L_d	Average Transfer Length
KC-9 f'_{ci} = 5903 psi	At Release	19	17	18
	Day 7	19	19	19
	Day 14	17	19	18
	Day 21	18	19	19
	Before Test	16	19	18
KC-3 f'_{ci} = - psi	At Release	12	27	20
	Day 7	14	26	20
	Day 14	18	27	23
	Day 21	18	28	23
	Before Test	17	20	19
MQ-9 f'_{ci} = 5615 psi	At Release	29	26	28
	Day 7	28	28	28
	Day 14	27	21	24
	Day 21	27	21	24
	Before Test	27	18	23
MQ-3 f'_{ci} = 5363 psi	At Release	16	18	17
	Day 7	15	19	17
	Day 14	14	20	17
	Day 21	15	20	18
	Before Test	15	18	17
STA-9 f'_{ci} = 5161 psi	At Release	17	18	18
	Day 7	17	17	17
	Day 14	17	17	17
	Day 21	17	16	17
	Before Test	17	17	17
STA-3 f'_{ci} = 5834 psi	At Release	18	18	18
	Day 7	21	17	19
	Day 14	21	16	19
	Day 21	21	17	19
	Before Test	22	16	19

Table 7-8 Transfer Lengths 95% Average Maximum Method (End Detensioned Second)

		100% Ld	80% Ld	Average Transfer Length
KC-9 f'_{ci} = 5903 psi	At Release	16	15	16
	Day 7	16	18	17
	Day 14	15	18	17
	Day 21	16	18	17
	Before Test	16	18	17
KC-3 f'_{ci} = - psi	At Release	11	11	11
	Day 7	16	14	15
	Day 14	12	10	11
	Day 21	13	15	14
	Before Test	12	14	13
MQ-9 f'_{ci} = 5615 psi	At Release	14	29	22
	Day 7	15	19	17
	Day 14	16	19	18
	Day 21	16	20	18
	Before Test	20	27	24
MQ-3 f'_{ci} = 5363 psi	At Release	13	13	13
	Day 7	12	15	14
	Day 14	13	16	15
	Day 21	12	15	14
	Before Test	12	15	14
STA-9 f'_{ci} = 5161 psi	At Release	20	24	22
	Day 7	18	29	24
	Day 14	18	29	24
	Day 21	18	30	24
	Before Test	17	30	24
STA-3 f'_{ci} = 5834 psi	At Release	22	23	23
	Day 7	19	22	21
	Day 14	19	21	20
	Day 21	19	23	21
	Before Test	19	23	21

The transfer length was also measured with end-slip readings as described in Section 6.6. The end-slip readings gave greater average transfer lengths before testing in all cases except for MQ-9 end detensioned first, where the two methods yielded equal transfer lengths. The data did not consistently show greater transfer lengths for either end. Additionally, the data did not yield consistent results between two slumps for a given coarse aggregate. The readings were sensitive to how the caliper was held, location on the beam the caliper was pressed against, and user

experience. Additionally, it was discovered the blade attached to the caliper that sat inside the notch on the strand began to bow. This deformation in the instrument could have given inconsistent results and skewed the data. Table 7-9 and Table 7-10 give the transfer lengths found using the end-slip method.

Table 7-9 Transfer Lengths from End-Slip Measurements (End Detensioned First)

		100% L_d	80% L_d	Average Transfer Length
KC-9 f'_{ci} = 5903 psi	At Release	19	22	21
	Day 7	19	21	20
	Day 14	19	21	20
	Day 21	19	21	20
	Before Test	19	22	21
KC-3 f'_{ci} = - psi	At Release	10	59	35
	Day 7	13	41	27
	Day 14	15	42	29
	Day 21	15	42	29
	Before Test	15	42	29
MQ-9 f'_{ci} = 5615 psi	At Release	30	14	22
	Day 7	32	14	23
	Day 14	33	14	24
	Day 21	33	15	24
	Before Test	32	14	23
MQ-3 f'_{ci} = 5363 psi	At Release	25	11	18
	Day 7	27	13	20
	Day 14	27	13	20
	Day 21	27	13	20
	Before Test	27	14	21
STA-9 f'_{ci} = 5161 psi	At Release	23	12	18
	Day 7	23	17	20
	Day 14	24	17	21
	Day 21	24	17	21
	Before Test	24	28	26
STA-3 f'_{ci} = 5834 psi	At Release	21	9	15
	Day 7	27	16	22
	Day 14	27	17	22
	Day 21	28	17	23
	Before Test	28	18	23

Table 7-10 Transfer Lengths from End-Slip Measurements (End Detensioned Second)

		100% L_d	80% L_d	Average Transfer Length
KC-9 f'_{ci} = 5903 psi	At Release	34	21	28
	Day 7	34	25	30
	Day 14	34	25	30
	Day 21	34	25	30
	Before Test	33	37	35
KC-3 f'_{ci} = - psi	At Release	13	15	14
	Day 7	17	18	17
	Day 14	18	18	18
	Day 21	19	18	19
	Before Test	20	19	19
MQ-9 f'_{ci} = 5615 psi	At Release	17	29	28
	Day 7	18	29	30
	Day 14	17	31	30
	Day 21	17	32	30
	Before Test	23	30	27
MQ-3 f'_{ci} = 5363 psi	At Release	14	16	15
	Day 7	16	18	17
	Day 14	15	20	18
	Day 21	15	20	18
	Before Test	20	19	19
STA-9 f'_{ci} = 5161 psi	At Release	34	25	29
	Day 7	32	26	29
	Day 14	33	26	29
	Day 21	35	26	30
	Before Test	35	26	31
STA-3 f'_{ci} = 5834 psi	At Release	24	21	23
	Day 7	32	29	30
	Day 14	32	30	31
	Day 21	32	31	31
	Before Test	32	32	32

7.3.3 Flexural Member Cracking

The crack pattern was recorded during loading at 85% and 100% of nominal-moment capacity. A black marker was used to trace the cracks at 85% of nominal capacity, and a red marker was used to trace further and new crack propagation at 100% nominal-moment capacity. Photos were then taken along the length of the beams to later diagram. Figure 7-19 shows MQ-3 80% L_d crack markings at nominal capacity; all other flexural members were recorded in the same manner. After testing, the crack propagation was plotted to give a relative comparison of crack magnitude and crack spacing. Figure 7-20 shows KC-9 100% Ld and KC-9 80% L_d crack diagrams. Figure A-15 through Figure **A-19** in Appendix A show the crack propagation diagrams for all other flexural members in the study. For the 100% development-length beams, the three-inch slump specimens experienced shorter crack spacing than the companion nine-inch slump specimens. However, KC-9 and STA-9 100% L_d specimens did not reach nominal-moment capacity, so the full crack pattern could not be diagramed. Comparing the 80% development-length beams, the same trend was found.

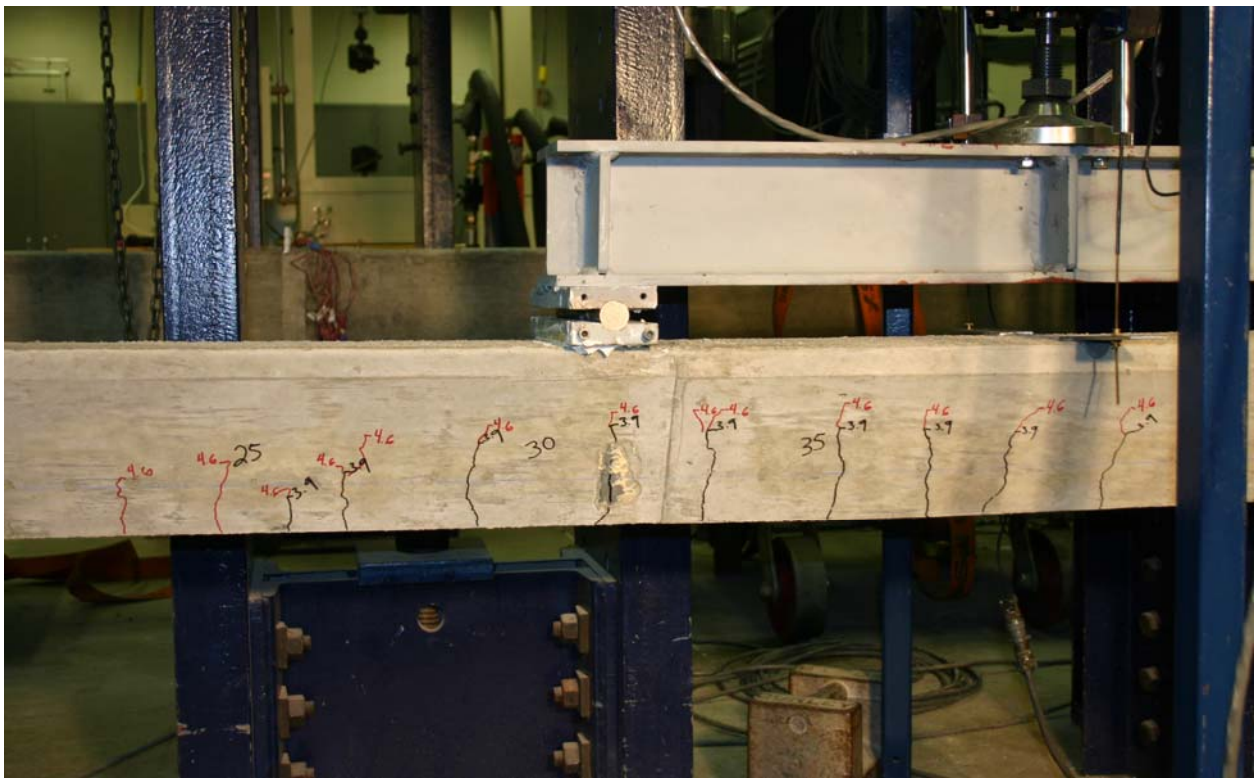

Figure 7-19 Typical Flexural Crack Markings

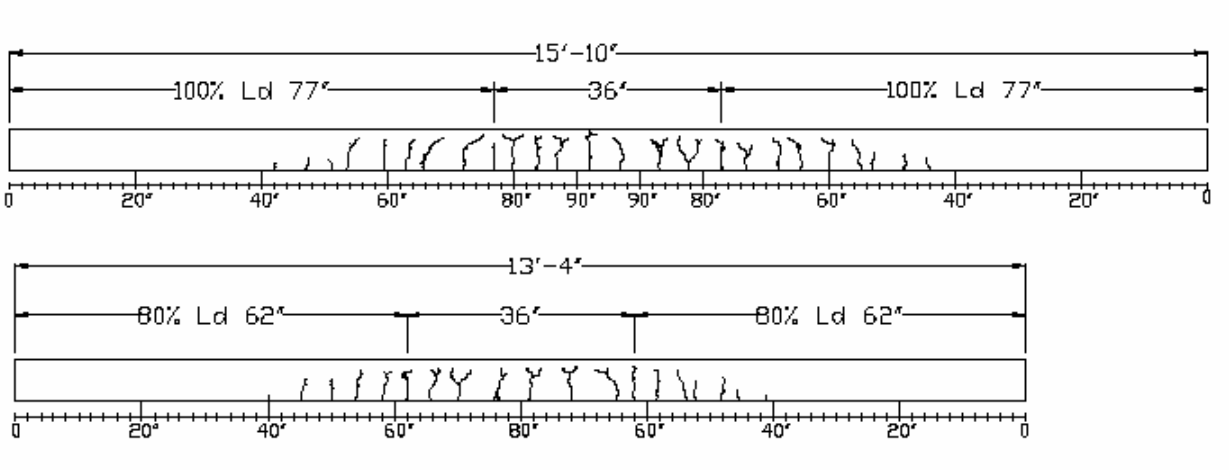

Figure 7-20 KC-9 100% L_d and KC-9 80% L_d Crack Propagation

7.3.4 Flexural Member Loading Results

The flexural members were tested with the MTS digitally controlled hydraulic actuator as described in Section 6.8. The member response obtained with the data acquisition was used to construct moment deflection and moment strand-slip plots. Each graph plots the results of a three-inch and nine-inch slump mix for a given coarse-aggregate and development-length. Figure 7-21 shows KC-9 and KC-3 100% development-length plots. Figure 7-22 displays results of KC-9 and KC-3 80% development-length beams. Figure A-20 through Figure A-23 in Appendix A show the moment-deflection curves for MQ and STA specimens. During testing, STA-3 100% L_d, the hydraulic actuator, rotated after the nominal-moment capacity had been reached. The test was stopped and the actuator was braced from rotating, and the beam was reloaded. The failure moment and deflection when the member was retested is shown on the graph with a square mark. Only KC-9 100% L_d and STA-9 100% L_d failed below nominal-moment capacity. Both beams failed in compression. Additionally, STA-9 80% L_d failed in shear as a result of strand slip after nominal-moment capacity had been reached. Table 7-11 gives a description of how each flexural member failed.

Due to the two failures, below nominal-moment capacity of KC-9 100% L_d and STA-9 100% L_d, a software package developed by Calvin Reed, former Kansas State University Master Student and later revised by Dr. Hayder Rasheed, associate professor at Kansas State University, was used to model the idealized behavior of the 100% L_d flexural members. The software was

written in Microsoft Excel and allows the user to input the beam's geometrical properties, loading conditions, strand stress, and hardened-concrete properties. The software imposes strain compatibility for a given load by iterations of the neutral axis. Additionally, the software continues the process until one of the input failure strains is reached. The software computes the deflections using the moment area theorem. The model considers changes in stiffness at the cracked portions of the member when numerically integrating the deflection. The experimentally found concrete material properties and strand stress was entered into the software to model the 100% L_d flexural members. The idealized behavior of the beams found using the software is shown in each moment-deflection plot and labeled "Analytical."

Table 7-11 Flexural Members Failure Description

KC-9 100% L_d	Compression Failure at Mid-Span
KC-3 100% L_d	Compression Failure at Mid-Span
KC-9 80% L_d	Compression Failure at Mid-Span
KC-3 80% L_d	Compression Failure at Mid-Span
MQ-9 100% L_d	Compression Failure at Mid-Span
MQ-3 100% L_d	Compression Failure at Crack Former
MQ-9 80% L_d	Compression Failure at Crack Former
MQ-3 80% L_d	Compression Failure at Mid-Span
STA-9 100% L_d	Compression Failure at Mid-Span
STA-3 100% L_d	Compression Failure at Mid-Span
STA-9 80% L_d	Shear Failure Caused by Strand Slip
STA-3 80% L_d	Compression Failure at Mid-Span

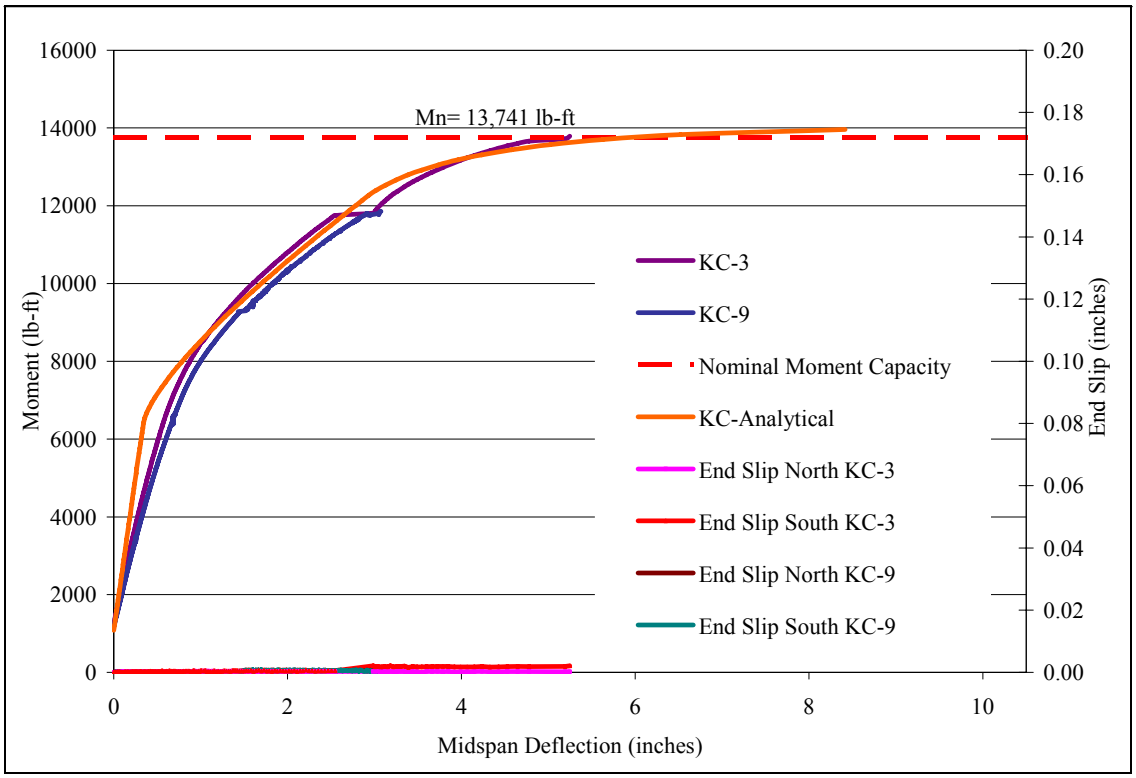

Figure 7-21 KC-9 and KC-3 100% L_d Moment-Deflection Curves

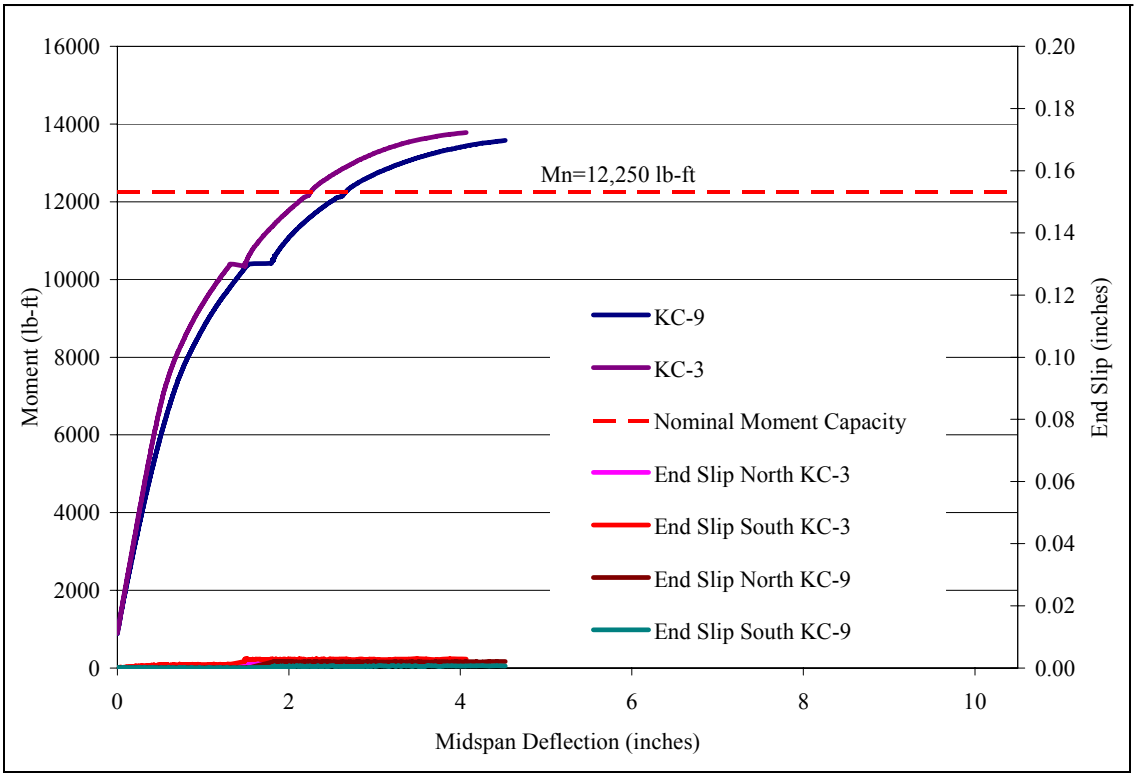

Figure 7-22 KC-9 and KC-3 80% L_d Moment-Deflection Curves

8 Discussion, Conclusions, and Recommendations

This section discusses the results reported in Section 7.0, and the conclusions and recommendations that can be drawn from them.

8.1 *Hardened Concrete Properties Discussion*

8.1.1 Compressive-Strength Testing Discussion

All concrete mixes met the specified 5000 psi compressive strength at 16 hours and the specified 28-day strength of 7000 psi. In addition to the compressive strengths reported in Table 7-1, many other cylinders were tested in the mix-design process. The Kansas City aggregate typically had higher coefficients of variation than comparable mixes made with the Marquette and Stalite aggregates. During compressive-strength testing, cylinders containing the Kansas City aggregate would begin to experience local aggregate failure at 50 to 75% of the failure load. This was detected by the "popping and cracking" noise heard during testing and the peak load dropping then regaining a new maximum load above the first peak. However, the early local aggregate failure did not affect the mix's ability to reach the specified compressive strength. All of the mixes experienced aggregate failure at the ultimate load in compressive-strength testing. The Kansas City mixes had the largest coarse-aggregate ratio as reported in Table 3-5. The local aggregate failure before the peak load at failure may be mitigated by decreasing the coarse-aggregate ratio for the Kansas City mix.

8.1.2 Split-Tensile and Modulus of Rupture Discussion

The split-tensile results shown in Table 7-2 can be used to predict the modulus of rupture according to ACI 318-05 Section 9.5.2.3. The predicted modulus of rupture found with Equation 7-1 is given in Table 7-3. The equation is used to predict the modulus of rupture for sand-lightweight aggregate in lieu of a specified split-tensile strength. If the split-tensile strength is specified or known, ACI recommends use of Equation 8-1 to calculate the modulus of rupture for lightweight mixes. The difference in the modulus of rupture using the prediction method of Equation 7-1 and the linear ratio of the split-tensile strength of Equation 8-1 is shown in Table 8-1. The method of predicting the modulus of rupture from Equation 7-1 yields greater values

then Equation 8-1. The brittle nature of lightweight aggregate used in the study is a likely cause for the lower values found using Equation 8-1. The brittle behavior is not as apparent in compressive-strength testing due to the nature of the test; however, it appears to be magnified in the split tensile-test. The ACI 318-05 equation used to predict the modulus of rupture, Equation 7-1, is a function of the compressive strength and therefore could over estimate the tensile capacity for concrete made with a brittle coarse-aggregate. If the constant 0.85 of Equation 7-1 is replaced with 0.76, the predicted modulus of rupture closely matches the values found with the split-tensile values.

$$f_r = 7.5\left(\frac{f_{ct}}{6.7}\right)$$

f_r = Modulus of Rupture for Lightweight Concrete Mixes 8-1

f_{ct} = Average Splitting Tensile Strength of Lightweight Concrete (psi)

Table 8-1 Difference in ACI 318-05 Methods to Specify Modulus of Rupture for Lightweight Concrete (psi)

Day	Marquette	Kansas City	Stalite
16-hour	13	59	106
3	130	78	26
7	35	39	0
14	82	99	22
21	-6	-3	28
28	66	19	102

8.1.3 Modulus of Elasticity Discussion

The experimental modulus of elasticity was different than the values predicted by ACI 318-05 Section 8.5 shown in Equation 7-2. The ACI value accounts for use of lightweight concrete in the unit-weight term of the function, but is also a function of the compressive strength. The commentary to ACI 318-05 Section 8.5 states that the modulus of the concrete is sensitive to the modulus of the aggregate and actual values vary from 80 to 120% of the predicted value. The experimentally found values differ from 79 to 101% of the predicted ACI 318-05 values. If the constant 33 of Equation 7-2 is changed to 29.75, the percent difference of

the ACI 318-05 equation and the experimental values range from 88 to 112%, with the majority of the values in the range of 93 to 105%. On the specified test days, for each mix, the experimental modulus of elasticity was on average 8.1%, 3.5%, and 9.7% less that the predicted values for KC, MQ and STA respectively.

8.1.4 Creep and Shrinkage Discussion

The ultimate creep coefficient, $v_{u,}$ found using the curve-fit method from ACI Committee 209 Report were 1.38, 1.32, and 1.36 for Kansas City, Marquette, and Stalite, respectively. The committee states that for "normal conditions," the average ultimate creep coefficient is 2.35 and the ultimate shrinkage strain is 780 $x10^{-6}$ inch/inch. The stated ultimate values were verified by two independent studies. One was carried out for 20 years on normal-weight concrete and the other was conducted with 479 creep data points and 356 shrinkage data points. The committee states that an estimated ultimate creep coefficient and shrinkage strain can be determined for concrete mixes based upon the ultimate values above and correction factors to adjust for conditions other than "normal", which the ultimate values were found under. The correction factors have shown to estimate the ultimate values for both normal and lightweight concrete mixes without consistent variation for either. The correction factors adjust the ultimate values for age at time of loading, volume-to-surface ratio, slump, percent fine-aggregate, cement content, air content, and humidity. Equations 8-2 and 8-3 show the prediction formulas for the ultimate creep coefficient and shrinkage strain. The correction factors shown in Equations 8-2 and 8-3 are the product of all applicable correction factors for conditions other than "normal" shown in Equations A-1 through A-12. The values obtained for each correction factor and the predicted ultimate creep coefficient and shrinkage strain of Equations 8-2 and 8-3 are shown in Table 8-2. The correction factors were found by substituting the specimen properties of the members used in the ACI-209 curve fit method. The relative humidity correction factor is an approximate average of the fluctuating humidity levels in the area where the creep and shrinkage specimens were stored. The values found for the ultimate creep coefficient from the ACI 209 predicted values with applicable correction factors differ from the values found with the curve-fit method described in Section 4.5.4. The difference in the ultimate creep coefficient from the two methods ranges from 0.42 to 0.02. The difference in the ultimate shrinkage strain from the two methods ranges from 19 micro-strain to 162 micro-strain. Despite the different values found

with the two methods, the values are in close enough agreement to serve the purpose of aiding the designer with values to predict the long-term creep and shrinkage behavior of structural members. Due to the large number of materials, member geometry, and environmental factors that can affect the creep and shrinkage, the goal is not to quantify the absolute creep and shrinkage values but to provide a good baseline value designers can use.

$$\upsilon_u = 2.35\gamma_c \qquad 8\text{-}2$$

$\upsilon_u =$ Ultimate Creep Coefficient

$\gamma_c =$ Product of Correction Factors

$$\left(\varepsilon_{sh}\right)_u = 780\gamma_{sh}x10^{-6}\,in/in \qquad 8\text{-}3$$

$\gamma_{sh} =$ Product of Correction Factors

Table 8-2 ACI 209 Predicted Creep Coefficient, Shrinkage, and Correction Factors

Correction Factor	KC Creep	KC Shrinkage	Maequette Creep	Marquette Shrinkage	Stalite Creep	Stalite Shrinkage
Time of Loading	$t_{la=}$ 28	$t_{la=}$ 28	$t_{la=}$ 28	$t_{la=}$ 28	$t_{la=}$ 28	$t_{la=}$ 28
Volume to Suface Ratio	v/s= 3.67	v/s= 3.67	v/s= 3.67	v/s= 3.67	v/s= 3.67	v/s= 3.67
Slump	s= 6.0	s= 6.0	s= 6.0	s= 6.0	s= 6.0	s= 6.0
Fine Aggregate Ratio	ψ= 56.1	ψ= 56.1	ψ= 61.0	ψ= 61.0	ψ= 61.0	ψ= 61.0
Cement Content	-	c= 725	-	c= 725	-	c= 725
Air Content	ά= 7.5	ά= 7.5	ά= 8.0	ά= 8.0	ά= 5.0	ά= 5.0
Relative Humidity	λ= 50	λ= 50	λ= 50	λ= 50	λ= 50	λ= 50
Product of Correction Factors	0.71	0.52	0.74	0.53	0.57	0.5
V_u ($\acute{\varepsilon}_{Creep}/\acute{\varepsilon}_{Elastic}$) or $(\acute{\varepsilon}_{sh})_u$ (με)	1.67	405.6	1.74	413	1.34	390

8.2 *Petrographic Examination Discussion*

The result of the concrete cores taken from existing bridge decks gave no clear indicator why the tested bridges expanded. Concerns that the locally used aggregates have expansive tendencies could not be attributed to alkali-silica reactivity or a physical property of the aggregate itself. However, the bridge deck at Belvue and Randolph, having significant cracking

concerns, were reported to have low air content. The bridge near Belvue had less than 1% of total air content and the bridge near Randolph had an air content of 1 to 4% of entrapped air. Additionally, both bridge decks were composed of a concrete mix containing a lightweight coarse and fine-aggregate. The bridge near Maple Hill had an air content of 3 to 5% and was composed of a sand lightweight mix. Cores from the bridge near Belvue had significant cracking that could be attributed to freeze-thaw action while saturated. The bridge near Randolph had similar cracking but the petrographic examination could not be deciphered if they were caused by freeze-thaw action or the milling process before the asphalt overlay was placed. However, KDOT personnel report the surface distress was present before the overlay was applied. The bridge near Maple Hill showed no top-surface cracking with minimal cracking in the body of the core. The reported expansion and poor performance of the Belvue and Randolph bridges could be caused by the freeze-thaw cycles of the decks with insufficient air entrainment.

8.3 *Large-Block Pull-Out Test Discussion*

As mentioned in Section 7.2, the only mix to meet the required average minimum pull-out force of 36 kips, specified by Logan, was MQ-3 as shown in Figure 7-9. KC-3, MQ-9 and STA-3 were close to the minimum load, achieving an average maximum pull-out force of 35, 34, and 31 kips, respectively. Logan cited that strands, using a single control mix, having average maximum pull-out force of 36 kips or greater, met ACI and AASHTO design transfer lengths. Additionally, Logan's flexural members cast with strand meeting the minimum 36-kip load failed in strand rupture and had ample deflection before failure. Only three surface-strain plots of the flexural members in this study yielded transfer lengths, based on the 95% average maximum strain method, greater then the ACI and AASHTO design values, the rest were below the design value of 28 inches. All flexural members in this study showed ample deflection before failure, even when failure was below nominal-moment capacity. Using the control strand obtained from Logan, all of the three-inch slump mixes had a higher pull-out force than the companion nine-inch slump mix. This phenomenon was mirrored in the flexural testing where the three-inch slump mixes had a higher moment capacity than the companion nine-inch slump mix. MQ-3, achieving the highest force at pull-out, exhibited the greatest moment capacity of the full-development-length flexural members. MQ-9 falling two kips short of the recommended 36-kip force had a flexural capacity considerably greater than the design capacity. However,

KC-3 and STA-3 falling one and five kips short of the recommended 36 kips, failed just above the design-moment capacity. The mixes having the lowest average maximum pull-out force, KC-9 at 28 kips and STA-9 at 24 kips, had full-development-length flexural specimens failing below nominal-moment capacity.

The six LBPT decreased in average load at first slip in the same order as the six mixes decreased in moment capacity for the full-development flexural members. There was a 2.8-kip difference in average load at first slip between STA-3 and KC-3, shown in Figure 7-10. The full-development-length flexural members corresponding to these two mixes had virtually the same moment capacity. KC-3 had a 0.7-kip greater average load at first slip than STA-9, but had an 1138 lb-ft greater moment capacity. Even though average load at first slip decreased in the same order of decreasing-moment capacity, a linear ratio was not shown between the two. Comparing two mixes with the same strand, the average force at first noticeable slip only gives an approximate comparison of the mix's flexural capacity.

The average strand displacement at first noticeable slip is determined through visual inspection, which creates subjective results. The displacements were also zeroed at a load of five kips to account for seating and imperfection of the load frame. The subjective determination of first slip and the zeroing of displacement for all specimens at the same load does not make the displacement at first slip a good indication of bond capacity. However, if the displacement at first slip is viewed as a percent of the total displacement at maximum pull-out force, the effects of zeroing at five kips is divided out and provides the same relative datum. Thus, the displacement is only subject to the error of observable slip. When this was done, the displacement at first slip accounted for 71.3% of the total displacement for KC-9, while the other mixes ranged from 29 to 37%. STA-9 100% L_d flexural member failed below nominal capacity, but the percentage of displacement at first slip to total displacement was only 33.3% for the LBPT. A low percentage of displacement at first slip may not guarantee good bond, but a high percentage may be an indication of inferior bond capacity.

The amount of total displacement at average maximum pull-out force is only subject to the error of zeroing the displacements at five kips. However, no consistent correlation could be found between maximum displacement and average maximum force.

Analyzing the data for average maximum force at pull-out and average load at first slip with four strands, disregarding the strands with the highest and lowest loads, yields average loads

almost identical to the six-strand average. This is evident by comparing Figure 7-9 and Figure 7-13, and Figure 7-10 and Figure 7-14. Figure 7-11 and Figure 7-15 give the displacement at first slip and pull-out for the six-strand and four-strand averages, respectively. The averages change between the two figures; however, the relative displacement of the different blocks is similar. The four-strand percent of displacement at first slip to the overall displacement is tightly grouped in the range of 23 to 38% for all blocks except KC-9 that has a larger ratio of 58.9%. The six-strand data gave this same grouping with the KC-9 outlier. The four-strand values also provided smaller coefficient of variations as shown in Figure 7-13 and Figure 7-14. The complete bond failure that takes place after initial slip occurs is a dynamic process that can be unique to each strand in a given block. The two mechanisms that provide bonding capacity after adhesion is broken, frictional resistance and mechanical interlock, can be affected by the ambient conditions of the concrete. The frictional resistance can vary based upon roughness of the paste next to the strand and small paste particles that break and provide wedging action between the strand and the surrounding concrete. The mechanical interlock provided by the bearing surface between the helix-shaped strand and molded concrete can vary based upon the strand twisting as it pulls out of the block or shearing of the concrete-bearing surface as it pulls out. Adding to the complexity, higher frictional resistance could dictate whether the strand twist around a bearing surface or shears through it. The complex nature of de-bonding is the likely contribution to the high coefficient of variation found in the LBPT. The data set obtained by disregarding the highest and lowest bonding strand of a six-strand test provides more predictable bond behavior evident by comparing Figure 7-12 and Figure 7-16. The linear portions of the curves in Figure 7-12 and Figure 7-16 represent the elastic stretch of the strand until first slip occurs. The non-linear portions of the curves in Figure 7-12 have several points of discontinuity, which does not model the physical process of smaller changes in load resulting in greater displacement due to less bonding surface as the strand pulls out of the block. Figure 7-16 have several small points of discontinuity in the non-linear portions of the curve but does not result in abrupt changes in the direction of the curve. The four-strand average actuator displacement versus average-load curves in Figure 7-16 shows the trend expected of the physical process taking place in the LBPT.

8.4 *Flexural Member Discussion*

8.4.1 Transfer-Length Discussion

The two methods of measuring transfer length, 95% average maximum and end-slip measurements, yielded different values. The end-slip measurements gave longer transfer lengths in almost all readings. As mentioned in Section 7.3.2, accuracy of the transfer lengths based on end-slip measurements is dependent on operator experience and consistency. Additionally, the bar on the micrometer that sat in the strand notch began to bow midway through testing. It was not reset due to concerns of loosing the zero point of the test already in progress. The surface strain measurements, 95% average maximum method, gave more consistent results and are dependent on 25 readings per transfer length, and thus are less sensitive to one individual reading.

The transfer lengths reported in Table 7-7 and Table 7-8 were found strictly on the procedure described in Section 7.3.2. Therefore, any anomalies that still existed in the smoothed-strain profile gave transfer lengths that were uncharacteristic of the transfer lengths found on the days before and after the value. Despite some anomalies in the data, the average transfer length was greater for the end detensioned first for the KC and MQ beams, except the MQ-9 before test which was one inch greater for the end detensioned second. Despite efforts to give both ends a sudden release, the end detensioned second experienced some relaxation when the opposite end was cut, thus resulting in a more gradual release. However, the beams cast with Stalite had greater transfer length for ends detensioned second for the majority of the readings. STA-9 100% L_d and STA-3 100% L_d had transfer lengths three to zero inches longer for the end detensioned second. STA-9 80% L_d and STA-3 80% L_d had transfer lengths 14 to five inches longer for the end detensioned second. All of the STA beam series tensioning, casting, and detensioning procedures were the same as the MQ and KC beams series. The rheological and hardened concrete properties provided no evidence why the end detensioned second had greater transfer lengths for the STA beam series.

Studying Table 7-7, 95% average maximum method end detensioned first, the average transfer length was greater for the KC-3 beams than the KC-9 beams. The average is misleading because KC-3 80% Ld was detensioned incorrectly causing a harsh transfer for the end detensioned first and gradual transfer for the second end. Thus comparing KC-9 80% L_d and

KC-3 80% L_d from Table 7-7 is unrealistic. The table does show that KC-9 100% L_d had initial transfer lengths greater then KC-3 100% L_d, but later began to converge. Both beams had transfer lengths below the ACI 318-05 equation of 28 inches and AASHTO equation of 30 inches shown in Appendix B. The MQ-9 beam series had average and individual transfer lengths greater than the MQ-3 beam series. For the days reported, MQ-9 100% L_d had transfer lengths between 27 and 29 inches. Despite the higher transfer lengths, MQ-9 was the only 100% L_d beam cast with a nine-inch slump to reach nominal-moment capacity. The table also shows that the average transfer length was greater for the STA-3 beams series than the STA-9 series. Comparing the 80% L_d Stalite beams, the transfer lengths are within one inch on the days reported. STA-3 100% L_d had a longer transfer length by one to five inches than the STA-9 100% Ld beam. However, STA-9 100% L_d did not make nominal-moment capacity.

Comparing the average and individual transfer lengths for the nine- and three-inch slump beams from Table 7-8, the transfer lengths were greater for the beams cast with a nine-inch slump concrete. However, none of the averaged transfer lengths were above the calculated 28 and 30 inches. Individually, STA-9 80% L_d had transfer lengths exceeding 28 inches. This was also the only beam to experience end slip during flexural testing. The end slip occurred after nominal-moment capacity was reached on the end with a transfer length greater then 28 inches, as shown in Figure A-23.

It is the author's belief that when comparing transfer lengths with the 95% average maximum method, the difference should be greater than five inches to substantiate any difference between the two. This is due to the nature of the method as described in Section 7.3.2 and the correlation of strand strain with surface strain. The end-slip method to measure transfer length has proven an effective means of capturing transfer length in many other studies. Due to the initial inexperience and issues with the tool, the end-slip readings in this study could not reliably be used to report the transfer length.

8.4.2 Flexural Testing Discussion

Two of the six full-development-length flexural specimens did not make nominal-moment capacity. The members not making the design strength, KC-9 100% L_d and STA-9 100% L_d, were beams cast with a nine-inch slump. The companion full-development-length, three-inch slump members to these two beams reached nominal-moment capacity and failed immediately afterwards as shown in Figure 7-21 and Figure A-22. The two nine-inch slump beams not attaining the nominal moment capacity failed at 86% and 94% of nominal moment capacity for KC-9 and STA-9 respectively. The strength reduction factor, φ, which would be applied in design, was 0.90 for the flexural members in this study. Both MQ-9 100% L_d and MQ-3 100% L_d achieved flexural capacities considerably higher than the design strength of 13,741 lb-ft shown in Figure A-20. All of the 80% development-length flexural members made nominal-moment capacity of 12,250 lb-ft. All of the specimens cast with a three-inch slump were able to sustain a higher moment than the companion nine-inch slump beam. Five of the six 80% L_d flexural members failed in compression except for STA-9 80% L_d, which failed in shear due to strain slip above nominal-moment capacity.

The design capacity of the flexural members was based upon the maximum prestressing force of 0.74 f_{pu} immediately after prestress transfer from ACI 318-05 Section 18.5.1 and prestress losses from the PCI. Due to safety concerns and elastic shortening of the prestress bed, the actual prestress force was lower than the 0.74 f_{pu}. The actual values of prestress force at release are given in Table 7-6**.** Additionally, the modulus of elasticity was estimated by Equation 7-2, which over estimated the experimentally found values reported in Table 7-4. The design capacity was also based upon f'_c on 7000 psi; greater compressive strengths were actually reached. Table 8-3 gives the design-moment capacity using the experimentally determined strand stress at release, modulus of elasticity, and compressive strengths with PCI losses to calculate the effective prestressing force. The table also gives the maximum moment attained during flexural testing.

Table 8-3 Design-Moment Capacity with Experimental Concrete Properties Values and Experimental-Moment Capacity

	Design Capacity Based Upon Actual $F_{ps,}$ F'_c and E_c (lb-ft)	Experimental Maximum Moment Capacity (lb-ft)
KC-3 100% L_d	13766	13786
KC-9 100% L_d	13769	11870
KC-3 80% L_d	11979	13783
KC-9 80% L_d	12102	13580
MQ-3 100% L_d	13848	14850
MQ-9 100% L_d	13486	14458
MQ-3 80% L_d	12035	15436
MQ-9 80% L_d	12035	14312
STA-3 100% L_d	13980	13787
STA-9 100% L_d	13984	13000
STA-3 80% L_d	12269	13783
STA-9 80% L_d	12218	12687

The superior performance of the of the three-inch slump flexural members compared to their companion nine-inch slump beam could be related to the fluidity of the mix at the time of casting. Once the concrete is cast, the free moisture in the mix rises to the top of the fresh concrete. As the water rises to the top, some of moisture could get trapped around the bottom of the strand. The amount of moisture trapped around the strand would then be dependent on the time it takes to reach initial set and the amount of free moisture in the mix. If the trapped water around the strand weakens the paste adjacent to it, this could affect the mechanical interlock and frictional forces developed between the strand and the paste. Fluid mixes have more free moisture and take longer to reach initial set. Therefore, due to increased trapped moisture, fluid mixes could have inferior bond capacity compared to low-slump mixes.

Both beams not attaining the nominal-moment capacity with the specified concrete properties, KC-9 100% L_d and STA-9 100% $L_{d,}$ failed in compression with no strand slip at the ends of the member. The design failure mode of the beams was crushing of the concrete at the ACI-recommended maximum concrete strain of 0.003. ACI 318-05 Section 10.2.3 sets the

maximum usable strain in concrete at 0.003, but the commentary to the section recognizes that maximum strain in compression can range from 0.003 to higher than 0.008 under special conditions. In an additional study not covered in this report, lightweight SCC beams of the same cross section, same lengths, same control strand, and same loading condition were tested. The beams were cast with Kansas City and Marquette coarse-aggregate. The only change to the concrete mix designs used in the study was the higher dosage of the superplasticizer to achieve the SCC condition. Also, a set of SCC beams with Kansas City and Marquette coarse-aggregate were cast with a retarding admixture to delay the set time. A total of eight SCC beams were cast and tested in the study. Four were cast with Kansas City coarse-aggregate, one set at 100% L_d and 80% L_d without a retarder and one set with a retarder. The same four beams were cast with the Marquette aggregate. The Stalite aggregate was not used in the additional study. The beams in this study were mounted with strain gages on the strand before casting and strain gages on the extreme compression fiber during flexural testing. All four 100% L_d beams failed in this study at a compression strain above 0.003 and below or at nominal-moment capacity. All four had a compression-failure mode similar to the beams failing below nominal-moment capacity in this study.

A possible explanation for the compression failures below nominal-moment capacity is localized bond slip without end slip of the strand. In the additional study, it was shown that the flexural members were failing at strain levels above the design maximum of 0.003, but below or at the design-moment capacity. If local bond failure occurs, then the strand stress will decrease. In order to sustain the demanded load, the moment arm between the strand and the centroid of the compression block increases. This results in a shallower depth of compression block and increased strain at the extreme compression fibers. If the strand stress continues to decrease, the moment arm increases to a depth that causes the compression block to fail. This phenomenon is shown in Figure 8-1 in a beam cast with Kansas City aggregate and a high dosage of superplasticizer to achieve an SCC mix and a retarder admixture to delay the set. The other concrete mix properties, cross section, loading conditions, and length were identical to the KC 100% L_d beams in this study.

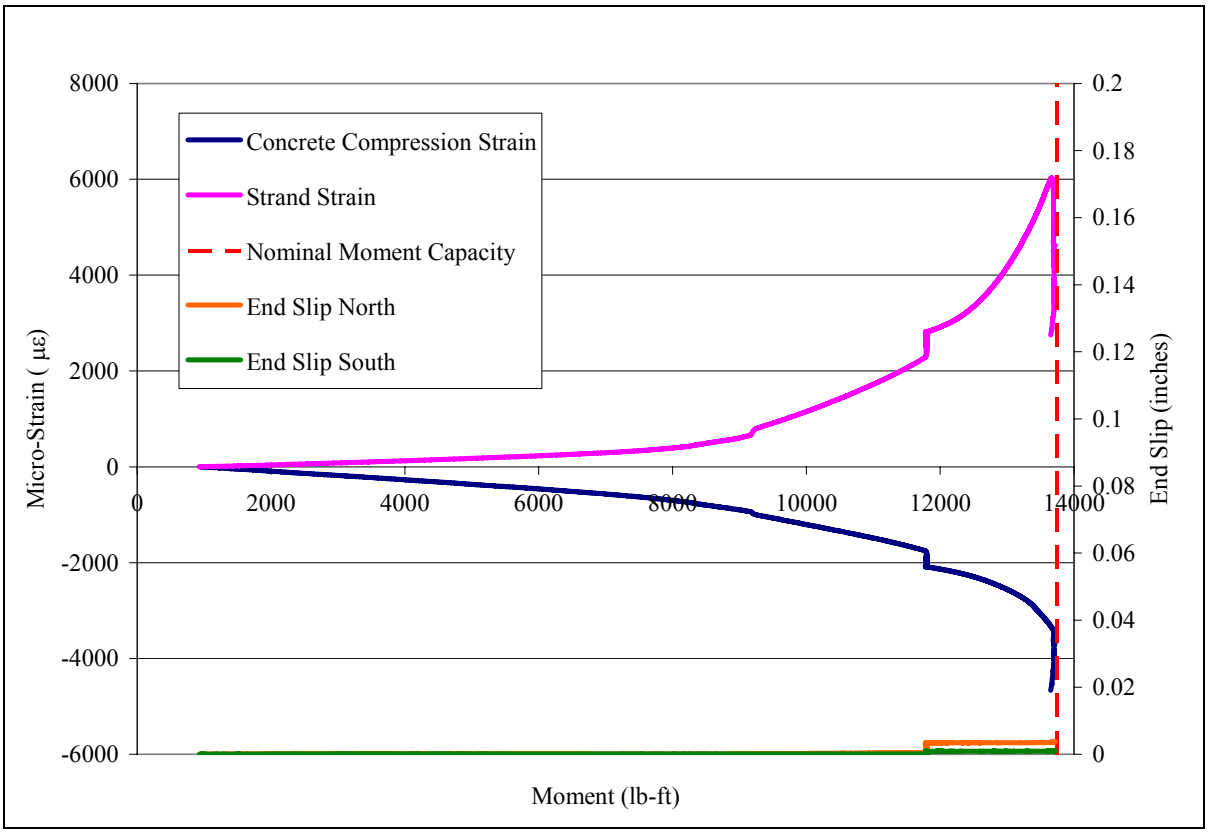

Figure 8-1 Flexural Test Displaying Possible Local Bond Failure

If local bond slip is occurring, the exact mechanism causing it is unclear. Additionally, the beams with underdeveloped strand, which could exaggerate the local bond slip, did not fail below the nominal-moment capacity. The superior performance of the 80% L_d beams may be a function of the actual development-length and the loading conditions of the test. If the actual full-development-length was shorter then the ACI 318-05 underdeveloped length of 62 inches, the 80% L_d beams are rotationally stiffer in the constant-moment region than the 100% L_d members due to the shorter length. Adding to the superior performance of the 80% L_d beams is the reduced maximum stress allowed in the strand due to the ACI 318-05-defined, underdeveloped strand. The reduced maximum stress, therefore, decreased the allowed-moment capacity. However, the 80% L_d beams attained moment capacities close to or exceeding the 100% L_d moment capacity except for STA-9. This suggests that the actual development is close to 62 inches for 80% Ld members, exceeding the 100% L_d design-moment capacity, and between 62 and 77 inches for 80% L_d beams failing at a moment capacity between the 80% L_d and 100% L_d design capacity.

Comparing the moment deflection curves for the 100% L_d and 80% L_d beams for each coarse-aggregate, the 100% L_d beams exhibited more creep deflection during the 24-hour hold of 85% of nominal-moment capacity. The creep deflection increased the strain in the compression block and strand for both development-lengths. The amount of creep strain experienced in the compression blocks during the 24-hour hold reduced the amount of strain increase the beams could have experienced after the hold up to failure. The amount of creep strain caused by the 24-hour held deflection increased from zero at the support to a maximum at the constant-moment region. Local bond failures may have occurred in the portions of high-creep strains, close to the constant-moment region, during the 24-hour hold due to the difference in elastic modulus between the strand and the surrounding concrete. The amount of slip would have depended upon the mechanical interlock and friction between the strand and the surrounding concrete. However, slip may not have occurred at the ends of the members due to the low levels of creep strain. This could be a possible explanation of a localized bond failure without end slip. The nine-inch slump 100% L_d beams, KC and STA, experienced more creep deflection then MQ, which did not fail below nominal-moment capacity.

The analytical model used to predict the moment-deflection behavior of the 100% L_d beams matched the experimental results relatively well for the members that reached nominal-moment capacity. The model over estimated the initial stiffness of MQ and STA beams but closely matched the stiffness of the KC beams. Actual and analytical results diverged at the hold of 85% of nominal capacity for 24 hours. At nominal-moment capacity, the experimental and model behavior converged and matched closely. The beams making nominal-moment capacity behaved in a manner that the model, based upon strain compatibility and moment-area-theorem, could accurately predict.

The entrained-air content of the nine-inch slump beams was greater than the three-inch slump beams. This was caused by allowing the concrete to continually mix until the desired slump was reached. The air content of the mix reduced during the increased mixing period. The difference in air content was 2.0% for KC-9 and KC-3 beams, 1.5% for MQ-9 and MQ-3 beams, and 3.5% for STA-9 and STA-3 beams as shown in Table A-1 through Table A-3. The difference in moment capacity for the 100% development-length members was 1919 lb-ft for KC beams, 392 lb-ft for MQ beams, and 787 lb-ft for STA beams. The difference in moment

capacity for the 80% development-length was 203 lb-ft for KC beams, 124 lb-ft for MQ beams, and 96 lb-ft for STA beams. The difference in air content did not increase consistently with difference in moment capacity when comparing both the 80 and 100% development-length beam series. Therefore, it is unlikely that the small difference in air content between the beams with a nine-inch and three-inch slump played a significant role in the flexural capacity

8.5 *Conclusions*

1. Lightweight concrete mixes were capable of attaining 5000 psi compressive strength in 16 hours, and 7000 psi at 28 days can be produced with all coarse-aggregates in the study.
2. Use of ACI 318-05 Section 8.5.1 to predict the modulus of elasticity over estimated the modulus of elasticity found experimentally using ASTM C469, for the mixes in this study.
3. Experimental creep and shrinkage data provide curves that can be matched with the ACI Committee 209 curve-fit method to determine the ultimate creep coefficient and shrinkage that can aid engineers in the design process.
4. Core samples taken from in-place lightweight bridge decks and sent to CTL for a petrographic examination revealed that the bridge decks with unsatisfactory performance had entrapped air contents between 1 and 4% and were composed of lightweight fine and coarse-aggregates. The bridge with a satisfactory performance had entrained air content between 3 to 5% and was composed of a sand lightweight mix. However, the petrographic examination could not definitively identify the reason the bridge decks expanded.
5. The only mix to meet the recommended minimum average maximum pull-out force of 36 kips was MQ-3. All other pull-out blocks fell above the 16-kip minimum at first observable slip, that can result in long transfer lengths, and below the 36-kip minimum to ensure acceptable transfer lengths. The coefficient of variation for the average maximum pull-out force was above 10%, using all six strands for KC-3, KC-9, STA-3, and STA-9. For each coarse-aggregate, the average maximum force at pull-out and first observable slip was higher for the block cast with a three-inch slump. Additionally, STA-9 had the lowest average force at pull-out, falling slightly below KC-9, and was the only mix to experience significant strand slip during flexural testing.

6. The four strand average method proved to be an appropriate method to analyze pull-out data with a high coefficient of variation. Analyzing the large-block pull-out data, disregarding the strands with the highest and lowest pull-out force, changed the average maximum pull-out force by zero to five kips and the average load at first slip by zero to 0.3 kips. The four-strand average gave coefficient of variations that were 10% or less for the average maximum force at pull-out and average force at first observable slip for all blocks except for KC-9, which was the only block that had an average change in force between the six-strand and four-strand averages greater then 1.0 kips. The order of decreasing load at first slip for the six blocks tested was the same order of decreasing-moment capacity for the full-development-length beams.
7. Only three individual transfer-length measurements, found with the 95% average maximum strain method, were greater than the calculated ACI value of 28 inches in Appendix B. The largest individual transfer length recorded was 30 inches. The three beams with transfer lengths greater than 28 inches made nominal-moment capacity in flexural testing. None of the average transfer lengths were greater than the ACI value of 28 inches and AASHTO value of 30 inches.
8. All of the 80% development-length specimens made nominal-moment capacity. Four of the six 100% development-length specimens made nominal-moment capacity. The two beams not reaching nominal-moment capacity, KC-9 and STA-9, failed in compression without strand end slip. The moment capacity was greater for three-inch slump members than the companion specimen placed with nine-inch slump concrete.

8.6 *Recommendations*

1. Lightweight concrete mixes developed for this study were adequate for the testing during this study. However, the aggregate ratio should be adjusted for the Kansas City mix to reduce the amount of coarse-aggregate and provide a more workable fresh concrete.
2. Use of Stalite aggregate shipped from North Carolina provided no substantial benefit to offset the extra cost of shipping to Kansas and needs no further investigation.
3. Stockpiling and soaking lightweight-aggregate on a large scale needs to be investigated for the effects of absorption on the porous coarse-aggregate used in this study.
4. A 0.92 multiplier should be applied to the ACI 318-05 modulus of elasticity prediction equation for the mixes in this study. Additionally, modulus-of-rupture flexural beams should be made and tested for each mix.
5. Creep-and-shrinkage testing should be continued for the specified timeframe of one year with a full scale AASHTO girder cross section exposed to the environment.
6. A larger data set of transfer lengths is required to substantiate a correlation between slump and implied transfer length from experimental results.
7. Flexural members should be tested with strain gages at the extreme compression fibers and several places between the mid-span and end of the member on the strand to investigate local bond failure without end slip. Loading conditions of point load and various lengths of constant-moment regions with and without the 24-hour hold of 85% nominal-moment capacity should be investigated and compared to the ultimate-moment capacity and maximum strain in the compression block.
8. SCC lightweight LBPT and beams should be tested and compared to the large block pull-out test and flexural member results found in this study.
9. Larger flexural members should be cast so that the design flexural failure mode is strand rupture. Shear stirrups should be provided as required by ACI 318-05.
10. Full-scale bridge girder cross sections should be cast and monitored for transfer length and prestress losses.

References

1. ACI Committee 209. *Report on Factors Affecting Shrinkage and Creep of Hardened Concrete*, ACI 209.1R-05, American Concrete Institute, 2005.

2. ACI Committee 213. *Guide for Structural Lightweight-Aggregate Concrete*, ACI 213R-03, American Concrete Institue, 2003.

3. ACI Committee 318. *Building Code Requirements for Structural Concrete*, 318-05, American Concrete Institue, 2005.

4. Barnes,R.W., J. W. Grove, and N. H. Burns. "Experimental Assessment of Factors Affecting Transfer Length." *ACI Structural Journal* 100.6, 2003: 740-8.

5. Bremner,T.W. "Elastic Compatibility and the Behavior of Concrete." *Journal of American Concrete Institute* 83.2, 1986: 244.

6. Brown, W.R. III, Larson, Torbjorn J. "Long Term Service Performance of Lightweight Concrete Bridge Structures." International Symposium of Structural Lightweight Aggregate.

7. Buckner,D.C. "A Review of Strand Development Length of Pretensioned Concrete Members." *PCI journal*, 1995: 84.

8. Canfield, S. R. Full Scale Testing of Prestressed, High Performance Concrete, Composite Bridge Girders. Georgia Institute of Technology, 2005 Georgia.

9. Federal Highway Administration. *Criteria for Designing Lightweight Concrete Bridges*, FHWA/RD-85/045, 1985.

10. Girgis,A.F.M., and C. Y. Tuan. "Bond Strength and Transfer Length of Pretensioned Bridge Girders Cast with Self-Consolidating Concrete." *PCI Journal* 50.6, 2005: 72-87.

11. Harmon, K. S. "Engineering Properties of Structural Lightweight Concrete." Stalite Company. 2007. <http://www.stalite.com/PDF/EngineeringProperties.pdf>.

12. Holm, T. A., and T. W. Bremner. "The Durability of Structural Lighweight Concrete." Durability of Concrete; Second International Confrence, Montreal, Canada. 1991.

13. Larson,K.H., R. J. Peterman, and A. Esmaeily. "Bond Characteristics of Self-Consolidating Concrete for Prestressed Bridge Girders." *PCI Journal* 52.4, 2007: 44-57.

14. Logan,D.R. "Acceptance Criteria for Bond Quality of Strand for Pretensioned Prestressed Concrete Applications." *PCI Journal* 42.2, 1997: 52-90.

15. Mitchell, D. W. "Bond Characteristics of High-Strength Lightweight Concrete." ACI Structural Journal 104.1 (2007): 22. .

16. Nawy, E. G.Prestress Concrete a Fundamental Approach. fifth ed. Upper Saddle River, New Jersey: Pearson Prentice Hall, 2006.

17. PCI Industry Handbook Committee.PCI Design Handbook Precast and Prestressed Concrete. 6th ed. USA: Precast/Prestressed Concrete Institute, 2004.

18. Peterman,R.J. "The Effects of as-Cast Depth and Concrete Fluidity on Strand Bond." *PCI Journal* 52.3, 2007: 72-101.

19. ---. "Influence of Flexure-Shear Cracking on Strand Development Length in Prestressed Concrete Members." *PCI journal* 45.5, 2000: 76.

20. Petrou,M.F., et al. "Excessive Strand End Slip in Prestressed Piles." *ACI Structural Journal* 97.5, 2000: 774-82.

21. Research Department, State Highway Commission of Kansas. *Availability and Suggested Usage of Lightweigt Aggregate Concrete for Kansas Highway Construction*, 1953.

22. ---. *Supplementary Report on Lightweight Aggregate Concrete Construction-1955, Bulletin NO.7*, 1955.

23. Russell, B. W., and Burns, N. H. *Design Guidelines for Transfer, Development and Debonding of Large Diameter Seven Wire Strands in Pretensioned Concrete Girders*, 1210-5F, Texas Department of Transportation, 1993.

Appendix A - Supplementary Figures, Tables, and Equations

Table A-1 Kansas City Concrete Mix Summary

Date	Name	Trial #	Aggregate Ratio	Aggregate Type	Air Admixture (oz./100 lb cement)	Super Admixture Type	Superplacticizer (oz./100 lb cement)	w/c	Cement Content (lb/yd^3)	Slump (in)	% Air (Rollometer)	% Air (Gravimeteric)	Unit Weight (Gravametric) (pcf)
5/8/2007	KC .34 750	J-1	60sand-40coarse	KC	0.55	Daracem 100	10.0	0.34	750	2.25	5.25	3.7	125.9
5/17/2007	KC III	3-1	60sand-40coarse	KC	0.52	Daracem 100	12.2	0.34	750	1.75	-	3.5	131.3
5/17/2007	KC III 2	3-2	60sand-40coarse	KC	0.58	Daracem 100	14.0	0.34	750	4.25	5.75	4.7	129.7
6/1/2007	8-1 KC	8-1	*	KC	0.58	Daracem 100	14.0	0.34	750	5.5	9.25	16.3	116.0
6/4/2007	9-1 KC	9-1	60sand-40coarse	KC	0.52	Daracem 100	14.0	0.34	750	0.5	-	8.7	124.6
6/6/2007	10-1 KC	10-1	60sand-40coarse	KC	0.15	AdvaCast 530	6.0	0.34	750	2.5	4	10.3	122.6
6/6/2007	10-2 KC	10-2	60sand-40coarse	KC	0.17	AdvaCast 530	6.1	0.34	750	5	6	12.7	119.8
6/7/2007	11-1 KC	11-1	60sand-40coarse	KC	0.18	AdvaCast 530	6.4	0.34	750	2.5	5	10.9	122.0
6/14/2007	12-1 KC	12-1	60sand-40coarse	KC	0.18	AdvaCast 530	6.7	0.34	725	9.25	-	15.5	116.8
6/19/2007	13-1 KC	13-1	60sand-40coarse	KC	0.15	AdvaCast 530	6.9	0.34	725	4	6.5	12	120.8
6/20/2007	14-1 KC NO SSD	14-1	60sand-40coarse	KC	0.15	AdvaCast 530	6.9	0.34	725	3	-	13	122.5
10/19/2007	KC 3" creep #1	trial 1 creep	44sand-56coarse	KC	0.15	AdvaCast 530	6.9	0.34	725	3" @pour	8	8.25	116.0
11/6/2007	KC 3" creep #2	creep	44sand-56coarse	KC	0.15	AdvaCast 530	6.1	0.34	725	3" @pour	7.5	5.1	119.7
8/15/2007	LBPT KC 3"	LBPT	44sand-56coarse	KC	0.30	AdvaCast 530	5.4	0.34	725	3" @pour	3.75	4.1	120.9
8/21/2007	LBPT KC 9"	LBPT	44sand-56coarse	KC	0.30	AdvaCast 530	6.4	0.34	725	9" @pour	5	9.1	115.0
10/23/2007	KC shrinkage	shrinkage	44sand-56coarse	KC	0.14	AdvaCast 530	6.7	0.34	725	7	8	8.1	116.2
1/28/2008	KC 9" beam	beams	44sand-56coarse	KC	0.35	AdvaCast 530	6.1	0.34	725	9" @pour	6	9.1	115.0
3/24/2008	KC 3" beam	beams	44sand-56coarse	KC	0.37	AdvaCast 530	5.4	0.34	725	3" @pour	4	2.5	122.9

Table A-2 Marquette Concrete Mix Summary

Date	Name	Trial #	Aggregate Ratio	Aggregate Type	Air Admixture (oz./100 lb cement)	Super Admixture Type	Superplacticizer (oz./100 lb cement)	w/c	Cement Content (lb/yd^3)	Slump (in)	% Air (Rollometer)	% Air (Gravimeteric)	Unit Weight (Gravametric) (pcf)
5/8/2007	Marq. .34 750	J-1	60sand-40coarse	Marq.	0.52	Daracem 100	7.3	0.34	750	0.5	2.5	2.3	124.8
5/9/2007	Marq. .32 750	J-2	60sand-40coarse	Marq.	0.67	Daracem 100	23.7	0.32	750	7.25	14	17.1	125.5
5/14/2007	Marq. 1 trial	sm-1	60sand-40coarse	Marq.	0.55	Daracem 100	12.8	0.34	750	0.5	-	2.9	128.6
5/14/2007	Marq. 2 trial	sm-2	60sand-40coarse	Marq.	0.55	Daracem 100	15.8	0.34	750	5.5	-	9	120.9
5/17/2007	Marq. III	3-1	60sand-40coarse	Marq.	0.64	Daracem 100	15.8	0.34	750	8	13	15.4	113.9
5/21/2007	4Marq. #1	4-1	60sand-40coarse	Marq.	0.58	Daracem 100	15.8	0.34	750	0.25	-	4.2	126.9
5/21/2007	4Marq. #2	4-2	60sand-40coarse	Marq.	0.58	Daracem 100	17.7	0.34	750	4.25	-	10.3	119.4
5/21/2007	4Marq. #3	4-3	60sand-40coarse	Marq.	0.55	Daracem 100	18.9	0.34	750	8.5	-	19.3	109.9
5/21/2007	4Marq. #4	4-4	60sand-40coarse	Marq.	0.52	Daracem 100	18.3	0.34	750	9.25	-	16.8	112.4
5/22/2007	5-1 Marq.	5-1	60sand-40coarse	Marq.	0.39	Daracem 100	17.7	0.34	750	6.25	9	12.2	117.3
5/22/2007	5-2 Marq.	5-2	60sand-40coarse	Marq.	0.34	Daracem 100	17.7	0.34	750	6.5	-	12.4	115.3
5/22/2007	5-3 Marq.	5-3	60sand-40coarse	Marq.	0.28	Daracem 100	17.7	0.34	750	8	-	14	115.3
5/30/2007	6-1 Marq.	6-1	60sand-40coarse	Marq.	0.00	Daracem 100	17.7	0.34	750	4	5.75	7.6	122.6
6/4/2007	9-1 Marq.	9-1	60sand-40coarse	Marq.	0.00	AdvaCast 530	7.3	0.34	750	8.5	6.5	6.6	123.8
6/6/2007	10-1 Marq.	10-1	60sand-40coarse	Marq.	0.12	AdvaCast 530	6.0	0.34	750	5.5	5.25	4.7	126.2
6/7/2007	11-1 Marq.	11-1	60sand-40coarse	Marq.	0.15	AdvaCast 530	5.5	0.34	750	2.75	4	2.9	128.6
6/14/2007	12-1 Marq.	12-1	60sand-40coarse	Marq.	0.15	AdvaCast 530	6.3	0.34	725	5.75	6	5.7	125.0
6/19/2007	13-1 Marq.	13-1	60sand-40coarse	Marq.	0.15	AdvaCast 530	6.5	0.34	725	6.5	6.5	5.9	124.8
6/20/2007	14-1 Marq. NO SSI	14-1	60sand-40coarse	Marq.	0.15	AdvaCast 530	6.5	0.34	725	3	5	7.8	126.9
6/26/2007	15-1 Marq. LBPT trial	15-1	60sand-40coarse	Marq.	0.10	AdvaCast 530	6.0	0.34	725	1	estimated 2-3%	-	-
7/3/2007	16-1 Marq. 3"	16-1	47.7sand-52.3coarse	Marq.	0.20	AdvaCast 530	6.2	0.34	725	4	5.75	5	119.8
7/3/2007	16-2 Marq. 9"	16-2	47.7sand-52.3coarse	Marq.	0.00	AdvaCast 530	8.2	0.34	725	8	7	6.3	118.2
7/26/2007	LBPT Marq. 3"	try #1 LBPT	47.7sand-52.3coarse	Marq.	0.25	AdvaCast 530	6.2	0.34	725	3" @pour	4	2.1	123.4
7/31/2007	LBPT Marq. 3" #2	LBPT	47.7sand-52.3coarse	Marq.	0.30	AdvaCast 530	5.9	0.34	725	3" @pour	3.5	0.6	125.4
8/13/2007	LBPT Marq. 9"	LBPT	47.7sand-52.3coarse	Marq.	0.00	AdvaCast 530	6.7	0.34	725	9" @pour	2.5	0.3	125.8
10/16/2007	Marq. 3" creep #1	trial 1 creep	47.7sand-52.3coarse	Marq.	0.15	AdvaCast 530	6.5	0.34	725	3" @pour	6.5	5.7	118.9
10/19/2007	Marq. 3" creep #2	trial 2 creep	47.7sand-52.3coarse	Marq.	0.15	AdvaCast 530	6.3	0.34	725	3" @pour	5	3.8	121.3
11/6/2007	Marq. 3" creep #3	creep	47.7sand-52.3coarse	Marq.	0.15	AdvaCast 530	6.5	0.34	725	3" @pour	8	8.6	115.6
10/23/2007	Marq. shrinkage	shrinkage	47.7sand-52.3coarse	Marq.	0.15	AdvaCast 530	6.4	0.34	725	7	8	7.2	117.2
1/14/2008	Marq. 9" beam	beams	47.7sand-52.3coarse	Marq.	0.30	AdvaCast 530	6.1	0.34	725	9" @pour	5.5	2.9	122.4
1/22/2008	Marq. 3" beam	beams	47.7sand-52.3coarse	Marq.	0.35	AdvaCast 530	5.5	0.34	725	3" @pour	4	2.9	122.4

Table A-3 Stalite Concrete Mix Summary

Date	Name	Trial #	Aggregate Ratio	Aggregate Type	Air Admixture (oz./100 lb cement)	Super Admixture Type	Superplacticizer (oz./100 lb cement)	w/c	Cement Content (lb/yd^3)	Slump (in)	% Air (Rollometer)	% Air (Gravimeteric)	Unit Weight (Gravametric) (pcf)
5/8/2007	Stalite .42 639	J-1	60sand-40coarse	Stalite	0.64	Daracem 100	8.6	0.42	639	7	6.5	8.2	125.7
5/9/2007	Stalite .32 750	J-2	60sand-40coarse	Stalite	0.67	Daracem 100	15.6	0.32	750	0.5	2	3.6	128.2
5/14/2007	Stalite .34 750	sm-1	60sand-40coarse	Stalite	0.49	Daracem 100	15.8	0.34	750	1	-	5.5	126.7
5/14/2007	Stalite .34 750	sm-2	60sand-40coarse	Stalite	0.49	Daracem 100	17.5	0.34	750	6.25	-	10.1	121.2
5/14/2007	Stalite .34 750	sm-3	60sand-40coarse	Stalite	0.43	Daracem 100	17.5	0.34	750	5.5	-	11.8	119.2
5/17/2007	Sta. III	3-1	60sand-40coarse	Stalite	0.43	Daracem 100	17.5	0.34	750	9	-	17.9	112.7
5/30/2007	6-1 Sta.	6-1	60sand-40coarse	Stalite	0.58	Daracem 100	15.8	0.34	750	3.5	8.5	9.5	121.8
5/30/2007	6-2 Sta.	6-2	60sand-40coarse	Stalite	0.52	Daracem 100	17.7	0.34	750	9	-	17	113.6
5/31/2007	7-1 Sta.	7-1	60sand-40coarse	Stalite	0.52	Daracem 100	16.8	0.34	750	1.25	-	8.1	123.6
5/31/2007	7-2 Sta.	7-2	60sand-40coarse	Stalite	0.43	Daracem 100	17.7	0.34	750	8.25	-	17	113.6
6/1/2007	8-1 Sta.	8-1	60sand-40coarse	Stalite	0.46	Daracem 100	17.2	0.34	750	5.75	-	16.8	113.7
6/1/2007	8-2 Sta.	8-2	60sand-40coarse	Stalite	0.33	Daracem 100	17.2	0.34	750	3.5	6.75	10.4	120.8
6/4/2007	9-1 Sta.	9-1	60sand-40coarse	Stalite	0.33	Daracem 100	17.2	0.34	750	-	16	114.7	-
6/7/2007	11-1 Sta.	11-1	60sand-40coarse	Stalite	0.15	AdvaCast 530	6.4	0.34	750	4	5	7.5	124.2
6/14/2007	12-1 Stalite	12-1	60sand-40coarse	Stalite	0.15	AdvaCast 530	6.9	0.34	725	7.25	6.75	9.1	122.4
6/19/2007	13-1 Stalite	13-1	60sand-40coarse	Stalite	0.15	AdvaCast 530	6.9	0.34	725	6.5	6.5	8	123.7
6/20/2007	14-1 Stalite NO SSD	14-1	60sand-40coarse	Stalite	0.15	AdvaCast 530	6.9	0.34	725	6	6.5	9.5	122.9
10/19/2007	Sta. 3" creep #1	trial 1 creep	43.6sand-56.4coarse	Stalite	0.15	AdvaCast 530	6.6	0.34	725	3" @pour	6	7.2	117.2
11/6/2007	Sta. 3" creep #2	creep	43.6sand-56.4coarse	Stalite	0.15	AdvaCast 530	5.7	0.34	725	3" @pour	5	5.4	119.3
Oct. 2007?	LBPT Sta. 3"	LBPT	43.6sand-56.4coarse	Stalite	0.34	AdvaCast 530	4.9	0.34	725	3" @pour	3	6.3	118.2
11/20/2007	LBPT Sta. 9"	LBPT	43.6sand-56.4coarse	Stalite	0.30	AdvaCast 530	6.4	0.34	725	9" @pour	-	12.3	111.6
10/23/2007	Stalite shrinkage	shrinkage	43.6sand-56.4coarse	Stalite	0.15	AdvaCast 530	6.8	0.34	725	9	6	-	117.0
3/10/2008	Stalite 9" beam	beams	43.6sand-56.4coarse	Stalite	0.32	AdvaCast 530	6.2	0.34	725	9" @pour	7	7.7	116.6
3/31/2008	Stalite 3" beam	beams	43.6sand-56.4coarse	Stalite	0.39	AdvaCast 530	5.0	0.34	725	3" @pour	3.5	4.1	120.9
3/12/2008	PS Stalite shrinkage #2	shrinkage	43.6sand-56.4coarse	Stalite	0.15	AdvaCast 530	6.3	0.34	725	9	7.5	11.3	112.6

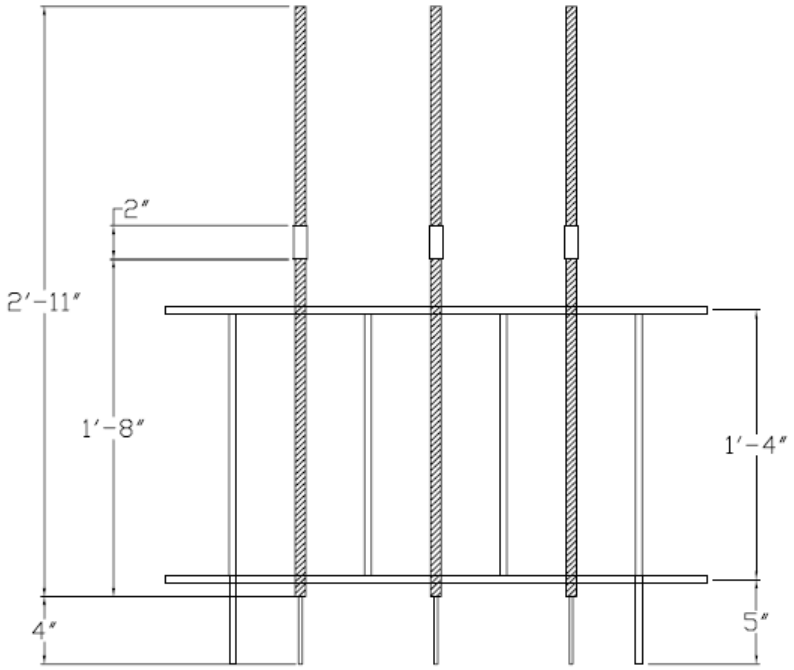

Figure A-1 LBPT Cage Dimensions and Strand-Spacing Side Elevation

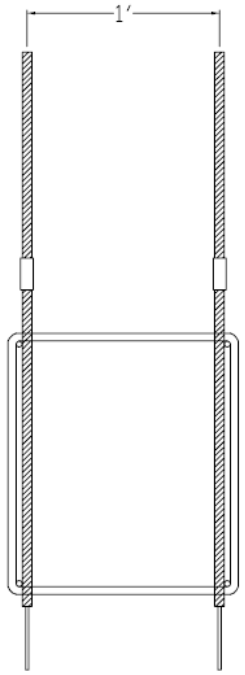

Figure A-2 LBPT Cage Dimensions and Strand-Spacing Front Elevation

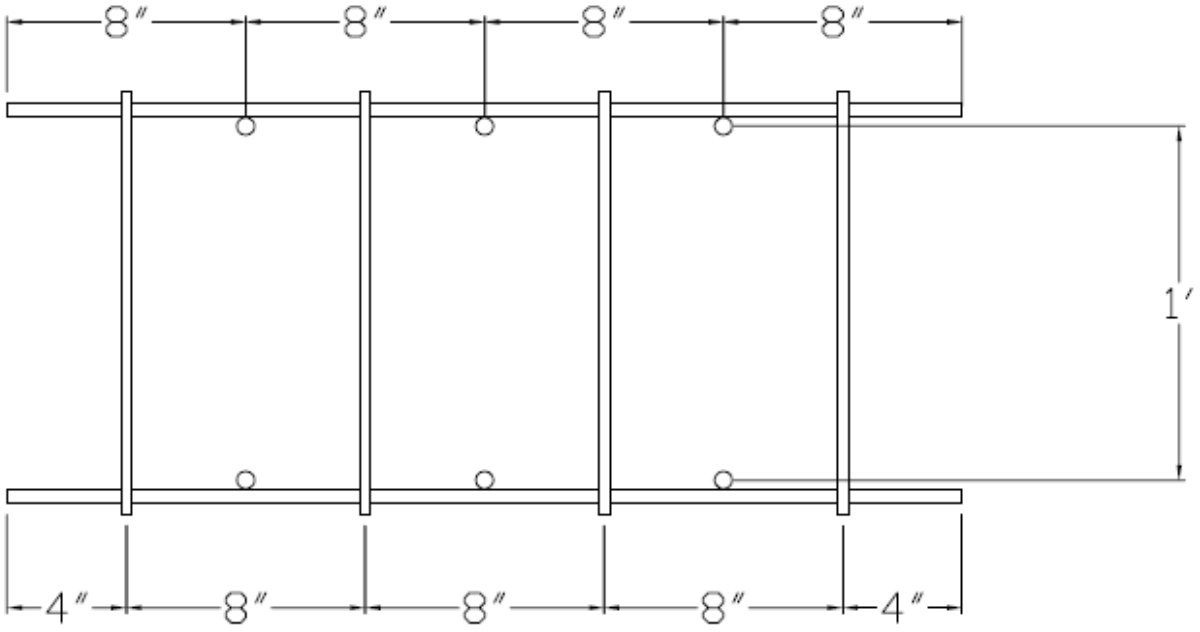

Figure A-3 LBPT Cage Dimensions and Strand-Spacing Plan View

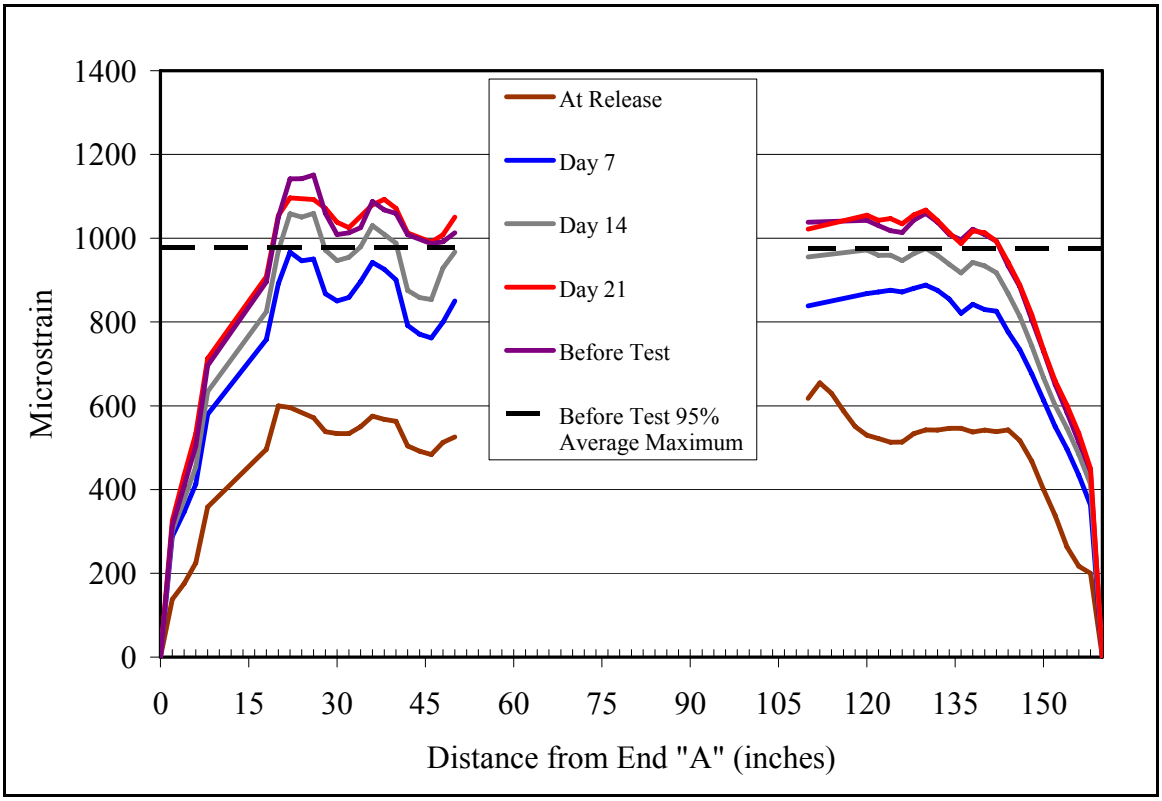

Figure A-4 KC-9 80% L_d Surface-Strain Profile

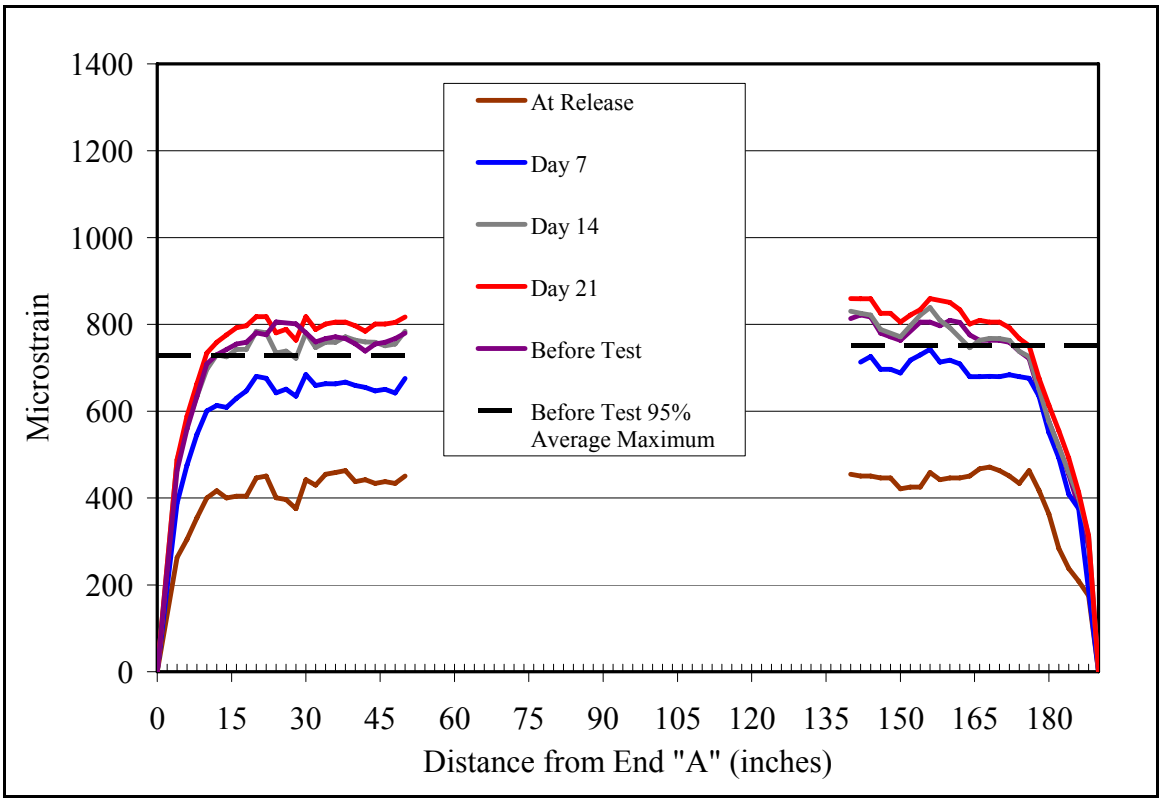

Figure A-5 KC-3 100% L_d Surface-Strain Profile

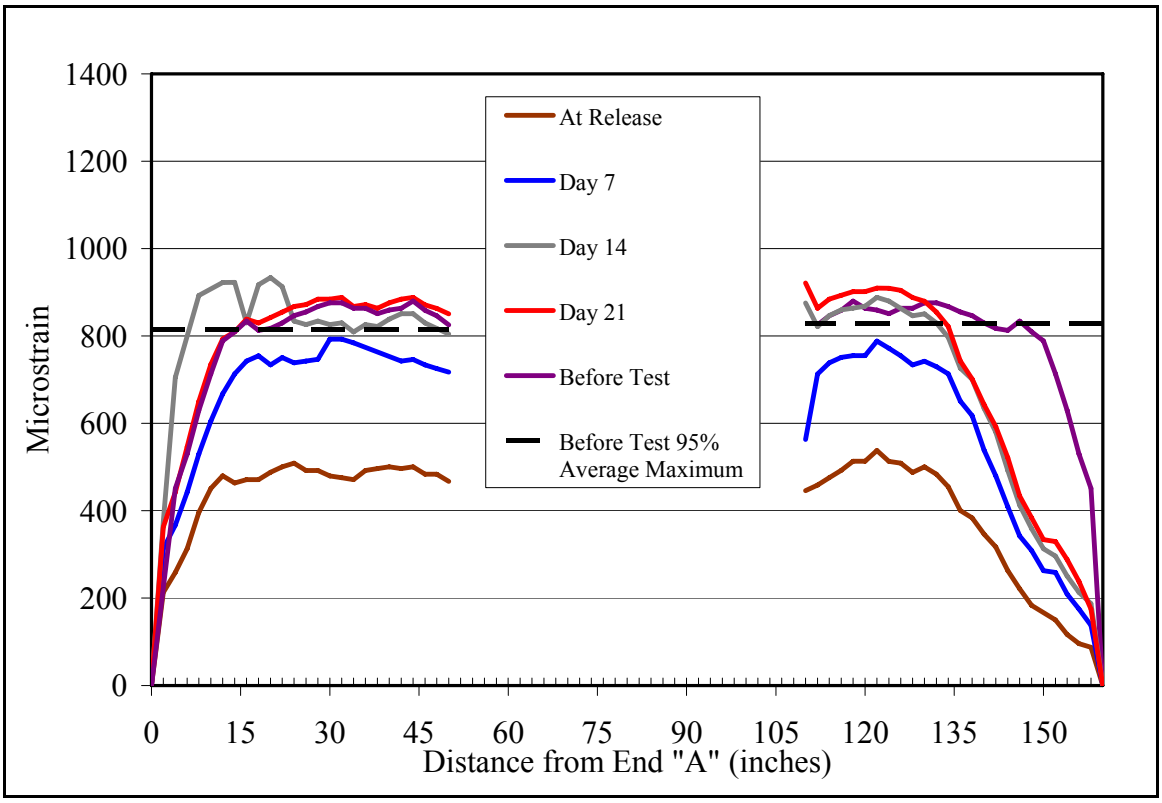

Figure A-6 KC-3 80% L_d Surface-Strain Profile

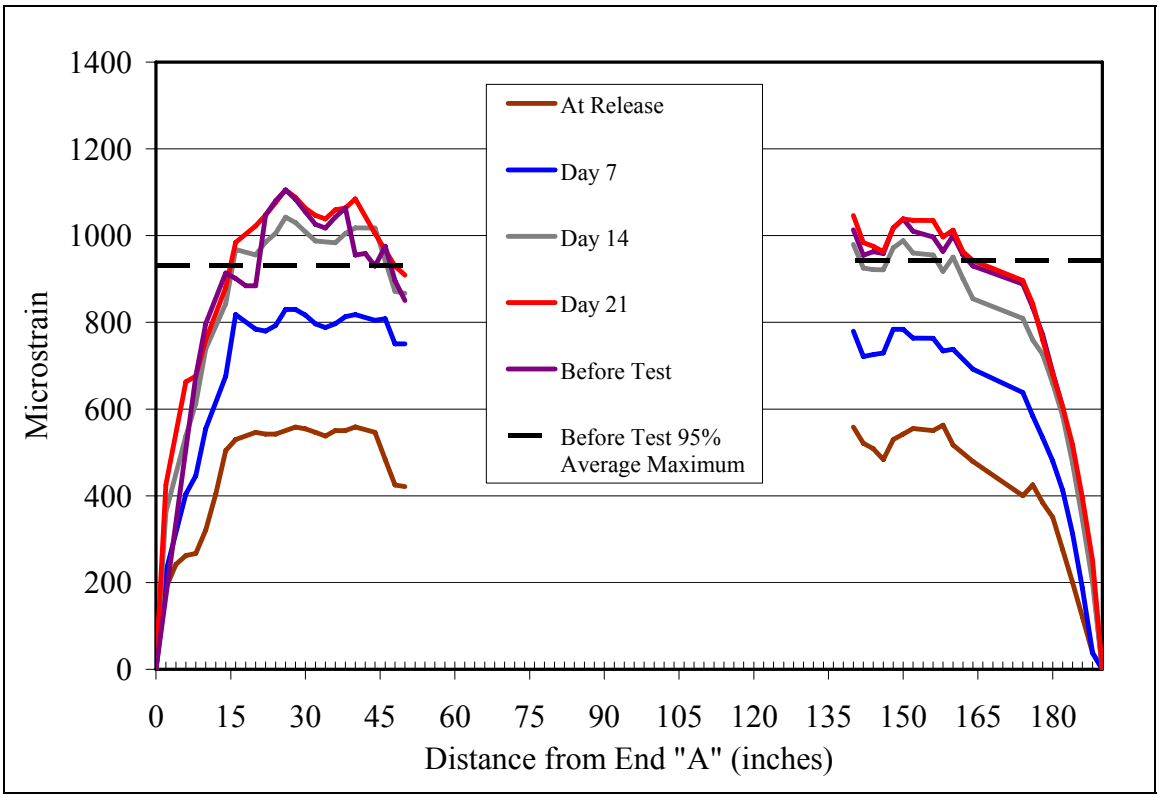

Figure A-7 MQ-9 100% L_d Surface-Strain Profile

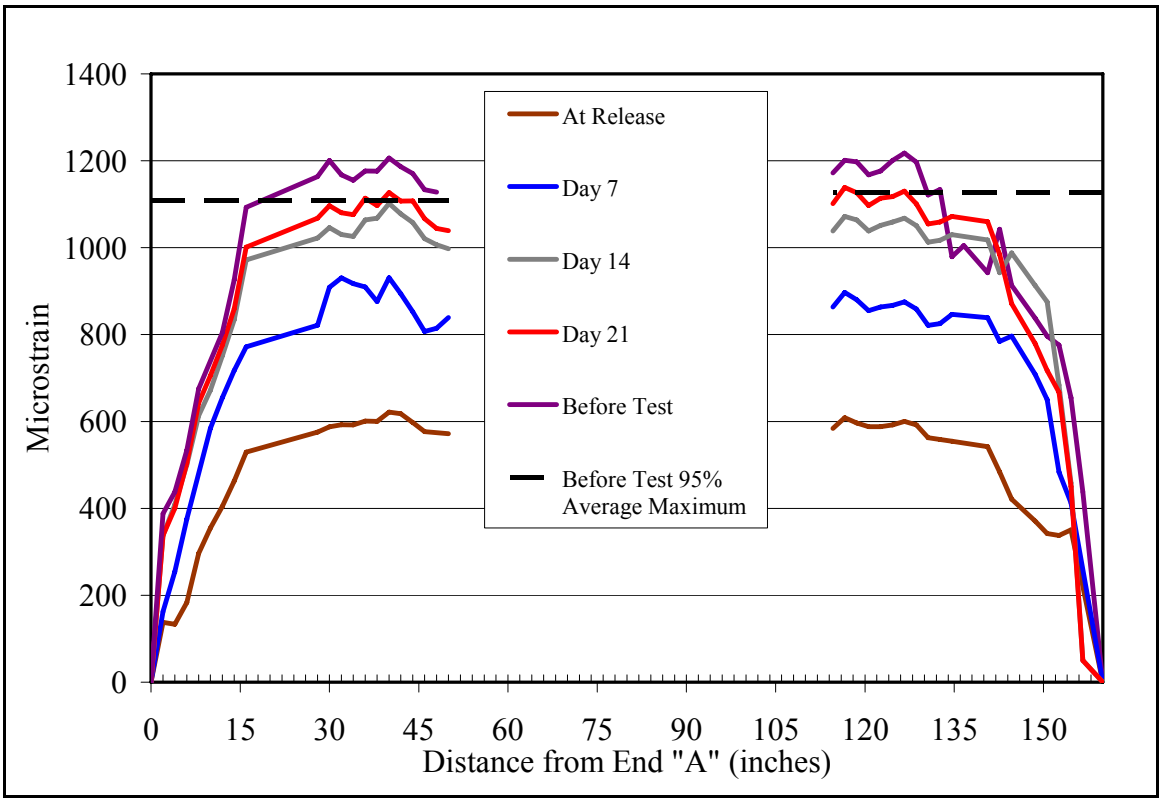

Figure A-8 MQ-9 80% L_d Surface-Strain Profile

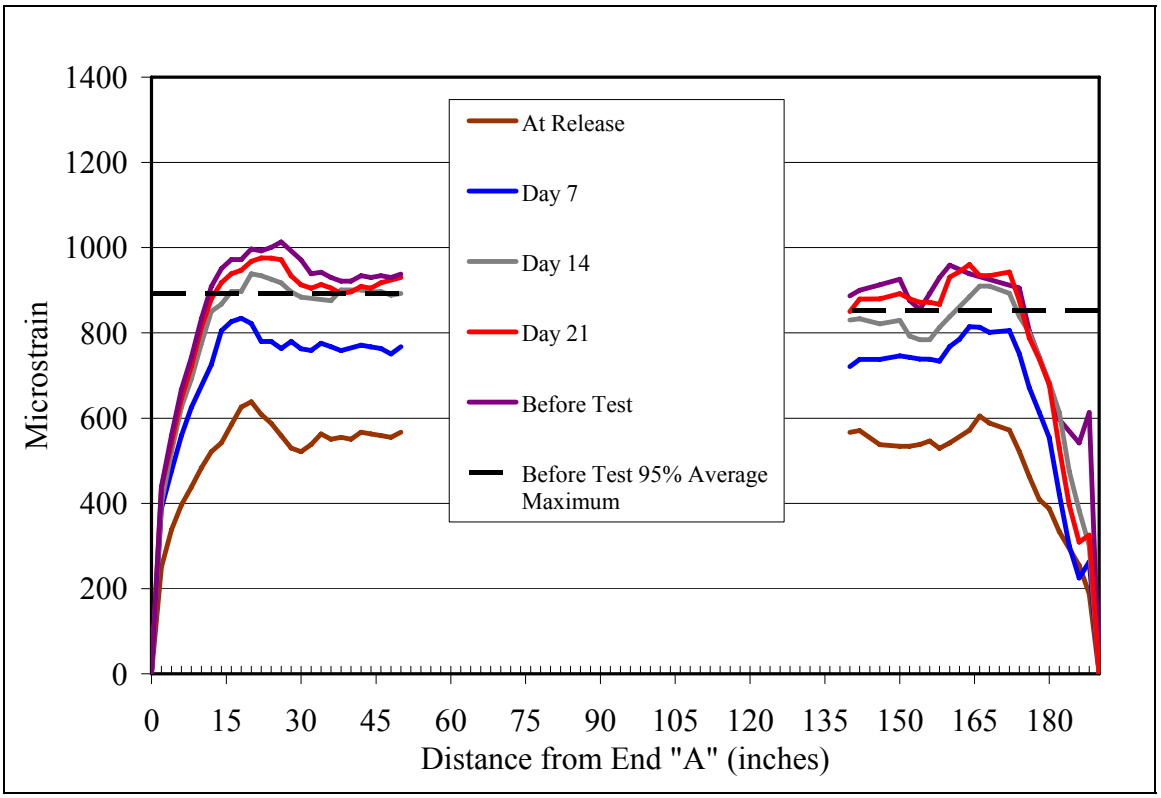

Figure A-9 MQ-3 100% Ld Surface-Strain Profile

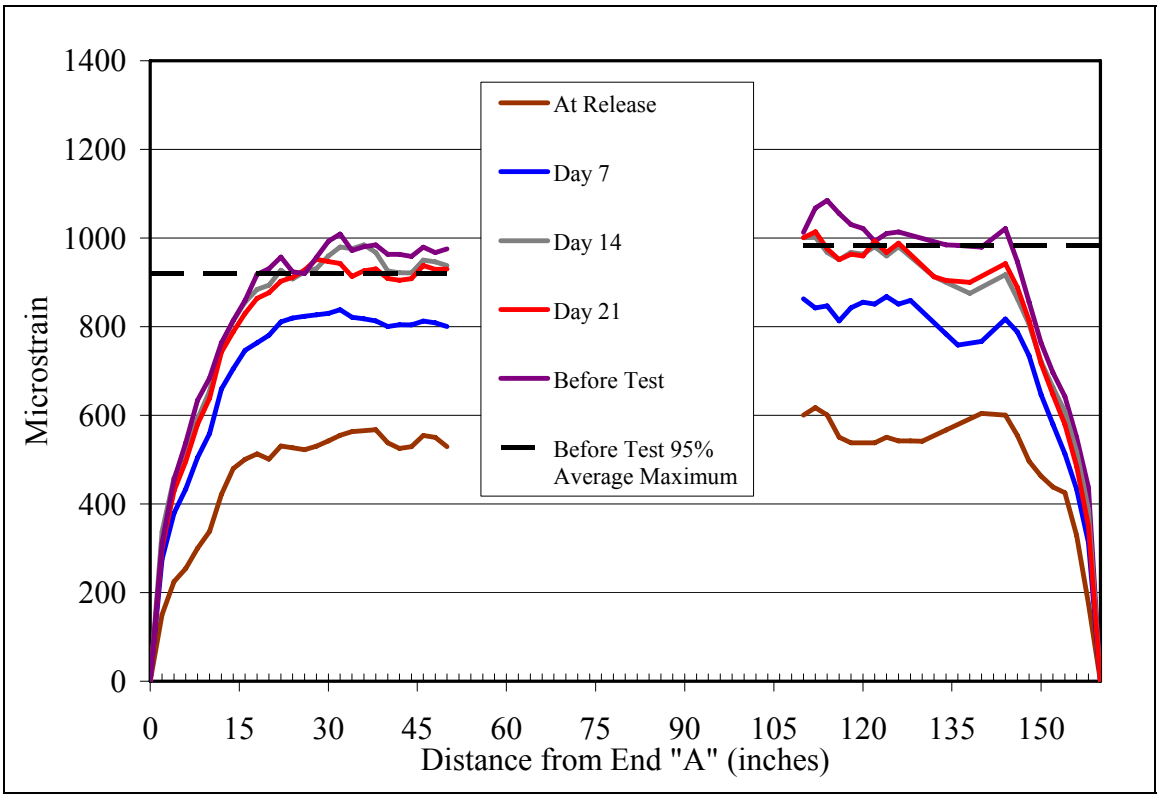

Figure A-10 MQ-3 80% Ld Surface-Strain Profile

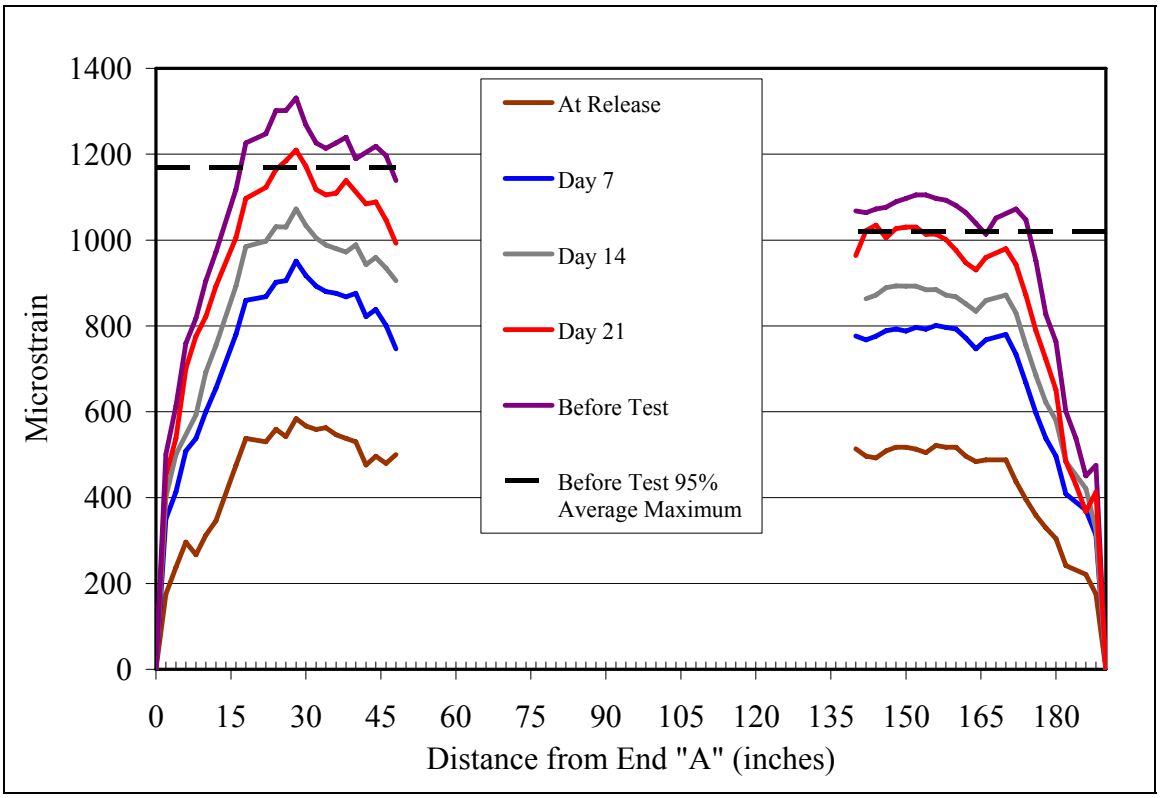

Figure A-11 STA-9 100% Ld Surface-Strain Profile

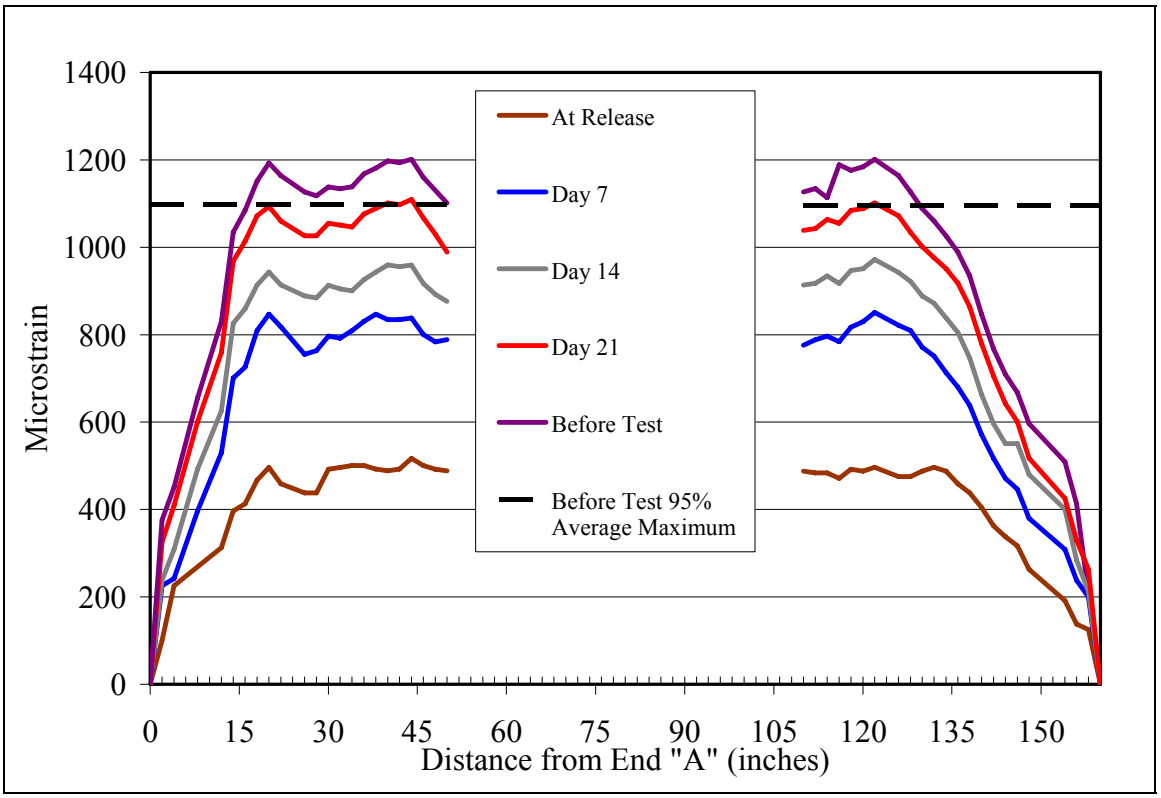

Figure A-12 STA-9 80% Ld Surface-Strain Profile

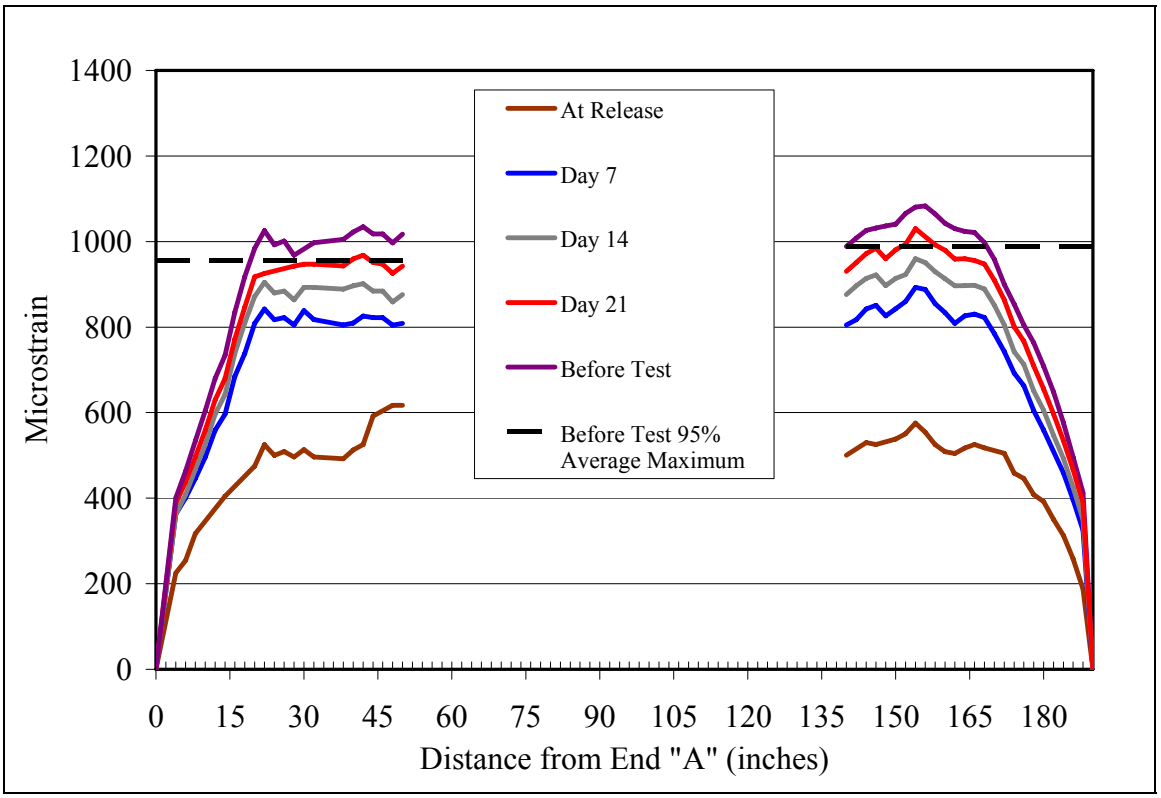

Figure A-13 STA-3 100% L_d Surface-Strain Profile

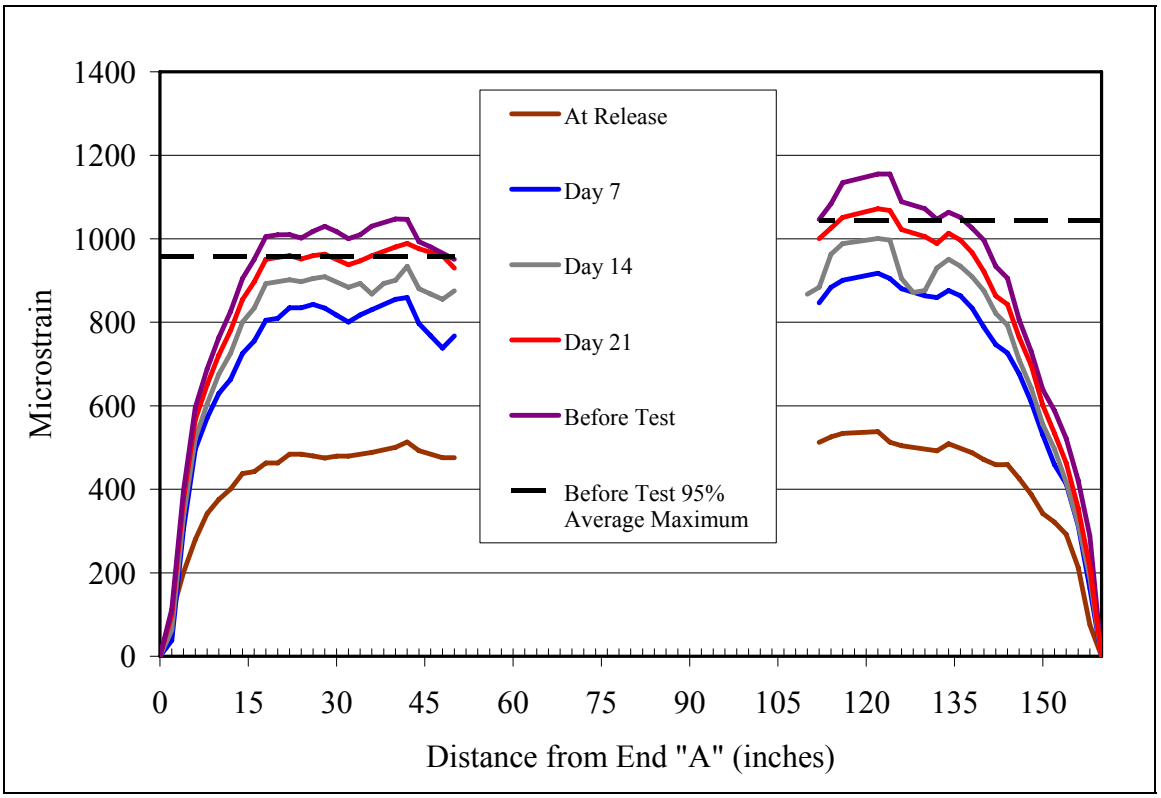

Figure A-14 STA-3 80% Ld Surface-Strain Profile

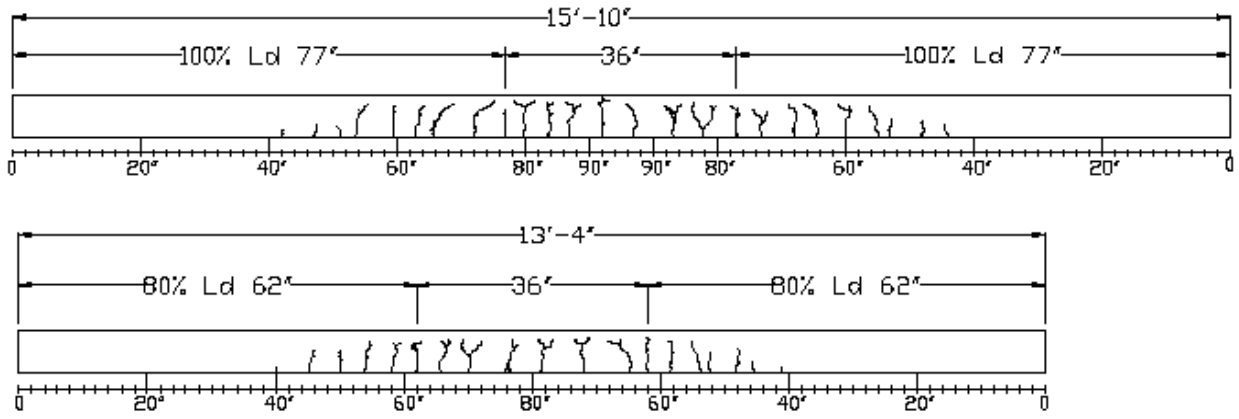

Figure A-15 KC-3 100% L_d and KC-3 80% L_d Crack Propagation

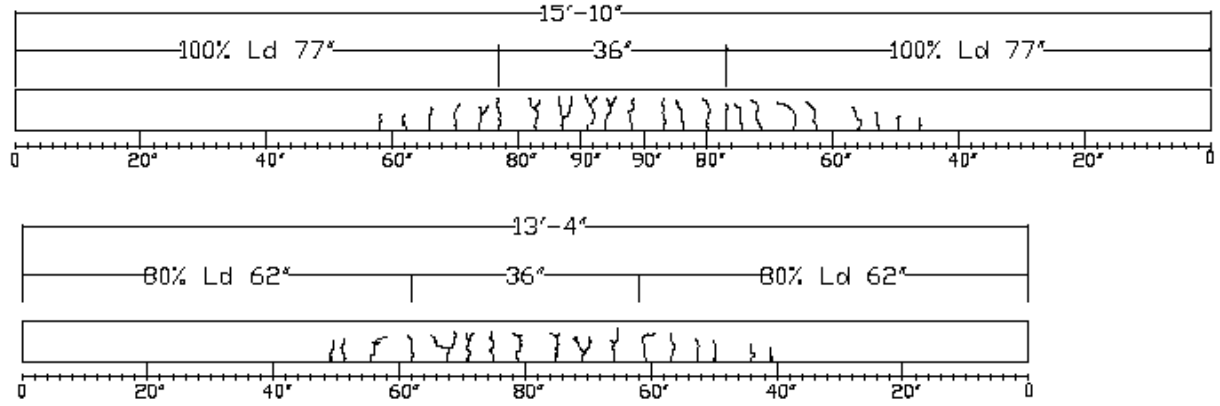

Figure A-16 MQ-9 100% L_d and MQ-9 80% L_d Crack Propagation

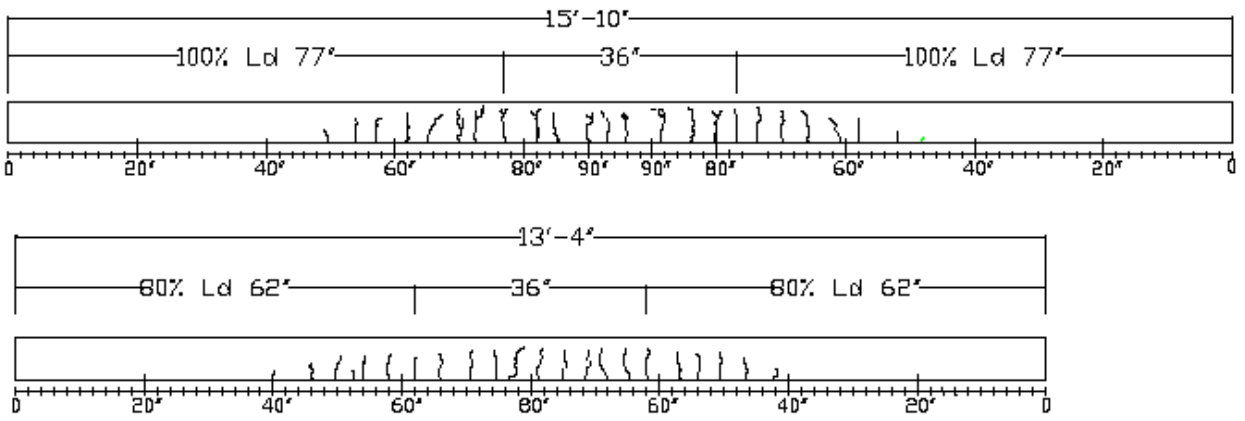

Figure A-17 MQ-3 100% L_d and MQ-3 80% L_d Crack Propagation

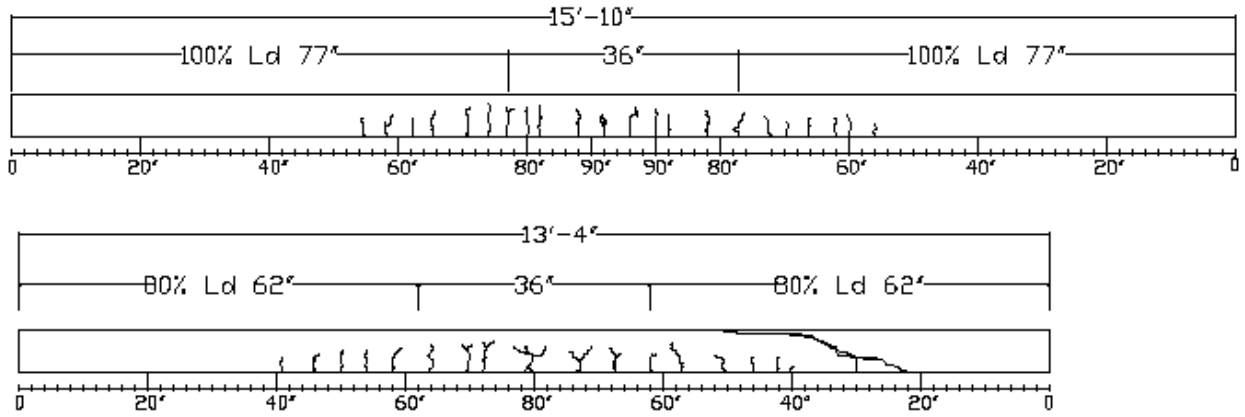

Figure A-18 STA-9 100% L_d and STA-9 80% L_d Crack Propagation

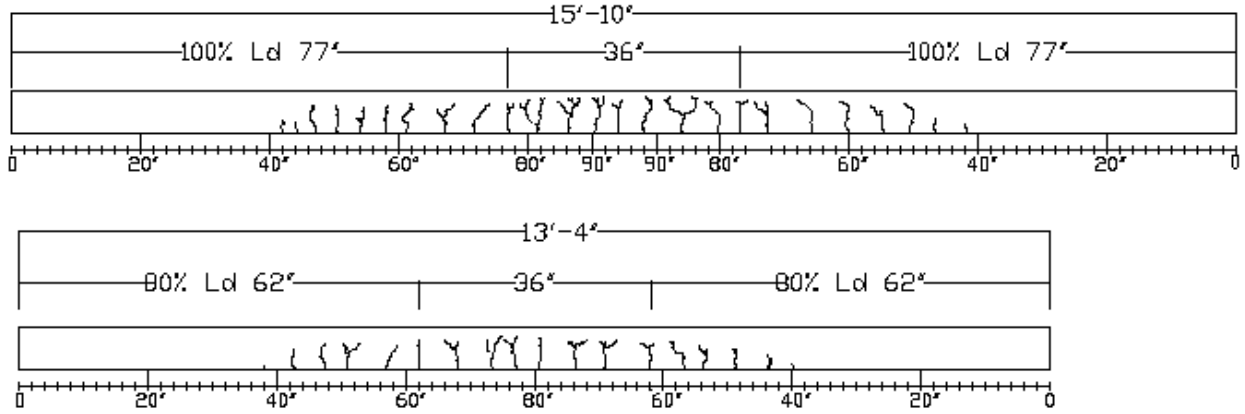

Figure A-19 STA-3 100% L_d and STA-3 80% L_d Crack Propagation

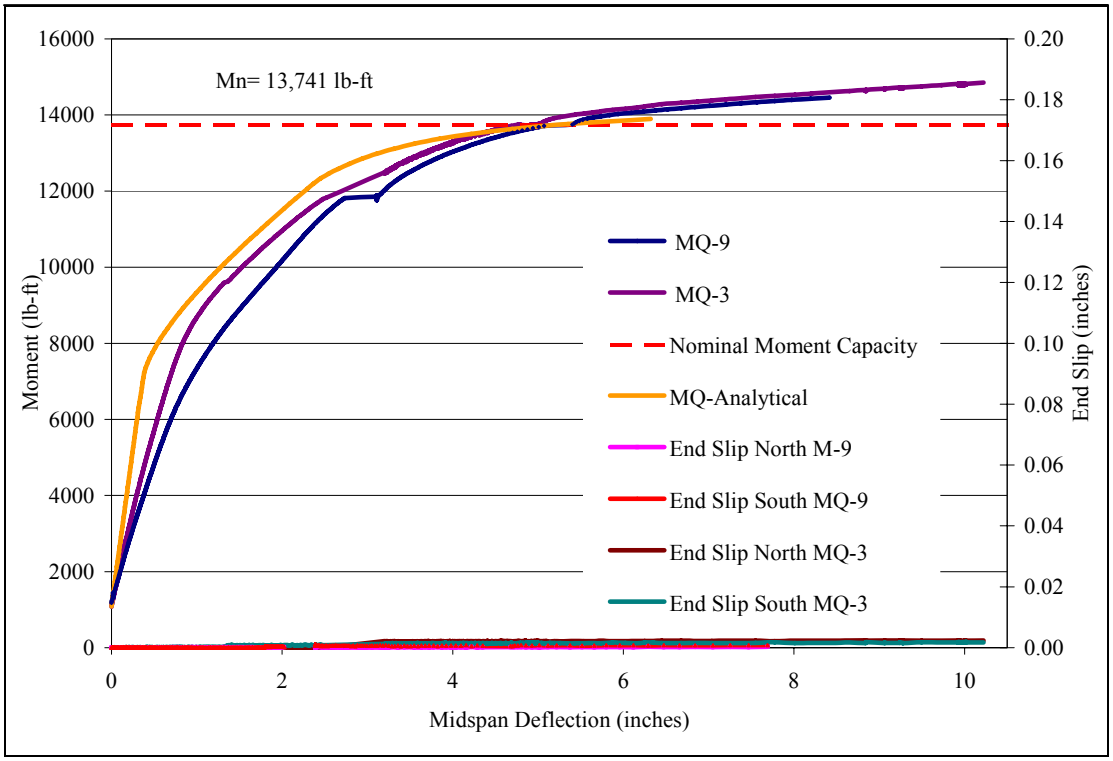

Figure A-20 MQ-9 and MQ-3 100% L_d Moment-Deflection Curves

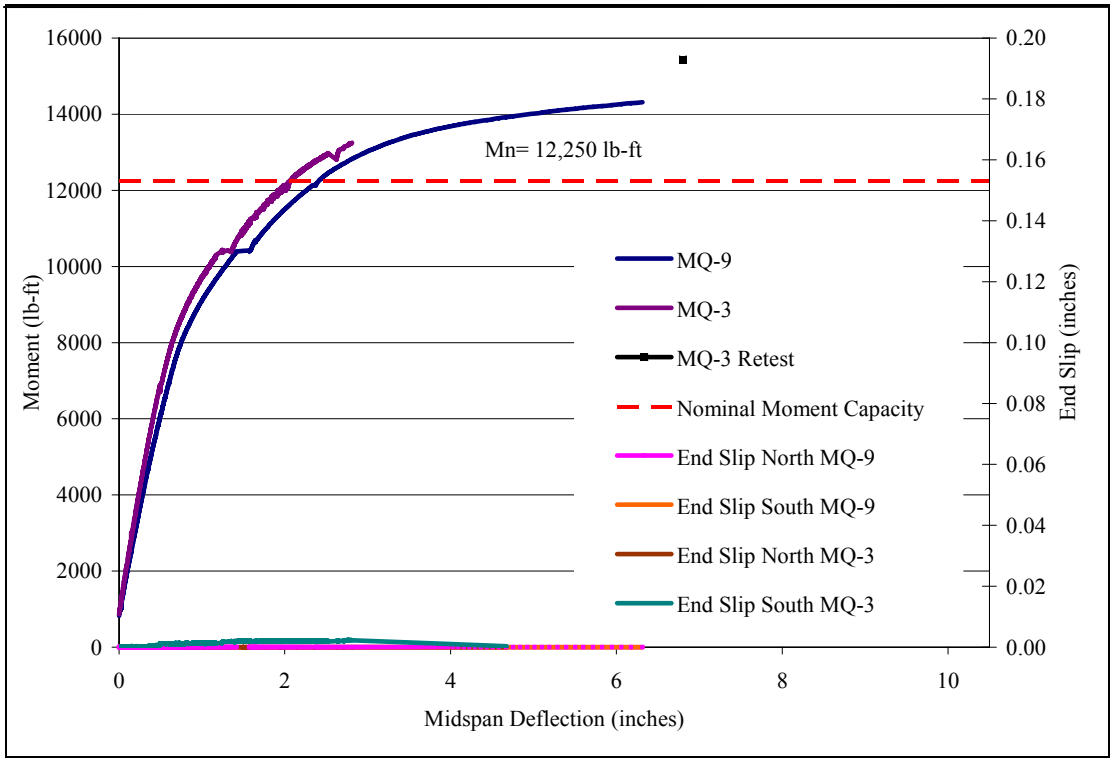

Figure A-21 MQ-9 and MQ-3 80% L_d Moment-Deflection Curves

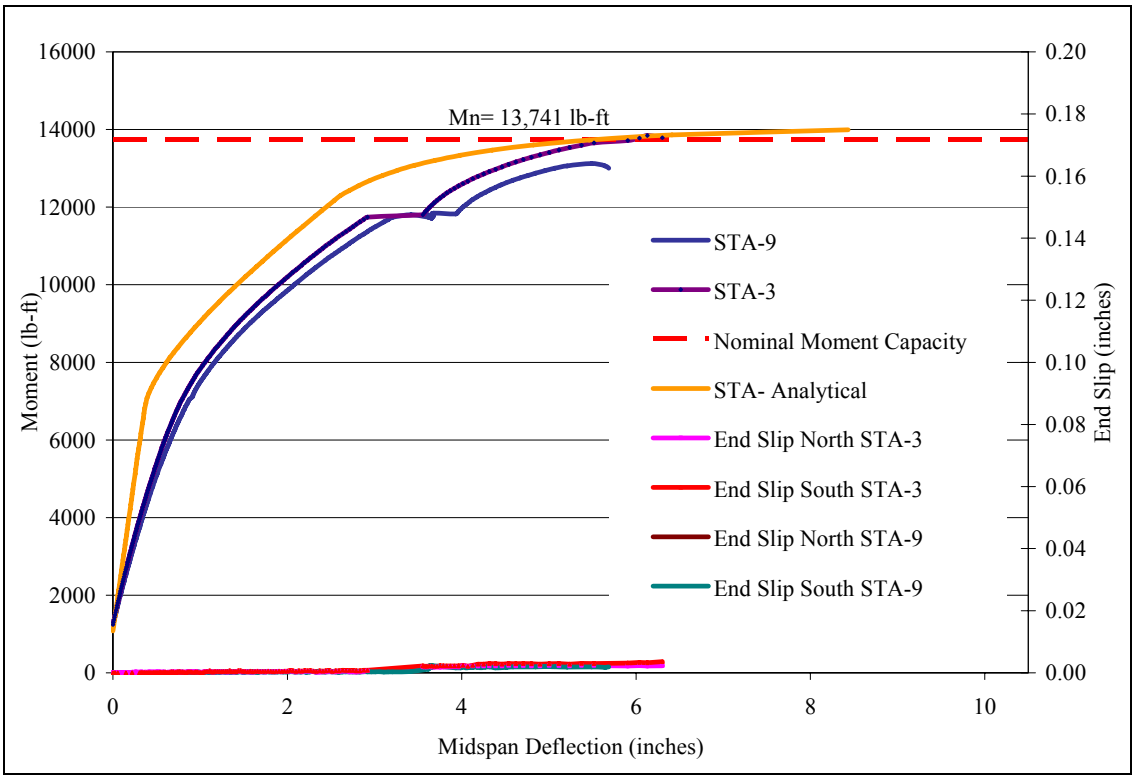

Figure A-22 STA-9 and STA-3 100% Ld Moment-Deflection Curves

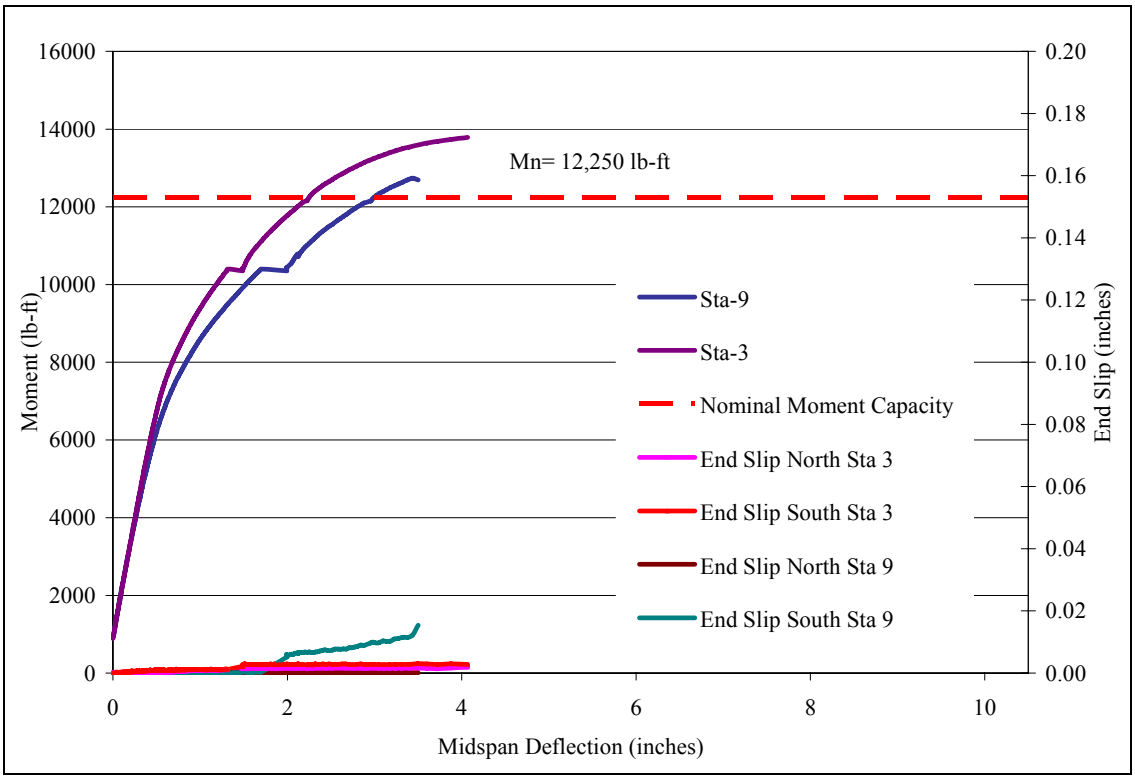

Figure A-23 STA-9 and STA-3 80% L_d Moment-Deflection Curves

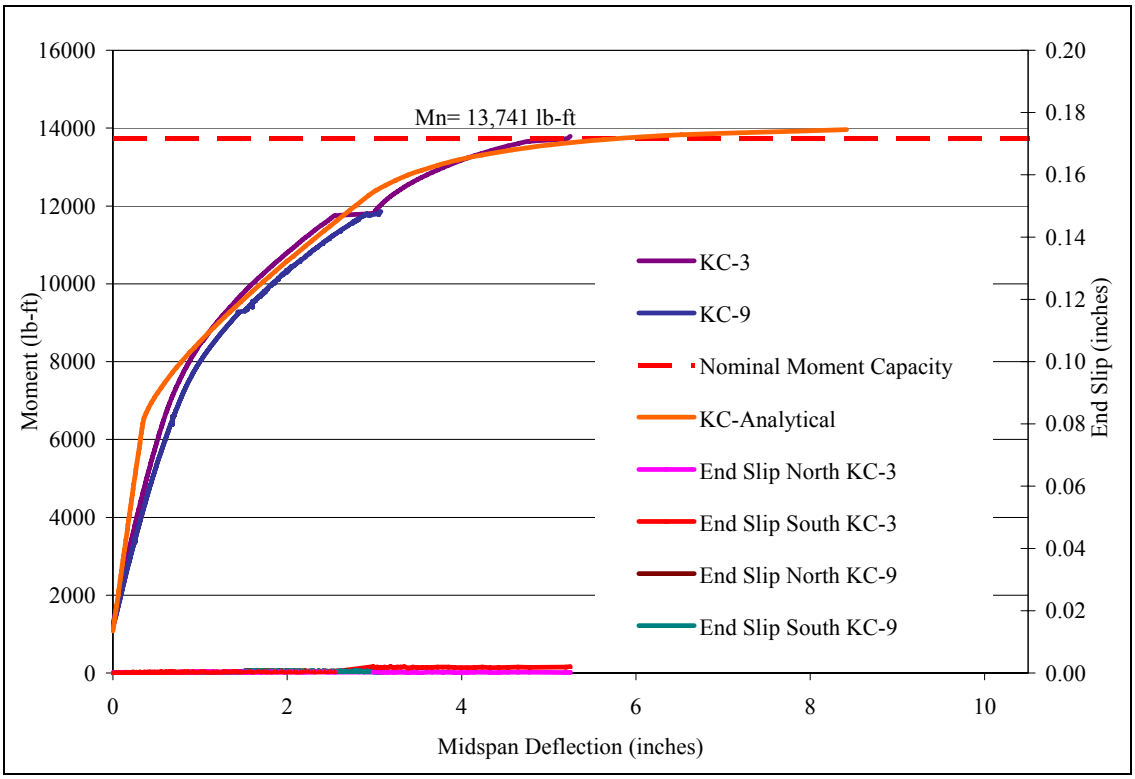

Figure A-24 KC-9 and KC-3 100% Ld Moment-Deflection Curves

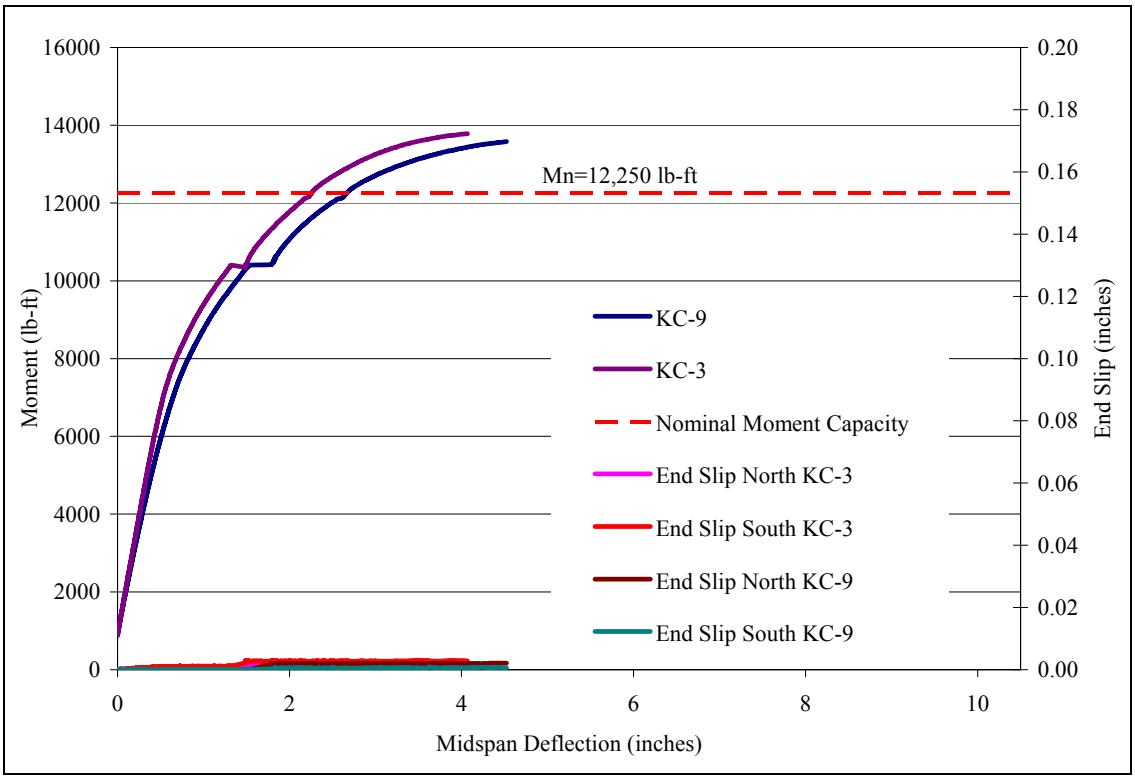

Figure A-25 KC-9 and KC-3 100% Ld Moment-Deflection Curves

$$\gamma_{la} = 1.28\left(t_{la}\right)^{-0.118}$$

γ_{la} = Correction Factor for Time of Loading A-1

t_{la} = Time of Loading (days)

$$\gamma_{vs} = \tfrac{2}{3}\left(1 + 1.13e^{-0.0213(v/s)}\right)$$

γ_{vs} = Creep Volume-Surface Ratio Correction Factor A-2

v / s = Volume to Surface Ratio of Creep Specimen

$$\gamma_{vs} = 1.2e^{-0.00472(v/s)}$$

γ_{vs} = Shrinkage Volume-Surface Ratio Correction Factor A-3

v / s = Volume to Surface Ratio

$$\gamma_s = 0.82 + 0.67s$$

γ_s = Creep Slump Correction Factor A-4

s = Concrete Slump (inches)

$$\gamma_s = 0.89 + 0.041s$$

γ_s = Shrinkage Slump Correction Factor A-5

s = Concrete Slump (inches)

$$\gamma_\psi = 0.88 + 0.0024\psi$$

γ_ψ = Fine Aggregate Percentage Correction Factor A-6

ψ = Fine Aggregate Ratio (%)

$$\gamma_\psi = 0.90 + 0.002\psi$$

γ_ψ = Shrinkage Fine Aggregate Percentage Correction Factor A-7

ψ = Fine Aggregate Ratio (%)

$\gamma_c = 0.75 + 0.00036c$

$\gamma_c =$ Shrinkage Cement Content Correction Factor A-8

$c =$ Cement Content (pounds per cubic yard)

$\gamma_a = 0.46 + 0.09\alpha \geq 1.0$

$\gamma_a =$ Creep Air Content Correction Factor A-9

$\alpha =$ Air Content (%)

$\gamma_a = 0.95 + 0.008\alpha$

$\gamma_a =$ Shrinkage Air Content Correction Factor A-10

$\alpha =$ Air Content (%)

$\gamma_\lambda = 1.27 - 0.0067\lambda$

$\gamma_\lambda =$ Creep Ambient Relative Humidity Correction Factor A-11

$\lambda =$ Ambient Relative Humidity (%) $(\lambda \geq 40\%)$

$\gamma_\lambda = 1.40 - 0.0102\lambda$

$\gamma_\lambda =$ Shrinkage Ambient Relative Humidity Correction Factor A-12

$\lambda =$ Ambient Relative Humidity (%) $(40\% \leq \lambda \leq 80\%)$

Appendix B - Flexural Members Design Calculations

Concrete and Prestressing Tendon Properties

$A = 38.25in^2$

$y_b = 3.759in$

$I = 122.44in^4$

$s_b = 32.57in^3$

$s_t = 44.67in^3$

$e_s = 1.76in$

$w_{self} = 122\frac{lbf}{ft^3}\cdot A$

$L_1 = 15.83ft$

$f_c = 7000psi$

$d_p = 4.5in$

$A_{ps} = 0.153in^2$

$E_{ps} = 28500ksi$

$f_{pu} = 270ksi$

$d_{ps} = 0.5in$

$e = 1.759in$

$E_{ci} = 122^{1.5}\cdot 33\cdot\sqrt{5000}\cdot psi$

$E_c = 122^{1.5}\cdot 33\cdot\sqrt{7000}\cdot psi$

Prestress Losses PCI Method

TL =ES+CR+SH+RE

TL = Total Loss (psi)
ES = Loss Due to Elastic Shortening (psi)
CR = Loss Due to Creep of Concrete (psi)
SH = Loss Due to Shrinkage of Concrete (psi)
RE = Loss Due to Relaxation of Tendon (psi)

Elastic Shortening Loss

$$ES = \frac{K_{es} \cdot E_{ps} \cdot f_{cir}}{E_{ci}}$$

$$K_{es} = 1.0$$

$$f_{cir} = K_{cir} \cdot \left(\frac{P_i}{A} + \frac{P_i \cdot e_s^{\,2}}{I} \right) - \frac{M_g \cdot e_s}{I}$$

$$K_{cir} = 0.9$$

$$M_g = \frac{w_{self} \cdot L_1^{\,2}}{8}$$

$$P_i = A_{ps} \cdot 0.74 \cdot 270\,\text{ksi}$$

$$ES = 11.24\ \text{ksi}$$

E_{ps} = Modulus of Elasticity of Prestressing Steel

E_{ci} = Modulus of Elasticity of Concrete at Transfer of Prestress Force

f_{cir} = Net Compressive Stress in Concrete at Center of Gravity of Prestressing Force Immediatley After the Prestress has Been Applied to the Concrete

K_{es} = 1.0 for Pretensioned Members

K_{cir} = 0.9 for Pretensioned Members

Creep Loss

$$CR = K_{cr} \cdot \left(\frac{E_{ps}}{E_c} \right) \cdot \left(f_{cir} - f_{cds} \right)$$

$$f_{cds} = \frac{M_{sd} \cdot e_s}{I}$$

$$M_{sd} = \frac{w_{self} \cdot L_1^{\,2}}{8}$$

$$K_{cr} = 1.6$$

$$CR = 13.05 \text{ ksi}$$

f_{cds} = The Concrete Stress at the Center of Gravity of Prestressing Steel Due to All Dead Loads at the Time Prestressing Force is Applied

K_{cr} = 1.6 for Sand Lightweight Concrete

Shrinkage Loss

$$SH = 8.2 \cdot 10^{-6} \cdot K_{sh} \cdot E_{ps} \cdot (1.0 - 0.06 \cdot VS) \cdot (100 - RH)$$

$$K_{sh} = 1.0$$

$$VS = 1.5249$$

$$RH = 65$$

$$SH = 7.4 \text{ ksi}$$

K_{sh} = 1.0 for Pretensioned Members

RH = Average Relative Humidity in Percent. For Kansas, this may be taken as 65 percent

VS = Volume to Surface Ratio

Relaxation of Prestressing Steel Loss

$$RE = \left[K_{re} - J \cdot (SH + CR + ES) \right] \cdot C$$

$$K_{re} = 5000 \text{ psi}$$

$$J = 0.040$$

$$C = \begin{cases} 1 + 9 \cdot \left(\frac{f_{pi}}{f_{pu}} - 0.7 \right) & \text{if } 0.75 \geq \frac{f_{pi}}{f_{pu}} \geq 0.70 \\ \text{otherwise} \\ \quad \begin{cases} \frac{\frac{f_{pi}}{f_{pu}}}{0.19} \cdot \left(\frac{\frac{f_{pi}}{f_{pu}}}{0.85} \right) - 0.55 & \text{if } 0.70 > \frac{f_{pi}}{f_{pi}} \geq 0.51 \\ \frac{\frac{f_{pi}}{f_{pu}}}{3.83} & \text{otherwise} \end{cases} \end{cases}$$

$$f_{pi} = \frac{P_i}{A_{ps}}$$

$$C = 1.36$$

$$RE = 5.07 \text{ ksi}$$

K_{re} = 5000 psi for 270 Grade Low-Relaxation Strand

J = 0.040 for 270 Grade Low-Relaxation Strand

The values of SH, CR, ES, are those computed previously.

Total Losses

$$TL = ES + CR + SH + RE$$

$$TL = 36.8 \text{ ksi}$$

Nominal-Moment Capacity Calculation Based on Strain Compatibility with PCI Losses

$f_{se} = 0.74 \cdot 270\text{ksi} - TL$

$f_{se} = 163.00\,\text{ksi}$

$\varepsilon_1 = \dfrac{f_{se}}{E_{ps}}$

$\varepsilon_1 = 0.00572$

$\varepsilon_2 = \dfrac{f_{se} \cdot A_{ps}}{A \cdot E_c} + \dfrac{f_{se} \cdot A_{ps} \cdot e^2}{I \cdot E_c}$

$\varepsilon_2 = 0.00034$

$\varepsilon_3(c_1) = \dfrac{0.003 \cdot (d_p - c_1)}{c_1}$

$$f_{ps}(c_1) = \begin{cases} 270\text{ksi} - \left(\dfrac{0.04}{\varepsilon_1 + \varepsilon_2 + \varepsilon_3(c_1) - 0.007} \right)\text{ksi} & \text{if } \varepsilon_1 + \varepsilon_2 + \varepsilon_3(c_1) > 0.0086 \\ 28500\text{ksi} \cdot (\varepsilon_1 + \varepsilon_2 + \varepsilon_3(c_1)) & \text{otherwise} \end{cases}$$

$comp(c_1) = 0.85 \cdot 8\text{in} \cdot \beta_1 \cdot c_1 \cdot f_c$

$ten(c_1) = A_{ps} \cdot f_{ps}(c_1)$

$comp(c_1) = ten(c_1)$

$c_1 = 1.21\,\text{in}$

$a = c_1 \cdot \beta_1$

$\beta_1 = 0.70$

$a = 0.85\,\text{in}$

$M_n = ten(c_1) \cdot \left(d_p - \dfrac{a}{2} \right)$

$M_n = 13.74\,\text{kip} \cdot \text{ft}$

Transfer and Development-length with PCI Losses

$$L_{tr} = \left(\frac{f_{se}}{3ksi}\right)\cdot d_{ps}$$

$$L_{tr} = 27.17\,in$$

$$L_d = L_{tr} + \left(f_{ps}(c_1) - f_{se}\right)\cdot\frac{1}{ksi}\cdot d_{ps}$$

$$L_d = 77.88\,in$$

Design Stress for Underdeveloped Strands (80% of Required Development-length) with PCI Losses

$$0.80\cdot L_d = 62.31\,in$$

$$f_{pd} = f_{se} + \frac{\left(f_{ps}(c_1) - f_{se}\right)\cdot\left(62in - L_{tr}\right)}{L_d - L_{tr}}$$

$$f_{pd} = 232.67\,ksi$$

Moment Capacity for Underdeveloped Members with PCI Losses

$$a_2 = \frac{A_{ps}\cdot f_{pd}}{0.85\cdot f_c\cdot 8in}$$

$$a_2 = 0.75\,in$$

$$M_n = A_{ps}\cdot f_{pd}\cdot\left(d_p - \frac{a_2}{2}\right)$$

$$M_n = 12.24\,kip\cdot ft$$

Shear Capacity of Member at Critical Section d_p from Support (ACI 318-05)

$$V_{ci} = 0.6 \cdot \frac{f_{ct}}{6.7} \cdot b_w \cdot d_p + V_d + \frac{V_i \cdot M_{cre}}{M_{max}}$$

$f_{ct} = 460\text{psi}$

$V_d = 229.54\text{lbf}$ $\quad b_w = 5.5\text{in}$

$M_{max} = 1251.6\text{lbf}\cdot\text{ft}$ $\quad d_p = 4.50\,\text{in}$

$V_i = 2304.5\text{lbf}$

$$M_{cre} = \left(\frac{I}{y_b}\right) \cdot \left(6 \cdot \frac{460\text{psi}}{6.7} + f_{pe} - f_d\right)$$

$M_{cre} = 5530.54\,\text{lbf}\cdot\text{ft}$

$V_{ci} = 11432.17\ \text{lbf}$

$$V_{cw} = \left(3.5 \cdot \frac{f_{ct}}{6.7} + 0.3 \cdot f_{pc}\right) \cdot 5.5\text{in} \cdot 4.5\,\text{in} + 0$$

$$f_{pc} = \frac{f_{se} \cdot A_{ps}}{A}$$

$f_{pc} = 652.00\ \text{psi}$

$V_{cw} = 10788.46\ \text{lbf}$

V_{cw} Controls Shear Strength of Member at Distance d_p from Support

AASHTO Development-length

$$L_{tr} = 60 \cdot d_{ps}$$

$d_{ps} = 0.5\,\text{in}$

$L_{tr} = 30.0\,\text{in}$

Prestressing Losses KDOT Method

$Dfs = SH + ES + CR_C + CR_S$

D_{fs} = Total Loss (psi)

SH = Loss Due to Shrinkage of Concrete (psi)

ES = Loss Due to Elastic Shortening (psi)

CR_C = Loss Due to Creep of Concrete (psi)

CR_S = Loss Due to Relaxation of Tendon (psi)

Shrinkage Loss

$RH = 65$

$SH = 17000\text{psi} - 150\text{psi} \cdot RH$

$SH = 7.25\,\text{ksi}$

RH = Average Relative Humidity in Percent. For Kansas, this may be taken as 65 percent

Elastic Shortening Loss

$$ES = \left(\frac{E_{ps}}{E_{ci}}\right) f_{cir}$$

$$f_{cir} = \left(\frac{P_{si}}{A} + \frac{P_{si} \cdot e_s^{\,2}}{I}\right) - \frac{M_g \cdot e_s}{I}$$

$$M_g = \frac{w_{self} \cdot L_1^{\,2}}{8}$$

$$P_{si} = A_{ps} \cdot f_{si}$$

$ES = 12.86\,\text{ksi}$

E_{ps} = Modulus of Elasticity of Prestressing Steel

E_{ci} = Modulus of Elasticity of Concrete at Transfer of Prestress Force

f_{cir} = Net Compressive Stress in Concrete at Center of Gravity of Prestressing Force Immediatley After the Prestress has Been Applied to the Concrete

Creep Loss

$CR_c = 12 \cdot f_{cir} - 7 f_{cds}$

$f_{cds} = 0.0$

$CR_c = 17.02\,\text{ksi}$

f_{cds} = The Concrete Stress at the Center of Gravity of Prestressing Steel Due to All Dead Loads Except the Dead Loads Present at the Time Prestressing Force is Applied

Relaxation of Prestressing Steel Loss

$CR_s = 5000\text{psi} - 0.10 \cdot ES - 0.05 \cdot \left(SH + CR_c \right)$

$CR_s = 2.50\,\text{ksi}$

The values of SH, CR, ES, are those computed previously.

Total Losses

$\Delta fs = SH + ES + CR_c + CR_s$

$\Delta fs = 39634.09$ psi

Nominal-Moment Capacity Calculation Based on Strain Compatibility with KDOT Losses

$f_{se} = 0.74 \cdot 270\text{ksi} - \Delta fs$

$f_{se} = 160.17\,\text{ksi}$

$\varepsilon_1 = \dfrac{f_{se}}{E_{ps}}$

$\varepsilon_1 = 0.00562$

$\varepsilon_2 = \dfrac{f_{se} \cdot A_{ps}}{A \cdot E_c} + \dfrac{f_{se} \cdot A_{ps} \cdot e^2}{I \cdot E_c}$

$\varepsilon_2 = 0.00034$

$\varepsilon_3(c_1) = \dfrac{0.003 \cdot (d_p - c_1)}{c_1}$

$$f_{ps}(c_1) = \begin{cases} 270\text{ksi} - \left(\dfrac{0.04}{\varepsilon_1 + \varepsilon_2 + \varepsilon_3(c_1) - 0.007} \right)\text{ksi} & \text{if } \varepsilon_1 + \varepsilon_2 + \varepsilon_3(c_1) > 0.0086 \\ 28500\text{ksi} \cdot (\varepsilon_1 + \varepsilon_2 + \varepsilon_3(c_1)) & \text{otherwise} \end{cases}$$

$comp(c_1) = 0.85 \cdot 8\text{in} \cdot \beta_1 \cdot c_1 \cdot f_c$

$ten(c_1) = A_{ps} \cdot f_{ps}(c_1)$

$comp(c_1) = ten(c_1)$

$c_1 = 1.21\,\text{in}$

$a = c_1 \cdot \beta_1$

$\beta_1 = 0.70$

$a = 0.85\,\text{in}$

$M_n = ten(c_1) \cdot \left(d_p - \dfrac{a}{2} \right)$

$M_n = 13.74\,\text{kip} \cdot \text{ft}$

Transfer and Development-length with KDOT Losses

$$L_{tr} = \left(\frac{f_{se}}{3ksi}\right)\cdot d_{ps}$$

$$L_{tr} = 26.69\,in$$

$$L_d = L_{tr} + \left(f_{ps}(c_1) - f_{se}\right)\cdot\frac{1}{ksi}\cdot d_{ps}$$

$$L_d = 78.79\,in$$

Design Stress for Underdeveloped Strands (80% of Required Development-length) with KDOT Losses

$$0.80\cdot L_d = 63.03\,in$$

$$f_{pd} = f_{se} + \frac{\left(f_{ps}(c_1) - f_{se}\right)\cdot\left(62in - L_{tr}\right)}{L_d - L_{tr}}$$

$$f_{pd} = 230.78\,ksi$$

Moment Capacity for Underdeveloped Members with KDOT Losses

$$a_2 = \frac{A_{ps}\cdot f_{pd}}{0.85\cdot f_c\cdot 8in}$$

$$a_2 = 0.74\,in$$

$$M_n = A_{ps}\cdot f_{pd}\cdot\left(d_p - \frac{a_2}{2}\right)$$

$$M_n = 12.15\,kip\cdot ft$$

Appendix C - Petrographic Examination Reports from Construction and Technology Laboratories Group

CTL GROUP
Building Knowledge. Delivering Results.
CONSTRUCTION TECHNOLOGY LABORATORIES
ENGINEERS & CONSTRUCTION TECHNOLOGY CONSULTANTS
www.CTLGroup.com

REPORT OF PETROGRAPHIC EXAMINATION

Date: April 3, 2008

CTL Project No.: 152872

Re: Petrographic Examination of Concrete Cores from Bridge Decks in Belvue and Maple Hill, Kansas

Three partial-depth concrete cores, designated as Cores B1 (Fig. 1), BNT1 (Fig. 2), and MH1 (Fig. 3), were received on January 2, 2008 from Mr. Jake Perkins, Kansas State University, Manhattan, Kansas. The cores were reportedly taken from light-weight concrete bridge decks at the above-specified locations due to concern with localized surface scaling and spalling (local flaking and peeling away of the near-surface portion of concrete). Cores B1 and BNT1 were taken from separate bridges in Belvue, Kansas, which are 10 miles away from each other. Core BNT1 was taken from a distressed portion of the bridge deck, and Core B1 was taken from an area of the bridge deck exhibiting a better condition. Core MH1 was taken from a bridge in Maple Hill, Kansas, where the entire deck was in good condition. Reportedly, the concrete represented by the cores is approximately 30 years old. Petrographic examination (ASTM C 856) is requested to determine possible causes of the reported surface distress, and to describe general quality and characteristics of the concrete represented by the cores.

FINDINGS

Main findings are described below. Selected petrographic observations for each core are summarized in Table 1 for comparison. Additional information is provided in the attached figure pages and data sheets.

- Top surface of Core B1 exhibits no significant distress. However, microscopical examination of the core reveals closely-spaced, sub-parallel hairline cracks to depths of 1.3 in., and closely-spaced, sub-parallel microcracks to depths of 2.0 in. from the top surface (Fig. 4a). The core tends to split along the sub-parallel hairline cracks when hit with a hammer in the laboratory, indicating that the observed hairline cracks create localized sub-surface zones of weakness in the concrete (incipient scaling). Based on microscopical examination, these observed sub-parallel hairline cracks and microcracks

Corporate Office: 5400 Old Orchard Road Skokie, Illinois 60077-1030 Phone: 847-965-7500 Fax: 847-965-6541
Washington D.C. Office: 9030 Red Branch Road, Suite 110 Columbia, Maryland 21045-2003 Phone: 410-997-0400 Fax: 410-997-8480

are consistent with damage caused by cyclic freezing and thawing of non-air-entrained concrete while critically saturated with water. The concrete represented by the core is not air entrained with an estimated total air content of less than 1% (Fig. 4b). Hardened paste in the core is moderately soft to moderately hard and absorptive (water drops applied to fresh fractures are quickly absorbed into the paste), which indicates concrete made and placed with a moderate to moderately high water-cement ratio (w/c).

- Top surface of Core BNT1 is rough and distressed with many exposed and fractured aggregate particles (Fig. 2a). Based on petrographic examination, the observed distress is mainly attributed to cyclic freezing and thawing of non-air-entrained concrete while critically saturated with water. Microscopical examination reveals a few sub-parallel hairline cracks near the distressed top surface. Closely-spaced, sub-parallel microcracks and associated randomly-oriented microcracks are observed through the full depth of the core (Fig. 5). The concrete represented by the core is not air entrained with an estimated total air content of less than 1%. Hardened paste in the core is moderately soft and absorptive, which indicates concrete made and placed with a moderately high w/c.

- The concrete represented by Core MH1 is in good condition. The core does not exhibit surface distress or any significant cracking in the core body (Fig. 6). The concrete was air entrained with an estimated air content of approximately 3 to 5% (Fig. 6b). The core exhibits somewhat improved physical paste properties compared to Cores B1 and BNT1. The paste in the core is moderately hard. The paste is somewhat absorptive overall but is denser compared to the paste in Cores B1 and BNT1. Estimated w/c is moderate, which is lower than the estimated w/c for Cores B1 and BNT1 (Fig. 7).

PETROGRAPHIC OBSERVATIONS

Both Cores B1 and BNT1 exhibit similar concrete composition. Concrete represented by the cores contains manufactured light-weight coarse and fine aggregates (expanded shale) in a portland cement paste. Core MH1 exhibits slightly different composition (mainly the fine aggregate composition) compared to Cores B1 and BNT1. The concrete represented by Core MH1 contains manufactured light-weight coarse aggregate (expanded shale) and siliceous sand fine aggregate in a portland cement paste. Aggregate particles in the concrete represented by all three cores are evenly graded to an observed top size of 0.3 in. (8 mm), and uniformly

distributed throughout the body of the cores. The concrete is well consolidated (no unusually large voids are observed). Paste properties such as hardness and paste-aggregate bond are generally consistent throughout the depth of the cores. The concrete does not show any evidence of alkali-aggregate reaction, chemical attack, or other deleterious reactions involving aggregates and/or paste constituents.

Many voids, cracks, and microcracks in Cores B1 and BNT1 are lined with secondary ettringite (calcium sulfoaluminate hydrate) deposits (Fig. 8). A few voids in Core MH1 are lined with secondary ettringite deposits. Presence of void-filling, secondary ettringite deposits is not considered deleterious, and is indicative of moisture infiltration into the concrete. The hardened paste in Cores B1 and BNT1 is depleted in calcium hydroxide (calcium hydroxide was leached out of the concrete), further indicating migration of water through the concrete.

DISCUSSION

Cores B1 and BNT1 exhibit freezing and thawing damage manifested as numerous closely-spaced hairline cracks and microcracks oriented sub-parallel to the top surface. Based on microscopical examination, both of the cores are non-air-entrained with an estimated total air content of less than 1%. American Concrete Institute (ACI 201.2R) currently recommends total target air content of 7.5 (±1.5)% for concrete containing 3/8-in. top size aggregate in conditions of severe exposure. Severe exposure is considered to be concrete exposed to wet freeze-thaw conditions, deicers, or other aggressive agents. Bridge decks in Kansas are generally considered to experience severe exposure (ASTM C 33, Fig. 1).

The hardened paste in Cores B1 and BNT1 is absorptive. A more absorptive and permeable paste microstructure is often the result of using a relatively high w/c in a concrete mix. Further testing and evaluation can address whether the concrete represented by the cores conforms to the specified maximum w/c and/or minimum compressive strength requirements for the given exposure condition.

Further field evaluation should also address whether the reported surface distress was contributed to by other possible causes not fully revealed by petrographic examination of the submitted cores, such as corrosion of embedded steel reinforcing bars.

TABLE 1 SELECTED PETROGRAPHIC OBSERVATIONS

Characteristics	Core B1	Core BNT1	Core MH1
Top surface	Rough, worn surface; no surface distress	Rough, distressed surface with fractured aggregate particles exposed; original top surface was lost due to distress and not available for examination	Rough, worn surface; no surface distress
Cracks/ microcracks	Closely-spaced, sub-parallel hairline cracks to depths of 1.3 in. from top surface Closely-spaced sub-parallel microcracks to depths of 2.0 in. from top surface A few vertical microcracks to depths of 1.5 in. from top surface	A few sub-parallel hairline cracks near distressed top surface Closely-spaced, sub-parallel microcracks and associated randomly-oriented microcracks through depth of core	A few vertical microcracks to depth of 2.0 in.
Paste hardness	Moderately soft to moderately hard	Moderately soft	Moderately hard
Paste absorptivity	Absorptive	Absorptive	Somewhat absorptive
Paste-aggregate bond	Tight	Tight	Tight
*Estimated water-cement ratio	Moderate to moderately high (approximately 0.50 to 0.60)	Moderately high (approximately 0.55 to 0.65)	Moderate (approximately 0.45 to 0.55)
Estimated air content	Less than 1%; not air entrained	Less than 1%; not air entrained	3 to 5%; air entrained
Carbonation	0.7 to 1.0 in. from top surface	0.2 in. from existing distressed top surface	0.1 to 0.2 in. from top surface
Secondary deposits	Voids, cracks, and microcracks are lined with secondary ettringite deposits	Voids, cracks, and microcracks are lined with secondary ettringite deposits	A few voids are lined with secondary ettringite deposits
Coarse aggregate	Manufactured light-weight aggregate (expanded shale)	Manufactured light-weight aggregate (expanded shale)	Manufactured light-weight aggregate (expanded shale)
Fine aggregate	Manufactured light-weight aggregate (expanded shale)	Manufactured light-weight aggregate (expanded shale)	Siliceous sand (mainly quartz, quartzite, feldspar, and granitic rocks)

*Estimation based on observed physical properties and microscopical characteristics of the hardened paste. The numeric estimates are somewhat speculative due to reported old age and apparent evidence of continued cement hydration in the paste.

METHODS OF TEST

Petrographic examination was performed in accordance with ASTM C 856-04, "Standard Practice for Petrographic Examination of Hardened Concrete." The cores were visually inspected and photographed. Epoxy was applied to the distressed top surface region of Core BNT1 to prevent damage during samples preparation and to preserve as-received condition. After the epoxy set, each core was cut in half perpendicular to the top surface and one side of each was lapped for further study. Lapped and freshly broken surfaces were examined at magnifications up to 45X using a stereomicroscope. After inspection of the cut surfaces, a rectangular block measuring approximately 1.0-in. (25-mm) wide, 1.8-in. (45-mm) long, and 0.4-in. (10-mm) thick was cut from top surface portion of each core for thin-section preparation. One side of each thin-section block was finely ground to produce a smooth, flat surface. After cleaning and drying, the prepared surfaces were mounted on separate ground glass microscope slides with epoxy resin. Following epoxy hardening, the thickness of the mounted blocks was reduced to approximately 0.0008 in. (20 μm). The resulting thin sections were examined at magnifications up to 400x using a polarized-light microscope to evaluate aggregate and paste mineralogy and microstructure.

Estimated water-cement ratio (w/c), when reported, is based on concrete and paste properties including, but not limited to: relative amounts of residual (unhydrated) portland cement clinker particles, paste hardness, color, and luster, paste-aggregate bond, and relative absorptivity of paste as indicated by a freshly fractured surface's readiness to accept applied water droplets. These techniques have been widely used by industry professionals to estimate w/c.

Depth and extent of paste carbonation was determined by the application of a pH indicator (phenolphthalein) solution to freshly fractured and saw-cut surfaces of the concrete. The solution imparts a deep magenta stain to high-pH, non-carbonated, cement paste but does not stain reduced-pH, carbonated, paste. Extent of paste carbonation was also confirmed during microscopical examination of the thin sections.

Notes:

1) The samples will be retained for 30 days, after which they will be discarded unless we hear otherwise from you.
2) This report may not be reproduced except in its entirety.
3) This examination represents specifically the samples submitted.

Sang Y. Lee, Ph.D.
Microscopist
Microscopy Group

SYL

152872

Attachments

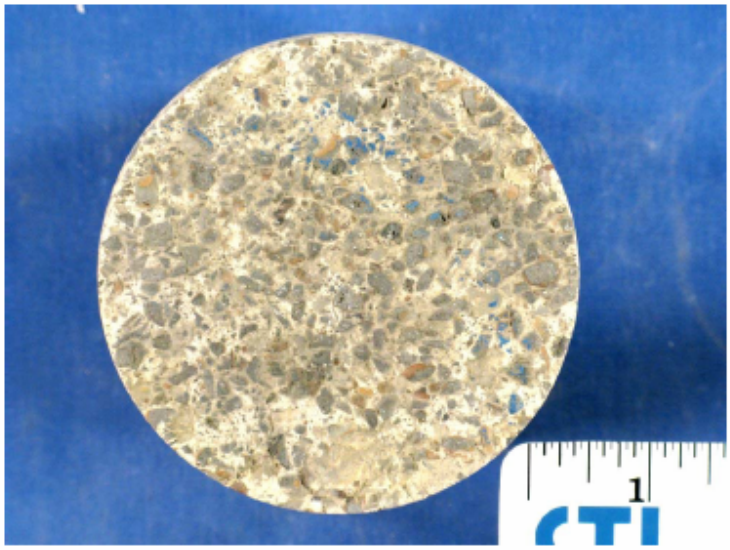

1a. Top surface.

1b. Side view. Top surface is up.

Fig. 1 Core B1 as-received for examination. Scale is marked in inches.

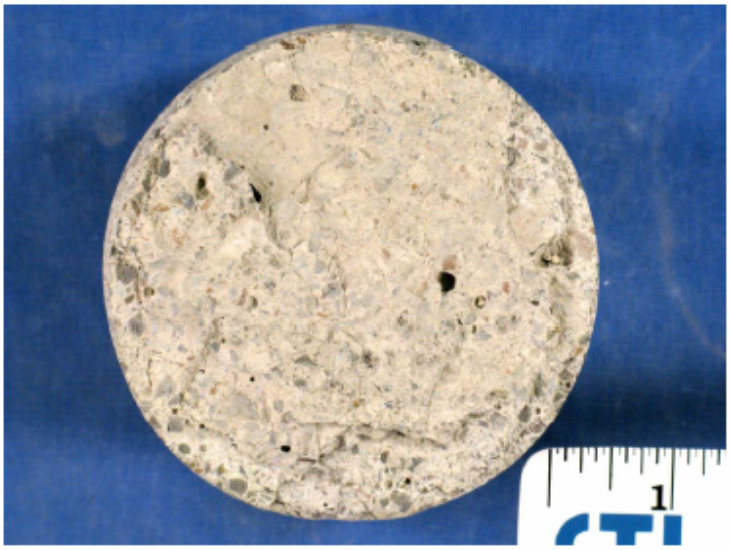

2a. Distressed top surface. Original concrete top surface was removed due to distress and not provided for examination.

2b. Side view. Top surface is up.

Fig. 2 Core BNT1 as-received for examination. Scale is marked in inches.

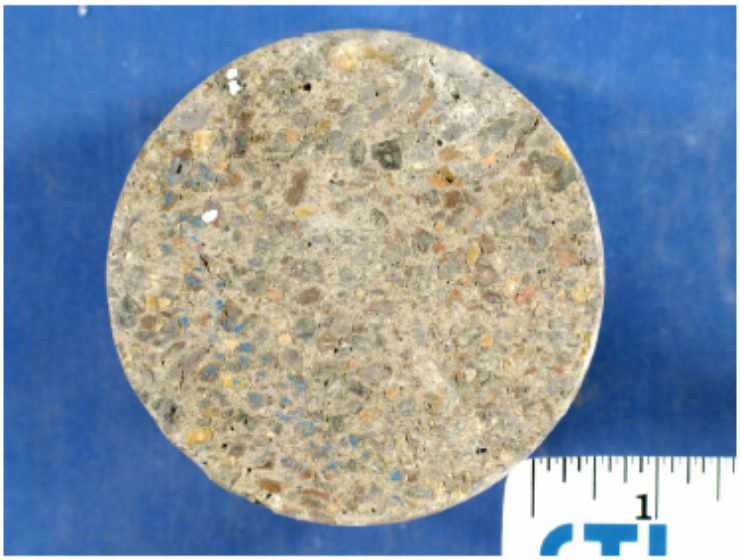

3a. Top surface.

3b. Side view. Top surface is up.

Fig. 3 Core MH1 as-received for examination. Scale is marked in inches.

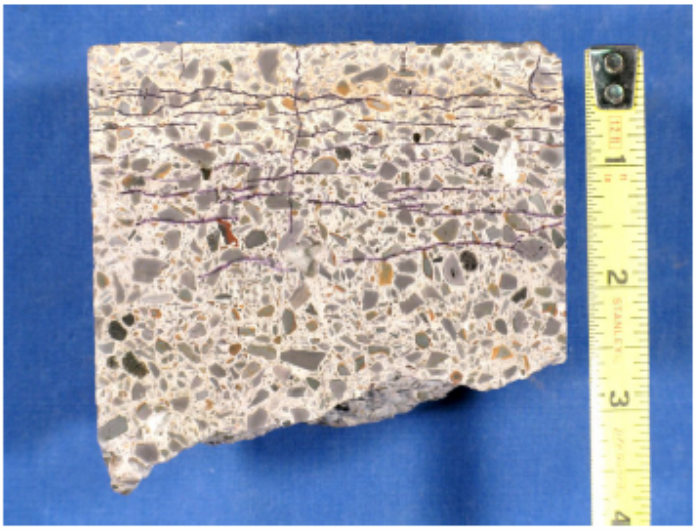

4a. General view. Some of the observed hairline cracks and microcracks are marked by black pen (actual widths of cracks and microcracks are significantly more narrow). Scale is in inches.

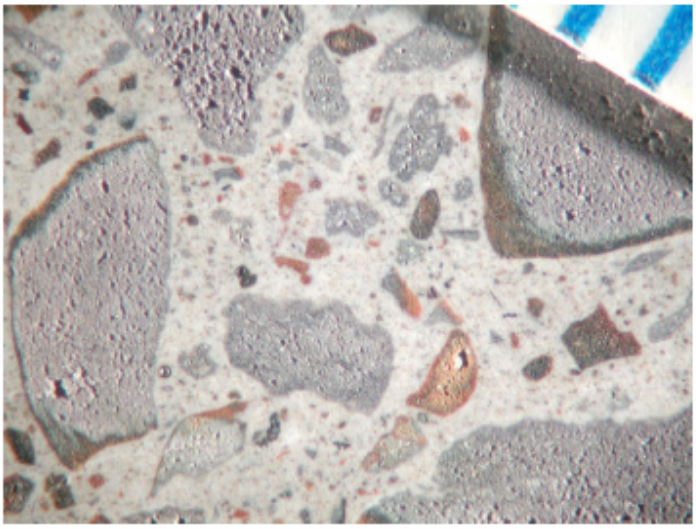

4a. Stereomicroscope image showing a representative field of the lapped surface shown in Fig. 4a. Lack of small, spherical air voids in the paste indicates that the concrete represented by the core was not air entrained. Scale increments are 0.04 in.

Fig. 4 Cut and lapped cross-section of Core B1.

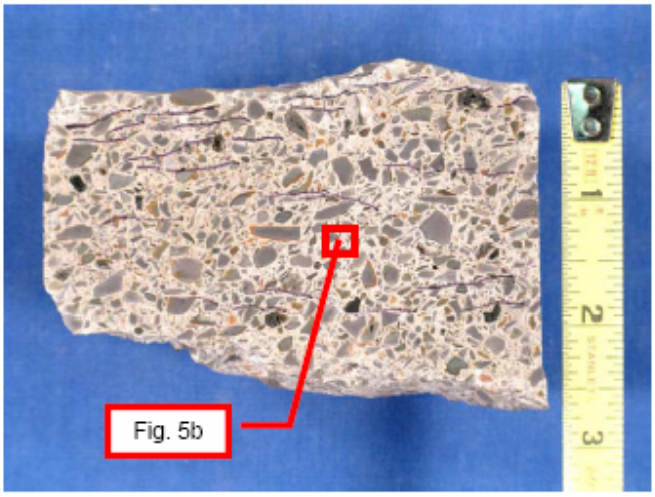

5a. Cut and lapped cross-section. Some of the observed hairline cracks and microcracks are marked by black pen (actual widths of cracks and microcracks are significantly more narrow). Epoxy was applied to the top surface of the core in the laboratory to prevent damage during sample preparation. Scale is in inches.

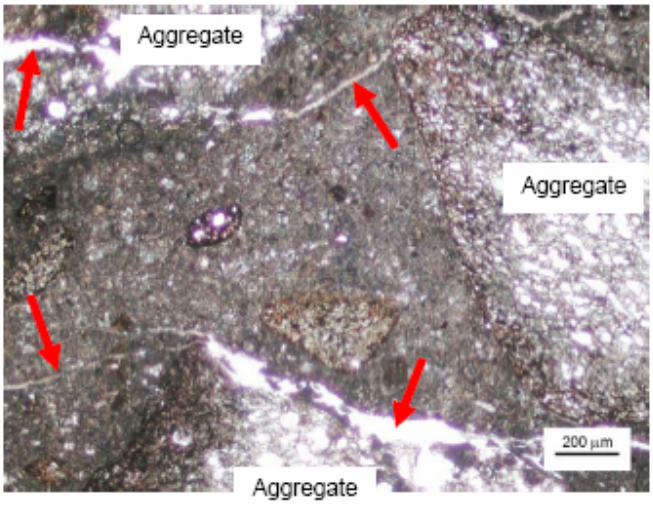

5b. Transmitted (plane-polarized) light photomicrograph of thin-section showing sub-parallel microcracks in the area marked by the red box in Fig. 5a. Top surface is up.

Fig. 5 Images showing sub-parallel hairline cracks and microcracks in Core BNT1.

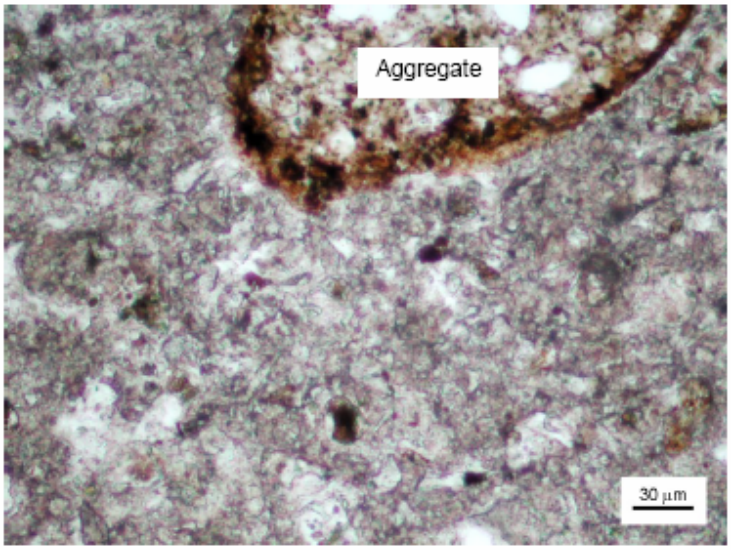

7a. Core BNT1.

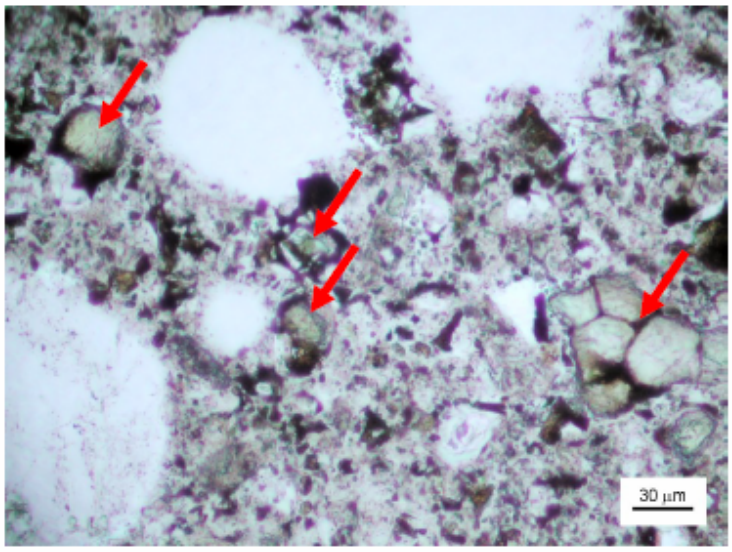

7b. Core MH1.

Fig. 7 Transmitted (plane-polarized) light photomicrograph of thin-sections showing a representative field of hardened paste in each core. The paste in Core MH1 contains higher volume of residual portland cement clinker particles (red arrows) compared to the paste in Core BNT1, consistent with a lower water-cement ratio.

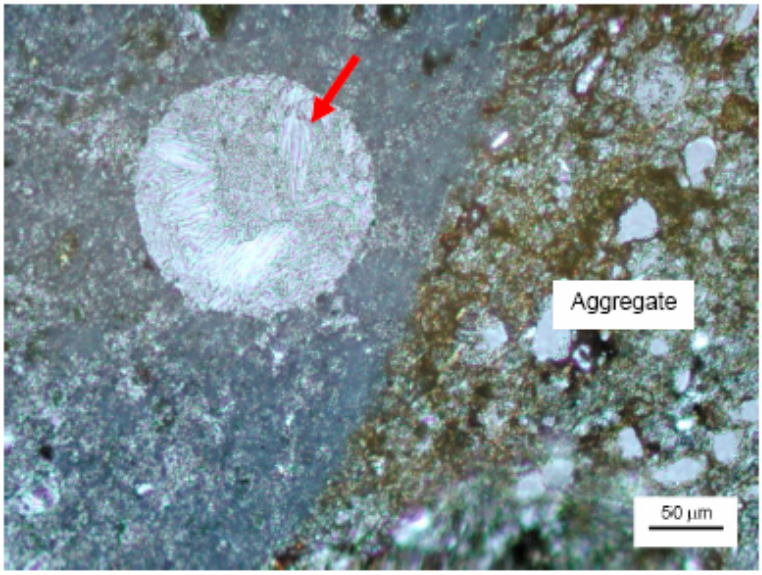

Fig. 8 Transmitted (cross-polarized) light photomicrograph of thin-section showing secondary ettringite deposits filling a void in Core BNT1 (red arrow).

PETROGRAPHIC EXAMINATION OF HARDENED CONCRETE, ASTM C 856

CTLGROUP PROJECT NO.: 152872 | *DATE REPORTED*: April 3, 2008

CLIENT: Kansas State University | *DATE RECEIVED*: January 2, 2008

STRUCTURE: Bridge deck | *EXAMINED BY*: Sang Lee

LOCATION: Belvue, Kansas |

SAMPLE

Identification: Core B1; an area of bridge deck in Belvue, Kansas, exhibiting relatively good condition.

Dimensions: Core diameter = 4.0 in. (102 mm); length = approximately 2.0 to 4.0 in. (51 to 102 mm); partial deck thickness.

Top Surface: Rough and worn surface with partially exposed aggregate particles.

Bottom Surface: Uneven, rough, fractured surface.

Cracks, Joints, or Large Voids: Closely-spaced, sub-parallel, hairline cracks are observed to depths of 1.3 in. (33 mm) from top surface, passing through aggregate particles. No joints or unusually large voids are observed.

Reinforcement: No reinforcement is observed in core segment.

AGGREGATES

Coarse: Manufactured, light-weight aggregate (expanded shale).

Fine: Manufactured, light-weight aggregate (expanded shale) and occasional quartz.

Gradation & Top Size: Evenly graded to an observed top size of 0.3 in. (8 mm).

Shape & Distribution: Aggregate particles are angular to sub-angular and equant to elongate; distribution is uniform.

PASTE

Color: Light gray; carbonated top approximate 0.7 to 1.0 in. (18 to 25 mm) of paste is light-beige gray.

Hardness: Moderately soft to moderately hard.

Luster: Dull.

Paste-Aggregate Bond: Tight; fresh fractures pass through almost all aggregate particles.

Depth of Carbonation: Approximately 0.7 to 1.0 in. (18 to 25 mm) from top surface.

Air Content: Less than 1%; the concrete is not air entrained based on scarcity of small, spherical air voids.

Calcium Hydroxide*: Almost none (less than 1%).

Unhydrated Portland Cement Clinker Particles*: Approximately 1% of partially hydrated portland cement clinker particles; relicts of in-situ hydrated portland cement clinker particles are common in hardened paste.

Supplementary Cementing Materials*: None observed.

Secondary Deposits: Voids, cracks, and microcracks are lined with secondary ettringite deposits.

MICROCRACKING: Closely-spaced, sub-parallel, microcracks are observed to depths of approximately 2.0 in. (50 mm), passing through aggregate particles. Randomly oriented microcracks are commonly observed in remaining bottom portion of core. A few vertical microcracks extend to depths of approximately 1.5 in. (38 mm) from top surface.

ESTIMATED WATER-CEMENT RATIO (W/C): Moderate to moderately high (approximately 0.50 to 0.60) based on observed physical properties and microscopical characteristics of hardened paste. The numeric estimate is somewhat speculative due to apparent evidence of continued cement hydration and reported old age.

MISCELLANEOUS: Hardened paste is absorptive; water drops applied on fresh fractures are quickly absorbed into paste.

*percent by volume of paste

PETROGRAPHIC EXAMINATION OF HARDENED CONCRETE, ASTM C 856

CTLGROUP PROJECT NO.: 152872 | *DATE REPORTED*: April 3, 2008

CLIENT: Kansas State University | *DATE RECEIVED*: January 2, 2008

STRUCTURE: Bridge deck | *EXAMINED BY*: Sang Lee

LOCATION: Belvue, Kansas |

SAMPLE

Identification: Core BNT1; an area of bridge deck in Belvue, Kansas, exhibiting distress. This bridge is approximately 10 miles away from the bridge where Core B1 was taken.

Dimensions: Core diameter = 4.0 in. (102 mm); length = approximately 1.9 to 2.8 in. (48 to 71 mm); partial deck thickness.

Top Surface: Irregular, rough, distressed surface with fractured aggregate particles exposed. Original concrete top surface was lost due to distress and not available for examination.

Bottom Surface: Uneven, rough, fractured surface.

Cracks, Joints, or Large Voids: A few surface-parallel hairline cracks are locally observed near distressed top surface region. No joints or unusually large voids are observed.

Reinforcement: No reinforcement is observed in core segment.

AGGREGATES

Coarse: Manufactured, light-weight aggregate (expanded shale).

Fine: Manufactured, light-weight aggregate (expanded shale) and occasional quartz.

Gradation & Top Size: Evenly graded to an observed top size of 0.3 in. (8 mm).

Shape & Distribution: Aggregate particles are angular to sub-angular and equant to elongate; distribution is uniform.

PASTE

Color: Light gray; carbonated top approximate 0.2 in. (5 mm) of paste is somewhat lighter.

Hardness: Moderately soft to moderately hard.

Luster: Dull.

Paste-Aggregate Bond: Tight; fresh fractures pass through almost all aggregate particles.

Depth of Carbonation: Approximately 0.2 in. (5 mm) from distressed top surface.

Air Content: Less than 1%; the concrete is not air entrained based on scarcity of small, spherical air voids.

Calcium Hydroxide*: Almost none (less than 1%).

Unhydrated Portland Cement Clinker Particles*: Almost completely hydrated (less than 1%); relicts of in-situ hydrated portland cement clinker particles are common in hardened paste.

Supplementary Cementing Materials*: None observed.

Secondary Deposits: Voids, cracks, and microcracks are lined with secondary ettringite deposits.

MICROCRACKING: Closely-spaced, sub-parallel microcracks and associated randomly-oriented microcracks are observed through depth of core.

ESTIMATED WATER-CEMENT RATIO (W/C): Moderately high (approximately 0.55 to 0.65) based on observed physical properties and microscopical characteristics of hardened paste. The numeric estimate is somewhat speculative due to apparent evidence of continued cement hydration and reported old age.

MISCELLANEOUS: Hardened paste is absorptive; water drops applied on fresh fractures are quickly absorbed into paste.

*percent by volume of paste

PETROGRAPHIC EXAMINATION OF HARDENED CONCRETE, ASTM C 856

CTLGROUP PROJECT NO.: 152872 | *DATE REPORTED*: April 3, 2008

CLIENT: Kansas State University | *DATE RECEIVED*: January 2, 2008

STRUCTURE: Bridge deck | *EXAMINED BY*: Sang Lee

LOCATION: Maple Hill, Kansas |

SAMPLE

Identification: Core MH1; a bridge deck in Maple Hill, Kansas, exhibiting relatively good condition.

Dimensions: Core diameter = 4.0 in. (102 mm); length = approximately 3.9 to 4.3 in. (99 to 109 mm); partial deck thickness.

Top Surface: Rough and worn surface with partially exposed aggregate particles.

Bottom Surface: Uneven, rough, fractured surface.

Cracks, Joints, or Large Voids: No cracks, joints, or unusually large voids are observed.

Reinforcement: No reinforcement is observed in core segment.

AGGREGATES

Coarse: Manufactured, light-weight aggregate (expanded shale).

Fine: Siliceous sand consisting mainly of quartz, quartzite, feldspar, and granitic rocks. Sand-size particles of manufactured, light-weight aggregate (expanded shale) are equally abundant.

Gradation & Top Size: Evenly graded to an observed top size of 0.3 in. (8 mm).

Shape & Distribution: Coarse aggregate particles are angular to sub-angular and equant to elongate; distribution is uniform. Fine aggregate particles are angular to rounded and equant to elongate; distribution is uniform.

PASTE

Color: Medium-gray.

Hardness: Moderately hard.

Luster: Dull to subvitreous.

Paste-Aggregate Bond: Tight; fresh fractures pass through almost all aggregate particles.

Depth of Carbonation: Approximately 0.1 to 0.2 in. (3 to 5 mm) from top surface.

Air Content: Estimated 3 to 5%; the concrete is air entrained based on abundance of small, spherical air voids. Air voids distribution is locally non-uniform in core body. No significant reduction of entrained air voids are observed in top surface region.

Calcium Hydroxide*: Estimated 5 to 8% of calcium hydroxide; calcium hydroxide mostly occurs as fine crystals scattered in paste and along periphery of a few aggregate particles.

Unhydrated Portland Cement Clinker Particles*: Estimated 4 to 7% of unhydrated or partially hydrated portland cement clinker particles. Relicts of hydrated portland cement clinker particles are common.

Supplementary Cementing Materials*: None observed.

Secondary Deposits: A few voids are lined with secondary ettringite deposits.

MICROCRACKING: A few vertical microcracks extend to depths of approximately 2.0 in. (50 mm) from top surface. Other randomly-oriented, discontinuous microcracks are commonly observed throughout core body.

ESTIMATED WATER-CEMENT RATIO (W/C): Moderate (approximately 0.45 to 0.55) based on observed physical properties and microscopical characteristics of hardened paste.

MISCELLANEOUS: Hardened paste is somewhat absorptive; water drops applied on fresh fractures are readily absorbed into paste.

*percent by volume of paste

Copy No. 1

Materials & Research, Kansas Department of Transportation

Project Number 152885

Petrographic Examination of Concrete Cores from Bridge Deck – Randolph Bridge, Kansas

Date:
July 7, 2008

Submitted by:
Sang Y. Lee

CTLGroup
5400 Old Orchard Road
Skokie, Illinois 60077-1030
(847) 965-7500

www.CTLGroup.com

CTLGROUP
Building Knowledge. Delivering Results.

CTL GROUP
Building Knowledge. Delivering Results.
CONSTRUCTION TECHNOLOGY LABORATORIES
ENGINEERS & CONSTRUCTION TECHNOLOGY CONSULTANTS
www.CTLGroup.com

REPORT OF PETROGRAPHIC EXAMINATION

Date: July 8, 2008

CTL Project No.: 152885

Re: Petrographic Examination of Concrete Cores from Bridge Deck – Randolph Bridge, Kansas

Three partial-depth concrete cores, designated as Cores C1S2 (Fig. 1), C2S3 (Fig. 2), and C3S4 (Fig. 3), were received on May 5, 2008 from Mr. David Meggers, Materials and Research, Kansas Department of Transportation, Topeka, Kansas. The cores were reportedly taken from a light-weight concrete bridge deck at the above-specified location. Petrographic examination (ASTM C 856) is requested to evaluate the presence of alkali-silica reaction (ASR) in the concrete represented by the cores.

FINDINGS

Based on petrographic examination, the concrete presented by each core exhibits no apparent evidence of alkali-aggregate reaction (such as ASR) or other expansive deleterious reactions involving aggregates and/or paste constituents.

Each core exhibits a vertical crack extending through the depth of concrete (Figs. 1 through 6). The cracks typically narrow toward the top surface and pass through aggregate particles. In concrete exhibiting no deleterious reactions, cracks exhibiting these features are typically related to drying shrinkage, thermal stresses, or other structural causes which cannot be fully evaluated by petrographic examination. Further field and laboratory evaluation would be needed to determine the exact causes of the observed cracking in the deck concrete. Excluding the localized vertical cracking, the concrete presented by the cores is in good condition and is of relatively good quality.

Other findings are described below. Additional information is provided in the attached figure pages and data sheets.

1. The submitted cores consist of an asphaltic topping and the underlying concrete (Figs. 1 through 6). The concrete contains crushed light-weight coarse and fine aggregates

Corporate Office: 5400 Old Orchard Road Skokie, Illinois 60077-1030 Phone: 847-965-7500 Fax: 847-965-6541
Washington D.C. Office: 9030 Red Branch Road, Suite 110 Columbia, Maryland 21045-2003 Phone: 410-997-0400 Fax: 410-997-8480

(expanded shale) in a portland cement paste (Fig. 7). The aggregate particles are evenly graded to an observed top size of 0.3 in., and uniformly distributed throughout the concrete. Holding all other factors equal, concrete with such small aggregate size is known to be generally more susceptible to drying shrinkage compared to concrete containing larger size aggregates.

2. Top surface of the concrete is rough with many fractured aggregate particles partially exposed. Microfractures and microcracks oriented sub-parallel to the surface are locally observed in the top approximately 0.1 to 0.2 in. of the concrete. These microfractures and microcracks may be related to: (1) localized damage due to abrasive concrete surface preparation for the topping application, or (2) pre-existing surface distress (such as freezing and thawing distress) before the topping had been applied. A few vertical microcracks are locally observed in the top surface region of the concrete. Randomly oriented, discontinuous microcracks are common throughout the body of the concrete. Some of these vertical and randomly-oriented microcracks are judged to be shrinkage-related.

3. The hardened paste in the concrete represented by the cores is overall moderately hard and fairly dense. Paste-aggregate bond in the concrete is tight (fresh fractures pass through majority of aggregate particles). These observed physical paste properties are generally consistent with concrete made and placed with a moderate water-cement ratio (w/c). The concrete exhibits small, irregular patches of lighter and softer paste along the periphery of some aggregate particles and in the nearby paste, which may be related to localized increase of w/c of the paste around the pre-wetted light-weight aggregates. However, quality of the concrete does not appear to be significantly compromised by presence of such localized patches of softer paste, as evidenced by the overall good physical concrete properties.

4. The concrete in the cores is not air entrained based on scarcity of small, spherical air voids. Estimated entrapped air content is 1 to 3% in Core C1S2, and 2 to 4% in Cores C2S3 and C3S4. Many of the entrapped voids in the concrete are lined with secondary ettringite deposits. Presence of such void-filling ettringite is not considered deleterious, and typically indicates presence of moisture in the concrete.

METHODS OF TEST

Petrographic examination was performed in accordance with ASTM C 856-04, "Standard Practice for Petrographic Examination of Hardened Concrete." The cores were visually inspected and photographed. Each core was cut in half perpendicular to the top surface and one side of each was lapped for further study. Lapped and freshly broken surfaces were examined at magnifications up to 45X using a stereomicroscope. After inspection of the cut surfaces, a rectangular block measuring approximately 1.0-in. (25-mm) wide, 1.8-in. (45-mm) long, and 0.4-in. (10-mm) thick was cut from the concrete body of each core for thin-section preparation. One side of each thin-section block was finely ground to produce a smooth, flat surface. After cleaning and drying, the prepared surfaces were mounted on separate ground glass microscope slides with epoxy resin. Following epoxy hardening, the thickness of the mounted blocks was reduced to approximately 0.0008 in. (20 μm). The resulting thin sections were examined at magnifications up to 400x using a polarized-light microscope to evaluate aggregate and paste mineralogy and microstructure.

Estimated water-cement ratio (w/c), when reported, is based on concrete and paste properties including, but not limited to: relative amounts of residual (unhydrated) portland cement clinker particles, paste hardness, color, and luster, paste-aggregate bond, and relative absorptivity of paste as indicated by a freshly fractured surface's readiness to accept applied water droplets. These techniques have been widely used by industry professionals to estimate w/c.

Depth and extent of paste carbonation was determined by the application of a pH indicator (phenolphthalein) solution to freshly fractured and saw-cut surfaces of the concrete. The solution imparts a deep magenta stain to high-pH, non-carbonated, cement paste but does not stain reduced-pH, carbonated, paste. Extent of paste carbonation was also confirmed during microscopical examination of the thin sections.

Notes:

1) The samples will be retained for 30 days, after which they will be discarded unless we hear otherwise from you.
2) This report may not be reproduced except in its entirety.
3) This examination represents specifically the samples submitted.

METHODS OF TEST

Petrographic examination was performed in accordance with ASTM C 856-04, "Standard Practice for Petrographic Examination of Hardened Concrete." The cores were visually inspected and photographed. Each core was cut in half perpendicular to the top surface and one side of each was lapped for further study. Lapped and freshly broken surfaces were examined at magnifications up to 45X using a stereomicroscope. After inspection of the cut surfaces, a rectangular block measuring approximately 1.0-in. (25-mm) wide, 1.8-in. (45-mm) long, and 0.4-in. (10-mm) thick was cut from the concrete body of each core for thin-section preparation. One side of each thin-section block was finely ground to produce a smooth, flat surface. After cleaning and drying, the prepared surfaces were mounted on separate ground glass microscope slides with epoxy resin. Following epoxy hardening, the thickness of the mounted blocks was reduced to approximately 0.0008 in. (20 μm). The resulting thin sections were examined at magnifications up to 400x using a polarized-light microscope to evaluate aggregate and paste mineralogy and microstructure.

Estimated water-cement ratio (w/c), when reported, is based on concrete and paste properties including, but not limited to: relative amounts of residual (unhydrated) portland cement clinker particles, paste hardness, color, and luster, paste-aggregate bond, and relative absorptivity of paste as indicated by a freshly fractured surface's readiness to accept applied water droplets. These techniques have been widely used by industry professionals to estimate w/c.

Depth and extent of paste carbonation was determined by the application of a pH indicator (phenolphthalein) solution to freshly fractured and saw-cut surfaces of the concrete. The solution imparts a deep magenta stain to high-pH, non-carbonated, cement paste but does not stain reduced-pH, carbonated, paste. Extent of paste carbonation was also confirmed during microscopical examination of the thin sections.

Notes:

1) The samples will be retained for 30 days, after which they will be discarded unless we hear otherwise from you.
2) This report may not be reproduced except in its entirety.
3) This examination represents specifically the samples submitted.

1a. Top surface.

2b. Side view. Arrows indicate a vertical crack in the concrete. The photo was taken while drying after being wetted with water to highlight the crack. Top surface is to left.

Fig. 1 Core C1S2 as-received for examination. The core consists of an asphaltic topping and the underlying concrete. Scale is marked in inches.

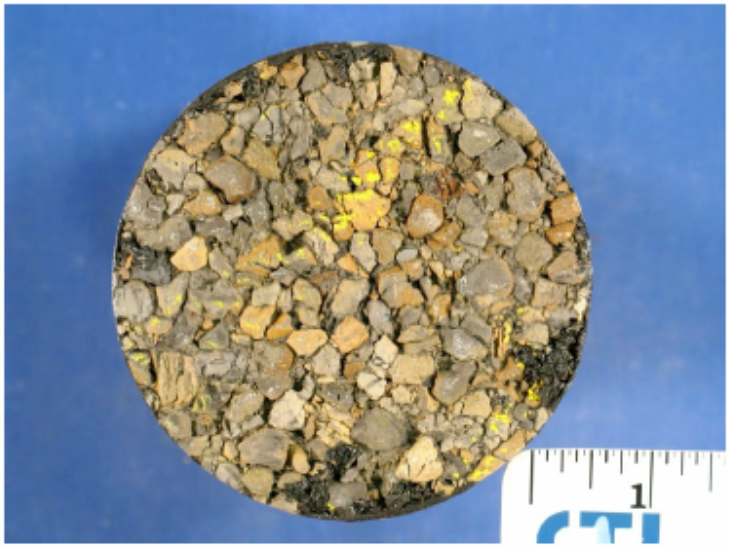

2a. Top surface.

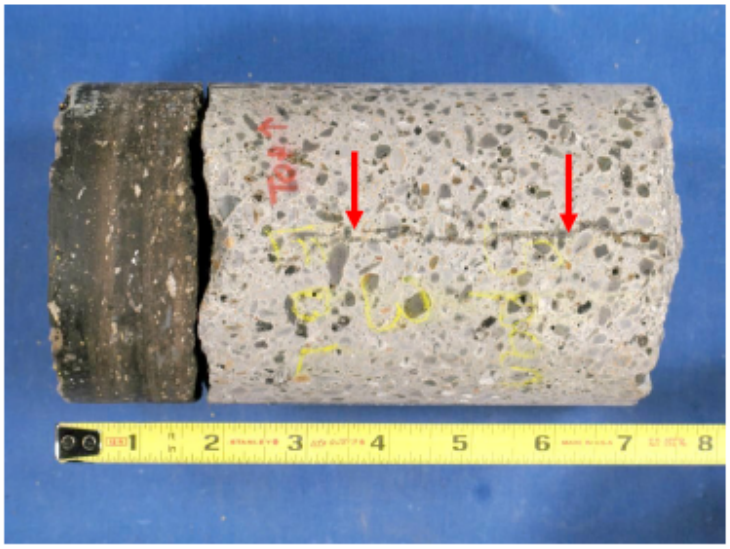

2b. Side view. Arrows indicate a vertical crack in the concrete. The photo was taken while drying after being wetted with water to highlight the crack. Top surface is to left.

Fig. 2 Core C2S3 as-received for examination. The core consists of an asphaltic topping and the underlying concrete. Scale is marked in inches.

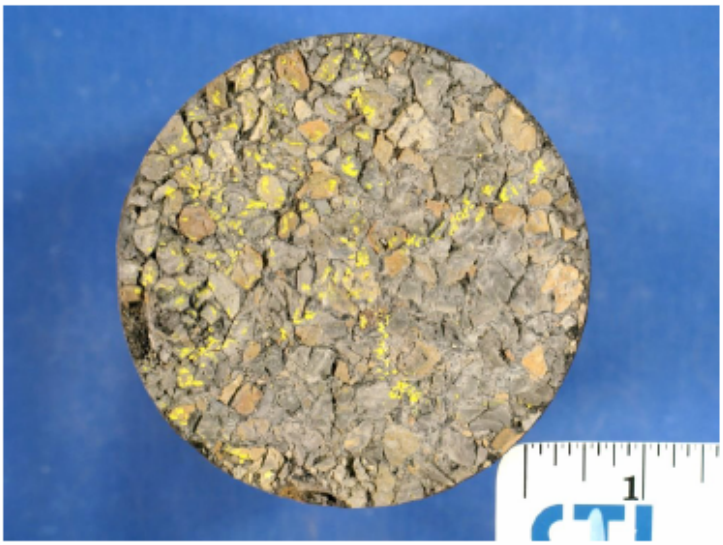

3a. Top surface.

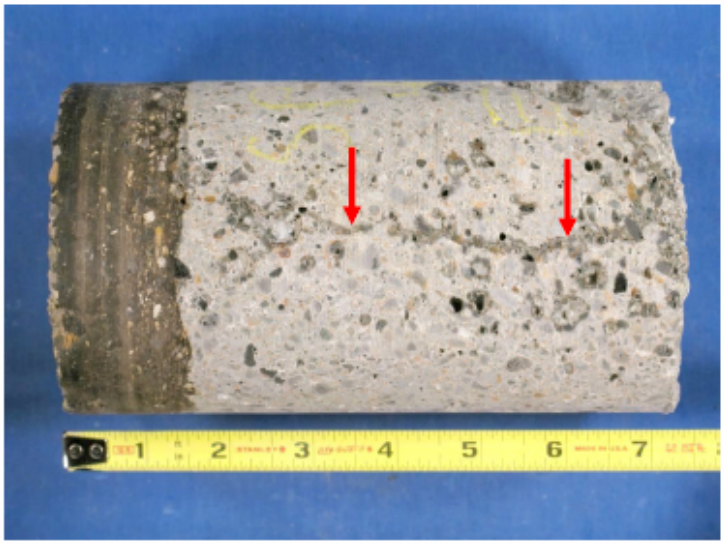

3b. Side view. Arrows indicate a vertical crack in the concrete. The photo was taken while drying after being wetted with water to highlight the crack. Top surface is to left.

Fig. 3 Core C3S4 as-received for examination. The core consists of an asphaltic topping and the underlying concrete. Scale is marked in inches.

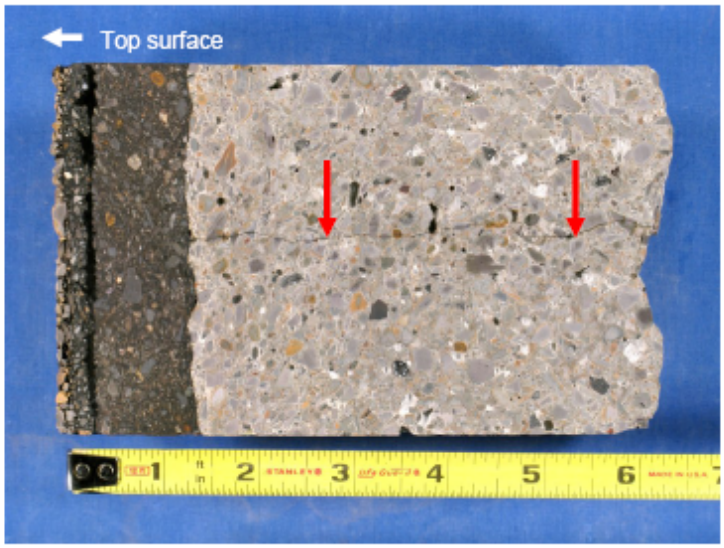

Fig. 4 Cut and lapped cross-section of Core C1S2 showing general appearance of the topping and the concrete. Arrows indicate a vertical crack in the concrete. Top surface is to the left. Scale is marked in inches.

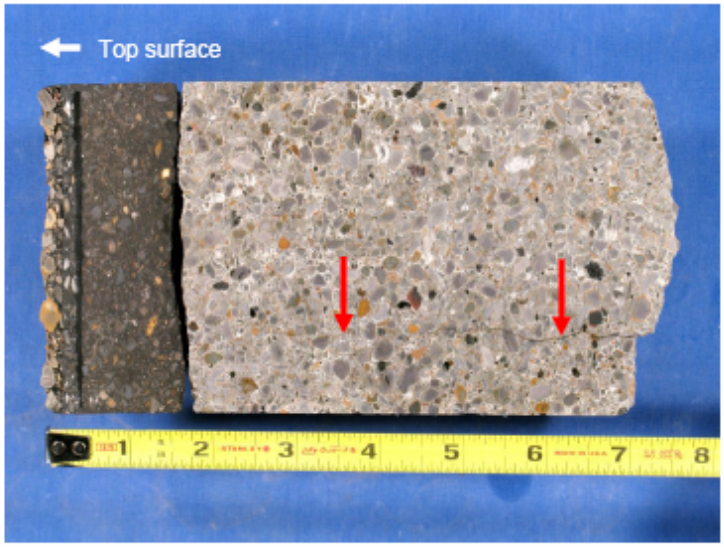

Fig. 5 Cut and lapped cross-section of Core C2S3 showing general appearance of the topping and the concrete. Arrows indicate a vertical crack in the concrete. Top surface is to the left. Scale is marked in inches.

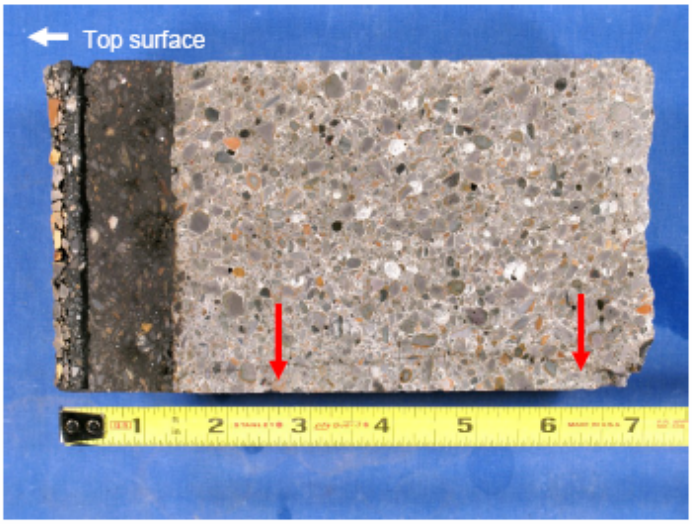

Fig. 6 Cut and lapped cross-section of Core C3S4 showing general appearance of the topping and the concrete. Arrows indicate a vertical crack in the concrete. Top surface is to the left. Scale is marked in inches.

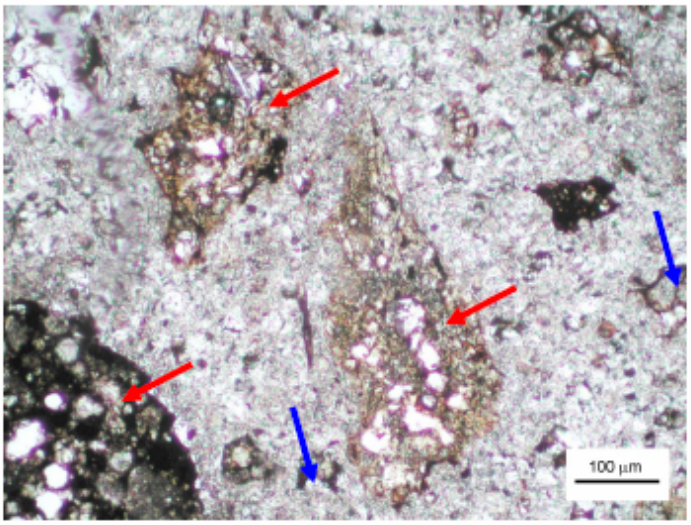

Fig. 7 Transmitted (plane-polarized) light photomicrograph of thin-section showing a representative field of the hardened concrete in Core C1S2. No apparent evidence of alkali-aggregate reaction is observed in the concrete. Red arrows indicate crushed light-weight fine aggregate (expanded shale) particles. Blue arrows indicate residual portland cement clinker particles in the hardened paste.

PETROGRAPHIC EXAMINATION OF HARDENED CONCRETE, ASTM C 856

CTLGROUP PROJECT NO.: 152885 | *DATE REPORTED*: July 7, 2008

CLIENT: Kansas Department of Transportation | *DATE RECEIVED*: May 5, 2008

STRUCTURE: Bridge deck | *EXAMINED BY*: Sang Lee

LOCATION: Randolph Bridge, Kansas |

SAMPLE

Identification: Core C1S2.

Dimensions: Core diameter = 4.0 in. (102 mm); length = approximately 6.1 to 6.5 in. (155 to 165 mm); partial deck thickness. The core consists of approximately 1.5-in. (38-mm) thick asphaltic topping and underlying deck concrete.

Top Surface: Rough asphaltic topping surface with exposed aggregates.

Bottom Surface: Uneven, rough, fractured concrete surface.

Cracks, Joints, or Large Voids: A fine vertical crack extends through depth of concrete, passing through aggregate particles. The crack slightly narrows toward top surface. Coarse entrapped voids up to 0.2 in. (5 mm) are commonly observed in body of concrete. No joint is observed in the concrete.

Reinforcement: No reinforcement is observed in core segment.

AGGREGATES

Coarse: Manufactured, light-weight aggregate (expanded shale).

Fine: Manufactured, light-weight aggregate (expanded shale).

Gradation & Top Size: Evenly graded to an observed top size of 0.3 in. (8 mm).

Shape & Distribution: Aggregate particles are angular to sub-angular and equant to elongate; distribution is uniform.

PASTE

Color: Mottled, dark-medium gray, medium gray, and locally light gray.

Hardness: Moderately hard to locally moderately soft.

Luster: Subvitreous to locally dull.

Paste-Aggregate Bond: Tight; fresh fractures pass through almost all aggregate particles.

Depth of Carbonation: Locally up to 0.04 in. (1 mm) from concrete top surface.

Air Content: Estimated 1 to 3% of entrapped voids. The concrete is not air entrained based on scarcity of small, spherical air voids.

Calcium Hydroxide*: Estimated 5 to 10%; calcium hydroxide mostly occurs as fine crystals and irregular patches in the paste and along periphery of some aggregate particles.

Unhydrated Portland Cement Clinker Particles*: Estimated 2 to 4% of residual portland cement clinker particles are somewhat non-uniformly distributed; relics of hydrated portland cement clinker particles are common.

Supplementary Cementing Materials*: None observed.

Secondary Deposits: Many voids are lined with secondary ettringite deposits.

MICROCRACKING: A few vertical microcracks extend to depths of approximately 1.0 in. (25 mm) from concrete top surface. A few surface-parallel microcracks are locally observed in top approximately 0.2 in. (5 mm) of concrete. Randomly-oriented, discontinuous microcracks are commonly observed in body of concrete.

ESTIMATED WATER-CEMENT RATIO (W/C): Moderate (approximately 0.45 to 0.55) based on observed physical properties and microscopical characteristics of hardened paste. The numeric estimate is somewhat speculative due to apparent evidence of continued cement hydration.

MISCELLANEOUS: (1) Hardened paste is fairly dense to locally somewhat absorptive. (2) Concrete top surface is rough with many fractured aggregate particles partially exposed. (3) Small, irregular patches of lighter and softer paste are locally observed along periphery of some aggregate particles and in nearby paste.

*percent by volume of paste

PETROGRAPHIC EXAMINATION OF HARDENED CONCRETE, ASTM C 856

SAMPLE

Identification: Core C2S3.

Dimensions: Core diameter = 4.0 in. (102 mm); length = approximately 7.0 to 7.4 in. (178 to 188 mm); partial deck thickness. The core consists of approximately 1.6 to 1.7-in. (41 to 43-mm) thick asphaltic topping and underlying deck concrete. Topping was separated from underlying concrete.

Top Surface: Rough asphaltic topping surface with exposed aggregates.

Bottom Surface: Uneven, rough, fractured concrete surface.

Cracks, Joints, or Large Voids: A fine vertical crack extends through depth of concrete, passing through aggregate particles. The crack narrows toward top surface to a microcrack width. Coarse entrapped voids up to 0.2 in. (5 mm) are commonly observed in body of concrete. No joint is observed in the concrete.

Reinforcement: No reinforcement is observed in core segment.

AGGREGATES

Coarse: Manufactured, light-weight aggregate (expanded shale).

Fine: Manufactured, light-weight aggregate (expanded shale).

Gradation & Top Size: Evenly graded to an observed top size of 0.3 in. (8 mm).

Shape & Distribution: Aggregate particles are angular to sub-angular and equant to elongate; distribution is uniform.

PASTE

Color: Mottled, dark-medium gray, medium gray, and locally light gray.

Hardness: Moderately hard to locally moderately soft.

Luster: Subvitreous to locally dull.

Paste-Aggregate Bond: Tight; fresh fractures pass through almost all aggregate particles.

Depth of Carbonation: Locally up to 0.05 in. (1 mm) from concrete top surface.

Air Content: Estimated 2 to 4% of entrapped voids. The concrete is not air entrained based on scarcity of small, spherical air voids.

Calcium Hydroxide*: Estimated 5 to 10%; calcium hydroxide mostly occurs as fine crystals and irregular patches in the paste and along periphery of some aggregate particles.

Unhydrated Portland Cement Clinker Particles*: Estimated 2 to 4% of residual portland cement clinker particles are somewhat non-uniformly distributed; relics of hydrated portland cement clinker particles are common.

Supplementary Cementing Materials*: None observed.

Secondary Deposits: Many voids are lined with secondary ettringite deposits.

MICROCRACKING: A few vertical microcracks extend to depths of approximately 0.9 in. (23 mm) from concrete top surface. A few surface-parallel microcracks are locally observed in top approximately 0.15 in. (4 mm) of concrete. Randomly-oriented, discontinuous microcracks are commonly observed in body of concrete.

ESTIMATED WATER-CEMENT RATIO (W/C): Moderate (approximately 0.45 to 0.55) based on observed physical properties and microscopical characteristics of hardened paste. The numeric estimate is somewhat speculative due to apparent evidence of continued cement hydration.

MISCELLANEOUS: (1) Hardened paste is fairly dense to locally somewhat absorptive. (2) Concrete top surface is rough with many fractured aggregate particles partially exposed. (3) Small, irregular patches of lighter and softer paste are locally observed along periphery of some aggregate particles and in nearby paste.

*percent by volume of paste

PETROGRAPHIC EXAMINATION OF HARDENED CONCRETE, ASTM C 856

CTLGROUP PROJECT NO.: 152885 | *DATE REPORTED*: July 7, 2008

CLIENT: Kansas Department of Transportation | *DATE RECEIVED*: May 5, 2008

STRUCTURE: Bridge deck | *EXAMINED BY*: Sang Lee

LOCATION: Randolph Bridge, Kansas

SAMPLE

Identification: Core C3S4.

Dimensions: Core diameter = 4.0 in. (102 mm); length = approximately 7.0 to 7.4 in. (178 to 188 mm); partial deck thickness. The core consists of approximately 1.5-in. (38-mm) thick asphaltic topping and underlying deck concrete.

Top Surface: Rough asphaltic topping surface with exposed aggregates.

Bottom Surface: Uneven, rough, fractured concrete surface.

Cracks, Joints, or Large Voids: A fine vertical crack extends through depth of concrete, passing through aggregate particles. The crack narrows toward top surface to a microcrack width. Coarse entrapped voids up to 0.3 in. (8 mm) are commonly observed in body of concrete. No joint is observed in the concrete.

Reinforcement: No reinforcement is observed in core segment.

AGGREGATES

Coarse: Manufactured, light-weight aggregate (expanded shale).

Fine: Manufactured, light-weight aggregate (expanded shale).

Gradation & Top Size: Evenly graded to an observed top size of 0.3 in. (8 mm).

Shape & Distribution: Aggregate particles are angular to sub-angular and equant to elongate; distribution is uniform.

PASTE

Color: Mottled, dark-medium gray, medium gray, and locally light gray.

Hardness: Moderately hard to locally moderately soft.

Luster: Subvitreous to locally dull.

Paste-Aggregate Bond: Tight; fresh fractures pass through almost all aggregate particles.

Depth of Carbonation: Locally up to 0.04 in. (1 mm) from concrete top surface.

Air Content: Estimated 2 to 4% of entrapped voids. The concrete is not air entrained based on scarcity of small, spherical air voids.

Calcium Hydroxide*: Estimated 5 to 10%; calcium hydroxide mostly occurs as fine crystals and irregular patches in the paste and along periphery of some aggregate particles.

Unhydrated Portland Cement Clinker Particles*: Estimated 2 to 4% of residual portland cement clinker particles are somewhat non-uniformly distributed; relics of hydrated portland cement clinker particles are common.

Supplementary Cementing Materials*: None observed.

Secondary Deposits: Many voids are lined with secondary ettringite deposits.

MICROCRACKING: A few vertical microcracks extend to depths of approximately 1.5 in. (38 mm) from concrete top surface. A few surface-parallel microcracks are locally observed in top approximately 0.15 in. (4 mm) of concrete. Randomly-oriented microcracks are commonly observed in body of concrete.

ESTIMATED WATER-CEMENT RATIO (W/C): Moderate (approximately 0.45 to 0.55) based on observed physical properties and microscopical characteristics of hardened paste. The numeric estimate is somewhat speculative due to apparent evidence of continued cement hydration.

MISCELLANEOUS: (1) Hardened paste is fairly dense to locally somewhat absorptive. (2) Concrete top surface is rough with many fractured aggregate particles partially exposed. (3) Small, irregular patches of lighter and softer paste are locally observed along periphery of some aggregate particles and in nearby paste.

*percent by volume of paste